Order Number 8810499

The relation between surface and basal velocity variations in glaciers, with application to the mini-surges of variegated glacier

Balise, Michael John, Ph.D.

University of Washington, 1988

U·M·I
300 N. Zeeb Rd.
Ann Arbor, MI 48106

PLEASE NOTE:

In all cases this material has been filmed in the best possible way from the available copy. Problems encountered with this document have been identified here with a check mark __√__.

1. Glossy photographs or pages _____
2. Colored illustrations, paper or print _____
3. Photographs with dark background _____
4. Illustrations are poor copy _____
5. Pages with black marks, not original copy __✓__
6. Print shows through as there is text on both sides of page _____
7. Indistinct, broken or small print on several pages __✓__
8. Print exceeds margin requirements _____
9. Tightly bound copy with print lost in spine _____
10. Computer printout pages with indistinct print _____
11. Page(s) _____ lacking when material received, and not available from school or author.
12. Page(s) _____ seem to be missing in numbering only as text follows.
13. Two pages numbered _____. Text follows.
14. Curling and wrinkled pages __✓__
15. Dissertation contains pages with print at a slant, filmed as received _____
16. Other _____

_____

_____

THE RELATION BETWEEN SURFACE AND BASAL VELOCITY VARIATIONS IN GLACIERS, WITH APPLICATION TO THE MINI-SURGES OF VARIEGATED GLACIER

by

Michael John Balise

A dissertation submitted in partial fulfillment
of the requirements for the degree of

Doctor of Philosophy

University of Washington

1988

Approved by Charles F. Raymond
(Chairperson of Supervisory Committee)

Program Authorized
to Offer Degree Geophysics Program

Date 16 December, 1987

Doctoral Dissertation

In presenting this dissertation in partial fulfillment of the requirements for the Doctoral degree at the University of Washington, I agree that the Library shall make its copies freely available for inspection. I further agree that extensive copying of this dissertation is allowable only for scholarly purposes, consistent with "fair use" as prescribed in the U.S. Copyright Law. Requests for copying or reproduction of this dissertation may be referred to University Microfilms, 300 North Zeeb Road, Ann Arbor, Michigan 48106, to whom the author has granted "the right to reproduce and sell (a) copies of the manuscript in microform and/or (b) printed copies of the manuscript made from microform."

Signature Michael John Balise

Date 16 December 1987

University of Washington

Abstract

THE RELATION BETWEEN SURFACE AND BASAL VELOCITY VARIATIONS IN GLACIERS, WITH APPLICATION TO THE MINI-SURGES OF VARIEGATED GLACIER

by Michael John Balise

Chairperson of the Supervisory Committee: Prof. C. F. Raymond

Geophysics Program

The relation between surface and basal velocity variations in glaciers is systematically studied, so that basal velocities of glaciers can be determined from measured surface velocities. Linear viscous, visco-elastic, and non-linear power law rheologies are used.

For the forward problem (prescribed basal velocity anomaly), the surface response depends on the length scale of the basal velocity anomaly as compared to the thickness of the ice. Four different length scales are defined: very short, short, intermediate, and long. At short and intermediate scales (anomaly lengths between 1 and 10 ice thicknesses) a cross-component effect allows normal motions at the surface to be caused by longitudinal motions at the base, and the spatial form of the longitudinal component at the surface may be very different from that component at the bed. The magnitude of the surface response increases as the length scale increases.

These length scales apply to both the linear and non-linear rheologies, although the magnitude of the surface response is less and the scales shift towards longer wavelengths for the non-linear rheology. Importantly, the anomalous solution is coupled to the steady-state solution for the non-linear rheology.

The inverse problem (prescribed surface velocity anomaly) is solved exactly for linear rheology. The solution for the basal velocity anomaly becomes infinite in amplitude as the wavelength of the prescribed surface anomaly goes to zero. This is dealt with by reducing the short wavelength components of the surface velocity. The non-linear inverse problem

is solved numerically.

When data from Variegated Glacier are used for the surface velocity anomalies, the calculated basal velocities have greater amplitude than the surface velocities. The structure is of similar roughness between surface and bed, but the velocity maxima and minima are often in different spatial positions. Multiple peaks in the surface velocity may be associated with only a single peak in the basal velocity. Substantial normal motions at the bed are calculated, but the uncertainties of the solution process do not allow definite conclusions about basal cavitation. Better spatial-resolution surface data is necessary to more accurately calculate the basal velocity anomalies.

TABLE OF CONTENTS

LIST OF FIGURES

LIST OF SYMBOLS

a,b,c	coefficients in visco-elastic solution
$a(t)$	time-varying amplitude
A	coefficient in solutions to biharmonic equation, or non-linear inverse viscosity parameter
B	coefficient in solutions to biharmonic equation, or non-linear viscosity parameter
C,D	coefficients in solutions to biharmonic equation
e_{ij}	strain tensor
F	a filter
$F_{ub},F_{us},F_{vb},F_{vs}$	effective filters for trade-off solutions
g	acceleration of gravity
G_s	Green's function
H	thickness of glacier
i,j	node numbers (as superscripts)
k	wave number
k_1	fundamental wave number for non-linear sliding law solution
K	elastic bulk modulus
m	exponent in sliding law
n	exponent in Glen's flow law, or order of derivative, or an integer
p	pressure
(pbv)	refers to prescribed basal velocity solution (as superscript)
p_{ij},q_i	coefficients in visco-elastic solution
r	half of horizontal distance of a "ramp"
s	Laplace transform variable
(sl)	refers to sliding law solution (as superscript)
$S_{ub},S_{vb},S_{ub}^{total},S_{vb}^{total}$	sums to minimize

t	time variable
t_o	reference time
T^{slide}	sliding law transfer function
$T^{uu}, T^{vu}, T^{uv}, T^{vv}$	forward transfer functions evaluated between bed and surface
T^{τ}	basal shear stress transfer function
$T_b^{uu}, T_b^{vu}, T_b^{uv}, T_b^{vv}$	inverse transfer functions evaluated at bed
$T_s^{uu}, T_s^{vu}, T_s^{uv}, T_s^{vv}$	forward transfer functions evaluated at surface
u	longitudinal (x direction) component of velocity
$u_b, u_b^a, u_b^{anomaly}$	anomalous longitudinal component of basal velocity
u_b^i	estimate of the total longitudinal component of the basal velocity at node i
u_b^s, u_b^{steady}	steady-state longitudinal component of basal velocity
u_b^t, u_b^{total}	total longitudinal component of basal velocity
u_s	anomalous longitudinal component of surface velocity
u_s^d	non-linear surface deformation velocity for no velocity anomaly
u_s^f	filtered anomalous longitudinal component of surface velocity
u_s^m	modified anomalous longitudinal component of surface velocity
u_s^s	steady-state longitudinal component of surface velocity
$\overline{u_s}$	mean longitudinal component of surface velocity
u_s^t	total longitudinal component of surface velocity
$\mathbf{u}$	anomalous velocity distribution
$\mathbf{u}^s$	steady-state velocity distribution
U_b	amplitude of anomalous longitudinal component of basal velocity
v	normal (y direction) component of velocity
v_b	anomalous normal component of basal velocity
v_b^i	estimate of the total normal component of the basal velocity at node i
v_s	anomalous normal component of surface velocity
v_s^f	filtered anomalous normal component of surface velocity

v_s^m	modified anomalous normal component of surface velocity
V_b	amplitude of anomalous normal component of basal velocity
w	wave propagation speed
W	total sliding law parameter
W^a	anomalous sliding law parameter
W^s	steady-state sliding law parameter
x	longitudinal coordinate (direction parallel to bed)
x_o	reference position
$\mathbf{x}$	spatial position vector
$\mathbf{x_b}$	spatial position vector at base
y	normal coordinate (direction normal to bed)
z	transverse coordinate (cross-slope)
α	wave amplitude decay or increase factor
$\alpha_i,\beta_i,\gamma_i$	coefficients in visco-elastic solution
β	trade-off parameter
γ	bed slope angle
δ	phase lead (in space)
$\delta(k-k_1)$	Dirac delta function
δ_{ij}	Kronecker delta function
δ_u,δ_v	basal velocity perturbations for Frechet derivative
δu_b^i	necessary changes in basal velocity
δu_s^i	necessary changes in surface velocity
$\delta u_s^{ij},\delta v_s^{ij}$	resulting surface velocity perturbations for Frechet derivative
δu_s^{ij*}	Frechet derivative
ε	difference between successive solutions in finite element model
$\varepsilon_u,epsilon_v$	assumed errors in measured surface velocity
ζ_{ij}	strain deviator tensor
η	dynamic viscosity
η^{eff}	non-linear effective viscosity

λ	wavelength
$\lambda_{u1},\lambda_{u2},\lambda_{v1},\lambda_{v2}$	Lagrange multipliers
μ	elastic shear modulus
ν	Poisson's ratio
ρ	density
σ	standard deviation
σ_{ij}	stress tensor
σ_{xy}	anomalous shear stress
σ_{yy}	anomalous normal stress
σ	anomalous stress distribution
σ^s	steady-state stress distribution
$\tau_b,\tau_b^a,\tau_b^{anomaly}$	anomalous basal shear stress
τ_b^s,τ_b^{steady}	steady-state basal shear stress
τ_b^t,τ_b^{total}	total basal shear stress
τ_{ij}	stress deviator tensor
ψ	biharmonic stream function
ω	angular frequency
∇	gradient
∇^2	biharmonic operator
*	dimensionless quantity or complex conjugate (as superscript)
*	convolution (between two quantities)
$\dot{f}$	time derivative of f
$\hat{f}$	Fourier transform of f
$\tilde{f}$ or $L\{f\}$	Laplace transform of f

PREFACE

Chapter 2 has been published (Balise and Raymond, 1985) and was written in collaboration with co-author C. F. Raymond. The notation has been changed to match the rest of the dissertation. Chapters 4 and 5, along with Chapter 2, were presented at the International Workshop on Hydraulic Effects at the Glacier Bed held at Interlaken, Switzerland, September 16-19, 1985. Preliminary versions of Chapters 6 and 7 were presented at the annual meeting of Northwest Glaciologists held in Seattle, Washington, December 4-5, 1986.

ACKNOWLEDGMENTS

Many people have helped to keep this dissertation on course. First, sincere thanks to Professer Charles Raymond for all of his invaluable input, both in the field and in the theoretical work. I would also like to thank the rest of my supervisory committee: Professor John Booker, for information on inverse theory; Professor Bernard Hallet, for good advice on many aspects of the dissertation; Professor Stephen Malone, for much information on how to operate "his" computer; and Professor Stephen Burges for a non-glaciological perspective, and helping to keep the rest of the committee honest! In addition, I would like to thank Ed Waddington, Tomas Johannesson, and Torquil Smith, for doing very useful reviews of various chapters.

I would like to thank all of my various officemates for humor and advice: especially Tad Pfeffer, who was also wading through the morass of putting together a finished dissertation; Neil Humphrey, who showed us that it could be done; and Magnus Magnusson, for a splendid tour of Iceland. I would also especially like to thank Lisa Peterson and Kathy Sharpe for information on text formatting, and taking care of various bureaucratic hassles. And an apology is due to all those anonymous and not-so-anonymous people who have tried to call on the telephone in the last few monthes, only to find the line occupied by a computer!

And last, I would like to thank my wife Mardi and our little boy Jamie, for putting up with me while I wrote this dissertation, and helping me to keep things in proper perspective.

CHAPTER 1

GENERAL DESCRIPTION OF PROBLEM AND ORGANIZATION OF DISSERTATION

The measurement of velocities at the bases of glaciers or ice sheets is a fundamental observational problem. A method to determine these velocities is necessary for developing an understanding of the sliding process, and the testing of sliding laws for practical predictions of glacier speeds. Although the bases of glaciers can be reached by various means for direct observation of sliding speed and factors affecting it (e.g, Engelhardt and others, 1978; Vivian, 1980), these techniques are difficult and usually very expensive.

For this reason it is natural to attempt to estimate sliding speed from measurements made at the surface. There are a number of cases involving various spatial and temporal scales where this has been attempted (e.g. Haefeli, 1970; Hodge, 1974; Bindschadler, 1983; Raymond and Harrison, submitted). Some of the most exciting recent discoveries and progress in understanding the sliding process have resulted from careful measurement of both the horizontal and vertical components of velocity at the glacier surface on a daily or shorter time scale, by standard surveying and photogrammetric methods (Iken, 1977; Iken and others, 1983; Kamb and Engelhardt, 1987). This kind of approach involves the estimation of velocity differences between the surface and the bed caused by ice deformation.

In the case where the changes happen on a seasonal or longer time scale and glacier geometry and associated internal stresses obviously vary, changes in ice deformation rate have been estimated from changes in depth and slope using results derived assuming deformation in simple shear parallel to the surface (Nye, 1952). In the case of short-scale variations for which glacier geometry is essentially constant, it has been assumed that the changes at the surface are nearly equal or at least proportional to those at the base. While this approach gives useful zero-order estimates of the relation between surface and basal velocity variations, it is clear that there are errors arising from uncertainties about the ice rheology and changes in stress distribution. In particular, if the spatial scale of the velocity variations is short, longitudinal interactions associated with longitudinal stress gradients will affect the form of this relation. Although the effect of these longitudinal stress gradients on the relation between basal topography changes, surface topography changes, and

internal motions has been studied (Langdon and Raymond, 1978; Hutter and others, 1981; Whillans and Johnsen, 1983), the relation between surface and basal velocities has not been systematically examined for short spatial-scale velocity variations. In addition, if the time scale of the velocity variations is short, visco-elastic effects may be important. These visco-elastic effects have not been well examined for glacier flow. This dissertation provides an analysis of the relation between surface and basal velocity variations, with careful consideration of these problems which may be caused by short spatial and temporal scales.

The immediate motivation for this analysis is the mini-surge behavior of Variegated Glacier (Raymond and Malone, 1986; Harrison and others, 1986; Kamb and Engelhardt, 1987). In these mini-surges the glacier did not speed up simultaneously at all locations. Instead, fast motion was confined to a rather narrow propagating zone, with high compression below it and extension above it. This means that the ice underwent a rapid transition from compression to tension as a given mini-surge propagated down-glacier. In general temporal changes in glacier speed, whether propagating or not, can be expected to show some localization and resulting longitudinal stress changes, which will tend to damp variations at the surface in comparison to the bed. Thus there is ample motivation for studying the relation between surface and basal velocity variations.

The analysis of velocity variations can be approached in two different ways. The first method is to start with a given basal velocity or basal sliding law, and then calculate the resulting surface velocity; the second method is to start with a given surface velocity and then attempt to calculate the corresponding basal velocity. The first method may be referred to as the "forward" problem and is used in Chapters 2 through 5. The forward problem is a standard boundary value problem. The second method is referred to as the "inverse" problem and is developed in Chapters 6 and 7. This inverse problem involves boundary conditions which result in instabilities in the solution process, and therefore special solution techniques are required. Since almost all velocity data from glaciers are surface data, the inverse method is very useful for analyzing real data. This method is applied to velocity data from the mini-surges of Variegated Glacier.

The assumed rheology of the glacier ice is clearly important in any study of velocity changes. Several different rheologies are used, for both the forward and the inverse solutions. These include a linear viscous rheology, a visco-elastic rheology, and a non-linear Glen's flow law rheology. The results using the linear and non-linear rheologies can be

compared to check the importance of non-linear effects. The visco-elastic rheology is useful for examining the possible importance of elastic straining during short time-scale velocity variations.

Various simplifying assumptions are used to make the analysis of velocity variations more tractable. These assumptions are described in some detail at the beginning of the appropriate chapters; particularly at the beginning of Chapter 2 (the first chapter on forward solutions) and at the beginning of Chapter 6 (the first chapter on inverse solutions). These assumptions will be summarized here.

The first major assumption is the specification of a planar geometry and plane strain. This means that only two components of velocity are allowed: a component u in the x direction (referred to as the "longitudinal" component), and a component v in the y direction (referred to as the "normal" component). Thus velocity and strain-rate components across the slope are assumed to everywhere be equal to zero. This assumption also means that width effects (e.g., from valley sides) are not considered.

The next major assumption is the separation of the problem into steady-state and anomalous parts. The flow in the steady-state problem is assumed not to vary in time or in the x direction (for the planar geometry), and this steady-state flow balances the average forces arising from gravity, atmospheric pressure, and the stresses at the glacier bed. The anomalous flow is assumed to be due to changes in the glacier boundary conditions at the bed (e.g., changes in the force balance at the bed from changes in the basal water pressure). Furthermore acceleration terms are assumed to be negligible for the anomalous flow. This separation into steady-state and anomalous parts will be shown to be of varying validity, depending on the rheology and the boundary conditions. When necessary, the total solution for the combined steady-state and anomalous problems will be derived.

The last major assumption is that the planar geometry remains essentially constant (with a constant surface slope parallel to a constant bed slope). This means that geometry changes arising from the anomalous flow must be negligible. The easiest analytical method of insuring negligible geometry changes is to look at the solutions in time-independent form; thus most of the solutions are a "snapshot" of the flow pattern within the ice at a certain specific time. In physical reality, this assumption of negligible geometry changes will be met if the velocity anomaly occurs over a sufficiently short time

scale, or if the velocity anomaly does not significantly affect the surface geometry even over longer time scales (see Appendix A).

CHAPTER 2

LINEAR VISCOUS FORWARD SOLUTIONS

2.1 Chapter introduction

The goal of this chapter is to do an initial analysis of short-scale velocity variations. This initial analysis will involve prescribing a basal sliding velocity, and then calculating the resulting englacial and surface velocities (the "forward" problem). A simple linear viscous rheology will be used. Examination of more complicated rheologies and the "inverse" problem is done in following chapters.

2.2 Mathematical description of problem

2.2.1 Definition of steady-state and anomalous motions

The effect on glacier motion of changes in sliding velocity is most simply examined by separating the added anomalous motion $\mathbf{u}(\mathbf{x},t)$ caused by a specific anomalous sliding velocity distribution from a steady-state motion $\mathbf{u}^s(\mathbf{x})$ that would occur without the anomaly. The velocity anywhere in the glacier is then expressed as $\mathbf{u}^s(\mathbf{x}) + \mathbf{u}(\mathbf{x},t)$.

The steady-state velocity distribution $\mathbf{u}^s(\mathbf{x})$ and the corresponding stress distribution $\sigma^s(\mathbf{x})$ satisfy the field equations for flow under the action of gravity, with atmospheric pressure at the upper surface and the steady-state sliding $\mathbf{u}^s(\mathbf{x}_b)$ at the bed. The sum of the steady-state and anomalous distributions must also satisfy these field equations, with the boundary conditions changed to include the additional anomalous sliding velocity $\mathbf{u}(\mathbf{x}_b,t)$.

2.2.2 Geometrical assumptions and coordinate system

Planar slab geometry is assumed. Coordinates are chosen as shown in Figure 2-1, with the x axis on the bed and positive down the slope, the y axis normal to the bed and positive towards the surface, and the z axis horizontal across the slope. The steady-state velocity distribution $\mathbf{u}^s(\mathbf{x})$ is assumed to be compatible with planar geometry and a constant ice thickness H, under a prescribed mass balance distribution. The anomalous motion is

assumed to be planar: the x ("longitudinal") component of velocity u and the y ("normal") component of velocity v may be non-zero functions of x, y, and t, but anomalous motion across the slope in the z direction is everywhere zero.

This chapter is concerned with the instantaneous velocity distribution at a specified time and for a specified planar geometry. A more complex and less well-defined problem would be the subsequent evolution of the geometry and velocity. Any basal velocity anomaly is likely to cause an anomalous normal velocity at the upper surface and gradually change the geometry of the glacier. This geometry change would feed back to affect the velocity distribution (Langdon and Raymond, 1978; Hutter, 1983; Kamb and Echelmeyer, 1986; Echelmeyer and Kamb, 1986). If the time scale of interest is short, or the velocity anomalies are small compared to the steady-state velocity $\mathbf{u}^s$, then the geometry changes and corresponding velocity changes may be negligible. Under these restrictive conditions the problem of the eventual evolution of the surface geometry would not arise. These restrictions are examined in more detail in Appendix A.

2.2.3 Rheological assumptions and field equations

The ice is assumed to flow as a Newtonian fluid of uniform dynamic viscosity η. The relevant field equations are the equation of continuity for incompressible flow, and the Navier-Stokes equations. Velocity anomalies are assumed to vary slowly enough that acceleration terms are negligible. From the assumptions that the motion is planar and that the steady-state distributions $\mathbf{u}^s$ and $\boldsymbol{\sigma}^s$ satisfy the equations with body force from gravity, standard considerations yield the following field equations for the velocity anomaly components u and v, and the anomalous pressure p:

$$\frac{\partial u}{\partial x} + \frac{\partial v}{\partial y} = 0 \tag{2-1}$$

$$\eta\left[\frac{\partial^2 u}{\partial x^2} + \frac{\partial^2 u}{\partial y^2}\right] - \frac{\partial p}{\partial x} = 0 \tag{2-2}$$

$$\eta\left[\frac{\partial^2 v}{\partial x^2} + \frac{\partial^2 v}{\partial y^2}\right] - \frac{\partial p}{\partial y} = 0 \tag{2-3}$$

The gravity body force does not appear in these equations because the steady-state stress distribution $\boldsymbol{\sigma}^s$ is in static equilibrium with gravity, and the linearity of the equations results

in the anomaly fields being independent of and additional to the steady-state distribution.

2.2.4 Boundary conditions

The boundary conditions to be applied are atmospheric pressure on the upper surface and a prescribed velocity at the base. At the upper surface the steady-state distributions $\mathbf{u}^s$ and $\boldsymbol{\sigma}^s$ correspond to atmospheric pressure. The additional stress on this surface from the anomaly distributions $\mathbf{u}$ and $\boldsymbol{\sigma}$ must therefore be zero. For the given coordinate system this is expressed as

$$\sigma_{yy}(x,H,t) = \left[2\eta\frac{\partial v}{\partial y} - p\right]_{y=H} = 0 \tag{2-4a}$$

$$\sigma_{xy}(x,H,t) = \eta\left[\frac{\partial u}{\partial y} + \frac{\partial v}{\partial x}\right]_{y=H} = 0 \tag{2-4b}$$

keeping in mind the restrictions on the geometry of the upper surface discussed in the previous section. At the base, a prescribed velocity anomaly is expressed as

$$u(x,0,t) = u_b(x,t) \tag{2-5a}$$

$$v(x,0,t) = v_b(x,t) \tag{2-5b}$$

Equation (2-5a) is appropriate to slip along a flat base, and Equation (2-5b) allows for a simple approximation of the opening and closing of basal cavities.

A physically based sliding law relating basal velocity to basal stress, with spatially or temporally varying parameters, can also be used instead of Equation (2-5a). This sliding law boundary condition is used in Chapter 3, in order to better understand the physical origin of basal velocity anomalies. However, from an observational point of view, it is better to relate surface velocity directly to basal velocity, especially since in practice a realistic sliding law is not known.

The mathematical formulations for these two approaches are somewhat different. However, in many cases the results of one formulation can be interpreted in terms of the other (see Chapter 3).

2.2.5 Solution technique

Equations (2-1) to (2-3) are solved using a stream function ψ such that

$$u = \frac{\partial \psi}{\partial y} \qquad v = -\frac{\partial \psi}{\partial x} \tag{2-6}$$

Equation (2-1) is trivially satisfied for any choice of ψ. Substitution of Equation (2-6) into Equations (2-2) and (2-3) gives two corresponding equations for ψ and p. Differentiation of Equation (2-2) with respect to y and Equation (2-3) with respect to x and the requirement $\partial^2 p/\partial x \partial y = \partial^2 p/\partial y \partial x$ implies that ψ must be biharmonic, that is

$$\frac{\partial^4 \psi}{\partial x^4} + 2\frac{\partial^4 \psi}{\partial x^2 \partial y^2} + \frac{\partial^4 \psi}{\partial y^4} = 0 \tag{2-7}$$

Furthermore, when ψ is biharmonic, p can always be found from a path-independent integration of Equations (2-2) and (2-3). Thus the solution of Equations (2-1) to (2-3) is reduced to the solution of Equation (2-7).

To solve Equation (2-7) the boundary conditions (2-4) and (2-5) must be expressed in terms of ψ. Treatment of Equation (2-4a) is simplified if it is equivalently expressed as $\partial \sigma_{yy}(x,H,t)/\partial x = 0$, plus the requirement that at some point on $y = H$, $\sigma_{yy} = 0$ (e.g. $\sigma_{yy}(0,H,t) = 0$). In this differentiated form of Equation (2-4a), $\partial p/\partial x$ and $\partial^2 v/\partial x \partial y$ can be calculated in terms of ψ from Equations (2-2) and (2-6) to find

$$-\eta\left[3\frac{\partial^3 \psi}{\partial x^2 \partial y} + \frac{\partial^3 \psi}{\partial y^3}\right]_{y=H} = 0 \tag{2-8a}$$

Substitution of Equation (2-6) into Equations (2-4b), (2-5a), and (2-5b) gives

$$\eta\left[\frac{\partial^2 \psi}{\partial y^2} - \frac{\partial^2 \psi}{\partial x^2}\right]_{y=H} = 0 \tag{2-8b}$$

$$\frac{\partial \psi}{\partial y}\Big|_{y=0} = u_b(x,t) \tag{2-9a}$$

$$-\frac{\partial \psi}{\partial x}\Big|_{y=0} = v_b(x,t) \tag{2-9b}$$

2.2.6 Some properties of solutions

Because of the linearity of Equations (2-1) to (2-3) or equivalently Equation (2-7), it is apparent that if $\psi^{(a)}$ and $\psi^{(b)}$ are solutions, then $\psi = \psi^{(a)} + \psi^{(b)}$ is also a solution. Furthermore, if $\psi^{(a)}$ and $\psi^{(b)}$ satisfy the boundary conditions in Equations (2-8) and (2-9) corresponding to $u_b^{(a)}$ and $u_b^{(b)}$ in Equation (2-9a) and $v_b^{(a)}$ and $v_b^{(b)}$ in Equation (2-9b), then ψ also satisfies the boundary conditions with $u_b = u_b^{(a)} + u_b^{(b)}$ and $v_b = v_b^{(a)} + v_b^{(b)}$. This expresses the well-known principle of superposition of solutions. It is also evident that if $v_b = 0$, so that ψ is a solution corresponding to a basal velocity u_b, then $\partial\psi/\partial x$ is also a solution and corresponds to a basal velocity $\partial u_b/\partial x$. These properties can be used to generate new solutions from existing ones.

Another important property of the equations is that they depend on time only through the boundary conditions in Equations (2-9a) and (2-9b). This arises because of the assumed fluid rheology and the absence of acceleration terms, so that the internal flow responds to the basal boundary condition without time lag. An important consequence of this is illustrated by the following example. Suppose $v_b = 0$, so that $\psi(x,y)$ is a solution corresponding to $u_b(x)$; then $a(t)\psi(x-wt,y)$ is a solution corresponding to $a(t)u_b(x-wt)$. Thus a solution for a certain time-independent, fixed spatial distribution can easily be modified to give a time-varying amplitude, or a propagating solution of the same wave shape. The solutions in the following sections will only be written in time-independent form, with the understanding that the corresponding propagating solutions can easily be determined.

Finally, it is noteworthy that the dynamic viscosity η drops out of all of the Equations (2-7) through (2-9b) which determine ψ. This arises because there are no prescribed stress boundary conditions other than the free upper surface, and no body force. In consequence, the anomalous velocity is independent of η and differences in the velocity distribution arise only from differences in the kinematic boundary conditions in Equations (2-9a) and (2-9b). However, the anomalous stress distribution will depend on η, although this distribution is not examined explicitly in this chapter. (Also, the velocity solution for a basal sliding law will depend on η; see Chapter 3).

2.3 Solution methods

2.3.1 Harmonic longitudinal basal velocity anomaly

Suppose the velocity anomaly at the base of the glacier is

$$u_b(x) = U_b \sin kx \tag{2-10a}$$

$$v_b(x) = 0 \tag{2-10b}$$

where U_b is the amplitude of the basal anomaly. With the given rheology and assumptions, the velocity throughout the ice mass will also vary harmonically. A solution to Equation (2-7) varying harmonically with x is

$$\psi = \left[\frac{A_u(k)}{k}e^{-ky} + B_u(k)ye^{-ky} + \frac{C_u(k)}{k}e^{ky} + D_u(k)ye^{ky}\right]U_b \sin kx \tag{2-11}$$

The boundary conditions in Equations (2-8) and (2-9) give four equations which determine the coefficients A_u, B_u, C_u, and D_u as follows:

$$A_u = -C_u = -\frac{2k^2H^2}{e^{-2kH}+2+4k^2H^2+e^{2kH}} \tag{2-12a}$$

$$B_u = \frac{1+2kH+e^{2kH}}{e^{-2kH}+2+4k^2H^2+e^{2kH}} \tag{2-12b}$$

$$D_u = \frac{e^{-2kH}+1-2kH}{e^{-2kH}+2+4k^2H^2+e^{2kH}} \tag{2-12c}$$

The velocity anomaly at any point (x,y) can be found from Equations (2-6), (2-11), and (2-12). The longitudinal component at (x,y) is

$$u(x,y) = \frac{\partial \psi(x,y)}{\partial y} \tag{2-13a}$$

$$= [-A_u e^{-ky} + [B_u - B_u ky]e^{-ky} + C_u e^{ky} + [D_u + D_u ky]e^{ky}]U_b \sin kx$$

$$= T^{uu}(k,y)u_b(x)$$

and the normal component is

$$v(x,y) = -\frac{\partial \psi(x,y)}{\partial x} \tag{2-13b}$$

$$= -\,[A_v e^{-ky} + B_v k y e^{-ky} + C_v e^{ky} + D_v k y e^{ky}]U_b \cos kx$$

$$= T^{vv}(k,y)u_b(x-\frac{\pi}{2k})$$

Here

$$T^{uu}(k,y) \equiv -A_u e^{-ky} + [B_u - B_u k y]e^{-ky} + C_u e^{ky} + [D_u + D_u k y]e^{ky} \tag{2-14a}$$

and

$$T^{uv}(k,y) \equiv A_u e^{-ky} + B_u k y e^{-ky} + C_u e^{ky} + D_u k y e^{ky} \tag{2-14b}$$

The velocities consist of a transfer or filter function multiplying the basal velocity u_b. The longitudinal velocity component anywhere in the glacier is in phase with the longitudinal velocity component at the base; the normal velocity component is everywhere 90^o out of phase from the longitudinal velocity component.

The velocity transfer functions evaluated at the surface ($y = H$) are

$$T_s^{uu}(k) \equiv T^{uu}(k,y)\Big|_{y=H} = \frac{[2+2kH]e^{-kH} + [2-2kH]e^{kH}}{e^{-2kH} + 2 + 4k^2H^2 + e^{2kH}} \tag{2-15a}$$

for the longitudinal velocity component, and

$$T_s^{uv}(k) \equiv T^{uv}(k,y)\Big|_{y=H} = \frac{2kHe^{-kH} + 2kHe^{kH}}{e^{-2kH} + 2 + 4k^2H^2 + e^{2kH}} \tag{2-15b}$$

for the normal component.

Schematics of the internal motion for harmonic longitudinal basal velocity anomalies of a short and a long non-dimensional wavelength λ/H are shown in Figures 2-2a and 2-2b. The important difference between these two cases is that for the short wavelength the velocity anomaly recirculates, while for long wavelengths it does not. This leads to interesting effects at the surface; particularly for short wavelengths the longitudinal component will have opposite direction at the surface to that at the base. (This can either be viewed as a sign change or a 180^o phase shift.) Also, at a certain intermediate wavelength $\lambda/H \approx 5.2$, the amplitude at the surface of the longitudinal velocity component is zero. At this wavelength the surface amplitude of the normal component reaches its maximum. These effects are summarized in Figure 2-3.

2.3.2 Harmonic normal basal velocity anomaly

Now suppose that the velocity anomaly at the base of the glacier is

$$u_b(x) = 0 \tag{2-16a}$$

$$v_b(x) = V_b \cos kx \tag{2-16b}$$

where V_b is the amplitude of the basal anomaly. A solution to Equation (2-7) then is

$$\psi = \left[\frac{A_v(k)}{k}e^{-ky} + B_v(k)ye^{-ky} + \frac{C_v(k)}{k}e^{ky} + D_v(k)ye^{ky}\right]V_b \sin kx \tag{2-17}$$

Using the boundary conditions in Equations (2-8) and (2-9) the coefficients A_v, B_v, C_v, and D_v are found to be

$$A_v = \frac{-1+2kH-2k^2H^2-e^{2kH}}{e^{-2kH}+2+4k^2H^2+e^{2kH}} \tag{2-18a}$$

$$B_v = \frac{-1+2kH-e^{2kH}}{e^{-2kH}+2+4k^2H^2+e^{2kH}} \tag{2-18b}$$

$$C_v = \frac{-e^{-2kH}-1-2kH-2k^2H^2}{e^{-2kH}+2+4k^2H^2+e^{2kH}} \tag{2-18c}$$

$$D_v = -\frac{e^{2kH}+1+2kH}{e^{-2kH}+2+4k^2H^2+e^{2kH}} \tag{2-18d}$$

The resulting velocity anomaly at a point (x,y) is

$$u(x,y) = \frac{\partial\psi(x,y)}{\partial y} \tag{2-19a}$$

$$= [-A_v e^{-ky} + (B_v - B_v ky)e^{-ky} + C_v e^{ky} + (D_v + D_v ky)e^{ky}]V_b \sin kx$$

$$= T^{vu}(k,y)v_b\left(x-\frac{\pi}{2k}\right)$$

and

$$v(x,y) = -\frac{\partial\psi(x,y)}{\partial x} \tag{2-19b}$$

$$= - [A_v e^{-ky} + B_v ky e^{-ky} + C_v e^{ky} + D_v ky e^{ky}] V_b \cos kx$$

$$= T^{vv}(k,y) v_b(x)$$

where

$$T^{vu}(k,y) \equiv -A_v e^{-ky} + [B_v - B_v ky] e^{-ky} + C_v e^{ky} + [D_v + D_v ky] e^{ky} \qquad (2\text{-}20a)$$

and

$$T^{vv}(k,y) \equiv -A_v e^{-ky} - B_v ky e^{-ky} - C_v e^{ky} - D_v ky e^{ky} \qquad (2\text{-}20b)$$

The velocity transfer functions evaluated at the surface ($y=H$) are

$$T_s^{vu}(k) \equiv T^{vu}(k,y)\Big|_{y=H} = \frac{2kHe^{-kH} + 2kHe^{kH}}{e^{-2kH}+2+4k^2H^2+e^{2kH}} \qquad (2\text{-}21a)$$

for the longitudinal velocity component, and

$$T_s^{vv}(k) \equiv T^{vv}(k,y)\Big|_{y=H} = \frac{[2-2kH]e^{-kH} + [2+2kH]e^{kH}}{e^{-2kH}+2+4k^2H^2+e^{2kH}} \qquad (2\text{-}21b)$$

for the normal component.

Comparison of Equation (2-21a) with Equation (2-15b) shows that $T_s^{vu} = T_s^{uv}$, i.e. the "cross-component" transfer functions are equal at the surface.

Schematics of the flow for harmonic normal basal anomalies of a short and a long non-dimensional wavelength are shown in Figures 2-2c and 2-2d. The major difference is that the amplitude of the surface velocity is greater for the longer wavelength anomaly. The amplitudes at the surface of the longitudinal and normal components also vary relative to each other depending on the wavelength, although not in a significant manner for the schematics shown. These effects are summarized in Figure 2-3.

2.3.3 Fourier transform solution

The Fourier transform method theoretically allows surface solutions to be found for any pattern of basal velocity u_b and v_b. The Fourier transform and the inverse transform are defined as

$$\hat{f}(k) \equiv \int_{-\infty}^{\infty} f(x)e^{-ikx}dx \tag{2-22a}$$

$$f(x) \equiv \frac{1}{2\pi}\int_{-\infty}^{\infty} \hat{f}(k)e^{ikx}dk \tag{2-22b}$$

Using Equation (2-22a), the transform of Equation (2-7) is

$$k^4\hat{\psi} - 2k^2\frac{\partial^2\hat{\psi}}{\partial y^2} + \frac{\partial^4\hat{\psi}}{\partial y^4} = 0 \tag{2-23}$$

A solution for $\hat{\psi}$ is

$$\hat{\psi} = \frac{A(k)}{k}e^{-ky} + B(k)ye^{-ky} + \frac{C(k)}{k}e^{ky} + D(k)ye^{ky} \tag{2-24}$$

By transforming the boundary conditions (Equations (2-8) and (2-9)), the coefficients A, B, C and D are found, and are most simply written in terms of the coefficients in Equations (2-12) and (2-18):

$$A = A_u\hat{u}_b - iA_v\hat{v}_b \tag{2-25a}$$

$$B = B_u\hat{u}_b - iB_v\hat{v}_b \tag{2-25b}$$

$$C = C_u\hat{u}_b - iC_v\hat{v}_b \tag{2-25c}$$

$$D = D_u\hat{u}_b - iD_v\hat{v}_b \tag{2-25d}$$

Here $\hat{u}_b(k)$ is the Fourier transform of the longitudinal component of the basal velocity anomaly, and $\hat{v}_b(k)$ is the transform of the normal component of the basal velocity anomaly. These equations are analogous to those found for a single harmonic component in Sections 2.3.1 and 2.3.2.

The actual basal anomaly components $u_b(x)$ and $v_b(x)$ must be specified (as two of the boundary conditions). From the transformed basal velocity components $\hat{u}_b$ and $\hat{v}_b$ the transformed stream function $\hat{\psi}$ is determined using Equations (2-24) and (2-25). This is used to calculate the transformed velocities anywhere in the glacier:

$$\hat{u}(k,y) = \frac{\partial\hat{\psi}(k,y)}{\partial y} \tag{2-26a}$$

$$\hat{v}(k,y) = -ik\hat{\psi}(k,y) \tag{2-26b}$$

If these are written out in terms of the individual coefficients (Equations (2-25)), then the transformed velocities can easily be rewritten in terms of the transfer functions (Equations (2-14) and (2-20)). Then when evaluated at the surface, the transformed velocity components are:

$$\hat{u}_s = T_s^{uu}\hat{u}_b - iT_s^{uv}\hat{v}_b \tag{2-27a}$$

$$\hat{v}_s = -iT_s^{uv}\hat{u}_b + T_s^{vv}\hat{v}_b \tag{2-27b}$$

These surface transfer functions are given explicitly in Equations (2-15) and (2-21). T_s^{uv} is used instead of T_s^{vu} in Equation (2-27a), since these two transfer functions are identical.

The Fourier transform solutions in the following sections were calculated using a discrete Fourier transform routine. The discrete Fourier transform assumes that the function is periodic. The surface effects of this assumption can be minimized by having a length of at least $2.5H$ on each side of the region of interest in the basal function (since this is about the maximum distance to which surface effects spread out from the basal function).

2.4 Solutions for basal velocity fronts and peaks

2.4.1 Surface response to basal front

An anomaly in the longitudinal component of basal velocity that has the form of a front of amplitude (half-height) U_b can be expressed as:

$$u_b(x) = \begin{cases} U_b & x < 0 \\ -U_b & x > 0 \end{cases} \tag{2-28a}$$

$$v_b(x) = 0 \tag{2-28b}$$

The corresponding surface response can be calculated using Equation (2-27) and a discrete Fourier transform routine.

Surface and basal velocities are compared in Figure 2-4 for such a basal front. The abrupt change in u at the basal front is spread out over about $5H$ at the surface. Also, the trend of u at the surface is not as smooth as would be expected. Instead, there is a flat of

width about $1H$ in the surface velocity over the basal discontinuity. The flat in the longitudinal component of the surface velocity occurs because of reverse contributions when the high wave-number Fourier components of u_b are filtered to the surface through the transfer function. These high wave-number components dominate near the basal front, and their reverse surface contributions break the larger-scale trend established by the lower wave number contributions.

2.4.2 Surface response for ramp at base

An anomaly in the longitudinal component of the basal velocity that has the form of a ramp can be written as

$$u_b(x) = \begin{cases} U_b & x < -r \\ \dfrac{-U_b}{r}x & -r \le x \le r \\ -U_b & x > r \end{cases} \qquad \text{(2-29a)}$$

$$v_b(x) = 0 \qquad \text{(2-29b)}$$

The slope of the ramp is $-U_b/r$, where $2r$ is the horizontal distance taken up by the ramp.

Basal and surface velocities for $r = 0.25H$ are shown in Figure 2-4. This produces a ramp in u_b of width $0.5H$. At the plotting scale, the calculated surface velocity components are almost indistinguishable from those for a sharp basal front.

If the basal velocity ramp width is increased, the flat in u_s becomes less prominent, and the maximum amplitude of v_s decreases (see Figure 2-4). However, the width of the basal ramp does not noticeably affect the width of the zone of the surface velocity anomaly, as long as the basal ramp is less than about $5H$ wide.

2.4.3 Surface solution for Gaussian peak at base

A pulse in basal velocity is plausible for both the normal and longitudinal components. An anomaly in the longitudinal component at the bed which has the spatial form of a Gaussian peak is expressed as

$$u_b(x) = U_b \frac{1}{\sqrt{2\pi}\sigma} e^{-\frac{1}{2}\left[\frac{x}{\sigma}\right]^2} \tag{2-30}$$

where σ is the standard deviation. The surface effects vary depending on the ratio of the standard deviation of the peak to the thickness of the ice (σ/H). Three results are shown: a wide peak (Figure 2-5a), a medium width peak (Figure 2-5b) and a narrow peak (Figure 2-5c). As the peak is made narrower, u_s develops a dip over the center of the basal peak, and v_s becomes more pronounced. These effects are summarized in Figure 2-6. The high wave-number terms of the basal velocity are the source of these variations (as was explained in Section 2.4.1).

If a Gaussian pulse is made narrower and taller while holding the area constant in the limit of zero width, it approaches a delta function. The delta function solution can also be found by differentiation of the solution for a basal front. From this point of view the dip in surface velocity directly above a basal delta function spike corresponds to the surface velocity "flat" above a discontinuous front. The delta function solution is qualitatively the same as Figure 2-5c for the narrow Gaussian pulse.

The solution for a delta function anomaly in u_b provides the formal means for expressing the solution for any arbitrary spatial distribution of u_b in terms of a spatial decomposition based on a Green's function. (A similar solution is possible for a delta function anomaly in v_b.) Let the surface velocity at position x caused by a unit basal delta function at x' be expressed as $G_s(x,x') = G_s(x-x')$. Figure 2-5c approximates $G_s(x-x')$ with $x' = 0$. By superposition the surface solution for an arbitrary spatial distribution of $u_b(x,t)$ is

$$u_s(x,t) = \int_{-\infty}^{\infty} u_b(x',t) G_s(x-x') dx' \tag{2-31}$$

Since the analytical representation of $G_s(x-x')$ derived above is very complex, this approach does not seem generally useful now. If a simple analytic approximation were fitted to $G_s(x-x')$, then Equation (2-31) could be very useful, but this is not pursued here.

One property of $G_s(x-x')$ can be used to arrive simply at a useful result. This property is

$$\int_{-\infty}^{\infty} G_s(x-x') dx = 1 \tag{2-32}$$

This can be seen in several ways. For example, the solution for a basal delta function is the x derivative of the solution for a unit basal front at x'. Thus $G_s(x-x')$ for fixed x' gives the x derivative of surface velocity for a unit basal front at x', and when it is integrated over adequate distance from one side of the front to the other, it gives the total velocity jump at the surface and at the bed (Figure 2-4). From Equations (2-31) and (2-32)

$$\int_{-\infty}^{\infty} u_s(x,t)dx = \int_{-\infty}^{\infty}\int_{-\infty}^{\infty} u_b(x',t)G_s(x-x')dx'dx = \int_{-\infty}^{\infty} u_b(x',t)dx' \tag{2-33}$$

which shows that the integrated velocity is the same at the surface and bed for any basal velocity anomaly.

A Gaussian pulse in the normal component of basal velocity (perhaps caused by cavitation) can be represented as

$$v_b(x) = V_b \frac{1}{\sqrt{2\pi}\sigma} e^{\frac{-1}{2}\left[\frac{x}{\sigma}\right]^2} \tag{2-34}$$

Surface effects are shown for a wide peak (Figure 2-7a), a medium-width peak (Figure 2-7b), and a narrow peak (Figure 2-7c). The cross-component effects are the same as for the pulses in the longitudinal component of the basal velocity (since $T_s^{vu} = T_s^{uv}$). The normal component at the surface is reduced in amplitude and increased in longitudinal extent relative to the basal pulse, as the basal pulse is made narrower.

2.5 Discussion

2.5.1 Longitudinal scales of transfer

Based on the considerations of the foregoing sections, four longitudinal scales of differing behavior may be identified. Basal velocity anomalies of a long scale appear at the surface unattenuated, and deformation-induced cross-component motions are negligible. At an intermediate scale, the longitudinal and normal velocity components have nearly the same spatial pattern at the surface as at the bed, but with reduced amplitudes. At this scale, cross-component motions caused by ice deformation become noticeable. At a short scale, while the normal component at the surface is reduced in amplitude from that of the normal component at the base, the longitudinal component at the surface is significantly

altered in both amplitude and spatial pattern in comparison to at the bed. At this short scale cross-component motions are substantial. Finally there is a very short scale, at which there is essentially no response at the surface.

These systematics are best seen with reference to harmonic basal anomalies (Figure 2-3) and basal peaks (Figures 2-5, 2-6, and 2-7). The boundary between the four scales can be roughly identified as $10H$ (long to intermediate), $5H$ (intermediate to short), and $1H$ (short to very short). Since the change in behavior with longitudinal scale is gradational, these boundaries cannot be positioned precisely. Furthermore, the positions of the boundaries depend to some extent on the spatial pattern as can be seen from comparison of Figures 2-3 and 2-6. Any real pattern of basal velocity variation will likely have features at a variety of scales. A basal velocity front is one example for which there are effects at all of these scales (Figure 2-4).

2.5.2 Deformation-induced normal motions and estimates from surface strain rate

For intermediate and short scales, Figures 2-3 and 2-6 show that a basal velocity anomaly such that $u_b \neq 0$ and $v_b = 0$ causes both u_s and v_s to be non-zero, and v_s may be larger than u_s. From ice continuity (Equation (2-1)), and assuming $v_b = 0$, v_s is

$$v(x,H,t) = \int_0^H \frac{\partial v}{\partial y}(x,y,t)\, dy = \int_H^0 \frac{\partial u}{\partial x}(x,y,t) dy = -H\left[\frac{\partial u}{\partial x}\right]_H \tag{2-35}$$

(where $[\partial u/\partial x]_H$ refers to the average over the depth). If the anomalous longitudinal motion were independent of depth, then the average of $\partial u/\partial x$ could be found from $\partial u_s/\partial x$ measured at the surface. The problem is that in general u is attenuated toward the surface and $\partial u_s/\partial x$ will underestimate the magnitude of the average of $\partial u/\partial x$ over depth. Furthermore, at the short scale the signs can be opposite. These problems are illustrated in Figure 2-8.

2.5.3 Problems of interpretation of measured surface velocity and uplift variations

On Variegated Glacier, propagating "mini-surges" occurred quasi-periodically during the early melt seasons for several years prior to the main surge. These were characterized by a zone of accelerated motion which propagated down-glacier at about 0.1 to 0.6 $km\ hr^{-1}$. At a given location, speed rose rapidly over a few hours to a sharp peak, dropped rapidly and then more slowly over about 1 d^{-1} as the zone approached and passed (Kamb and

Engelhardt, 1987). Often there was a secondary velocity peak following the first principal one by several hours (Raymond and Malone, 1986).

The longitudinal velocity anomalies u_s averaged over 1 d were of the order of 0.5 to 1 $m\,d^{-1}$ and resulted in extra anomalous surface displacements of 0.5 to 1 m over the 1 d interval of a mini-surge. The peaks in u_s were of the order of 3 to 4 times larger than the day-averaged values. In addition there was a noticeable anomaly v_s, which produced a relatively rapid uplift rate of up to about 1 $m\,d^{-1}$ over 1 to several hr, followed by a slower more extended subsidence. The maximum uplift was about 0.1 m and occurred after the peak in u_s by 1 or 2 hr.

These time intervals and propagation speeds correspond to spatial scales of from about 1 km to more than 10 km, which can be compared to the ice thickness of about 0.4 km. Therefore, the surface velocity patterns of these mini-surges have features from the small to the large scale.

Figure 2-9 shows an example constructed from a superposition of ramps and a Gaussian spike for u_b, and a Gaussian pulse for v_b. Surface velocities are shown both with and without the effects from v_b. This example shows some of the qualitative features of mini-surge velocity variation. However, it is not as accurate as the direct calculation of the basal velocity anomaly from mini-surge surface velocity data (this direct calculation is the inverse problem; see Chapters 6 and 7). Nevertheless, some semi-quantitative conclusions are possible. The broad scale asymmetric peak in mini-surge velocity is of long enough scale that it probably resembles in shape and amplitude the actual variation at a similar scale at the bed, except for some broadening of the velocity rise at the surface in comparison to the bed. The narrow principal peak and the subsequent secondary peak at the surface may be indicative of a single sharp peak at the bed of substantially higher velocity and represent intermediate to short scale features. The principal peak at the surface has a half-width of about one depth, which suggests the peak at the bed could be narrower and have a velocity anomaly more than 3 times that at the surface. Furthermore, the positions of the peak at the bed may be shifted relative to the principal peak at the surface, probably toward the secondary peak. Finally, at this scale the deformation-induced normal velocity component at the surface will have an amplitude similar to the anomalous longitudinal component at the surface. Uplift determined by integration of v_s when $v_b = 0$ shows a rapid rise and a subsequent slower fall. The maximum uplift is ≈ 0.13 times the anomalous

longitudinal displacement caused by the passage of the velocity wave; this is seen by comparison of the areas under the positive parts of the v_s and the u_s curves. This shows that a large fraction or possibly all of the surface uplift during mini-surges could be explained by internal deformation, without uplift at the bed.

Iken and others (1983) have observed variations in surface velocity and elevation on Unteraargletscher at an approximately 4 *d* time resolution. At this time resolution they find a correlated velocity increase and uplift of the surface during an approximately seven-month summer season. Several short-term velocity and uplift events lasting more than four days are superimposed on it. These short-term velocity variations have some resemblances to the mini-surges of Variegated Glacier; however, little is known about their spatial variation or propagation. Assuming the Unteraargletscher events propagate at speeds similar to or faster than the Variegated Glacier mini-surges, which is consistent with the description of available information, the durations of the features would indicate that these events have large spatial scale and are free from the complexities of the short and intermediate scales in the foregoing analyses. Iken and others (1983) have carefully considered in detail various possible contributions to the surface uplift and conclude that its major features must arise from the opening of cavities at the bed, but based on limited measurements of surface strain-rate changes they caution that ice straining in the direction normal to the bed could be a major contribution. We emphasize here the possible major errors when using surface values of longitudinal strain rate to estimate averages over depth unless the spatial scale of velocity variation is well known. Furthermore, unlike a velocity measurement, which represents an average over time, an uplift measurement is a sample at a single time and may not be representative of the time interval over which the velocity has been averaged.

2.5.4 Limitations of the model

A major limitation of the model is the assumption of a linear viscous fluid rheology to represent ice behavior. Some of the features of the strain-rate pattern during Variegated Glacier mini-surges show dramatic changes on time scales short compared to the time needed to establish steady-state creep in experiments. This indicates possible visco-elastic effects. This problem has been examined using a visco-elastic Maxwell rheology, which gives some differences in behavior in comparison to the purely viscous rheology, but these differences are not major (see Chapter 4). More importantly, ice creep is better

approximated by a power law with power of 3 to 4 than by a linear fluid (power of 1). This could lead to some substantial differences in behavior. In the limit in which the velocity anomalies induced at the bed and their strain-rate contributions are much smaller than the steady-state velocity and strain rate, the velocity anomaly field will occur in a distribution of effective viscosity controlled by the straining associated with the steady-state motions. In this circumstance, a perturbation solution could be attempted (Hutter, 1983). The effective viscosity will then tend to be low near the bed and high near the surface (Whillans and Johnsen, 1983). This will tend to promote recirculation of the velocity anomaly near the bed and probably increase the length for transition between the short and intermediate scales described above. If the velocity anomalies and corresponding strain rates are large in comparison to the steady-state motion, then the anomalies themselves will significantly alter both the normal and longitudinal structure of the effective viscosity field with possible major effects on the transfer of amplitude and pattern between the surface and bed. In both of these limits the behavior of the ice will be equally or more complex than for the linear fluid rheology, and no easing of the difficulties of interpreting surface variations in terms of those at the bed will occur.

If basal velocity variations do not extend over widths significantly larger than the depth, their transmission to the surface may be different from that calculated here. Three-dimensional flow calculations would be needed to account for this.

Finally, these calculations do not address the question of what sliding velocity variations are physically possible. Some of the mathematically illustrative solutions derived represent idealizations that likely could not exist in reality (for example, a sharp basal velocity front). Nevertheless, in the absence of a compelling sliding law, an appropriate step is to attempt measurement of basal velocity from the surface. From that point of view this chapter begins to show what is possible and what is not.

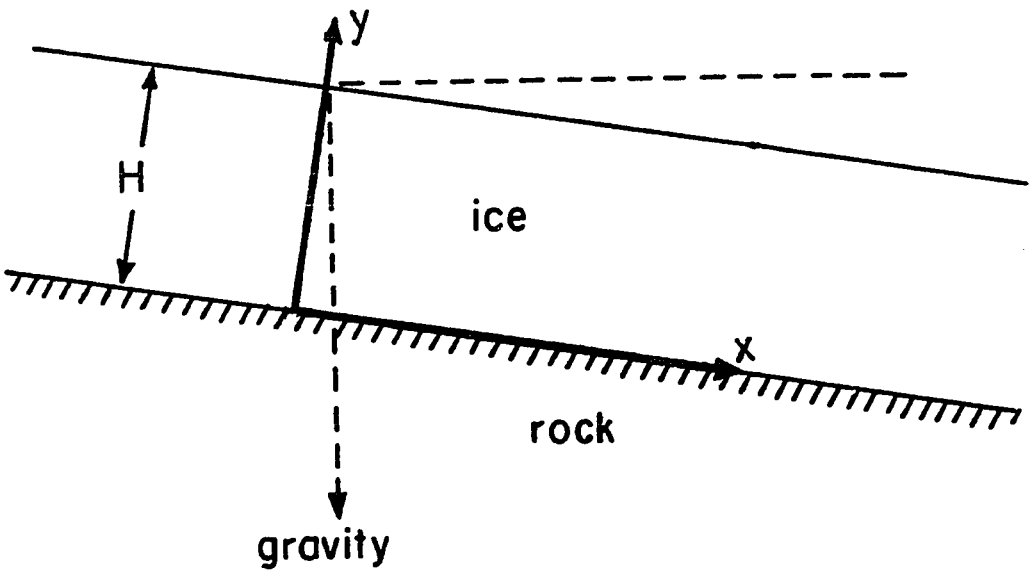

Figure 2-1. Definition of geometrical quantities and coordinate system.

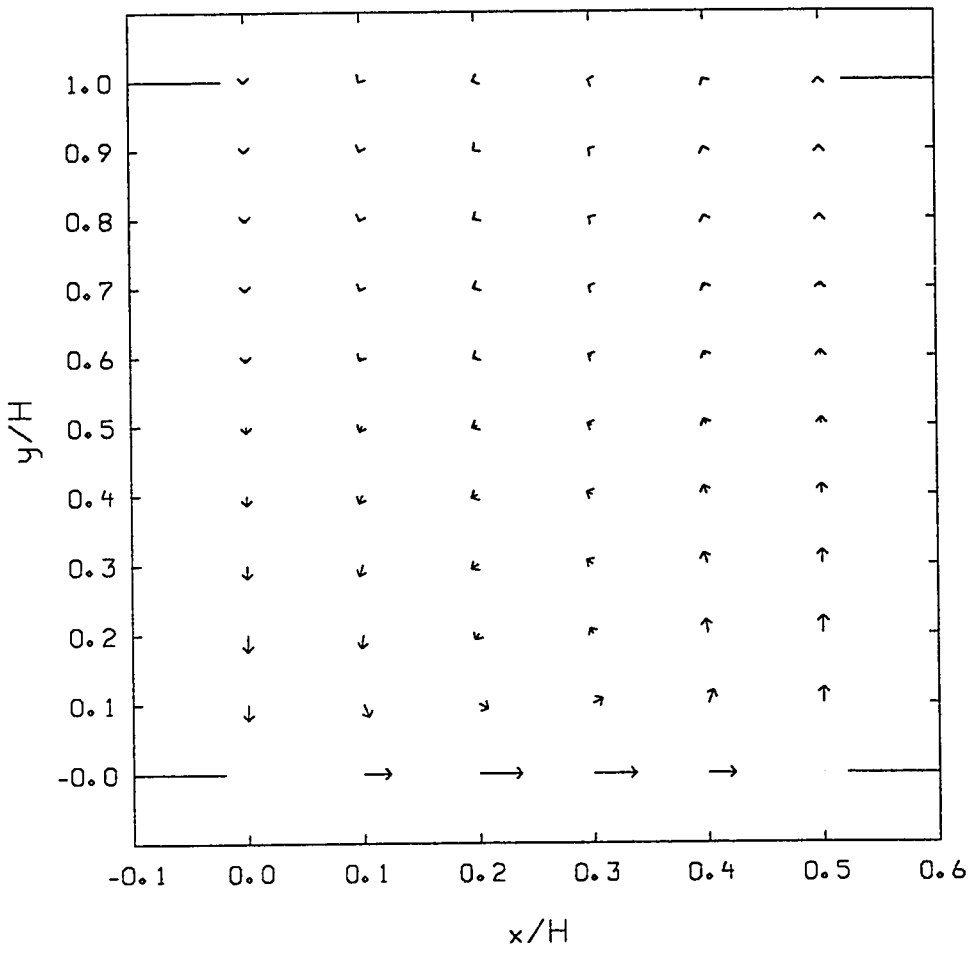

Figure 2-2a. Pattern of motion represented schematically for harmonic longitudinal basal velocity anomaly, short wavelength $\lambda/H = 1$, for linear viscous rheology (shown for a half wavelength). Note differences in proportions between horizontal and vertical scales compared to Figure 2-2a.

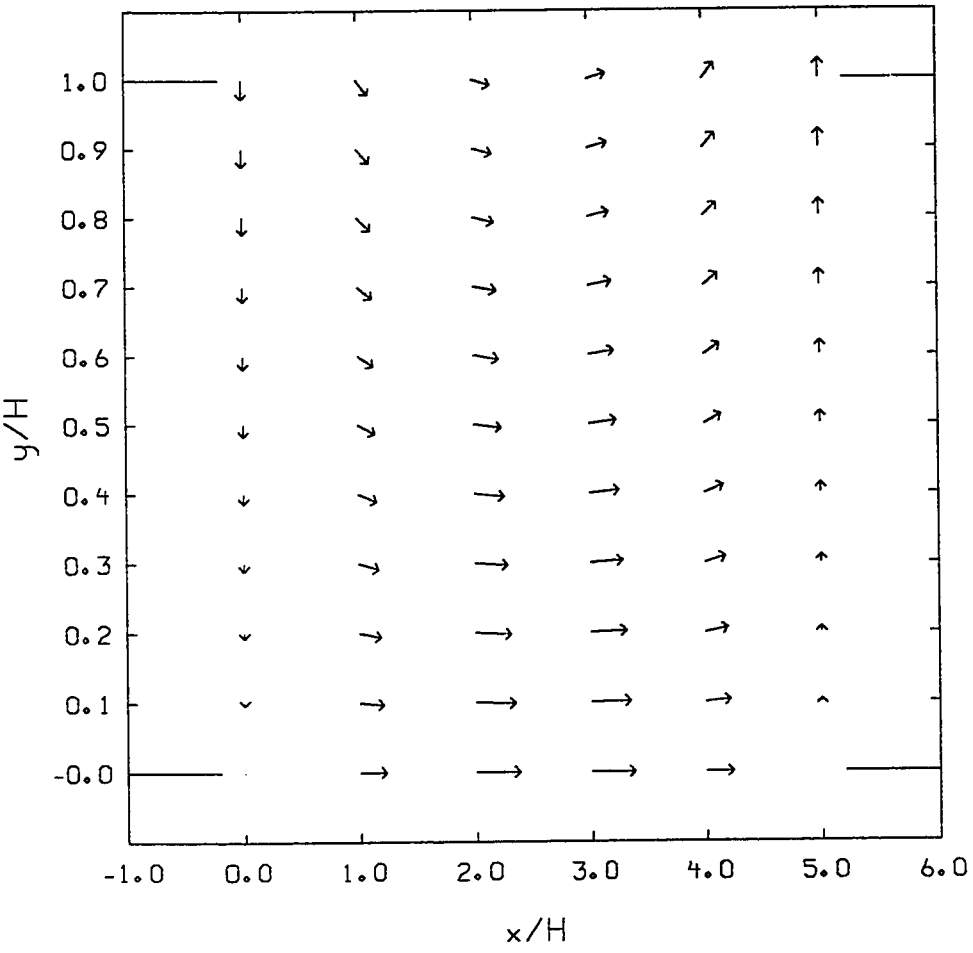

Figure 2-2b. Pattern of motion represented schematically for harmonic longitudinal basal velocity anomaly, long wavelength $\lambda/H = 10$, for linear viscous rheology (shown for a half wavelength).

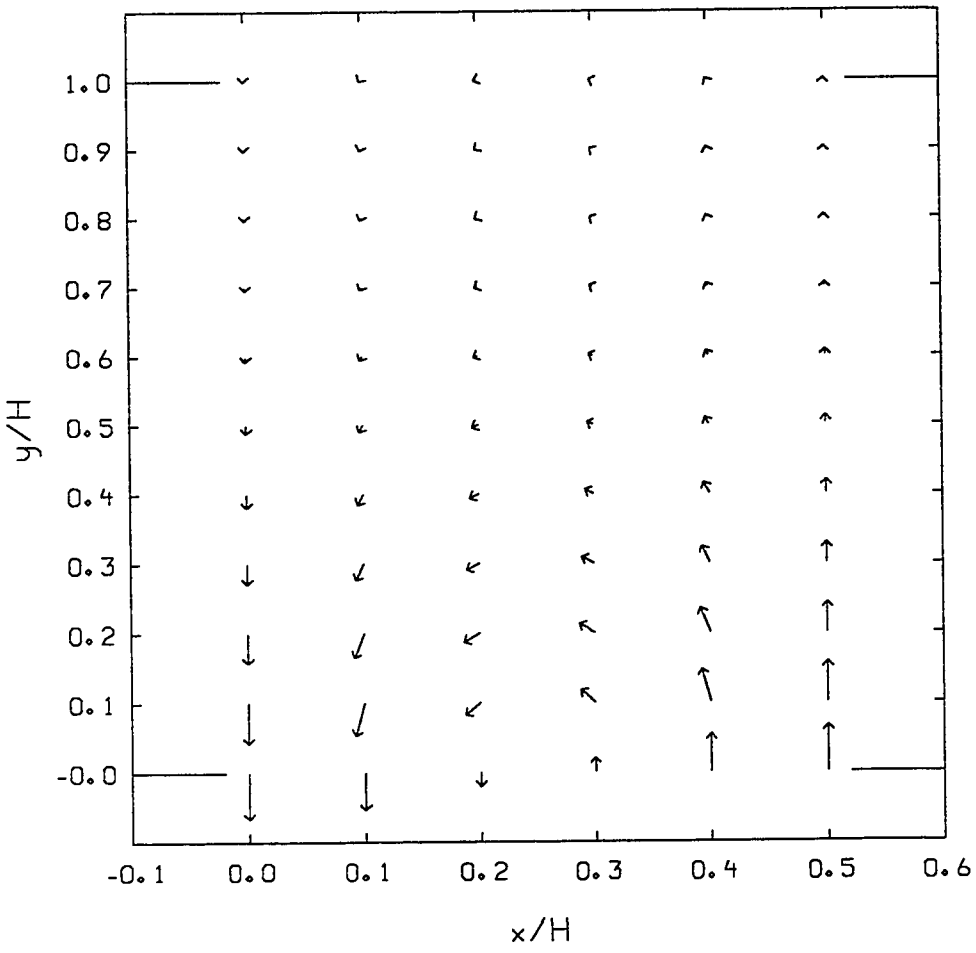

Figure 2-2c. Pattern of motion represented schematically for harmonic normal basal velocity anomaly, short wavelength $\lambda/H = 1$, for linear viscous rheology (shown for a half wavelength). Note differences in proportions between horizontal and vertical scales compared to Figure 2-2d.

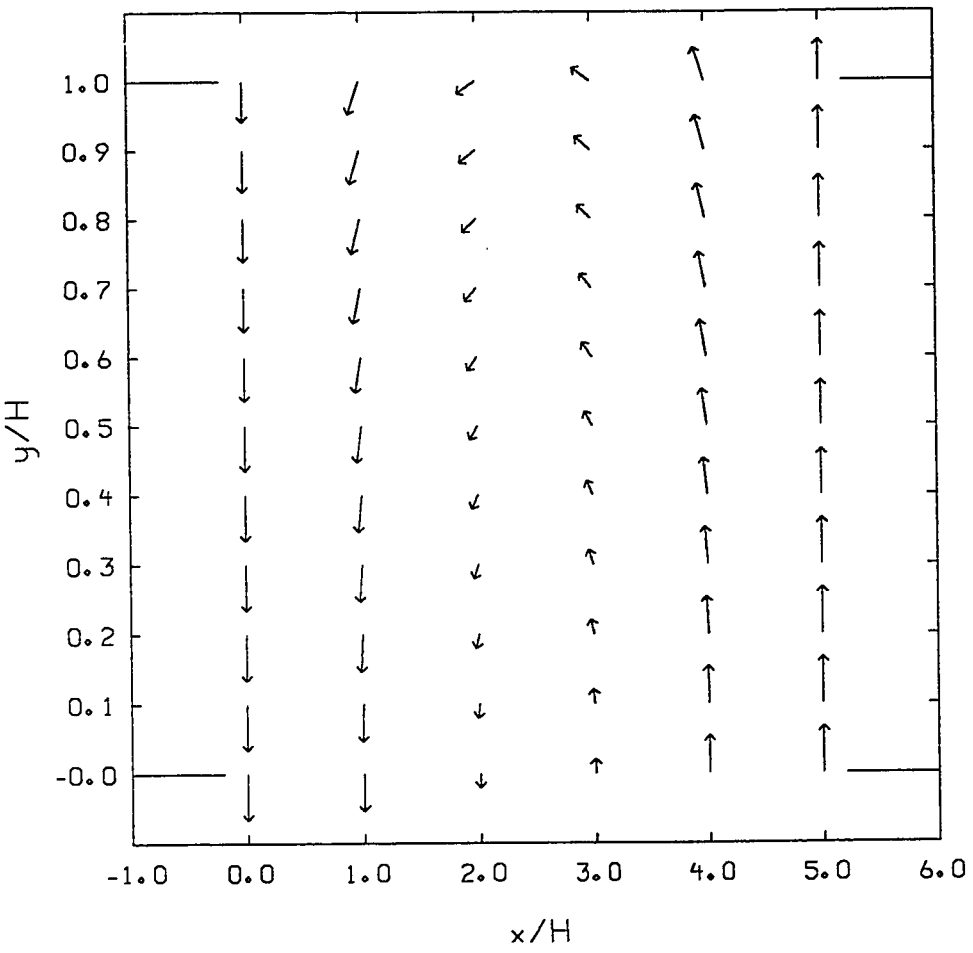

Figure 2-2d. Pattern of motion represented schematically for harmonic normal basal velocity anomaly, long wavelength $\lambda/H = 10$, for linear viscous rheology (shown for a half wavelength).

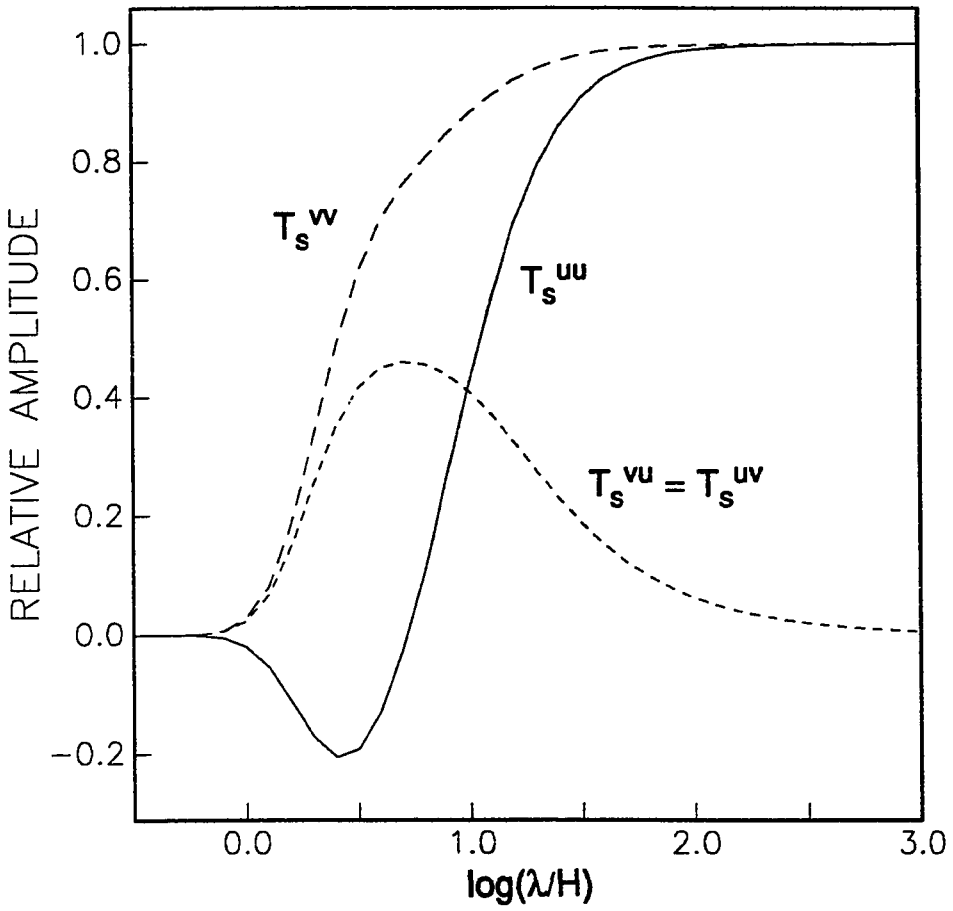

Figure 2-3. Forward transfer functions for linear viscous rheology. These are the relative amplitudes of surface velocity caused by harmonic variation in the basal velocity (of unit amplitude). Solid line = T_s^{uu}, long dashed line = T_s^{vv}, short dashed line = T_s^{uv} = T_s^{vu}.

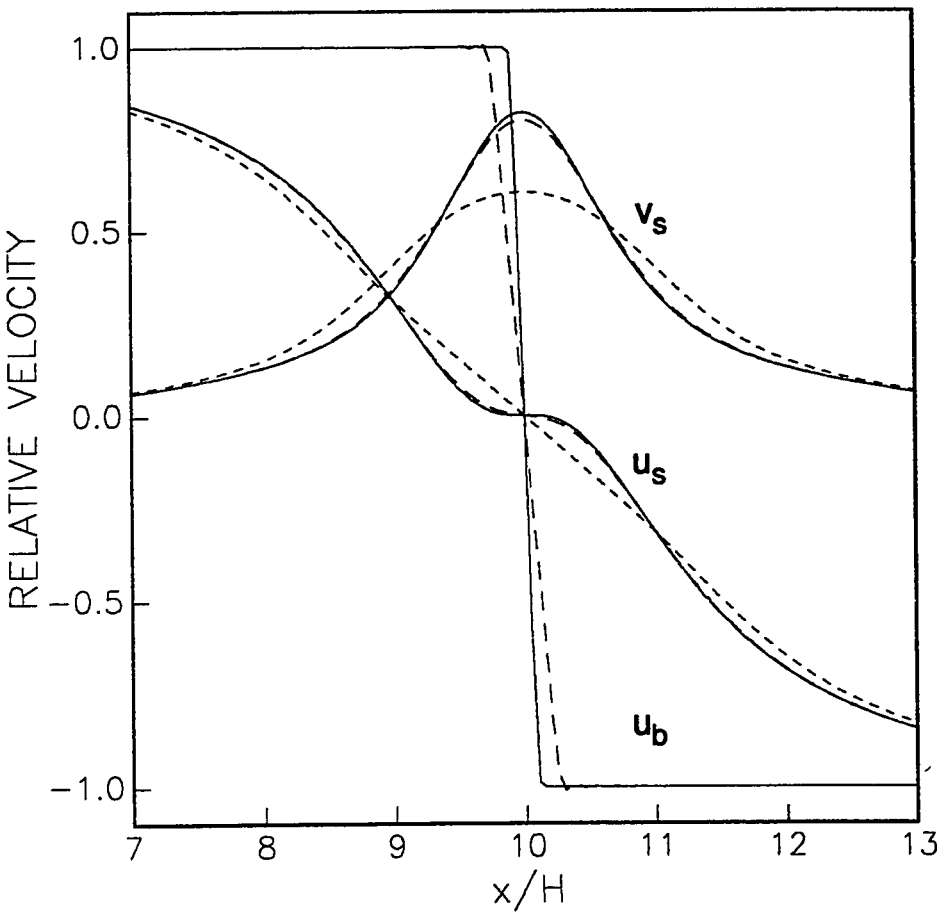

Figure 2-4. Basal and surface velocities for a basal velocity anomaly u_b, for linear viscous rheology: a sharp front shown by solid lines, a steep ramp wave (r = 0.025), shown by long dashed lines where distinguishable, and a less steep ramp wave (r = 0.1), shown by short dashed lines.

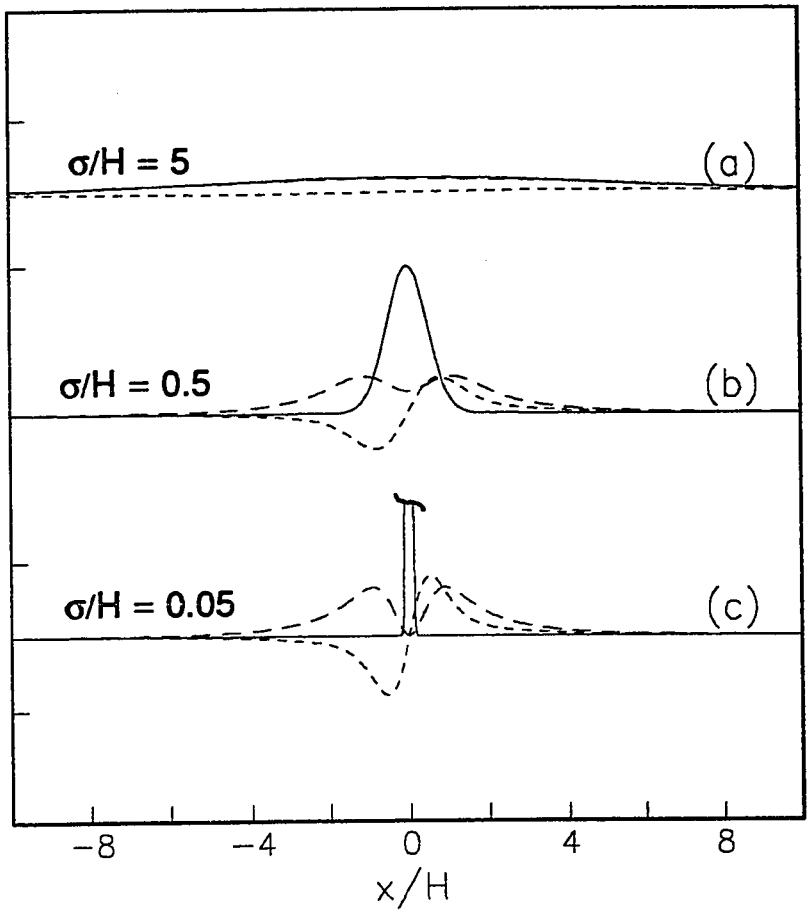

Figure 2-5. Relative basal and surface velocities for Gaussian pulse basal velocity anomalies u_b, for linear viscous rheology. (a) $\sigma/H = 5$, (b) $\sigma/H = 0.5$, and (c) $\sigma/H = 0.05$. Solid line = u_b, long dashed line = u_s (where distinguishable from u_b), short dashed line = v_s. Basal velocity anomalies integrated over distance are equal in all three cases.

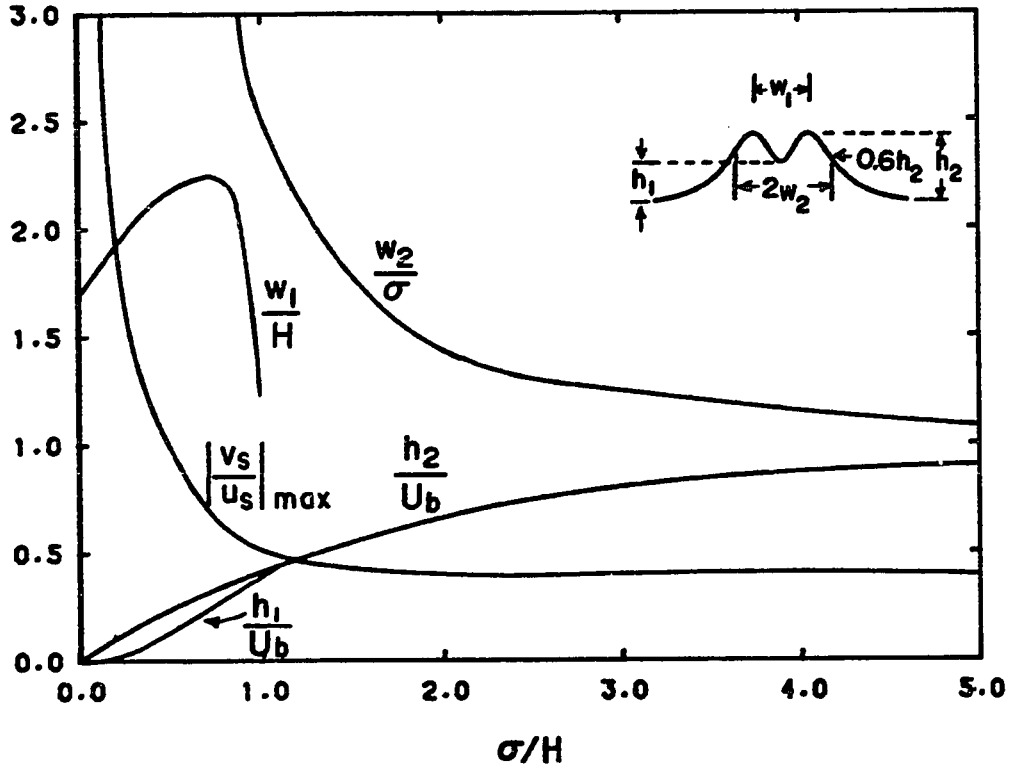

Figure 2-6. Characteristics of u_z in response to Gaussian pulse basal velocity anomalies u_b, and their dependence on the longitudinal scale of the pulse, for linear viscous rheology.

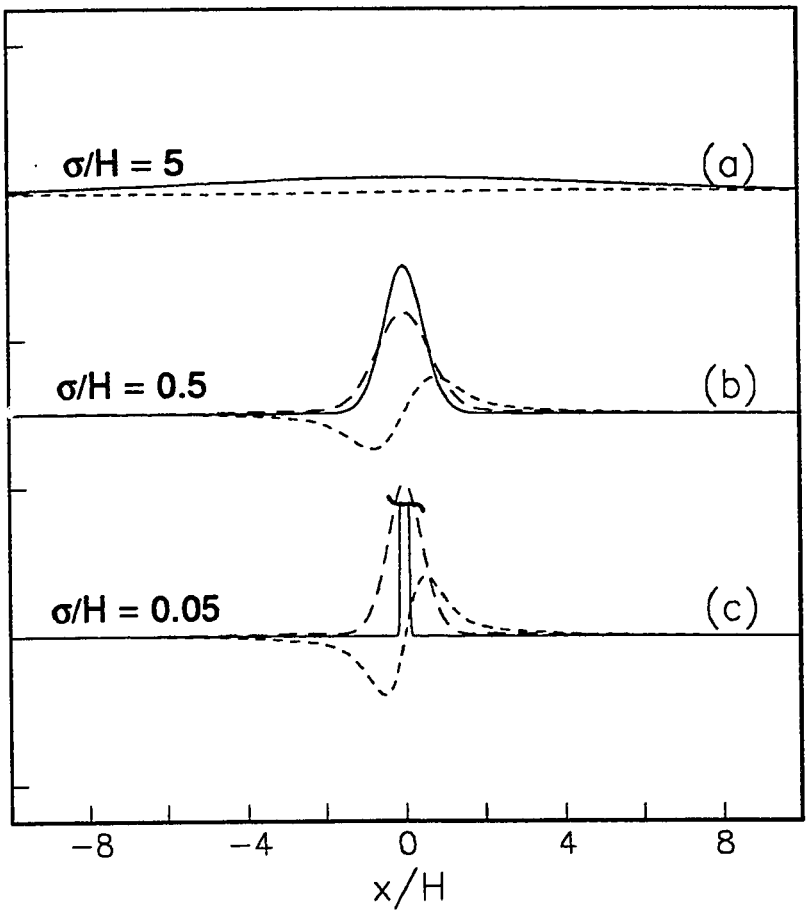

Figure 2-7. Relative basal and surface velocities for Gaussian pulse basal velocity anomalies v_b, for linear viscous rheology. (a) $\sigma/H = 5$, (b) $\sigma/H = 0.5$, and (c) $\sigma/H = 0.05$. Solid line = v_b, long dashed line = v_s (where distinguishable from v_b), short dashed line = u_s. Basal velocity anomalies integrated over distance are equal in all three cases.

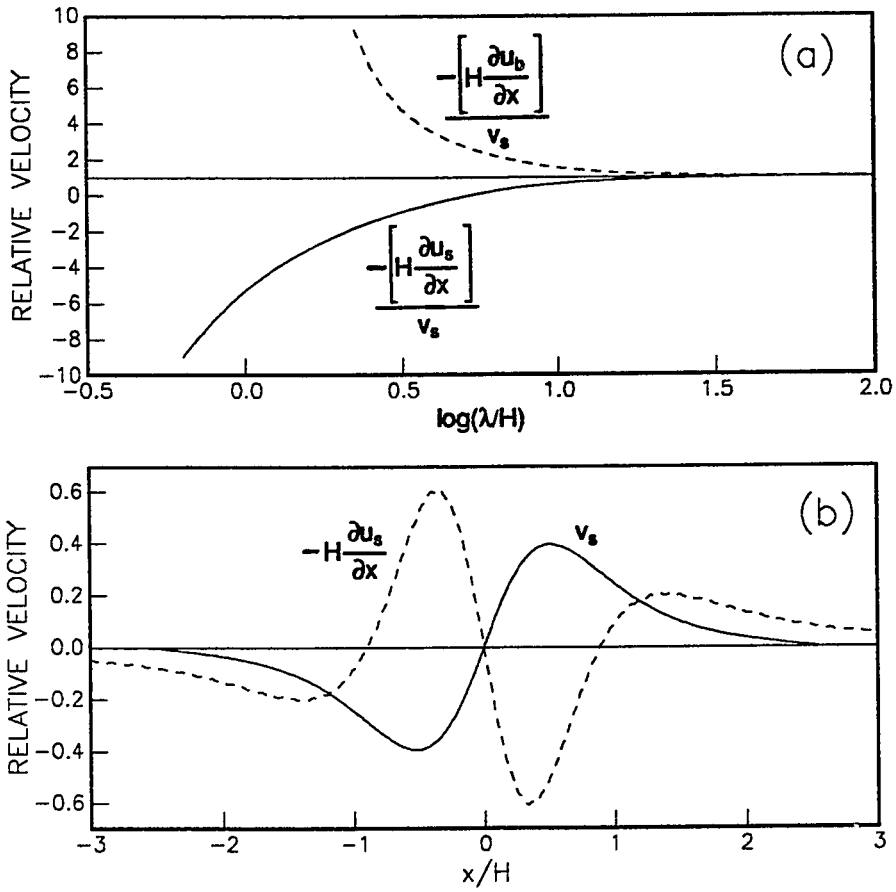

Figure 2-8. (a) Normal component of surface velocity for linear viscous rheology, calculated as $-H\partial u/\partial x$ scaled by v_s from mathematical model, for harmonic basal velocity anomaly u_b. Solid line = $[-H\partial u_s/\partial x]/v_s$, dashed line = $[-H\partial u_b/\partial x]/v_s$. (b) Normal component of surface velocity for linear viscous rheology, calculated as $-H\partial u_s/\partial x$ (dashed line) compared with v_s from mathematical model (solid line), for a Gaussian pulse basal velocity anomaly u_b with $\sigma/H = 0.05$, of maximum amplitude $u_b(0) = 10$.

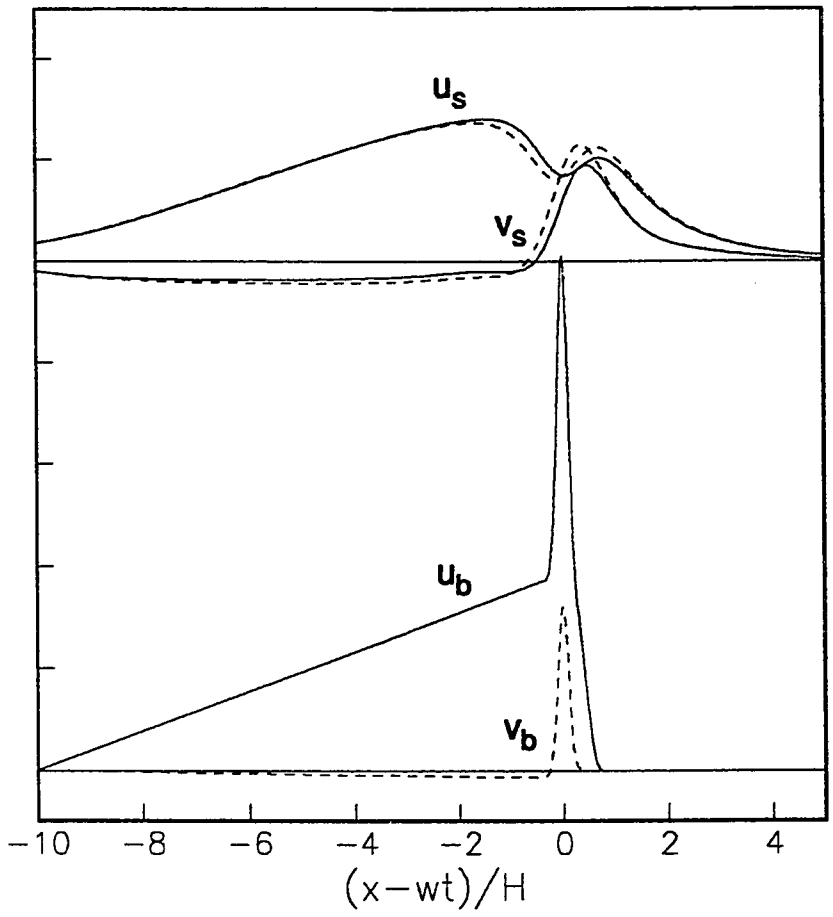

Figure 2-9. Hypothetical mini-surge for linear viscous rheology. Surface velocity components u_s and v_s (upper two solid curves) for a hypothetical basal velocity anomaly with component u_b (lower solid curve). Addition of basal component v_b (lower dashed curve) results in total surface components u_s and v_s (shown by upper two dashed curves). Anomalies propagating with speed w.

CHAPTER 3

LINEAR VISCOUS FORWARD SOLUTIONS USING A BASAL SLIDING LAW

3.1 Field equations, basal sliding law, and other boundary conditions

3.1.1 Field equations

The applicable field equations for the planar geometry and the linear viscous rheology are again reduced to (as in Section 2.2.5):

$$\frac{\partial^4\psi}{\partial x^4} + 2\frac{\partial^4\psi}{\partial x^2\partial y^2} + \frac{\partial^4\psi}{\partial y^4} = 0 \tag{3-1}$$

where ψ is the stream function. This equation can again be Fourier transformed to

$$k^4\hat{\psi} - 2k^2\frac{\partial^2\hat{\psi}}{\partial y^2} + \frac{\partial^4\hat{\psi}}{\partial y^4} = 0 \tag{3-2}$$

3.1.2 Form of sliding law

Basal sliding laws for glacier ice have been developed by many authors; among these are Weertman (1957), Kamb (1970), Lliboutry (1975), Bindschadler (1983), and Iken and Bindschadler (1986). The general form of the sliding law which we wish to use is

$$u_b^{total} = W[\tau_b^{total}]^m \tag{3-3}$$

Here u_b^{total} is the basal sliding velocity (the longitudinal component of the basal velocity). The effective basal shear stress deviator is τ_b^{total} (which is equal to the effective basal shear stress). This effective basal shear stress is actually due to normal stresses exerted on the ice by the upstream sides of bumps in the bed, etc. The exponent m depends on the rheology of the ice; for a linear viscous material m=1. The sliding law parameter is W.

This sliding law says that as the sliding speed increases, the effective basal shear stress increases, for a given value of the parameter W. In the earlier versions of the sliding law (e.g., Weertman, Kamb, and Lliboutry) the value of this parameter only depends on the inverse of the actual roughness of the glacier bed. Thus the only ways to increase the

sliding speed in these early sliding laws are to increase the basal shear stress (by increasing the ice thickness or the surface slope), or to decrease the actual bed roughness.

In later versions of the sliding law (e.g., Bindschadler, and Iken and Bindschadler), and in flow laws which incorporate varying rheological parameters near the bed (Boulton and Hindmarsh, 1986; Clarke, 1986), the value of a sliding law parameter W can also depend on such things as the basal water pressure, the geometry of the basal hydraulic system, and the amount of deformable till overlying a solid bed. These can be included in an effective roughness of the glacier bed. Thus the sliding speed of the glacier will change if this effective roughness changes. In fact, the main motivation for studying a prescribed basal sliding law is to examine velocity variations caused by changes in this effective roughness (with these roughness changes being mathematically described as changes in the sliding law parameter).

It is important to note that in reality, a true basal sliding law for glaciers is probably not linear in velocity and shear stress, even if the assumption of linear rheology were valid. However, it is quite likely that the true sliding law is at least monotonic (although the possibility of a sliding law with multiple maxima has been proposed by several authors). We will use the given form of the sliding law for lack of a proven better form, and because the given form also results in reasonably tractable mathematics.

To determine the basal shear stress, we first note that for a glacier lying on a sloped bed (sloped at angle γ), the downslope component of the weight of the ice can either be balanced by the basal shear stress or a longitudinal stress gradient. If we look at a section of ice in our planar slab geometry which is sufficiently long to include any anomalous boundary conditions, or has periodic boundary conditions, the longitudinal stresses at the ends of the section will be equal. The average shear stress at the base of the section can then easily be calculated to be $\rho g H \sin\gamma$ (Paterson, 1981). This does not preclude variations in the basal shear stress within the section.

3.1.3 Separation into steady-state and anomalous equations

To separate the basal sliding law into steady-state and anomalous equations, we note that the rheology is linear, so velocity solutions can be superposed, and shear stress solutions can also be superposed. For the planar slab geometry, a longitudinally varying basal

sliding velocity (that is, varying in the x direction) can then be composed of steady-state and anomalous parts:

$$u_b^{total}(x) = u_b^{steady} + u_b^{anomaly}(x) \tag{3-4a}$$

(Thus the steady-state basal sliding does not change in the x direction.) Similarly, a longitudinally varying basal shear stress can be written:

$$\tau_b^{total}(x) = \tau_b^{steady} + \tau_b^{anomaly}(x) \tag{3-4b}$$

(From here on the superscripts *total*, *steady*, and *anomaly* will be shortened to t, s, and a.) Substituting Equations (3-4) into Equation (3-3), our sliding law then is

$$u_b^s + u_b^a(x) = W\left[\tau_b^s + \tau_b^a(x)\right] \tag{3-5}$$

In order to examine basal velocity anomalies and the associated surface velocity anomalies, it is necessary to prescribe a varying sliding law parameter $W(x)$. (If this parameter does not vary, it turns out that the velocity anomalies and stress anomalies are all equal to zero; see Section 3.3.2.) We therefore divide the sliding law parameter into a steady-state part W^s and an anomalous part W^a. We also note that the steady-state basal shear stress τ_b^s can in fact be set equal to the average basal shear stress $\rho g H \sin\gamma$ (with the anomalous basal shear stress $\tau_b^a(x)$ accounting for any variations from this average). The sliding law is then written:

$$u_b^s + u_b^a(x) = \left[W^s + W^a(x)\right]\left[\rho g H \sin\gamma + \tau_b^a(x)\right] \tag{3-6}$$

The next step is to divide this sliding law into a steady-state equation and an anomalous equation, where the steady-state equation has only terms which do not involve functions of x, and the anomalous equation has all the terms which do involve functions of x. This gives, for the steady-state equation

$$u_b^s = W^s \rho g H \sin\gamma \tag{3-7a}$$

The anomalous equation is

$$u_b^a(x) = W^s \tau_b^a(x) + W^a(x) \rho g H \sin\gamma + W^a(x) \tau_b^a(x) \tag{3-7b}$$

We will not be directly solving Equation (3-7a), which is the equation for the longitudinal component ot the steady-state basal velocity. (However, this equation will be used to

non-dimensionalize the anomalous velocity at the bed and surface.)

Equation (3-7b) is the equation for the longitudinal component of the anomalous basal velocity. The right side of this equation has three terms: $W^s\tau_b{}^a(x)$, which is the contribution to the anomalous basal sliding from the combination of the steady-state sliding parameter and the anomalous basal shear stress; $W^a(x)\rho gH\sin\gamma$, which is the contribution from the combinations of the anomalous sliding parameter and the steady-state basal shear stress; and $W^a(x)\tau_b{}^a(x)$, which is the contribution from the combination of the anomalous sliding parameter and the anomalous basal shear stress. This last term is non-linear.

Equation (3-7b) is one of the boundary conditions which we will use to solve for the anomalous basal shear stress, and the velocity anomalies at the base and surface of the glacier. It is important to realize that this boundary condition depends on both the anomalous and steady-state parts of the sliding law parameter, and that it also depends on both the anomalous and steady-state parts of the basal shear stress. Thus the anomaly solution will be coupled to the steady-state solution. This coupling complicates the solution process; however, if this coupling did not exist, the anomalous solution would be everywhere equal to zero (as will be shown in Section 3.3.2).

3.1.4 Magnitude of terms in anomalous sliding velocity equation

We will now examine Equation (3-7b) to check the relative importance of the three terms on the right side. This process is facilitated by non-dimensionalizing the equation, which is done by dividing by the steady-state basal sliding velocity $u_b{}^s = W^s\rho gH\sin\gamma$ (from Equation (3-7a)). This gives:

$$\frac{u_b{}^a(x)}{u_b{}^s} = \frac{\tau_b{}^a(x)}{\rho gH\sin\gamma} + \frac{W^a(x)}{W^s} + \left[\frac{W^a(x)}{W^s}\right]\left[\frac{\tau_b{}^a(x)}{\rho gH\sin\gamma}\right] \qquad (3\text{-}8a)$$

In this equation, the left side is the ratio of the anomalous basal velocity to the steady-state basal velocity. The first term on the right side is the ratio of the anomalous basal shear stress to the steady-state basal shear stress; the second term on the right side is the ratio of the anomalous sliding parameter to the steady-state sliding parameter. The third term on the right side is the product of the first and second terms on the right side; this is the non-linear term.

For any physically reasonable basal sliding law, $|W^a(x)| \leq W^s$ (or else the glacier could conceivably be sliding uphill!). Therefore we will require that $|W^a(x)| \leq W^s$, which means that the second term on the right side of Equation (3-8a) is less than or equal to one. However, meeting this requirement does not constrain the magnitude of the other terms in the equation, since these other terms all depend on the ratio of $\tau_b{}^a(x)$ to $\rho g H \sin\gamma$. Although we could intuitively expect the magnitude of this ratio to be somewhat dependent on the magnitude of $W^a(x)$, (i.e., the anomalous basal shear stress $\tau_b{}^a(x)$ will tend to vary proportionally to $W^a(x)$), we might also expect that the "roughness" of the spatial form of $W^a(x)$ would be important (i.e., if $W^a(x)$ had rapid changes or sharp jumps, we might expect that the anomalous basal shear stress would have high values in the vicinity of these rapid changes). However, we will show that if the non-linear last term on the right side of Equation (3-8a) is second-order (of the order of one-third or less), the ratio of $\tau_b{}^a(x)$ to $\rho g H \sin\gamma$ is less than or equal to the ratio of $W^a(x)$ to W^s (and thus less than or equal to one). If the non-linear last term on the right side of Equation (3-8a) is not second-order, the ratio of $\tau_b{}^a$ to $\rho g H \sin\gamma$ is not constrained.

3.1.5 Conditions for non-linear term being second-order

Equation (3-8a) will be much more easily solved when the non-linear last term on the right side is second-order, since this non-linear term can then be neglected. To meet this qualification, both ratios in this non-linear term must be significantly less than one (say of the order of one-third or less). For the ratio $W^a(x)/W^s$, this requirement is just a slightly more stringent case of the physically reasonable requirement that $|W^a(x)| \leq W^s$. Mathematically, this more stringent requirement is easy to satisfy, by simply increasing W^s to whatever value is required.

For the ratio $\tau_b{}^a(x)/\rho g H \sin\gamma$, it turns out that the requirement that this ratio be of the order of one-third or less is automatically satisfied by the requirement that the ratio $W^a(x)/W^s$ be of the order of one-third or less. (This occurs because the maximum possible value of the magnitude of $\tau_b{}^a/\rho g H \sin\gamma$ is the maximum magnitude of $W^a(x)/W^s$, when the magnitude of $W^a(x)/W^s$ is of the order of one-third or less; this will be shown in Section 3.3.3.) Therefore the only condition for the non-linear term in Equation (3-8a) to be second-order is that $|W^a(x)|/W^s$ be of the order of one-third or less.

It is important to note that this mathematical requirement may or may not correspond well with physical reality. The requirement that $|W^a(x)|/W^s$ be relatively small is easily met on some glaciers, such as the lower Columbia Glacier in Alaska (Krimmel and Vaughan, 1986). However, in other situations, such as the mini-surges of Variegated Glacier, the magnitude of $W^a(x)$ may be close to the value of W^s. (Also, the spatial form of $W^a(x)$ may have rapid changes in situations such as these mini-surges.) Thus the mathematical requirement for the non-linear last term in Equation (3-8a) being second-order may be quite restrictive in physical reality.

3.1.6 Other boundary conditions

To solve Equation (3-1) or (3-2), four boundary conditions are necessary, two of which will be at the surface and two at the bed. The first of the basal boundary conditions is the relation between the longitudinal component of the basal velocity anomaly and the basal shear stress anomaly, which has previously been given in dimensionless form in Equation (3-8a). The other basal boundary condition which we will use is a requirement that the normal component of the basal velocity anomaly be equal to zero:

$$v_b = 0 \tag{3-8b}$$

It is possible that a better form of this boundary condition would be to allow v_b to vary as some function of the parameters in the sliding law. However, this relation would be quite speculative, and would also greatly complicate our solution process. In this chapter we will use the much more simple requirement of Equation (3-8b).

The two surface boundary conditions are the requirement that the stress anomaly at the surface be equal to zero. These boundary conditions are written:

$$\sigma_{yy}|_{y=H} = 0 \tag{3-9a}$$

and

$$\sigma_{xy}|_{y=H} = 0 \tag{3-9b}$$

Here $\sigma_{yy}|_{y=H}$ is the normal component of the stress anomaly at the glacier surface, and $\sigma_{xy}|_{y=H}$ is the shear component of the stress anomaly at the glacier surface.

We will not allow these boundary conditions to vary with time, thus constraining our solutions to "snapshots" fixed in space at a certain time. The reasoning behind this restriction is explained in Section 2.2.6.

3.2 Mathematical solution neglecting non-linear term

3.2.1 General solution form

The solution will most easily be determined by using the Fourier transform. We first write the boundary conditions (Equations (3-8) and (3-9)) in terms of the stream function ψ, with Equation (3-8a) changed back to the dimensioned form and the last term on the right side neglected. The equations are then Fourier transformed. This gives, from Equations (3-8):

$$\frac{\partial \hat{\psi}}{\partial y}\Big|_{y=0} = W^s \eta \left[\frac{\partial^2 \hat{\psi}}{\partial y^2} + k^2 \hat{\psi}\right]_{y=0} + \hat{W}^a \rho g H \sin\gamma \tag{3-10a}$$

$$-ik\hat{\psi}\Big|_{y=0} = 0 \tag{3-10b}$$

From Equations (3-9):

$$\left[3k^2 \frac{\partial \hat{\psi}}{\partial y} - \frac{\partial^3 \hat{\psi}}{\partial y^3}\right]_{y=H} = 0 \tag{3-11a}$$

$$\left[\frac{\partial^2 \hat{\psi}}{\partial y^2} + k^2 \hat{\psi}\right]_{y=H} = 0 \tag{3-11b}$$

Here the caret (e.g. $\hat{\psi}$) signifies the Fourier transform, and these Fourier transformed variables are now functions of the wave number k. Note that in Equation (3-10a), the Fourier transform does not affect the constant sliding parameter W^s (which multiplies other terms which are affected by the transform); but the Fourier transform does affect the variable sliding parameter $W^a(x)$, transforming it to $\hat{W}^a$, (which multiplies a constant term). Also note that Equation (3-11a) is actually the transform of the x derivative of Equation (3-9a), as is explained in Section 2.2.5.

We can now consider the solution to Equation (3-2), for the Fourier transformed stream function $\hat{\psi}$. The form of this solution is

$$\hat{\psi} = \left[\frac{A(k)}{k}e^{-ky} + B(k)ye^{-ky} + \frac{C(k)}{k}e^{ky} + D(k)ye^{ky}\right]\hat{W}^a\rho gH\sin\gamma \qquad (3\text{-}12)$$

Using the boundary conditions (Equations (3-10) and (3-11)), we can solve for the coefficients A, B, C, and D. These solutions are

$$A = -C = \frac{-2k^2H^2}{(1-2W^s\eta k)e^{-2kH} + 2 + 8W^s\eta kkH + 4k^2H^2 + (1+2W^s\eta k)e^{2kH}} \qquad (3\text{-}13a)$$

$$B = \frac{1 + 2kH + e^{2kH}}{(1-2W^s\eta k)e^{-2kH} + 2 + 8W^s\eta kkH + 4k^2H^2 + (1+2W^s\eta k)e^{2kH}} \qquad (3\text{-}13b)$$

$$D = \frac{e^{-2kH} + 1 - 2kH}{(1-2W^s\eta k)e^{-2kH} + 2 + 8W^s\eta kkH + 4k^2H^2 + (1+2W^s\eta k)e^{2kH}} \qquad (3\text{-}13c)$$

These coefficients give us the solution for $\hat{\psi}$. This transformed stream function allows us to determine the velocity anomaly or stress anomaly anywhere in the glacier.

3.2.2 Basal shear stress solution

The equation to solve for the Fourier transform of the basal shear stress anomaly (which from now on in this chapter will be written without the superscript a as just $\hat{\tau}_b$) is

$$\hat{\tau}_b = \eta\left[\frac{\partial^2\hat{\psi}}{\partial y^2} + k^2\hat{\psi}\right]_{y=0} \qquad (3\text{-}14a)$$

$$= \left[A - B + C + D\right]2\hat{W}^a\eta k\rho gH\sin\gamma$$

Using the solutions for the coefficients A, B, C, and D, we get the solution for $\hat{\tau}_b$:

$$\hat{\tau}_b = \left[\frac{e^{-2kH} - 4kH - e^{2kH}}{(1-2W^s\eta k)e^{-2kH} + 2 + 8W^s\eta kkH + 4k^2H^2 + (1+2W^s\eta k)e^{2kH}}\right]2\hat{W}^a\eta k\rho gH\sin\gamma \qquad (3\text{-}14b)$$

3.2.3 Basal velocity solution

The equation to solve for the Fourier transform of the longitudinal component of the basal velocity anomaly (which from now on in this chapter will be written without the superscript a as just $\hat{u}_b$) is just the boundary condition of Equation (3-10a). In terms of the coefficients A, B, C, and D of $\hat{\psi}$, this is

$$\hat{u}_b = \left[-A + B + C + D\right]\hat{W}^a \rho g H \sin\gamma \tag{3-15a}$$

Using the solutions for the coefficients of $\hat{\psi}$, we get the solution for $\hat{u}_b$:

$$\hat{u}_b = \left[\frac{e^{-2kH} + 2 + 4k^2H^2 + e^{2kH}}{(1-2W^s\eta k)e^{-2kH} + 2 + 8W^s\eta kkH + 4k^2H^2 + (1+2W^s\eta k)e^{2kH}}\right]\hat{W}^a \rho g H \sin\gamma \tag{3-15b}$$

It is worth noting that the basal velocity is a function of the dynamic viscosity η, as contrasted to the case in Chapter 2 where the basal velocity was prescribed and did not depend on the viscosity. This occurs because in this chapter the boundary condition in Equation (3-8a) relates the basal velocity to the basal shear stress, and a velocity solution based on this boundary condition must depend on the viscosity. Chapter 2 does not use a similar boundary condition.

The Fourier transform of the normal component of the basal velocity anomaly is zero (which corresponds with this component being set equal to zero in the boundary condition Equation (3-8b)).

3.2.4 Surface velocity solution

The equation for the Fourier transform of the longitudinal component of the surface velocity anomaly $\hat{u}_s$ is

$$\hat{u}_s = \frac{\partial\hat{\psi}}{\partial y}\Big|_{y=H} \tag{3-16a}$$

$$= \left[-Ae^{-kH} + B[1-kH]e^{-kH} + Ce^{kH} + D[1+kH]e^{kH}\right]\hat{W}^a \rho g H \sin\gamma$$

Using the solutions for the coefficients of $\hat{\psi}$, we get the solution for $\hat{u}_s$

$$\hat{u}_s = \left[\frac{[2+2kH]e^{-kH} + [2-2kH]e^{kH}}{[1-2W^s\eta k]e^{-2kH} + 2 + 8W^s\eta kkH + 4k^2H^2 + [1+2W^s\eta k]e^{2kH}}\right]\hat{W}^a \rho g H \sin\gamma \tag{3-16b}$$

The equation for the Fourier transform of the normal component of the surface velocity anomaly $\hat{v}_s$ is

$$\hat{v}_s = -ik\hat{\psi}\Big|_{y=H} \tag{3-17a}$$

$$= -i\left[Ae^{-kH} + BkHe^{-kH} + Ce^{kH} + DkHe^{kH}\right]\hat{W}^a \rho g H \sin\gamma$$

Using the solutions for the coefficients of $\hat{\psi}$, we get the solution for $\hat{v}_s$

$$\hat{v}_s = -\left[\frac{2kHe^{-kH} + 2kHe^{kH}}{[1-2W^s\eta k]e^{-2kH} + 2 + 8W^s\eta kkH + 4k^2H^2 + [1+2W^s\eta k]e^{2kH}}\right]\hat{W}^a \rho g H \sin\gamma \quad (3\text{-}17b)$$

These surface velocity components are functions of the dynamic viscosity η, as contrasted with the case in Chapter 2 where the surface velocity anomaly did not depend on η. This difference occurs because for the basal sliding law the basal velocity anomaly u_b depends on η, and this basal velocity anomaly in turn drives the surface velocity anomaly.

3.3 Properties of mathematical solution neglecting non-linear term

3.3.1 Non-dimensionalization and adjustable parameters

The Fourier transformed solutions for the basal shear stress anomaly (Equation (3-14b)), the longitudinal component of the basal velocity anomaly (Equation (3-15b)), and the surface velocity anomaly (Equations (3-16b) and (3-17b)) all depend on various parameters. These parameters are the dynamic viscosity η, the steady-state sliding parameter W^s, the Fourier transformed anomalous sliding parameter $\hat{W}^a$, the wave number k, the ice thickness H, and steady-state basal shear stress $\rho g H \sin\gamma$.

These solutions can be non-dimensionalized by dividing the transformed basal shear stress anomaly by the steady-state basal shear stress $\rho g H \sin\gamma$, and dividing the transformed velocity anomalies by the steady-state basal sliding velocity $W^s \rho g H \sin\gamma$. The equation for the dimensionless Fourier transformed basal shear stress anomaly $\hat{\tau}_b^*$ then is

$$\hat{\tau}_b^* = \left[\frac{e^{-2kH} - 4kH - e^{2kH}}{[1-2W^s\eta k]e^{-2kH} + 2 + 8W^s\eta kkH + 4k^2H^2 + [1+2W^s\eta k]e^{2kH}}\right]2\hat{W}^a\eta k \quad (3\text{-}18a)$$

The equation for the dimensionless Fourier transformed longitudinal component of the basal velocity anomaly $\hat{u}_b^*$ is

$$\hat{u}_b^* = \left[\frac{e^{-2kH} + 2 + 4k^2H^2 + e^{2kH}}{[1-2W^s\eta k]e^{-2kH} + 2 + 8W^s\eta kkH + 4k^2H^2 + [1+2W^s\eta k]e^{2kH}}\right]\left[\frac{\hat{W}^a}{W^s}\right] \quad (3\text{-}18b)$$

The equations for the dimensionless Fourier transformed longitudinal and normal

components of the surface velocity anomaly $\hat{u}_s^*$ and $\hat{v}_s^*$ are

$$\hat{u}_s^* = \left[\frac{[2+2kH]e^{-kH} + [2-2kH]e^{kH}}{[1-2W^s\eta k]e^{-2kH} + 2 + 8W^s\eta kkH + 4k^2H^2 + [1+2W^s\eta k]e^{2kH}}\right]\left[\frac{\hat{W}^a}{W^s}\right] \qquad (3\text{-}18c)$$

and

$$\hat{v}_s^* = \left[\frac{2kHe^{-kH} + 2kHe^{kH}}{[1-2W^s\eta k]e^{-2kH} + 2 + 8W^s\eta kkH + 4k^2H^2 + [1+2W^s\eta k]e^{2kH}}\right]\left[i\frac{\hat{W}^a}{W^s}\right] \qquad (3\text{-}18d)$$

It is possible to combine the parameters so that the solutions in the dimensionless Equations (3-18) only depend on three dimensionless combinations of parameters. These combinations are: (1) the dimensionless viscosity $W^s\eta/H$, (2) the dimensionless Fourier transformed sliding parameter $\hat{W}^a/W^s$, and (3) the dimensionless wave number kH. Note that $\hat{W}^a\eta k = [W^s\eta/H][\hat{W}^a/W^s][kH]$ and $W^s\eta k = [W^s\eta/H][kH]$.

To calculate the Fourier transformed dimensionless basal shear stress anomaly and dimensionless velocity anomalies, we first specify the anomalous sliding law parameter as $W^a(x)/W^s$. We also specify the dimensionless viscosity $W^s\eta/H$. Given the ice thickness H, a fast Fourier transform routine will calculate the solutions for Equations (3-18), as functions of the dimensionless wave number kH. These solutions can then be inverse transformed to the space domain.

3.3.2 Effect of zero or constant terms in anomalous sliding velocity equation

We now look at the effect on the anomaly solutions of setting various terms in the sliding law boundary condition equal to zero or a constant. It will be easier to use dimensioned equations to see these effects. The dimensioned form of the sliding law boundary condition is Equation (3-7b); this equation Fourier transforms to

$$\hat{u}_b = W^s\hat{\tau}_b + \hat{W}^a\rho gH\sin\gamma + \hat{W}^a\hat{\tau}_b \qquad (3\text{-}19)$$

The dimensioned form of the Fourier transformed anomalous basal shear stress equation is Equation (3-14b); and the dimensioned forms of the Fourier transformed anomalous velocity component equations are Equations (3-15b), (3-16b), and (3-17b).

We first look at the coupling of the steady-state basal shear stress $\rho gH\sin\gamma$ to the anomaly solutions. This coupling can be seen by setting $\rho gH\sin\gamma$ equal to zero (e.g., no bed slope). We immediately see that the effect on these solutions of setting $\rho gH\sin\gamma$ equal to

zero is that all of the anomaly solutions are also equal to zero. *This illustrates the fact that the steady-state basal shear stress is necessary to drive the anomalous basal shear stress solution and the anomalous velocity solution.*

We next look at the case where the varying part of the sliding law parameter $W^a(x)$ is set equal to zero. In the wave number domain $W^a(x) = 0$ is transformed to $\hat{W}^a = 0$ for all wave numbers. The solutions in this case for the anomalous basal shear stress and anomalous velocity components are again equal to zero, as is to be expected.

We last look at the case where $W^a(x)$ equals a constant. The Fourier transform of this constant will only have power at k=0, so we look at the transformed anomalous solutions with k=0 and $\hat{W}^a$ equal to some constant. Examining Equation (3-14b) for the transformed anomalous basal shear stress, we see that it involves a multiplication by k; so the anomalous basal shear stress solution for k=0 is simply equal to zero. Solving for the transformed longitudinal components of the basal and surface velocity anomalies (Equations (3-15b) and (3-16b)) for k=0, we see that they are both equal to $\hat{W}^a \rho g H \sin\gamma$. (where $\hat{W}^a$ is equal to the constant). The transformed normal component of the velocity anomaly (Equation (3-17b) involves a multiplication by k, so it is also equal to zero when k=0. These solutions all show that setting $W^a(x)$ equal to a constant is analagous to changing the steady-state sliding parameter W^s by the same constant (for the steady-state solution see for example Paterson, 1981). This is not surprising and can be viewed as a check of the solution process.

3.3.3 Limits of solution at low and high wave numbers

The limits of the anomaly solutions at low and high wave numbers can be used to show several important properties of the solutions. The limits of the anomaly solutions as the wave number k goes to zero are derived in the previous section. This shows that a very long wavelength anomaly in the sliding law parameter becomes equivalent to adding the anomalous parameter $W^a(x)$ to the steady-state sliding law parameter W^s.

The limit of the anomalous basal shear stress solution as k goes to infinity is also useful to determine. Knowing from the previous section that the limit of τ_b is zero as k goes to zero, we can show that the limit at the other end of the wave number spectrum (high wave numbers) will be the maximum value of the Fourier transformed basal shear stress

anomaly (for a given value of $\hat{W}^a$ regardless of the wave number). This maximum value is crucial to whether or not the non-linear term on the right side of the dimensionless sliding law equation (Equation (3-8a)) is second-order and can be neglected, since this term is a function of $\tau_b(x)$. Taking the limit of the transformed anomalous basal shear stress in Equation (3-14b) as k goes to infinity, we see that this limit is

$$\lim_{k\to\infty} \hat{\tau}_b = -\frac{\hat{W}^a}{W^s}\rho g H \sin\gamma \tag{3-20a}$$

(It can be shown that for intermediate wave numbers the value of $\hat{\tau}_b$ is always less than this limit.) Thus we can show that in the space domain

$$\lim_{k\to\infty} \frac{\tau_b(x)}{\rho g H \sin\gamma} = -\frac{W^a(x)}{W^s} \tag{3-20b}$$

for the case where the non-linear last term on the right side of Equation (3-8a) was neglected. This means that if we neglect this term and make the preliminary requirement that the ratio $|W^a(x)|/W^s$ be of the order of one-third or less, the ratio $\tau_b(x)/\rho g H \sin\gamma$ will also be of the order of one-third or less, and the non-linear last term on the right side of Equation (3-8a) will be less than or equal to the square of the ratio $|W^a(x)|/W^s$. This non-linear term will then in fact be second-order, and we will have a self-consistent problem. *Therefore the only requirement for this non-linear term being second-order is that the magnitude of $W^a(x)$ be of the order of one-third or less the value of W^s.*

At high wave numbers, the limit of the solution for the longitudinal component of the basal velocity anomaly goes to zero (see Equation (3-15b)). This is interesting since we have seen that the anomalous shear stress will have power at high wave numbers if the anomalous sliding parameter has power. The explanation for this lack of a basal velocity anomaly at high wave numbers is that the longitudinal stresses become high enough such that the high wave number components of the basal velocity anomaly are damped out.

At high wave numbers, the limits of the solutions for the anomalous surface velocity components both go to zero. This is easily seen since these limits will be proportional to e^{kH}/e^{2kH}. This situation is entirely equivalent to the transfer functions in Chapter 2 going to zero at short wavelengths; at these high wave numbers a signal at the bed results in a vanishingly small signal at the surface.

3.3.4 Relation to prescribed basal velocity solution

The relation of the solutions which result from a basal sliding law with a varying parameter, to the solutions which result from a prescribed basal velocity (Chapter 2), is quite interesting. For this comparison, we will only use the longitudinal component of the Fourier transformed prescribed basal velocity anomaly $\hat{u}_b^{(pbv)}$; the normal component of the prescribed basal velocity anomaly will be set equal to zero, to correspond with this component being set equal to zero for the sliding law solutions. (Here the superscript *(pbv)* refers to a quantity from the prescribed basal velocity solutions of Chapter 2.)

We first look at the relation of the basal shear stress solutions. Since the solution for the basal shear stress anomaly was not explicitly derived in Chapter 2 (given a prescribed basal velocity), this solution in the wave number domain $\hat{\tau}_b^{(pbv)}$ is given here (for the case with $\hat{v}_b = 0$):

$$\hat{\tau}_b^{(pbv)} = \left[\frac{e^{-2kH} - 4kH - e^{2kH}}{e^{-2kH} + 2 + 4k^2H^2 + e^{2kH}}\right] 2\eta k \hat{u}_b^{(pbv)} \tag{3-21a}$$

This can also be written in terms of a "transfer function" T^{τ}, which relates the basal shear stress to the prescribed basal velocity anomaly:

$$\hat{\tau}_b^{(pbv)} = T^{\tau} \hat{u}_b^{(pbv)} \tag{3-21b}$$

Here T^{τ} is defined

$$T^{\tau} \equiv \left[\frac{e^{-2kH} - 4kH - e^{2kH}}{e^{-2kH} + 2 + 4k^2H^2 + e^{2kH}}\right] 2\eta k \tag{3-21c}$$

This transfer function is plotted in Figure 3-1. This transfer function T^{τ} relates stress to velocity at the same depth in the glacier (in this case at the bed), unlike the transfer functions of Chapter 2 which relate velocity to velocity at different depths in the glacier (e.g., from the base to the surface). Note that T^{τ} is always negative, e.g., for a prescribed basal velocity (longitudinal component) of one sign, the associated basal shear stress will always have the opposite sign.

Comparison of Equation (3-21a) with Equation (3-14b) shows that

$$\frac{\hat{\tau}_b^{(sl)}}{\hat{\tau}_b^{(pbv)}} = \left[\frac{e^{-2kH} + 2 + 4k^2H^2 + e^{2kH}}{(1-2W^s\eta k)e^{-2kH} + 2 + 8W^s\eta kkH + 4k^2H^2 + (1+2W^s\eta k)e^{2kH}}\right]\left[\frac{\hat{W}^a \rho g H \sin\gamma}{\hat{u}_b^{(pbv)}}\right] \tag{3-22a}$$

Here the superscript *(sl)* refers to a quantity from the sliding law solutions of this chapter.

Inspection of this equation shows that we can define a sliding law transfer function T^{slide} such that

$$\frac{\hat{\tau}_b^{(sl)}}{\hat{\tau}_b^{(pbv)}} = T^{slide}\frac{\hat{W}^a \rho g H \sin\gamma}{\hat{u}_b^{(pbv)}} \tag{3-22b}$$

with T^{slide} defined

$$T^{slide} \equiv \frac{e^{-2kH} + 2 + 4k^2H^2 + e^{2kH}}{(1-2W^s\eta k)e^{-2kH} + 2 + 8W^s\eta kkH + 4k^2H^2 + (1+2W^s\eta k)e^{2kH}} \tag{3-22c}$$

Comparison of the equations for the basal and surface components of the velocity anomaly in Chapter 2 with these components for the basal sliding law shows that they all are related by the same transfer function T^{slide} multiplying the same ratio $\hat{W}^a \rho g H \sin\gamma / \hat{u}_b^{(pbv)}$. That is:

$$\frac{\hat{u}_b^{(sl)}}{\hat{u}_b^{(pbv)}} = T^{slide}\frac{\hat{W}^a \rho g H \sin\gamma}{\hat{u}_b^{(pbv)}} \tag{3-23a}$$

$$\frac{\hat{u}_s^{(sl)}}{\hat{u}_s^{(pbv)}} = T^{slide}\frac{\hat{W}^a \rho g H \sin\gamma}{\hat{u}_b^{(pbv)}} \tag{3-23b}$$

$$\frac{\hat{v}_s^{(sl)}}{\hat{v}_s^{(pbv)}} = T^{slide}\frac{\hat{W}^a \rho g H \sin\gamma}{\hat{u}_b^{(pbv)}} \tag{3-23c}$$

The term $\hat{W}^a \rho g H \sin\gamma / \hat{u}_b^{(pbv)}$ is simply the dimensionless ratio between the prescribed anomalies for the two cases. Therefore the relation between the solutions for the prescribed basal velocity anomaly, and the solutions for the basal sliding law, can be viewed as being completely described by the sliding law transfer function T^{slide}. This transfer function is plotted in Figure 3-2, for different values of the dimensionless viscosity $W^s\eta/H$, as a function of the logarithm (to the base 10) of the dimensionless wavelength λ/H. The plots in this figure show that T^{slide} increases with increasing wavelength, and increases with decreasing viscosity. These characteristics are due to the fact that longitudinal interactions will always tend to damp out the effect on the stress and velocity fields of an anomaly in the sliding law parameter, except in the limits as the wavelength goes to infinity or the viscosity goes to zero. At these limits the value of T^{slide} is one (as can be seen from Equation (3-22c)); for shorter wavelengths or greater viscosity the value of T^{slide} is less than one. The coupling between the anomalous sliding parameter, and the basal

shear stress and basal velocity, is only perfect at these limits of infinite wavelength or zero viscosity.

The question of why the solutions for the prescribed basal velocity should be related to the solutions for the sliding law by one simple ratio is worth examining. This relation by the simple ratio T^{slide} means that the physics are the same for both problems, in that the stress and velocity are coupled in the same manner. It is fairly obvious that the surface and basal velocity should be related by the same transfer functions in both solutions; what is not quite so obvious is that in both solutions the basal shear stress anomaly and the longitudinal component of the basal velocity anomaly should be related by the same function T^{τ}. However, in one problem we specify the basal velocity and the physics give the basal shear stress; in the other problem we specify a relation between the basal velocity and the basal shear stress, and the physics give us the particular basal velocity and basal shear stress which satisfies both the physics and the specified relation. E.g., in the first problem we have one equation in one unknown, and in the second problem we have two equations in two unknowns. In both cases we end up with solutions for both the basal velocity anomaly and the basal shear stress anomaly, which are related in both cases by the transfer function T^{τ}, and are also related in the second case by the sliding law.

By using the prescribed basal velocity transfer functions T^{τ}, T_s^{uu}, and T_s^{uv}, and the sliding law transfer function T^{slide}, we can further simplify our notation in the sliding law solutions. We first multiply Equation (3-22b) and Equations (23) by their respective denominators from the left sides. We next substitute the appropriate prescribed basal velocity transfer function multiplying $\hat{u}_b^{(pbv)}$, for the basal shear stress and velocity components $\hat{\tau}_b^{(pbv)}$, $\hat{u}_b^{(pbv)}$, $\hat{u}_s^{(pbv)}$, and $\hat{v}_s^{(pbv)}$. This gives the following forms of the Fourier transformed solutions for the sliding law (which we will no longer write with the superscript reference to the sliding law):

$$\hat{\tau}_b = T^{\tau}T^{slide}\hat{W}^a \rho g H \sin\gamma \tag{3-24a}$$

$$\hat{u}_b = T^{slide}\hat{W}^a \rho g H \sin\gamma \tag{3-24b}$$

$$\hat{u}_s = T_s^{uu}T^{slide}\hat{W}^a \rho g H \sin\gamma \tag{3-24c}$$

$$\hat{v}_s = T_s^{uv}T^{slide}\hat{W}^a \rho g H \sin\gamma \tag{3-24d}$$

In Equation (3-24b) there is only the single transfer function T^{slide} (this occurs because no transfer function is necessary to calculate a prescribed basal velocity anomaly from itself). This shows that the sliding law transfer function T^{slide} directly relates the anomalous basal velocity to the prescribed anomaly in the form of $\hat{W}^a \rho g H \sin\gamma$, for the sliding law solution. This can also be quite simply concluded from Equation (3-23a).

3.4 Mathematical solution including non-linear term

3.4.1 Restrictions on solution

We now look at solutions for the basal shear stress and velocity anomalies, and the surface velocity anomaly, when the non-linear last term on the right side in the sliding law (Equation (3-8a)) is included. (This non-linear term is the contribution to the basal sliding velocity from the combination of the anomalous sliding parameter and the anomalous basal shear stress; this contribution will be significant when both of these anomalous parts are of the same order as the equivalent steady-state quantities.) When this non-linear term is second-order, the solutions derived here should not differ appreciably from the solutions of Sections 3.2 and 3.3. If this non-linear term is not second-order, the solutions in these previous sections are not valid. However, there is a limited range of situations where this non-linear last term on the right side of Equation (3-8a) is not second-order: the ratio $|W^a(x)|/W^s$ has to be greater than about one-third (so that the term is not second-order), but less than one (to be physically reasonable). It is in this limited range that we expect the solutions including the last term in Equation (3-8a) to be useful, and it is important to note that this term is not actually second-order in this range.

Another important restriction on the solutions which will be derived in this section, is that these solutions are strictly valid for only a single harmonic in the anomalous sliding parameter $W^a(x)$, since this is the form of anomaly for which we are able to reasonably derive solutions. The possibility of superposing solutions for various harmonic components will be examined in Section 3.5.4.

3.4.2 General solution form

The solution will again be determined by using the Fourier transform. This necessitates transforming all the terms in the equation for the basal sliding anomaly (Equation (3-8a)), as one of the basal boundary conditions. The non-linear last term on the right side must now be included. This term involves a multiplication of two functions of x, which will transform to a convolution of two functions of k in the wave number domain (Papoulis, 1962). The dimensioned form of the transform of Equation (3-8a) then is:

$$\frac{\partial\hat{\psi}}{\partial y}\Big|_{y=0} = W^{a}\eta\left[\frac{\partial^2\hat{\psi}}{\partial y^2} + k^2\hat{\psi}\right]_{y=0} + \hat{W}^{a}\rho gH\sin\gamma + \hat{W}^{a}\eta * \left[\frac{\partial^2\hat{\psi}}{\partial y^2} + k^2\hat{\psi}\right]_{y=0} \tag{3-25}$$

Here * denotes convolution.

The difficulty in this equation is caused by the convolution of $\hat{W}^{a}$ with terms of the transformed stream function $\hat{\psi}$. Since we wish to obtain a reasonably simple explicit solution for $\hat{\psi}$, we will choose a form for $\hat{W}^{a}$ which allows the convolution to be written as a multiplication. This will be true if $W^{a}(x)$ is harmonic, since the Fourier transform will then be a Dirac delta function. Thus we choose

$$W^{a}(x) = W^{a}\cos k_1 x \tag{3-26a}$$

Here W^{a} is now the amplitude of a cosine function, which has a fundamental wave number k_1. The Fourier transform then is

$$\hat{W}^{a} = W^{a}\delta(k-k_1) \tag{3-26b}$$

Here $\delta(k-k_1)$ is the Dirac delta function, which has infinite amplitude at $k=k_1$ and zero amplitude elsewhere, and which has an integrated value over all k of one.

This form of $\hat{W}^{a}$ is then substituted into Equation (3-25). Using the fact that $\delta(k-k_1)*f(k) = f(k-k_1)$, where the * again denotes convolution, this gives for one of the basal boundary conditions:

$$\frac{\partial\hat{\psi}}{\partial y}\Big|_{y=0} = W^{a}\eta\left[\frac{\partial^2\hat{\psi}}{\partial y^2} + k^2\hat{\psi}\right]_{y=0} + W^{a}\delta(k-k_1)\rho gH\sin\gamma \tag{3-27a}$$

$$+ W^{a}\eta\left[\frac{\partial^2\hat{\psi}(k-k_1)}{\partial y^2} + (k-k_1)^2\hat{\psi}(k-k_1)\right]_{y=0}$$

The other boundary conditions are the same as the corresponding boundary conditions in

Sections 3.3 and 3.4. That is

$$-ik\hat{\psi}|_{y=0} = 0 \tag{3-27b}$$

$$\left[3k^2\frac{\partial\hat{\psi}}{\partial y} - \frac{\partial^3\hat{\psi}}{\partial y^3}\right]_{y=H} = 0 \tag{3-27c}$$

$$\left[\frac{\partial^2\hat{\psi}}{\partial y^2} + k^2\hat{\psi}\right]_{y=H} = 0 \tag{3-27d}$$

The solution form for $\hat{\psi}$ will be

$$\hat{\psi} = \frac{A(k)}{k}e^{-ky} + B(k)ye^{-ky} + \frac{C(k)}{k}e^{ky} + D(k)ye^{ky} \tag{3-28}$$

Note that here (as contrasted with Equation (3-12) where the non-linear term was neglected) the solution can not be assumed to be proportional to $\hat{W}^a\rho gH\sin\gamma$.

The solutions for the coefficients A, B, C, and D can then be determined. These solutions are somewhat complicated. It turns out that the solutions are sums over all positive integer multiples of the fundamental wave number k_1. The solutions for the coefficients for each multiple depend on the solutions for the previous multiple; thus the solution process is iterative.

We need to be able to begin the iteration by knowing the solutions for the coefficients at $k=k_1$. These solutions can in fact be determined, since the terms in Equation (3-27a) which are multiplied by $k-k_1$ become zero when $k=k_1$; this allows non-iterative solutions for the coefficients at this wave number $k=k_1$. The solutions for the coefficients at this fundamental wave number are:

$$A(k_1) = -C(k_1) = -\frac{2k_1^2H^2\rho gH\sin\gamma\delta(k-k_1)}{[1-2W^a\eta k_1]e^{-2k_1H} + 2 + 8W^a\eta k_1k_1H + 4k_1^2H^2 + [1+2W^a\eta k_1]e^{2k_1H}} \tag{3-29a}$$

$$B(k_1) = \frac{[1 + 2k_1H + e^{2k_1H}]\rho gH\sin\gamma\delta(k-k_1)}{[1-2W^a\eta k_1]e^{-2k_1H} + 2 + 8W^a\eta k_1k_1H + 4k_1^2H^2 + [1+2W^a\eta k_1]e^{2k_1H}} \tag{3-29b}$$

$$D(k_1) = \frac{[e^{-2k_1H} + 1 - 2k_1H]\rho gH\sin\gamma\delta(k-k_1)}{[1-2W^a\eta k_1]e^{-2k_1H} + 2 + 8W^a\eta k_1k_1H + 4k_1^2H^2 + [1+2W^a\eta k_1]e^{2k_1H}} \tag{3-29c}$$

We now define the wave number k_n such that $k_n = nk_1$, with n being a positive integer. The solutions for $n=1$ are given in Equations (3-29). Using these solutions for $A(k_1)$, $B(k_1)$, $C(k_1)$, and $D(k_1)$, we can iterate to write the solutions at all other ($n > 1$) positive integer multiples of the fundamental wave number. The solutions for the terms in the coefficients for $n=2$ to $n=\infty$ then are

$$\underset{n=2 \text{ to } \infty}{A(k_n)} = -\left[\frac{2k_n^2H^2}{[1-2W^s\eta k_n]e^{-2k_nH} + 2 + 8W^s\eta k_nk_nH + 4k_n^2H^2 + [1+2W^s\eta k_n]e^{2k_nH}}\right] \quad (3\text{-}30a)$$

$$\left[\frac{e^{-2k_{n-1}H} - 4k_{n-1}H - e^{2k_{n-1}H}}{-2k_{n-1}^2H^2}\right]2W^a\eta k_{n-1}A(k_{n-1})$$

$$\underset{n=2 \text{ to } \infty}{B(k_n)} = \left[\frac{1 + 2k_nH + e^{2k_nH}}{[1-2W^s\eta k_n]e^{-2k_nH} + 2 + 8W^s\eta k_nk_nH + 4k_n^2H^2 + [1+2W^s\eta k_n]e^{2k_nH}}\right] \quad (3\text{-}30b)$$

$$\left[\frac{e^{-2k_{n-1}H} - 4k_{n-1}H - e^{2k_{n-1}H}}{1 + 2k_{n-1}H + e^{2k_{n-1}H}}\right]2W^a\eta k_{n-1}B(k_{n-1})$$

$$\underset{n=2 \text{ to } \infty}{C(k_n)} = \left[\frac{2k_n^2H^2}{[1-2W^s\eta k_n]e^{-2k_nH} + 2 + 8W^s\eta k_nk_nH + 4k_n^2H^2 + [1+2W^s\eta k_n]e^{2k_nH}}\right] \quad (3\text{-}30c)$$

$$\left[\frac{e^{-2k_{n-1}H} - 4k_{n-1}H - e^{2k_{n-1}H}}{2k_{n-1}^2H^2}\right]2W^a\eta k_{n-1}C(k_{n-1})$$

$$\underset{n=2 \text{ to } \infty}{D(k_n)} = \left[\frac{e^{-2k_nH} + 1 - 2k_nH}{[1-2W^s\eta k_n]e^{-2k_nH} + 2 + 8W^s\eta k_nk_nH + 4k_n^2H^2 + [1+2W^s\eta k_n]e^{2k_nH}}\right] \quad (3\text{-}30d)$$

$$\left[\frac{e^{-2k_{n-1}H} - 4k_{n-1}H - e^{2k_{n-1}H}}{e^{-2k_{n-1}H} + 1 - 2k_{n-1}H}\right]2W^a\eta k_{n-1}D(k_{n-1})$$

The total solution for each coefficient, is the sum of these solutions for all positive integer multiples of the fundamental wave number k_1. The total solution for each coefficient has power at each of these multiples. (Note that in Equations (3-30) the solution for the value of a coefficients at a given wave number k_n is a function of that wave number, multiplying the value of the coefficient for the previous wave number k_{n-1}.)

The total solutions for the coefficients give the solution for the transformed stream function $\hat{\psi}$.

3.4.3 Basal shear stress solution

The Fourier transform of the basal shear stress anomaly $\hat{\tau}_b$ can be determined by substituting the solutions for the coefficients A, B, C, and D, as solved in the last section, into Equation (3-14a). For this case (including the non-linear term in the sliding law), the solution for the transformed basal shear stress anomaly will be iterative, because the coefficients are iterative. We first determine the solution for $\hat{\tau}_b$ at the fundamental wave number k_1:

$$\hat{\tau}_b(k_1) = \left[\frac{[e^{-2k_1H} - 4k_1H - e^{2k_1H}]W^a \rho g H \sin\gamma\delta(k-k_1)}{[1-2W^s\eta k_1]e^{-2k_1H} + 2 + 8W^s\eta k_1 k_1 H + 4k_1{}^2H^2 + [1+2W^s\eta k_1]e^{2k_1H}} \right] 2\eta k_1 \quad (3\text{-}31a)$$

We can then determine the transformed basal shear stress anomaly $\hat{\tau}_b$ for the multiples from n=2 to n=∞ of the fundamental wave number:

$$\underset{n=2\ to\ \infty}{\hat{\tau}_b(k_n)} = \left[\frac{[e^{-2k_nH} - 4k_nH - e^{2k_nH}]W^a \hat{\tau}_b(k_{n-1})}{[1-2W^s\eta k_n]e^{-2k_nH} + 2 + 8W^s\eta k_n k_n H + 4k_n{}^2H^2 + [1+2W^s\eta k_n]e^{2k_nH}} \right] 2\eta k_n \quad (3\text{-}31b)$$

Inspection of Equations (3-31) shows that if we define a term $\hat{\tau}_b(k_0)$, we can write a single equation which gives the solutions for $\hat{\tau}_b(k_n)$ for all the multiples of the fundamental wave number, from n=1 to n=∞. (Note that this term $\hat{\tau}_b(k_0)$ is not one of the terms which are summed to determine the total basal shear stress anomaly; $\hat{\tau}_b(k_0)$ is only used to begin the iteration process.) The definition of $\hat{\tau}_b(k_0)$ is

$$\hat{\tau}_b(k_0) = \rho g H \sin\gamma\delta(k-k_0) \quad (3\text{-}32a)$$

The equation for the *nth* wave number multiple of the transformed basal shear stress anomaly then is

$$\underset{n=1\ to\ \infty}{\hat{\tau}_b(k_n)} = \left[\frac{[e^{-2k_nH} - 4k_nH - e^{2k_nH}]W^a\hat{\tau}_b(k_{n-1})}{[1-2W^s\eta k_n]e^{-2k_nH} + 2 + 8W^s\eta k_nk_nH + 4k_n^2H^2 + [1+2W^s\eta k_n]e^{2k_nH}}\right]2\eta k_n \quad (3\text{-}32b)$$

The total solution for the Fourier transformed basal shear stress anomaly is the sum of these solutions for all positive integer multiples of the fundamental wave number k_1. The total solution has power at each of these multiples.

3.4.4 Basal velocity solution

The solution for the Fourier transformed longitudinal component of the basal velocity anomaly $\hat{u}_b$ is determined by substituting the solutions for the coefficients A, B, C, and D, as solved in Section 3.4.2, into Equation (3-15a). The solution for $\hat{u}_b$ will be iterative. The solution will be most easily written by using the "transfer function" $T^\tau(k)$ (defined in Equation (3-21c)). We first define a term $\hat{u}_b(k_0)$ as

$$\hat{u}_b(k_0) \equiv \frac{\rho g H \sin\gamma\delta(k-k_0)}{T^\tau(k_0)} \quad (3\text{-}33a)$$

(This term $\hat{u}_b(k_0)$ is not summed to determine the total basal velocity anomaly; it is only used to begin the iteration process.) The equation for the *nth* wave number multiple of the transformed longitudinal component of the basal velocity anomaly then is

$$\underset{n=1\ to\ \infty}{\hat{u}_b(k_n)} = \frac{\left[e^{-2k_nH} + 2 + 4k_n^2H^2 + e^{2k_nH}\right]W^aT^\tau(k_{n-1})\hat{u}_b(k_{n-1})}{[1-2W^s\eta k_n]e^{-2k_nH} + 2 + 8W^s\eta k_nk_nH + 4k_n^2H^2 + [1+2W^s\eta k_n]e^{2k_nH}} \quad (3\text{-}33b)$$

$$= \frac{1}{T^\tau(k_n)}\hat{\tau}_b(k_n)$$

The total solution for the Fourier transformed longitudinal component of the basal velocity anomaly is the sum of these solutions for all positive integer multiples of the fundamental wave number k_1. The Fourier transform of the normal component of the basal velocity anomaly is zero.

3.4.5 Surface velocity solution

The solution for the Fourier transformed longitudinal component of the surface velocity anomaly $\hat{u}_s$ is determined by substituting the solutions for the coefficients A, B, C, and D, as solved in Section 3.4.2, into Equation (3-16a). The solution for $\hat{u}_s$ will be iterative. The solution will be most easily written if we first define a term $\hat{u}_s(k_0)$ as

$$\hat{u}_s(k_0) \equiv \frac{\rho g H \sin\gamma \delta(k-k_0)}{T^c(k_0)} \tag{3-34a}$$

(This term $\hat{u}_s(k_0)$ is not summed to determine the total longitudinal component of the surface velocity anomaly.) The equation for the *nth* wave number multiple of the transformed longitudinal component of the surface velocity anomaly then is

$$\underset{n=1 \text{ to } \infty}{\hat{u}_s(k_n)} = \frac{\left[[2+2k_nH]e^{-k_nH} + [2-2k_nH]e^{k_nH}\right]W^a T^c(k_{n-1})\hat{u}_s(k_{n-1})}{[1-2W^s\eta k_n]e^{-2k_nH} + 2 + 8W^s\eta k_n k_n H + 4k_n^2H^2 + [1+2W^s\eta k_n]e^{2k_nH}} \tag{3-34b}$$

$$= \frac{T_s^{ua}(k_n)}{T^c(k_n)}\,\hat{\tau}_b(k_n)$$

The total solution for the Fourier transformed longitudinal component of the surface velocity anomaly is the sum of these solutions for all positive integer multiples of the fundamental wave number k_1.

The solution for the Fourier transformed normal component of the surface velocity anomaly $\hat{v}_s$ is determined by substituting the solutions for the coefficients A, B, C, and D, as solved in Section 3.4.2, into Equation (3-17a). The solution for $\hat{v}_s$ will be iterative. The solution will be most easily written if we first define a term $\hat{v}_s(k_0)$ as

$$\hat{v}_s(k_0) \equiv \frac{-i\rho g H \sin\gamma \delta(k-k_0)}{T^c(k_0)} \tag{3-35a}$$

(This term $\hat{v}_s(k_0)$ is not summed to determine the total normal component of the surface velocity anomaly.) The equation for the *nth* wave number multiple of the transformed normal component of the surface velocity anomaly then is

$$\underset{n=1 \text{ to } \infty}{\hat{v}_s(k_n)} = \frac{\left[2k_nH[e^{-k_nH} + e^{k_nH}]\right]W^a T^c(k_{n-1})\hat{v}_s(k_{n-1})}{[1-2W^s\eta k_n]e^{-2k_nH} + 2 + 8W^s\eta k_n k_n H + 4k_n^2H^2 + [1+2W^s\eta k_n]e^{2k_nH}} \tag{3-35b}$$

$$= \frac{-iT_s^{uv}(k_n)}{T^c(k_n)} \hat{\tau}_b(k_n)$$

The total solution for the Fourier transformed normal component of the surface velocity anomaly is the sum of these solutions for all positive integer multiples of the fundamental wave number k_1.

3.5 Properties of mathematical solution including non-linear term

3.5.1 Non-dimensionalization and adjustable parameters

The non-dimensionalization and adjustable parameters, are very similar for the solution including the non-linear term in the sliding law and the solution neglecting the non-linear term in the sliding law. The non-dimensionalization and adjustable parameters for the solution neglecting the non-linear term were examined in Section 3.3.1. The only differences in the case here (where the non-linear term is included) are due to the simple form of the sliding law anomaly, and the fact that the solutions are iterative.

The non-dimensionalization of the basal shear stress anomaly and the velocity anomalies are the same for both cases: the basal shear stress anomaly is divided by the steady-state basal shear stress $\rho gH\sin\gamma$, and the velocity anomalies are divided by the steady-state sliding velocity $W^s\rho gH\sin\gamma$.

The adjustable parameters are very similar for both cases. For the case including the non-linear term, the dimensionless Fourier transformed sliding parameter $\hat{W}^a/W^s$ becomes $W^a\delta(k-k_1)/W^s$, and the dimensionless wave number kH becomes $k_nH = nk_1H$, where n is a positive integer and k_1 is the fundamental wave number.

3.5.2 Limits of solution

The limits of the solution including the non-linear term in the sliding law can be briefly examined. The first limit which we will examine is the limit of the iterative solution for the Fourier transformed basal shear stress anomaly $\hat{\tau}_b(k_n)$.

As the wave number multiple k_n of the fundamental wave number k_1 goes to infinity, the limit of Equation (3-32b) for the transformed basal shear stress anomaly goes to

$[-W^a/W^s]\hat{\tau}_b(k_{n-1})$. Since W^a must be less than or equal to W^s for a physically reasonable sliding law, this limit shows that the maximum possible power at any wave number is less than or equal to the power at the previous wave number. Therefore in the case where $W^a = W^s$, we expect that the total solution (summed over all wave number multiples) for $\hat{\tau}_b$, when inverse Fourier transformed to the space domain, would converge to some type of delta function. This is in fact true, and is shown by the example for a harmonic anomaly $W^a(x)$ in Section 3.6.1. For values of W^a which are less than W^s, the solution in the space domain for τ_b converges to an intermediate case, between a delta function and the harmonic form of the basal shear stress anomaly $W^a\cos k_1 x$.

This information about the form of the basal shear stress anomaly is interesting, since it shows that the magnitude of this anomaly can be very large, for a simple harmonic anomaly in the sliding law parameter of much smaller magnitude. The requirement for this large anomaly in the basal shear stress is that the magnitude of the anomaly in the sliding law parameter be close to the value of the steady-state sliding law parameter. The "roughness" of the sliding law parameter does not appear to be crucial to whether or not the basal shear stress anomaly has a large magnitude.

The limits of the iterative solutions for the Fourier transformed velocity components $\hat{u}_b$, $\hat{u}_s$, and $\hat{v}_s$, as k_n goes to infinity, are all less than the limit for $\hat{\tau}_b$. (This can be seen by examining Equations (3-33), (3-34), and (3-35).) Thus we expect that these limits would always converge to the intermediate case somewhere between a delta function and a harmonic. This is shown in Section 3.6.1.

It is also useful to check that the solution including the non-linear term approaches the solution neglecting this non-linear term, when the ratio W^a/W^s becomes of the order of one-third (which means that the non-linear term is then second-order). This is fairly easy to see, since the limits of the various quantities at a high wave number k_n are proportional to W^a/W^s multiplying the quantity at the previous wave number. As the ratio W^a/W^s decreases, these limits will rapidly approach zero, since they will be proportional to $[W^a/W^s]^n$ (because the quantity at the previous wave number will also be proportional to W^a/W^s, and so forth). Therefore the wave number multiples will not have much power for W^a/W^s of the order of one-third; and only the solution for the fundamental wave number k_1 will be significant. Comparison of Section 3.2 with Section 3.4 shows that this solution for the fundamental wave number is in fact identical to the solution neglecting the non-

linear term, if the anomalous parameter W^a in the sliding law is harmonic.

3.5.3 Relation to prescribed basal velocity solution

The previous section shows that the solution including the non-linear term in the sliding law is similar to the solution neglecting this term, provided that the iterations in the solution for the case including the non-linear term rapidly approach zero. This suggests that it is possible to write the solutions for the basal shear stress anomaly and velocity anomaly for the non-linear case, in terms which relate them to the solutions for a prescribed basal velocity, since this is possible for the case which neglects the non-linear term. Inspection of Equations (3-32), (3-33), (3-34), and (3-35) shows that this is true; that is, we can write the solutions for the case including the non-linear term by using the transfer functions T^{τ}, T_s^{uu}, and T_s^{uv}, and the sliding law transfer function T^{slide}.

This gives the following forms for the solutions which include the non-linear term in the sliding law. The Fourier transformed basal shear stress anomaly $\hat{\tau}_b$ is:

$$\hat{\tau}_b(k_n) = T^{\tau}(k_n)T^{slide}(k_n)W^a\hat{\tau}_b(k_{n-1}) \tag{3-36a}$$

The Fourier transformed longitudinal component of the basal velocity anomaly $\hat{u}_b$ is:

$$\hat{u}_b(k_n) = T^{slide}(k_n)W^aT^{\tau}(k_{n-1})\hat{u}_b(k_{n-1}) \tag{3-36b}$$

The Fourier transformed longitudinal component of the surface velocity anomaly $\hat{u}_s$ is:

$$\hat{u}_s(k_n) = T_s^{uu}(k_n)T^{slide}(k_n)W^aT^{\tau}(k_{n-1})\hat{u}_s(k_{n-1}) \tag{3-36c}$$

The Fourier transformed normal component of the surface velocity anomaly $\hat{v}_s$ is:

$$\hat{v}_s(k_n) = T_s^{uv}(k_n)T^{slide}(k_n)W^aT^{\tau}(k_{n-1})\hat{v}_s(k_{n-1}) \tag{3-36d}$$

Here the transfer functions are evaluated at the wave number k_n, where the subscript n refers to the positive integer multiple of the fundamental wave number k_1. These solutions are summed as in Section 3.4 to determine the total transformed basal shear stress anomaly and velocity anomaly. The terms $\hat{\tau}_b(k_0)$, $\hat{u}_b(k_0)$, $\hat{u}_s(k_0)$, and $\hat{v}_s(k_0)$ are also as defined in Section 3.4.

3.5.4 Possibility of superposing solutions for various harmonic components

The solution for the case including the non-linear term in the sliding law has been done for a harmonic variation in the sliding law parameter. The question arises of whether the solutions for different harmonic anomalies could be summed, to give a solution for the combination of these harmonic anomalies. This would enable the solution for any arbitrary anomaly in the sliding law to be determined. This can be simply tested, by comparing the sum of the solutions for two different harmonic anomalies, to the solution which results from a sliding law which has an anomalous parameter consisting of two different harmonics.

To do this comparison, we can look at the solutions for just one part of the anomalies, e.g. the Fourier transformed longitudinal component of the basal velocity anomaly $\hat{u}_b$. The solution for this component is just the sliding law. We suppose that we have two different harmonic anomalies in the sliding law parameter:

$$W^{(1)}(x) = W^{(1)}\cos k_1 x \tag{3-37a}$$

$$W^{(2)}(x) = W^{(2)}\cos k_2 x \tag{3-37b}$$

Then the individual solution for $u_b^{(1)}(x)$, using the anomaly $W^{(1)}(x)$, can be found directly from Equation (3-7b):

$$u_b^{(1)}(x) = W^{\sigma}\tau_b^{(1)}(x) + W^{(1)}(x)\rho g H\sin\gamma + W^{(1)}(x)\tau_b^{(1)}(x) \tag{3-38a}$$

Here $\tau_b^{(1)}(x)$ is the corresponding basal shear stress solution. The individual solution for $u_b^{(2)}$, using the anomaly $W^{(2)}(x)$, is

$$u_b^{(2)}(x) = W^{\sigma}\tau_b^{(2)}(x) + W^{(2)}(x)\rho g H\sin\gamma + W^{(2)}(x)\tau_b^{(2)}(x) \tag{3-38b}$$

Here $\tau_b^{(2)}(x)$ is the corresponding basal shear stress solution.

We next directly add these two solutions. This gives:

$$u_b^{(1)} + u_b^{(2)} = W^{\sigma}[\tau_b^{(1)} + \tau_b^{(2)}] + [W^{(1)} + W^{(2)}]\rho g H\sin\gamma + W^{(1)}\tau_b^{(1)} + W^{(2)}\tau_b^{(2)} \tag{3-39a}$$

We now compare this additive solution with the presumed solution for a combined sliding law anomaly $W^{\alpha}(x) = W^{(1)}(x) + W^{(2)}(x)$. This presumed solution is

$$u_b^{(1)+(2)} = W^{\sigma}\tau_b^{(1)+(2)} + [W^{(1)} + W^{(2)}]\rho g H\sin\gamma + [W^{(1)} + W^{(2)}]\tau_b^{(1)+(2)} \tag{3-39b}$$

Equations (3-39a) and (3-39b) are not equal. If we set $\tau_b^{(1)+(2)} = \tau_b^{(1)} + \tau_b^{(2)}$, we see that the additive solution (Equation (3-39a)) is missing the terms $W^{(1)}\tau_b^{(2)}$ and $W^{(2)}\tau_b^{(1)}$. Consideration of the magnitude of the various terms shows that there is no valid reason to expect these missing terms to be smaller in magnitude than any of the terms which were included in the additive solution. We are forced to conclude that adding solutions for different harmonic anomalies is not valid, when the non-linear last term in the sliding law is not second-order.

It is worth noting that a direct analytic solution for an anomalous sliding law parameter which consists of two or more harmonics is theoretically possible. However, this solution would be very complicated. It might also be possible to determine analytic solutions for forms of the sliding law parameter other than a harmonic anomaly, such as a delta function. These solutions are not attempted in this dissertation.

3.6 Examples of shear stress and velocity solutions

3.6.1 Solutions for harmonic variation in sliding law parameter

We will now examine specific solutions for various different anomalies in the sliding law parameter. We will first look at a simple harmonic variation in the sliding law parameter, e.g., $W^a(x) = W^a \cos kx$. This simple form of the anomaly allows a comparison of the solutions both neglecting and including the non-linear term in the basal sliding law.

The solutions for a harmonic anomaly are first examined for the case neglecting the non-linear term in the sliding law. The dimensionless parameters for this case need to be chosen. We will choose intermediate values of these parameters, which hopefully will represent a typical situation for glacier ice. We therefore set the dimensionless viscosity $W^s\bar{\eta}/\bar{\imath}\bar{\imath}$ equal to one, the amplitude of the dimensionless sliding parameter W^a/W^s equal to one-third, and the dimensionless wave number of the harmonic anomaly kH equal to one. We note that although the choice of $W^a/W^s = 1/3$ can be considered an intermediate value, it is about the highest value of this parameter which can be used, while still validly neglecting the non-linear term in the sliding law.

The resulting solutions for the dimensionless basal shear stress anomaly and the dimensionless basal and surface velocity anomalies are plotted as the dashed lines in

Figures 3-3. There is nothing very surprising about these results. We note that the dimensionless longitudinal component of the basal velocity anomaly u_b^* has the same pattern and phase as the prescribed sliding law anomaly $W^a\cos kx$; the amplitude of u_b^* is somewhat lower than the amplitude of $W^a\cos kx$. This is as expected from the form of the transfer function T^{slide}, which relates u_b^* to $W^a(x)$ (see Equation (3-24b)). The dimensionless basal shear stress anomaly τ_b^* has a similar pattern, although with opposite phase and greater amplitude, when compared to u_b^*. This is to be expected from the form of T^{slide} and the transfer function T^τ (see Equation (3-24a)). We note that the amplitude of τ_b^* is less than the amplitude of the prescribed anomaly W^a; this is because the product $T^\tau T^{slide}$ is less than one in absolute value, for all wave numbers k.

The dimensionless components of the surface velocity anomaly u_s^* and v_s^* are as is to be expected from the transfer functions (see Equations (3-24c) and (3-24d)). There is no phase reversal between u_b^* and u_s^*, although this would occur if a sufficiently high wave number (kH greater than about 1.2) were used. The phase of v_s^* leads u_s^* by $\pi/2$. The amplitude of both u_s^* and v_s^* is less than the amplitude of u_b^*.

The case where the non-linear term in the sliding law is included is much more interesting. The same dimensionless parameters are used as for the case neglecting this term, except that the dimensionless amplitude W^a/W^s has been increased to a value of one. This is necessary for the non-linear term to be significant (not second-order), and affect the solutions in an interesting manner.

The resulting solutions for the dimensionless basal shear stress anomaly and the dimensionless velocity anomalies are plotted as the solid lines in Figures 3-3. These solutions are quite different than the solutions where the non-linear term is neglected (dashed lines). In particular, these new solutions are not harmonic, although the prescribed sliding law anomaly $W^a(x)$ is harmonic; this especially applies to the solutions for the dimensionless basal shear stress anomaly τ_b^* and the dimensionless longitudinal component of the basal velocity anomaly u_b^*. In addition, the amplitude of τ_b^* is greater than the amplitude of $W^a(x)$. These solutions for τ_b^* and u_b^* when the non-linear term in the sliding law is included can be approximately described as consisting of a series of delta functions (the solid lines in Figures 3-3b and 3-3c). The area under these curves is equal to zero, but the dimensionless basal shear stress anomaly consists of broad slightly negative regions alternating with sharply positive spikes, while the dimensionless longitudinal component of the

basal velocity anomaly consists of broad slightly positive regions alternating with fairly sharp negative spikes. The dimensionless surface velocity anomaly (u_s^* and v_s^*) is less extreme in pattern, but is also non-harmonic.

Mathematically, the form of the dimensionless basal anomalies τ_b^* and u_b^* is not too surprising (see Section 3.5.2). The fact that the magnitude of τ_b^* is greater than the magnitude of W^a is due to the summation process; the magnitude of u_b^* is still less than W^a. The physical basis for these basal anomalies is more difficult to determine. The main question to be answered is why the positive and negative parts of the basal anomalies are so different in form. If this question is answered for the dimensionless basal anomalies τ_b^* and u_b^*, the form of the dimensionless surface anomalies u_s^* and v_s^* is simply explained by applying the transfer functions T_s^{uu} and T_s^{uv} to the dimensionless basal anomaly u_b^*.

The form of the basal anomalies is probably due to the fact that the non-linear term in the sliding law makes the dimensionless anomalous basal shear stress solution τ_b^* highly non-linear as a function of the anomalous sliding law parameter W^a; and yet this dimensionless anomalous basal shear stress solution (which is driven by the steady-state basal shear stress) must have a mean value of zero. Therefore high values of τ_b^* must cover only a narrow range, if they are to be offset by regions of only slightly negative anomalous basal shear stress. The dimensionless longitudinal component of the basal velocity anomaly u_b^* is simply related to τ_b^* by the transfer function T^τ. The dimensionless components of the surface velocity anomaly are in turn related to the dimensionless basal velocity anomaly by the appropriate transfer functions.

It is useful to test that the solution (for a harmonic variation in the sliding law parameter) including the non-linear term in the sliding law approaches the solution neglecting this term, as the magnitude of the non-linear term is decreased. If we decrease the ratio W^a/W^s to a value of one-third, the solution including the non-linear term does in fact become very similar to the solution where the non-linear term is neglected.

3.6.2 Solution for step in sliding law parameter

We next look at the solution for a step in the anomalous sliding law parameter $W^a(x)$. It is necessary to use the solution neglecting the non-linear term in the sliding law, since the prescribed anomaly is non-harmonic. We set the ratio $|W^a|/W^s$ to a value of one-third,

where the anomalous amplitude $|W^a|$ is the half-height of the step. The dimensionless viscosity $W^s\eta/H$ is set equal to one. The wavelength of the periodic pattern (in the fast Fourier transform) for $W^a(x)$ is chosen to be $25H$ (where H is the thickness of the glacier.

The resulting dimensionless basal shear stress anomaly and dimensionless velocity anomalies are shown in Figure 3-4. For this case where the non-linear term in the sliding law is neglected, we see that the magnitude of these anomalies is less than the magnitude of the anomalous sliding law parameter. This again follows from the fact that the various transfer functions and products of transfer functions in Equations (3-24) are all less than one.

The dimensionless basal shear stress anomaly τ_b^* has sharp spikes associated with the step in the anomalous sliding law parameter W^a; the sign of τ_b^* is opposite to the sign of W^a. This is because the transfer function T^τ is negative, and has a large magnitude at the small wavelengths which dominate the Fourier transform of the step in W^a.

The dimensionless longitudinal component of the basal velocity anomaly u_b^* is simply a somewhat smoothed version of the prescribed anomaly W^a. This is interesting, because it shows that the spikes in the basal shear stress are not associated with sudden changes in the basal velocity, although physically the fairly extreme pattern of the basal shear stress might be expected to cause relatively rapid changes in the basal sliding velocity. (It is important to remember that the non-linear term in the sliding law has been neglected.)

The dimensionless surface velocity is as would be expected from the transfer functions T_s^{ua} and T_s^{uv}. The longitudinal component u_s^* is simply an even smoother version of u_b^*; there is no phase reversal due to the long wavelength of the prescribed anomaly W^a. The normal component v_s^* has a peak associated with the step in W^a.

It is interesting to compare this solution with the similar solution of Hutter and Olunloyo (1980). Hutter and Olunloyo prescribed an abrupt change from "perfect slip" to "no slip" as the basal sliding boundary condition; however, their surface boundary condition requires that the normal velocity component at the surface be equal to zero. The result is that Hutter and Olunloyo's basal shear stress and basal velocity solutions are similar to the solutions derived in this section, but their surface velocity solution is different than the solution derived here. The longitudinal component of the surface velocity in the

calculations of Hutter and Olunloyo reaches a maximum over the abrupt change in the basal sliding boundary condition; this is equivalent to the peak in the normal component of the surface velocity seen in the solution here (since we have allowed normal motions at the surface).

3.6.3 Solution for peak in sliding law parameter

We will now examine an anomaly for $W^a(x)$ which has the form of a Gaussian peak. We again choose a value of one for the dimensionless viscosity $W^s\eta/H$, and a value of one-third for the ratio $|W^a|/W^s$, where $|W^a|$ is the height of the peak. The standard deviation of the Gaussian is taken to be $0.5H$ (where H is the ice thickness). It is again necessary to use the solution where the non-linear term in the sliding law is neglected.

The resulting dimensionless basal shear stress anomaly and dimensionless velocity anomalies are plotted in Figures 3-5. It is useful to note that the resulting dimensionless longitudinal component of the basal velocity anomaly u_b^* has the form of a basal peak, although this peak in u_b^* is broader and of less amplitude than the prescribed peak for W^a. This peak in u_b^* means that the results for a prescribed peak in W^a are similar to the results for a peak in the prescribed basal velocity (see Section 2.4.3). This can be seen by comparison of Figures 2-5b and 3-5.

It is interesting to examine the dimensionless basal shear stress anomaly τ_b^* for the sliding law solution (the basal shear stress was not calculated for the prescribed basal velocity solution). This anomaly τ_b^* has a negative peak associated with the positive peaks in W^a and u_b^*. It also has lower amplitude positive peaks on either side of the negative peak (see Figure 3-5b). This shows that this form of basal shear stress anomaly is necessary for the peak to exist in the longitudinal component of the basal velocity anomaly u_b. This is verified by directly calculating the basal shear stress anomaly associated with a prescribed Gaussian peak in the longitudinal component of the basal velocity anomaly; this basal shear stress anomaly has the same form as Figure 3-5b.

3.6.4 Sliding law anomaly associated with a step in basal velocity

All of the examples in the previous sections have resulted in velocity anomalies which are continuous, with no sharp jumps. The solution neglecting the non-linear term in the sliding law resulted in smooth velocity anomalies for the various sliding law anomalies which we have examined; the solution including the non-linear term (for a harmonic sliding law anomaly) resulted in velocity anomalies which are still continuous, although the longitudinal component of the basal velocity anomaly u_b had relatively sharp peaks. The question arises of what form of anomaly in the sliding law parameter is necessary in order to get a sharp jump in the associated basal velocity, e.g. a step in u_b. This question is particularly important since this form of basal velocity anomaly is thought to be associated with the mini-surges and the main surge of Variegated Glacier, and with surges in other glaciers. (This form of basal velocity anomaly was prescribed in Chapter 2, and resulted in a very interesting surface velocity anomaly.)

This question can be answered by reversing the solution for the Fourier transformed longitudinal component of the basal velocity $\hat{u}_b$ in Equation (3-24b) (neglecting the non-linear term in the sliding law). The new equation which results is

$$\hat{W}^a = \frac{1}{T^{slide}\rho g H \sin\gamma}\hat{u}_b \tag{3-40}$$

This means that we can prescribe the transformed velocity $\hat{u}_b$, and then calculate the associated transformed anomalous sliding law parameter $\hat{W}^a$. We can also easily calculate the associated transformed basal shear stress anomaly and transformed surface velocity anomaly by using the calculated parameter $\hat{W}^a$ in Equations (3-24a), (3-24), and (3-24d).

An example of this solution is shown in Figure 3-6. A step is prescribed as the form of the dimensionless longitudinal component of the basal velocity anomaly u_b^*; this form of u_b^* is plotted in Figure 3-6c. (Here u_b^* has exactly the same form as the prescribed dimensionless anomalous sliding law parameter W^a/W^s in Figure 3-4a, with a half-height of 1/3). The dimensionless anomalous sliding law parameter and dimensionless basal shear stress anomaly τ_b^* associated with the step in u_b^* are plotted in Figures 3-6a and 3-6b. (The surface velocity anomaly is not plotted since it is of the same form as in Figure 2-4.)

This step in u_b^* results in the form of a sharp positive spike immediately next to a sharp negative spike for both W^a/W^s and τ_b^*, located at the position of the step in the basal

velocity anomaly. (The sign of W^a/W^s is reversed from that of τ_b^*.) This form of anomaly for the sliding law parameter and basal shear stress does not seem very plausible, since it is somewhat difficult to picture a physical basis for such an anomaly. This means that a step in the basal velocity anomaly is not very likely, *if we assume that the sliding law is an accurate description of the physics of the problem, and that the linear viscous rheology is valid.* It is quite likely that these assumptions are not true for a step in the basal velocity anomaly. Furthermore, forms of the basal velocity anomaly such as a smoothed step or a ramp have not been ruled out.

It is also important to note that our given choice of u_b^* results in a magnitude for W^a/W^s which is much too large for the non-linear term in the sliding law to be neglected. This could be remedied by decreasing the magnitude of the prescribed velocity anomaly; however, it would have to be decreased to of the order of one-hundredth of the steady-state sliding velocity. If we had a solution including the non-linear term in the sliding law, the magnitude of the anomaly u_b would still have to be decreased to of the order of one-thirtieth of the steady-state sliding velocity. This would be necessary for the ratio $|W^a|/W^s$ to be less than one (which we have decided is the criterion for a physically reasonable sliding law anomaly). Although we do not know the form of the solution including the non-linear term for the prescribed step in the basal velocity anomaly, we would intuitively expect it to be somewhat similar to the solution where the non-linear term is neglected, for this particular anomaly.

3.7 Discussion

The solutions for a prescribed anomaly in a basal sliding law have been shown to have several interesting features. If the magnitude of the anomalous sliding law parameter is of the order of one-third or less the value of the steady-state sliding law parameter, the non-linear term in the sliding law is second-order and can be neglected. For this solution, the most interesting feature is probably the fact that the basal shear stress anomaly and velocity anomalies can be directly related to the solution for a prescribed basal velocity anomaly, by using the transfer function T^{slide}. The results can be summarized as showing that very rapid changes in the anomalous sliding law parameter result in rapid changes in the basal shear stress anomaly, but that these are associated with relatively smooth changes in the velocity anomaly. The magnitude of the rapid changes in τ_b^* is less than the

magnitude of the anomalous sliding law parameter W^a. These results are not particularly surprising.

For situations where the magnitude of the anomalous sliding law parameter is between about one-third and one times the value of the steady-state sliding law parameter, the non-linear term in the sliding law must be included. For this case, the basal shear stress anomaly and velocity anomaly can not be as simply related to the solution for a prescribed basal velocity anomaly, since the solution for the sliding law involves a summation process. However, the sums can still be written in terms of the transfer function T^{slide}. For a harmonic anomalous sliding law parameter, rapid changes in the basal shear stress anomaly are associated with changes in the velocity anomaly which are somewhat rougher than those for the case where the non-linear term is neglected. The velocity anomaly is still smoother than the basal shear stress anomaly. In this case the magnitude of τ_b^* can be greater than the magnitude of W^a.

The possibility of the magnitude of the anomalous sliding law parameter exceeding the value of the steady-state sliding law parameter is generally assumed to not be physically reasonable. However, Section 3.6.4 showed that brief high-amplitude spikes in the anomalous sliding law parameter (with magnitude greater than the value of the steady-state sliding law parameter) could be associated with a much lower amplitude anomalous sliding velocity variation, such that the total sliding velocity (the sum of the anomalous and steady-state sliding velocities) would always be positive. Thus a physically reasonable sliding velocity can be associated with a physically unreasonable sliding law parameter. The total basal shear stress associated with the negative sliding law parameter is also negative, which is also physically unreasonable. The solution to this problem is probably that the abrupt step in the basal velocity is not possible in reality, and that real changes in the sliding velocity are required to be at least somewhat smoother. It is also quite likely that the sliding law is not a completely accurate description of the physics of the problem, and that the assumed linear viscous rheology is not a valid approximation of the true rheology for this particular case. It is important to note that this particular solution also neglected the non-linear term and thus is not really valid (since for this particular case the non-linear term is not second-order). The mathematical solutions derived in this chapter do not allow the inclusion of the non-linear term in this case. This means that the question of whether the an abrupt step in the basal sliding velocity is possible must be left unanswered.

Finally it is important to realize that the value of the dimensionless viscosity affects the form of the transfer function T^{slide}, which in turn affects the form of the solutions considered in this chapter. At high values for the dimensionless viscosity, the value of T^{slide} will be less than one (except at very long wavelengths). For this case the sliding law solutions for a prescribed anomalous sliding law parameter will be considerably different than the solutions for a prescribed basal velocity anomaly, when the prescribed anomalies have the same form. At low values of the dimensionless viscosity the value of T^{slide} will be much closer to one. In this case the sliding law solutions will be very similar to the solutions for a prescribed basal velocity anomaly, if the prescribed anomalies have the same form. In fact, simple calculations show that the dimensionless viscosity (which in this chapter has been defined as $W^*\eta/H$) is often quite low in value (of the order of 0.1), for various glaciers. This means that although the sliding law solutions have shown many interesting effects, in reality a prescribed basal velocity anomaly may be just as good a method for examining velocity anomalies in glaciers.

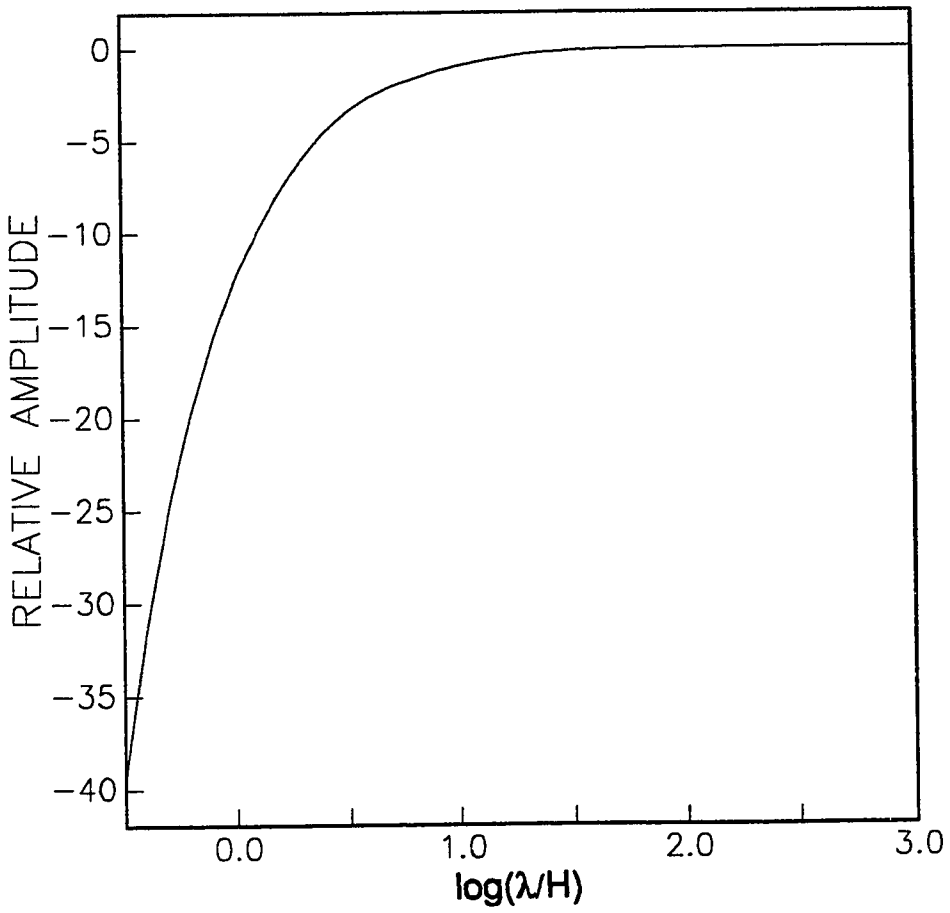

Figure 3-1. Transfer function T^{ε} for linear viscous rheology, plotted for dynamic viscosity $\eta = 1$.

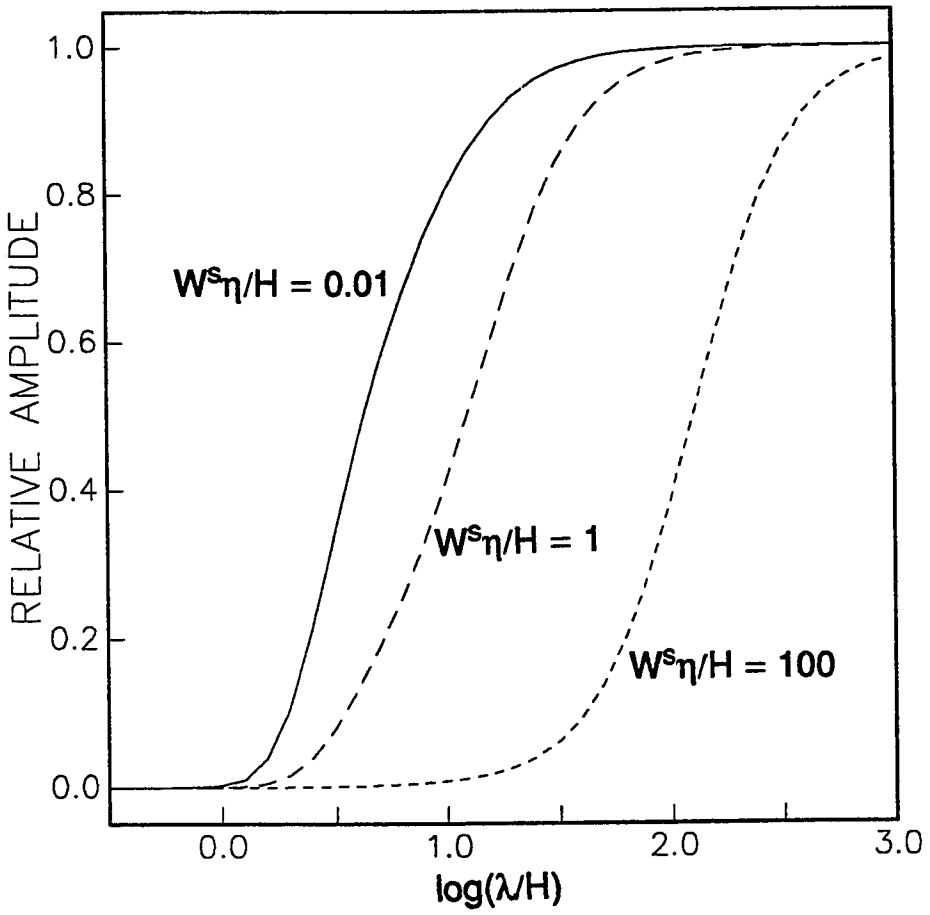

Figure 3-2. Transfer function T^{slide} for linear viscous rheology, plotted for $W^s\eta/H = 0.01$ (solid line), $W^s\eta/H = 1$ (long dashed line), and $W^s\eta/H = 100$ (short dashed line).

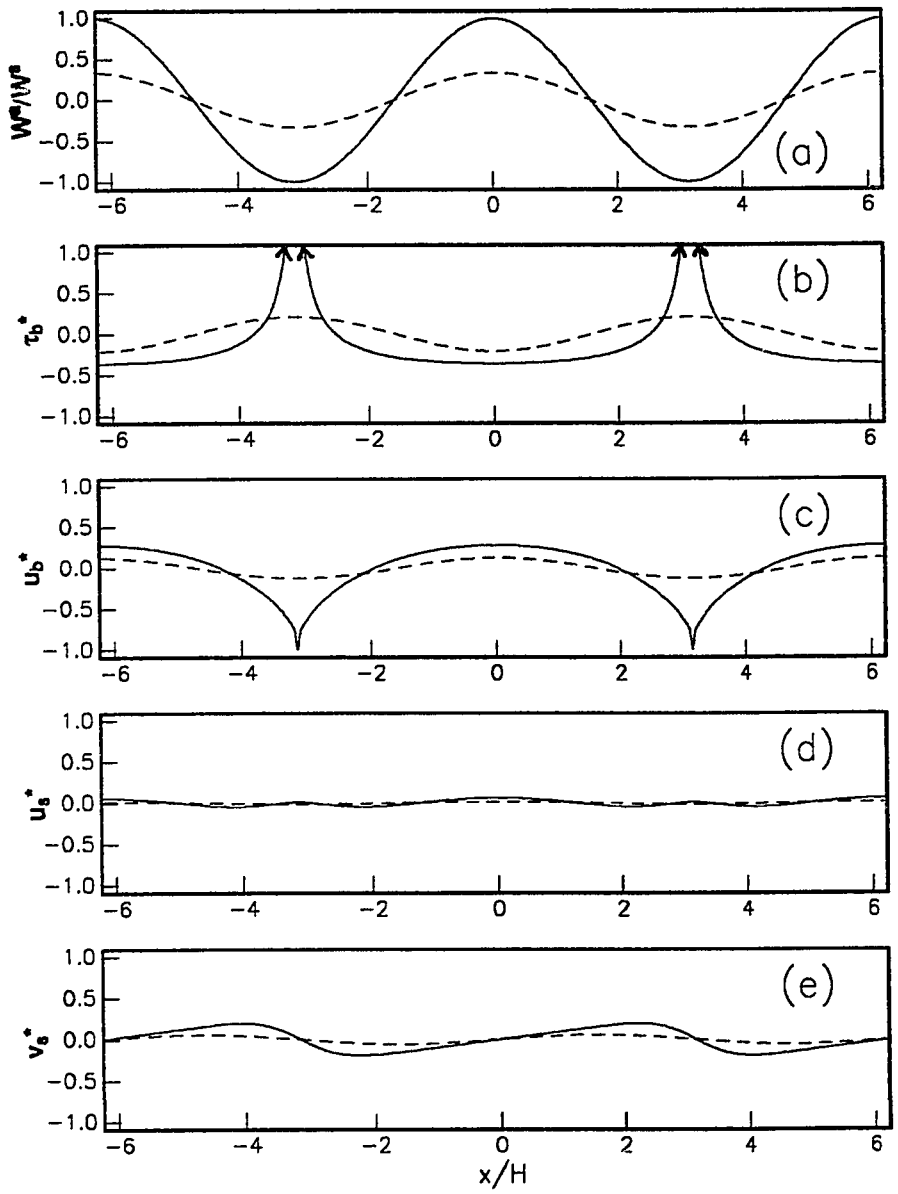

Figure 3-3. Dimensionless basal shear stress and velocity anomalies and dimensionless surface velocity anomalies, for linear viscous rheology, for harmonic variation in $W^a(x)$, $kH = 1$, $W^a\eta/H = 1$. Dashed lines: $|W^a(x)|/W^a = 1/3$ (non-linear term neglected). Solid lines: $|W^a(x)|/W^a = 1$ (non-linear term included). (a) W^a/W^a, (b) τ_b^*, (c) u_b^*, (d) u_s^*, and (e) v_s^*.

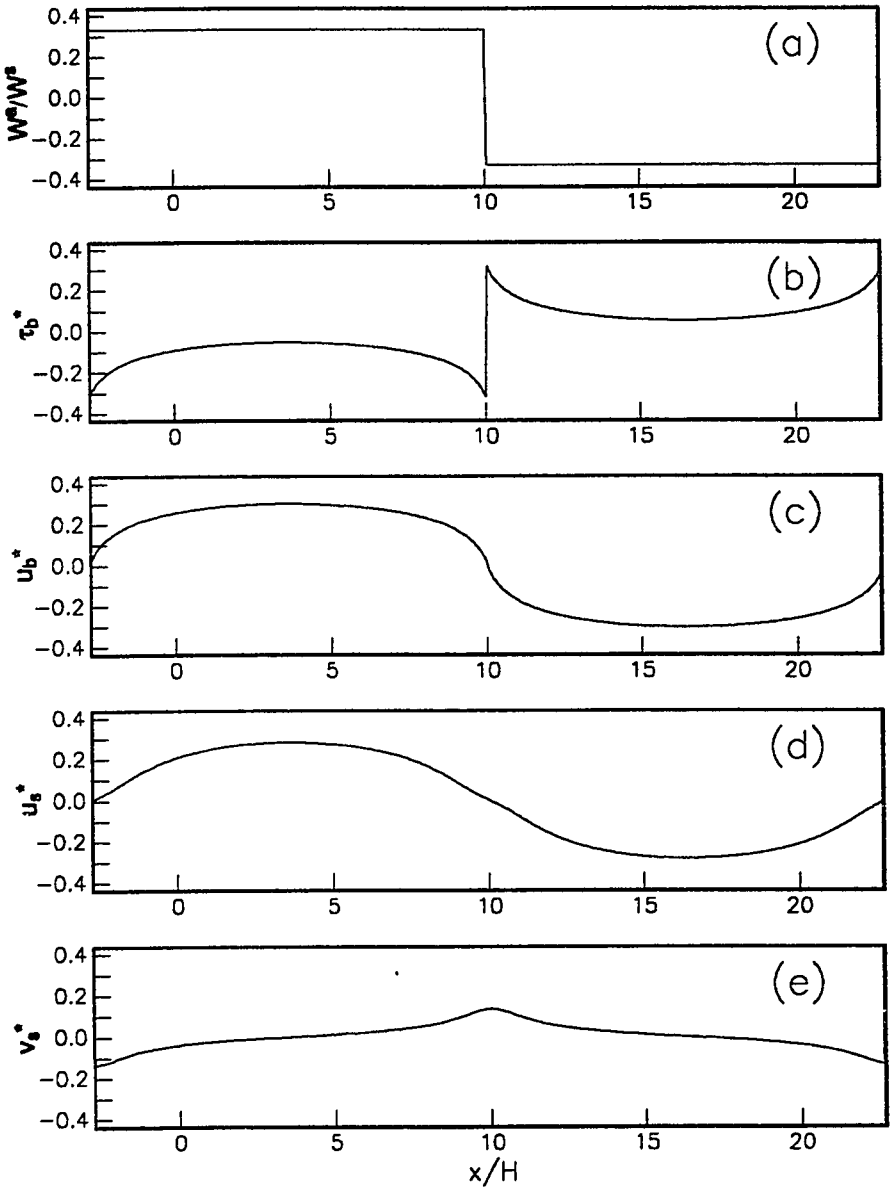

Figure 3-4. Dimensionless basal shear stress and velocity anomalies and dimensionless surface velocity anomalies, for linear viscous rheology, for step in $W^a(x)$, $|W^a(x)|/W^s = 1/3$ (non-linear term neglected), $W^s\eta/H = 1$. (a) W^a/W^s, (b) τ_b^*, (c) u_b^*, (d) u_s^*, and (e) v_s^*.

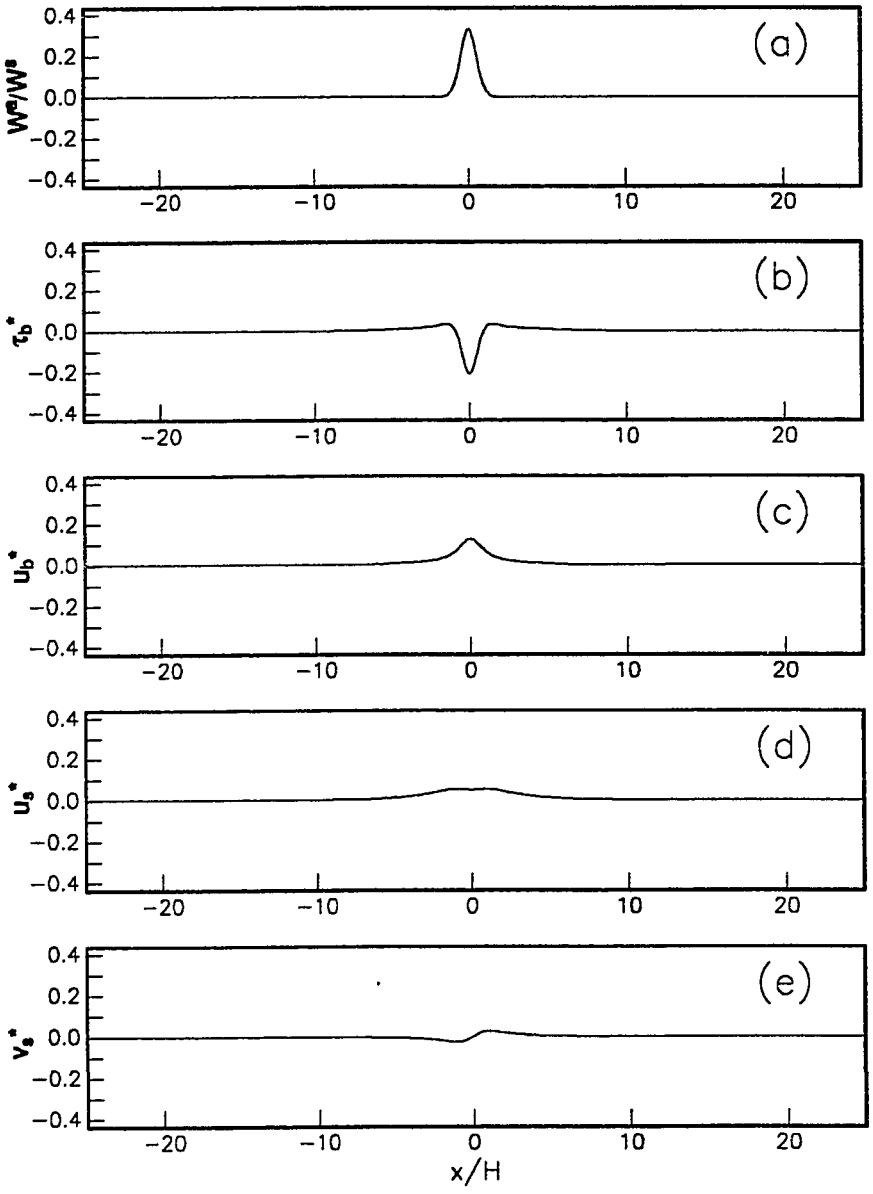

Figure 3-5. Dimensionless basal shear stress and velocity anomalies and dimensionless surface velocity anomalies, for linear viscous rheology, for Gaussian peak in $W^a(x)$, $\sigma/H = 0.5$, $|W^a(x)|/W^s = 1/3$ (non-linear term neglected), $W^s\eta/H = 1$. (a) W^a/W^s, (b) τ_b^*, (c) u_b^*, (d) u_s^*, and (e) v_s^*.

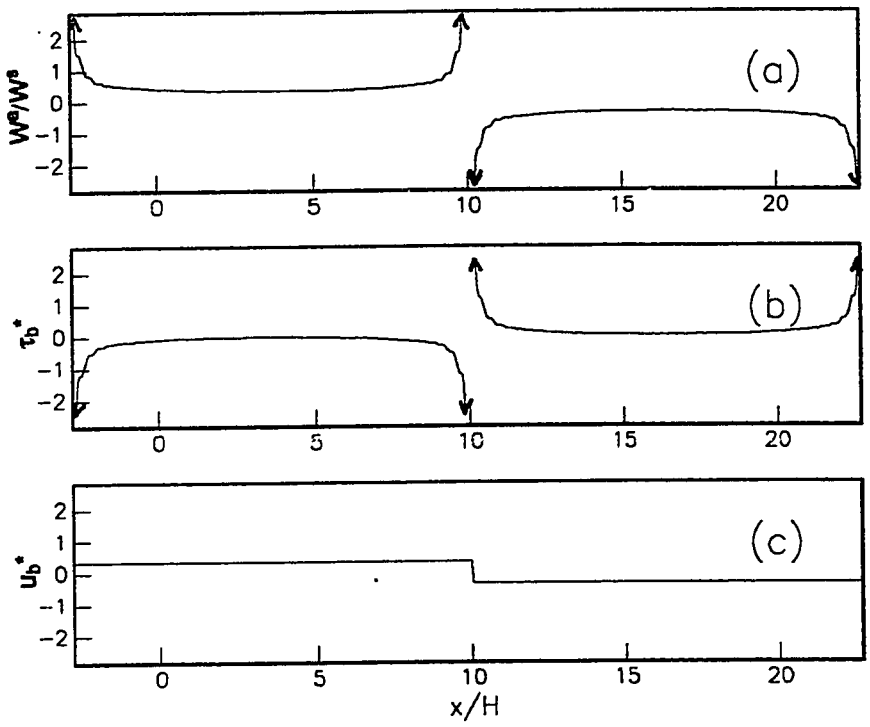

Figure 3-6. Dimensionless anomalous sliding law parameter and dimensionless basal shear stress anomaly, for linear viscous rheology, for step in $u_b(x)$, $|u_b(x)|/W^a \rho g H \sin\gamma = 1/3$ (non-linear term neglected), $W^a\eta/H = 1$. (a) W^a/W^a, (b) τ_b^*, and (c) u_b^*.

CHAPTER 4

VISCO-ELASTIC FORWARD SOLUTIONS

4.1 Constitutive equations

We now will examine the surface velocity solution for a Maxwell visco-elastic rheology, given a prescribed basal velocity anomaly. These solutions will be useful for studying possible transient creep (elastic strains) in glacier ice, for short time-scale velocity variations. The constitutive equations which relate the stress and strain rate (and the time derivative of the stress, which we will refer to as the stress rate) for the Maxwell rheology are (Peltier, 1974)

$$\dot{\sigma}_{ij} + \frac{\mu}{\eta}\left[\sigma_{ij} - \frac{1}{3}\sigma_{kk}\delta_{ij}\right] = 2\mu\dot{e}_{ij} + \left[K - \frac{2}{3}\mu\right]\dot{e}_{kk}\delta_{ij} \tag{4-1}$$

Here σ_{ij} are the nine stress components and $\dot{e}_{ij}$ are the nine strain rate components. The elastic bulk modulus is K, the elastic shear modulus is μ, and η is the dynamic viscosity. Repeated indices indicate summation and δ_{ij} is the Kronecker delta.

These constitutive equations are considerably more complicated than the constitutive equations for a viscous incompressible material (as first examined in Chapter 2), or an elastic compressible material (see Appendix B). However, the other equations which we need for our solution (i.e., force balance, and kinematic relations between velocity and strain rate) are exactly the same for the various rheologies. This fact will later be used to simplify the visco-elastic solution process.

4.2 General solution method

4.2.1 Separation of rheological operators and application of Laplace transform

The constitutive equations for the visco-elastic rheology involve not only the stress and the strain rate, but also the stress rate. This makes the solution for the surface velocity somewhat difficult. We will first put the visco-elastic constitutive equations into a simpler form before we attempt to solve for the surface velocity.

The first step which we will take is to separate the constitutive equations into two parts: one part relating the sum of the normal stress rates to the sum of the normal strain rates; and the other part relating the stress deviator components and stress rate deviator components to the strain rate deviator components. Summing Equations (4-1) for the normal components, we get

$$\dot{\sigma}_{kk} = 3K\dot{e}_{kk} \tag{4-2}$$

To relate the stress deviator components and stress rate deviator components to the strain rate deviator components, these deviators must first be defined. The stress deviators are defined:

$$\tau_{ij} \equiv \sigma_{ij} - \frac{1}{3}\sigma_{kk}\delta_{ij} \tag{4-3a}$$

(where δ_{ij} is the Kronecker delta). The stress rate deviator components are just defined as the time derivative of the stress deviator components. The strain rate deviators are defined:

$$\dot{\zeta}_{ij} \equiv \dot{e}_{ij} - \frac{1}{3}\dot{e}_{kk}\delta_{ij} \tag{4-3b}$$

These deviators are then substituted into Equations (4-1). The sums of the normal components which are in the resulting equation can be related by Equation (4-2) and cancel out. The remaining terms give a set of equations relating the stress deviators and the stress rate deviators, to the strain rate deviators:

$$\frac{\mu}{\eta}\tau_{ij} + \dot{\tau}_{ij} = 2\mu\dot{\zeta}_{ij} \tag{4-3c}$$

The other step which we will take to simplify the constitutive equations is to apply the Laplace transform. It is important to note that this means that any velocity solutions which we derive, using the Laplace transformed constitutive equations, will have to initially be solved in the Laplace transform domain.

The Laplace transform is defined:

$$\tilde{f}(s) \equiv \int_0^\infty e^{-st} f(t)dt \equiv L\{f(t)\} \tag{4-4a}$$

Here s is the transform variable. The inverse Laplace transform is then defined:

$$f(t) \equiv \int_{c-i\infty}^{c+i\infty} e^{st}\tilde{f}(s)ds \tag{4-4b}$$

Of special interest to our application is the fact that $L\{\frac{\partial f}{\partial t}\} = s\tilde{f}(s) - f(0)$. We can see that this allows us to turn the time derivatives in Equations (4-2) and (4-3c) into algebraic functions of s. This gives us our final simplified form of the visco-elastic constitutive equations. From Equation (4-2) we get

$$s\tilde{\sigma}_{kk} = 3Ks\tilde{e}_{kk} \tag{4-5a}$$

From Equation (4-3c) we get

$$\left[\frac{\mu}{\eta} + s\right]\tilde{\tau}_{ij} = 2\mu s\tilde{\zeta}_{ij} \tag{4-5b}$$

In these equations we have set $\sigma(0)$, $e(0)$, $\tau(0)$, and $\zeta(0)$ equal to zero to simplify the mathematics of our solution process.

4.2.2 Application of correspondence principle

Since we have Laplace transformed the constitutive equations, we must derive our solution for the surface velocity in the Laplace transform domain. Fortunately there exists a relatively simple method for deriving this solution. This method is known as the correspondence principle (Flugge, 1967).

The correspondence principle refers to a correspondence which can be derived between the visco-elastic and the elastic compressible rheological operators. This principle states that the substitution of the visco-elastic operators for the elastic compressible operators, will change the rheology from elastic compressible to visco-elastic, *in any equations which depend on the original constitutive equations.* In the Laplace transform domain, the correspondence is algebraic, since the time derivatives in the visco-elastic operators when Laplace transformed become algebraic functions of s, which simply multiply the other Laplace transformed functions in the equations which are being examined. (The Laplace transform does not affect the elastic compressible operators at all, since these operators are simply constant functions of time, which multiply other varying functions of time.) The correspondence principle allows us to fairly easily determine the Laplace transform of the visco-elastic surface velocity solution, by simply substituting the Laplace transformed

visco-elastic operators for the elastic compressible operators in the Laplace transformed elastic compressible surface velocity solution. (It is of course necessary to first have the elastic compressible surface velocity solution; this solution is derived in Appendix B.)

When the Laplace transformed visco-elastic solution has thus been determined, it must be inverse transformed to give the solution in the time domain. This inverse transform may be difficult, since the substitution of the visco-elastic operators for the elastic operators introduces various functions of the transform variable s into the transformed velocity equations. Since these transformed equations will have functions of s in addition to the operators (i.e., the Laplace transform for propagation of the velocity anomaly), the additional functions of s introduced by the transformed visco-elastic operators will complicate the inverse transform.

The correspondence principle could also be used to find the visco-elastic velocity anywhere within the glacier, or to find the visco-elastic basal shear stress, provided that we had the elastic compressible solutions for these quantities. However, we will only examine the visco-elastic surface velocity in this paper.

4.3 Surface velocity solution for prescribed basal velocity

4.3.1 Prescribed propagating basal velocity

The basal velocity anomalies which are used for the viscous incompressible surface velocity solution (Chapter 2) and the elastic compressible surface velocity solution (see Appendix B), are not propagating as a function of time. The only effect which propagation of the basal anomaly would have on the surface anomaly is to propagate the surface anomaly in a similar manner. The effect of this propagation at the surface can thus be very easily calculated (see Section 2.2.6). However, for a visco-elastic rheology, the propagation speed and the spatial pattern of a given basal velocity anomaly can both quite possibly affect the spatial pattern of the resulting surface velocity anomaly. It is therefore necessary to specify propagating velocity components $u_b(x,t)$ and $v_b(x,t)$ for the basal boundary conditions.

It is easiest to again use the Fourier transform in the solution process (in addition to the Laplace transform which is required for the algebraic use of the correspondence

principle). The Fourier transform is used in Appendix B for the linear elastic velocity solution; it is quite simple to just propagate the Fourier transformed velocity boundary conditions which are used in that appendix. These propagating boundary conditions (in the wave number domain) are:

$$\hat{u}_b(k,t) = \hat{u}_b(k)e^{-i\omega t} \tag{4-6a}$$

$$\hat{v}_b(k,t) = \hat{v}_b(k)e^{-i\omega t} \tag{4-6b}$$

Here $\hat{u}_b(k)$ and $\hat{v}_b(k)$ are the Fourier transforms of the x and y components of the spatially fixed basal velocity anomaly, and $e^{-i\omega t}$ is the term for propagation in the $+x$ direction. The angular frequency is ω; for all wave number components to propagate with a given wave speed w the angular frequency must be proportional to the wave number.

4.3.2 Laplace transform and substitution of visco-elastic rheological operators

We are now prepared to make use of the correspondence principle. We first must substitute the propagating Fourier transformed basal velocity anomaly (Equations (4-6)), for the fixed basal velocity anomaly in the Fourier transformed surface velocity solution for the linear elastic rheology (Equations B-11). We next take the Laplace transform. This gives:

$$\tilde{\hat{u}}_s = \left[\frac{[8-16\nu+8\nu^2+4kH-4\nu kH]e^{-kH} + [8-16\nu+8\nu^2-4kH+4\nu kH]e^{kH}}{[3-4\nu]e^{-2kH}+10-24\nu+16\nu^2+4k^2H^2+[3-4\nu]e^{2kH}}\right]\left[\frac{s-i\omega}{s^2+\omega^2}\right]\hat{u}_b \tag{4-7a}$$

$$+\left[\frac{[4-12\nu+8\nu^2-4kH+4\nu kH]e^{-kH} + [-4+12\nu-8\nu^2-4kH+4\nu kH]e^{kH}}{[3-4\nu]e^{-2kH}+10-24\nu+16\nu^2+4k^2H^2+[3-4\nu]e^{2kH}}\right]\left[\frac{s-i\omega}{s^2+\omega^2}\right]i\hat{v}_b$$

$$\tilde{\hat{v}}_s = \left[\frac{[-4+12\nu-8\nu^2-4kH+4\nu kH]e^{-kH} + [4-12\nu+8\nu^2-4kH+4\nu kH]e^{kH}}{[3-4\nu]e^{-2kH}+10-24\nu+16\nu^2+4k^2H^2+[3-4\nu]e^{2kH}}\right]\left[\frac{s-i\omega}{s^2+\omega^2}\right]i\hat{u}_b \tag{4-7b}$$

$$+\left[\frac{[8-16\nu+8\nu^2-4kH+4\nu kH]e^{-kH} + [8-16\nu+8\nu^2+4kH-4\nu kH]e^{kH}}{[3-4\nu]e^{-2kH}+10-24\nu+16\nu^2+4k^2H^2+[3-4\nu]e^{2kH}}\right]\left[\frac{s-i\omega}{s^2+\omega^2}\right]\hat{v}_b$$

In these equations ν is the elastic compressible Poisson's ratio. (We again note that the Laplace transform does not affect this elastic compressible ratio.) The terms $\hat{u}_b$ and $\hat{v}_b$ are the Fourier transforms of the spatial patterns of the two components of the basal velocity anomaly. The effect of the propagation is seen in the term $\frac{s-i\omega}{s^2+\omega^2}$.

We now need to substitute the Laplace transform of the visco-elastic operator $\bar{\nu}$ which corresponds with the elastic compressible Poisson's ratio. Comparison of Equations (4-5) with Equations (B-5) (from Appendix B) shows that: (a) the elastic compressible bulk modulus K corresponds with K in the Laplace transformed visco-elastic equations, and (b) the elastic compressible shear modulus μ corresponds with the operator $\frac{\mu\eta s}{\mu+\eta s}$ in the Laplace transformed visco-elastic equations. The solution for the Laplace transform of the visco-elastic operator $\bar{\nu}$ then is

$$\bar{\nu} = \frac{3K\mu + 3K\eta s - 2\mu\eta s}{6K\mu + 6K\eta s + 2\mu\eta s} \tag{4-8}$$

This operator is substituted for the elastic compressible Poisson's ratio in Equations (4-7). This substitution will add considerable complexity to these equations. The results of the substitution give us the Laplace transforms of the Fourier transforms of the visco-elastic surface velocity components $\tilde{\hat{u}}_s$ and $\tilde{\hat{v}}_s$.

4.3.3 Inverse Laplace transform of surface velocity

The inverse Laplace transform of the visco-elastic form of Equations (4-7) is not trivial, due to the substitution of the visco-elastic operator $\bar{\nu}$ (which is a function of the transform variable s) for the simple elastic compressible ratio ν (which is not a function of s). Without writing out all the steps involved in solving the inverse transform, it is sufficient to first note that the visco-elastic form of Equations (4-7) can be reduced to the following equations for the visco-elastic surface velocity components $\tilde{\hat{u}}_s$ and $\tilde{\hat{v}}_s$:

$$\tilde{\hat{u}}_s = \left[\frac{\alpha_1+\beta_1 s+\gamma_1 s^2}{a+bs+cs^2}\right]\left[\frac{s-i\omega}{[s+i\omega][s-i\omega]}\right]\hat{u}_b + \left[\frac{\alpha_2+\beta_2 s+\gamma_2 s^2}{a+bs+cs^2}\right]\left[\frac{s-i\omega}{[s+i\omega][s-i\omega]}\right] i\hat{v}_b \tag{4-9a}$$

$$\tilde{\hat{v}}_s = \left[\frac{\alpha_4+\beta_4 s+\gamma_4 s^2}{a+bs+cs^2}\right]\left[\frac{s-i\omega}{[s+i\omega][s-i\omega]}\right] i\hat{u}_b + \left[\frac{\alpha_3+\beta_3 s+\gamma_3 s^2}{a+bs+cs^2}\right]\left[\frac{s-i\omega}{[s+i\omega][s-i\omega]}\right]\hat{v}_b \tag{4-9b}$$

The coefficients α, β, γ, a, b, and c are explicitly written out in Appendix C. These coefficients are functions of the non-dimensional wave number kH, the bulk modulus K, the shear modulus μ, and the dynamic viscosity η. Equations (4-9) are in a form which can be inverse Laplace transformed (see for example Churchill, 1971); the inverse Laplace transforms give the solutions for the Fourier transformed surface velocity components $\hat{u}_s$

and $\hat{v}_s$. These solutions will each have four terms; however, two of the terms for each solution decay exponentially with time. These two terms are transient terms which arise from the fact that our Laplace transforms involved the assumptions that the initial stress and strain were equal to zero; thus we may ignore these terms. The third term for each solution is conveniently equal to zero. This leaves the only the final terms as the solutions for the Fourier transformed surface velocity components:

$$\hat{u}_s = \left[\frac{a\alpha_1 + [-a\gamma_1+b\beta_1-c\alpha_1]\omega^2 + c\gamma_1\omega^4}{a^2 + [-2ac+b^2]\omega^2 + c^2\omega^4}\right]\hat{u}_b e^{-i\omega t} \tag{4-10a}$$

$$+ \left[\frac{[-a\beta_1+b\alpha_1]\omega + [-b\gamma_1+c\beta_1]\omega^3}{a^2 + [-2ac+b^2]\omega^2 + c^2\omega^4}\right] i\hat{u}_b e^{-i\omega t}$$

$$- \left[\frac{[-a\beta_2+b\alpha_2]\omega + [-b\gamma_2+c\beta_2]\omega^3}{a^2 + [-2ac+b^2]\omega^2 + c^2\omega^4}\right] \hat{v}_b e^{-i\omega t}$$

$$+ \left[\frac{a\alpha_2 + [-a\gamma_2+b\beta_2-c\alpha_2]\omega^2 + c\gamma_2\omega^4}{a^2 + [-2ac+b^2]\omega^2 + c^2\omega^4}\right] i\hat{v}_b e^{-i\omega t}$$

and

$$\hat{v}_s = -\left[\frac{[-a\beta_4+b\alpha_4]\omega + [-b\gamma_4+c\beta_4]\omega^3}{a^2 + [-2ac+b^2]\omega^2 + c^2\omega^4}\right] \hat{u}_b e^{-i\omega t} \tag{4-10b}$$

$$+ \left[\frac{a\alpha_4 + [-a\gamma_4+b\beta_4-c\alpha_4]\omega^2 + c\gamma_4\omega^4}{a^2 + [-2ac+b^2]\omega^2 + c^2\omega^4}\right] i\hat{u}_b e^{-i\omega t}$$

$$+ \left[\frac{a\alpha_3 + [-a\gamma_3+b\beta_3-c\alpha_3]\omega^2 + c\gamma_3\omega^4}{a^2 + [-2ac+b^2]\omega^2 + c^2\omega^4}\right] \hat{v}_b e^{-i\omega t}$$

$$+ \left[\frac{[-a\beta_3+b\alpha_3]\omega + [-b\gamma_3+c\beta_3]\omega^3}{a^2 + [-2ac+b^2]\omega^2 + c^2\omega^4}\right] i\hat{v}_b e^{-i\omega t}$$

4.4 Properties of surface velocity solution

4.4.1 Choice of adjustable parameters

There are several parameters which we might wish to vary in order to look at the properties of the visco-elastic surface solution. The first of these is the non-dimensional wave number kH. We will look at our solutions as a function of the logarithm (to the base 10) of the non-dimensional wavelength λ/H, where this wavelength is related to the wave number in the usual manner ($\lambda/H=2\pi/kH$).

The other parameters which the velocity solutions are functions of are K, μ, and $\eta\omega$. (This can be seen from the full algebraic solution, which the reader has been spared.) All of these have units of stress. In fact, each of the terms in the numerators and the denominator of the surface velocity solution (e.g., $a\alpha_1$) come out as units of stress to the eighth power. (This means that the particular stress units used do not matter, provided that they are the same for K, μ, and $\eta\omega$.) *Thus the equations are dimensionless quantities multiplying the Fourier transformed basal velocity components $\hat{u}_b$ and $\hat{v}_b$.* We can vary K, μ, and $\eta\omega$ to change the relative elastic and viscous properties of the rheology.

For glacier ice, an acceptable value for the elastic compressible Poisson's ratio is about one third. If we set the bulk modulus K=1, Poisson's ratio will be correct for the shear modulus μ=0.375. The term $\eta\omega$ can then be varied over a wide range. Relatively low values of $\eta\omega$ correspond with a relatively viscous rheology; while relatively high values of $\eta\omega$ correspond with a relatively elastic rheology. At intermediate values of $\eta\omega$ we would expect to see the most interesting visco-elastic effects. The importance of these visco-elastic effects will also depend on the wavelength or wave number.

4.4.2 Magnitude and phase of forward transfer functions

The solutions for $\hat{u}_s$ and $\hat{v}_s$ (Equations (4-10) each have four terms: a real and an imaginary part multiplying both $\hat{u}_b$ and $\hat{v}_b$. These terms which multiply $\hat{u}_b$ and $\hat{v}_b$ are similar to the forward transfer functions of Chapter 2; however, the phase of the transfer for the visco-elastic rheology is more complicated, since there are both real and imaginary parts for each visco-elastic transfer function.

To calculate the magnitude and the phase of the visco-elastic transfer functions, we write Equations (4-10) in a simplified form. Simplifying Equation (4-10a):

$$\hat{u}_s = [A_1+iA_2]\hat{u}_b e^{-i\omega t} + [A_3+iA_4]\hat{v}_b e^{-i\omega t} \tag{4-11a}$$

Simplifying Equation (4-10b):

$$\hat{v}_s = [A_5+iA_6]\hat{u}_b e^{-i\omega t} + [A_7+iA_8]\hat{v}_b e^{-i\omega t} \tag{4-11b}$$

The magnitudes, and phase leads (in space), then are as follows:

$$|T_s^{uu}| = \sqrt{A_1^2+A_2^2}\ , \qquad \delta = \tan^{-1}\left[\frac{A_2}{A_1}\right] \tag{4-12a}$$

$$|T_s^{vu}| = \sqrt{A_3^2+A_4^2}\ , \qquad \delta = \tan^{-1}\left[\frac{A_4}{A_3}\right] \tag{4-12b}$$

$$|T_s^{uv}| = \sqrt{A_5^2+A_6^2}\ , \qquad \delta = \tan^{-1}\left[\frac{A_6}{A_5}\right] \tag{4-12c}$$

$$|T_s^{vv}| = \sqrt{A_7^2+A_8^2}\ , \qquad \delta = \tan^{-1}\left[\frac{A_8}{A_7}\right] \tag{4-12d}$$

The values of the phase leads δ are all between $-\pi$ and 0 (which means that *they are actually phase lags in space, which correspond to phase leads in time.* The magnitude and phase for each transfer function will depend on the wavelength or wave number, and the visco-elastic parameters. Fixing Poisson's ratio at $\nu = 1/3$, we then vary $\log(\lambda/H)$ and $\log(\eta\omega)$. The resulting plots of the transfer functions are shown in Figures 4-1.

Not surprisingly, we see that the magnitude and phase of the transfer functions for the relatively viscous rheology ($\log(\eta\omega) = -2.8$) are similar to those for the viscous transfer functions of Chapter 2; and the magnitude and phase of the transfer functions for the relatively elastic rheology ($\log(\eta\omega) = 1.2$) are similar to those for the elastic transfer functions of Appendix B. For the relatively visco-elastic rheology ($\log(\eta\omega) = -0.8$, which corresponds to $\omega = 10\ d^{-1}$ for glacier ice), the magnitude of the transfer functions is generally between the magnitudes for the viscous and elastic rheologies, which is not in any case much of a variation.

It is the phase of the transfer function T_s^{uu} which appears to be the most interesting for the relatively visco-elastic rheology, since there is a wide variation in the phase lag of

this transfer function when the visco-elastic rheology is compared to either the viscous or the elastic rheologies. This variation in the phase lag occurs in the range $0.6 \leq \log(\lambda/H) \leq 0.8$. The variation in the phase lag of the other transfer functions (as compared to the elastic or viscous rheologies) is not very pronounced. In fact, maximizing the variation in the phase lag for the transfer function T_s^{uu} was the criterion for choosing the value of $\log(\eta\omega)$ which would maximize the effects of the visco-elastic rheology (with the conclusion that a value of $\log(\eta\omega) = -0.8$ maximized these visco-elastic effects). However, we note that the magnitude of T_s^{uu} is relatively small for the wavelengths which have the large variation in the phase lag. This means that any interesting visco-elastic effects are not likely to be very pronounced.

4.4.3 Surface velocity solution for basal velocity front

To test for interesting visco-elastic effects, we will prescribe a basal velocity anomaly which consists of a "front" in the longitudinal velocity component u_b. The Fourier transform of this anomaly will include the wavelengths of interest. The transfer function T_s^{uu} can then be used to calculate the longitudinal component of the surface velocity anomaly u_s, thus testing the most likely situation for which we expect interesting visco-elastic effects to occur. We will also calculate the normal component of the surface velocity anomaly v_s. The basal velocity anomaly and resulting surface velocity anomaly are plotted as the solid lines in Figure 4-2.

This plot can be compared with the dashed lines in Figure 4-2, which are plots of the surface velocity anomaly using the linear viscous rheology (similar to the solid lines of Figure 2-4). The comparison shows that the amplitude of the surface velocity components for the visco-elastic rheology is slightly less than the amplitude of the same components for the linear viscous rheology. In addition, there is a slight shift in the pattern of u_s near the zero crossing, above the basal velocity front. However, these can not really be viewed as major differences between the results for the two different rheologies. This lack of major differences is significant, since the visco-elastic calculations in this section used a value of $\log(\eta\omega) = -0.8$, which we concluded was the Maxwell rheology which would give the most pronounced visco-elastic effects (when using a value of Poisson's ratio $\nu = 1/3$).

4.5 Discussion

The Maxwell visco-elastic rheology which we have used produces interesting complexity in the phase of the transfer function T_s^{uu}. However, the previous section showed that the calculated surface velocity, for a basal velocity front in the component u_b, is not much different as compared to the case for the linear viscous rheology. We can reasonably conclude that other forms for a basal velocity anomaly would also not have much difference between the visco-elastic and the linear viscous rheologies, since the basal velocity front is a fairly extreme case. The reason for the lack of difference between the results for the two rheologies (given the variation in the phase of the transfer function T_s^{uu}), is that the magnitude of T_s^{uu} is small when the phase variation is pronounced. The other transfer functions do not have significant differences when the two rheologies are compared.

It is possible that basal velocity anomalies could be prescribed for which the visco-elastic effects in the calculated surface velocity anomaly would be pronounced, although experimenting with various reasonable forms for basal velocity anomalies did not yield this result. It is also possible that visco-elastic effects might be important if a different visco-elastic rheology were used. However, the Maxwell rheology does show some of the possible visco-elastic effects in the transfer functions. The example of a calculated surface velocity using the Maxwell visco-elastic rheology suggests that the differences between linear viscous and visco-elastic rheologies may in most cases be fairly minor.

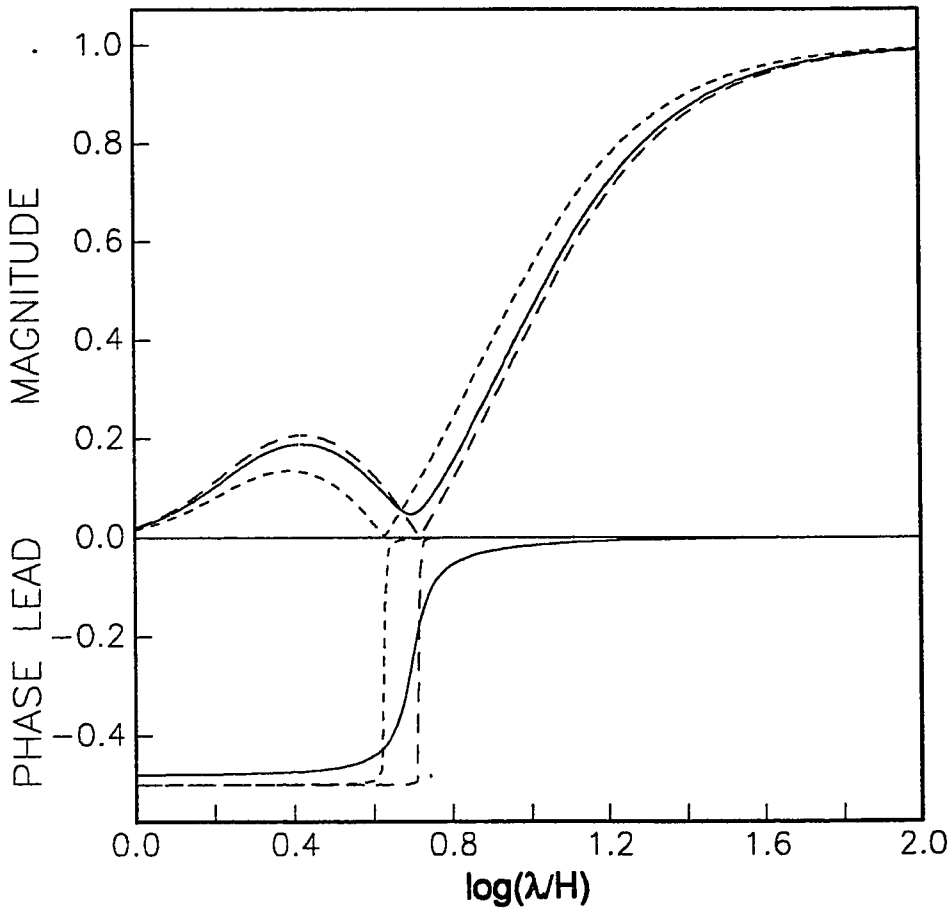

Figure 4-1a. Magnitude and normalized phase lead of forward transfer function T_z^{uu} for visco-elastic rheology, for three different values of log(ηω): long dashed line, log(ηω) = –2.8 ("viscous"); solid line, log(ηω) = –0.8 ("visco-elastic"); and short dashed line, log(ηω) = 1.2 ("elastic"). Poisson's ratio ν = 1/3.

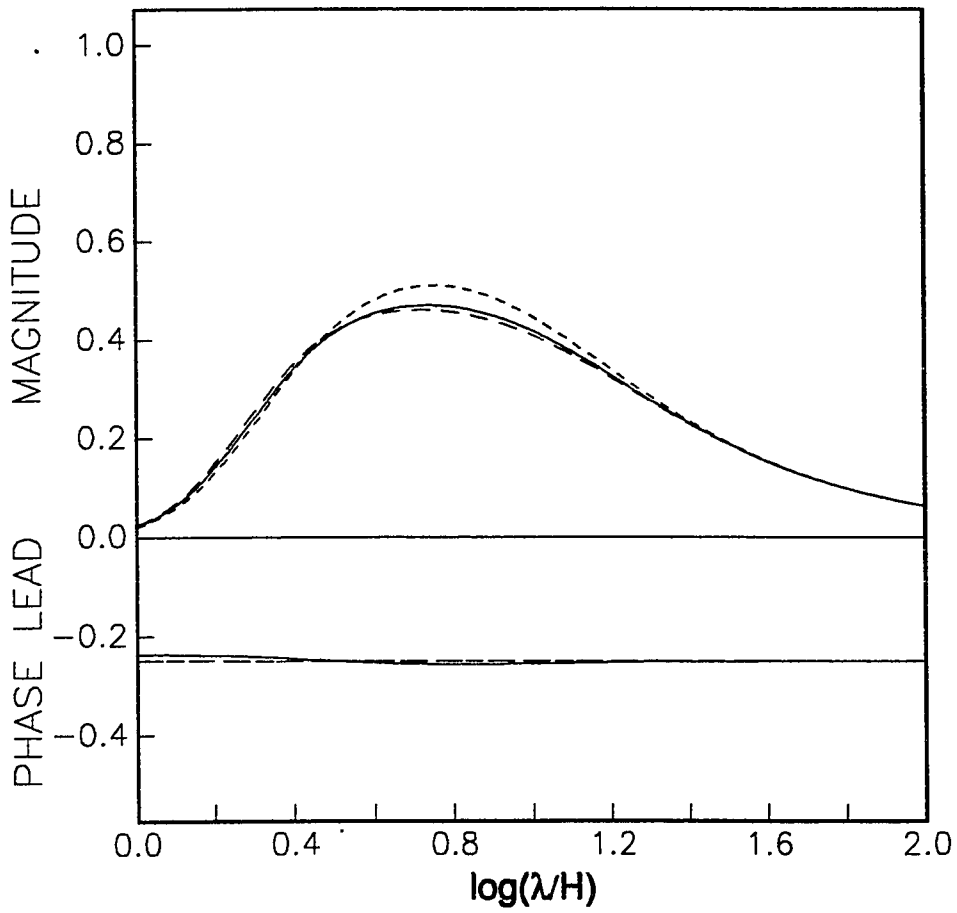

Figure 4-1b. Magnitude and normalized phase lead of forward transfer function T_z^{vu} for visco-elastic rheology, for three different values of log(ηω): long dashed line, log(ηω) = –2.8 ("viscous"); solid line, log(ηω) = –0.8 ("visco-elastic"); and short dashed line, log(ηω) = 1.2 ("elastic"). Poisson's ratio ν = 1/3.

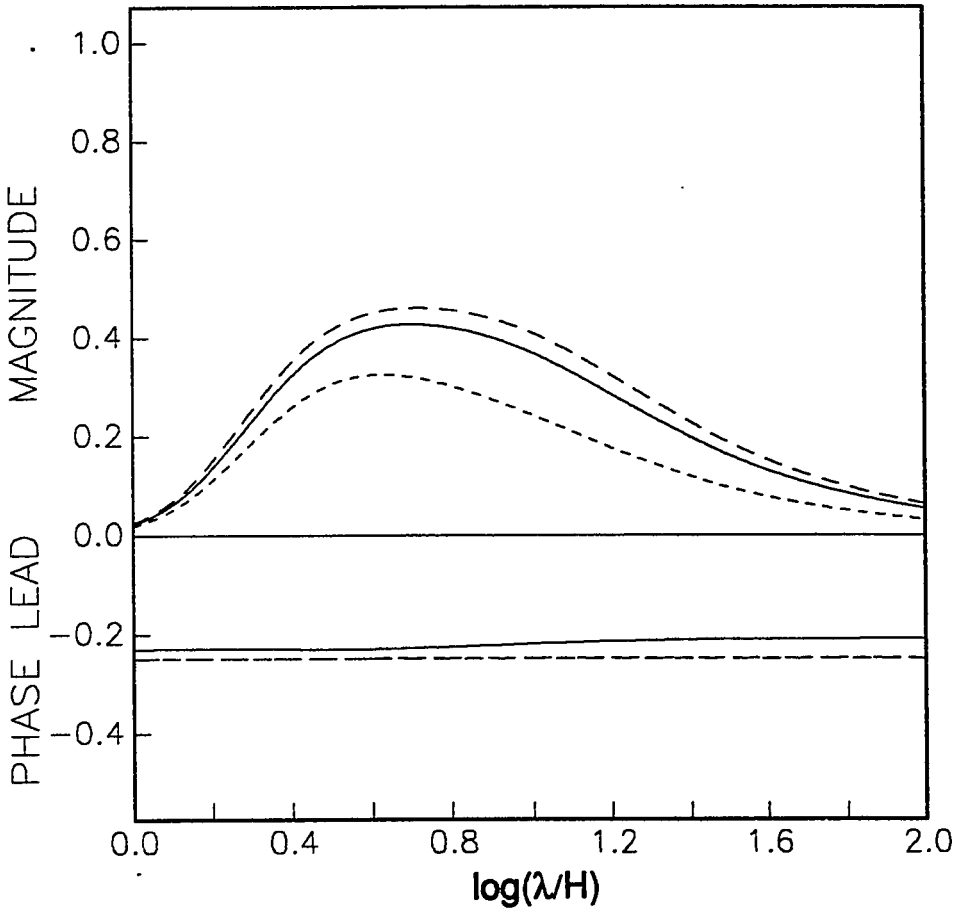

Figure 4-1c. Magnitude and normalized phase lead of forward transfer function T_z^{uv} for visco-elastic rheology, for three different values of log(ηω): long dashed line, log(ηω) = –2.8 ("viscous"); solid line, log(ηω) = –0.8 ("visco-elastic"); and short dashed line, log(ηω) = 1.2 ("elastic"). Poisson's ratio ν = 1/3.

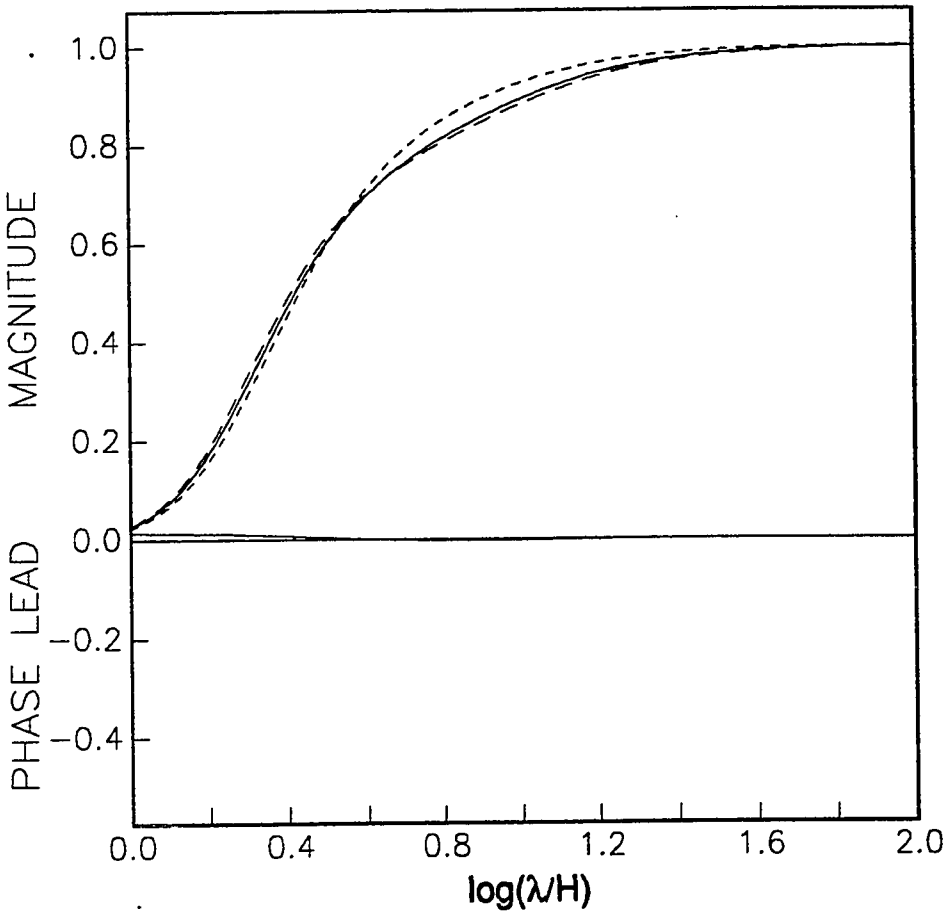

Figure 4-1d. Magnitude and normalized phase lead of forward transfer function T_s^{vv} for visco-elastic rheology, for three different values of log(ηω): long dashed line, log(ηω) = –2.8 ("viscous"); solid line, log(ηω) = –0.8 ("visco-elastic"); and short dashed line, log(ηω) = 1.2 ("elastic"). Poisson's ratio ν = 1/3.

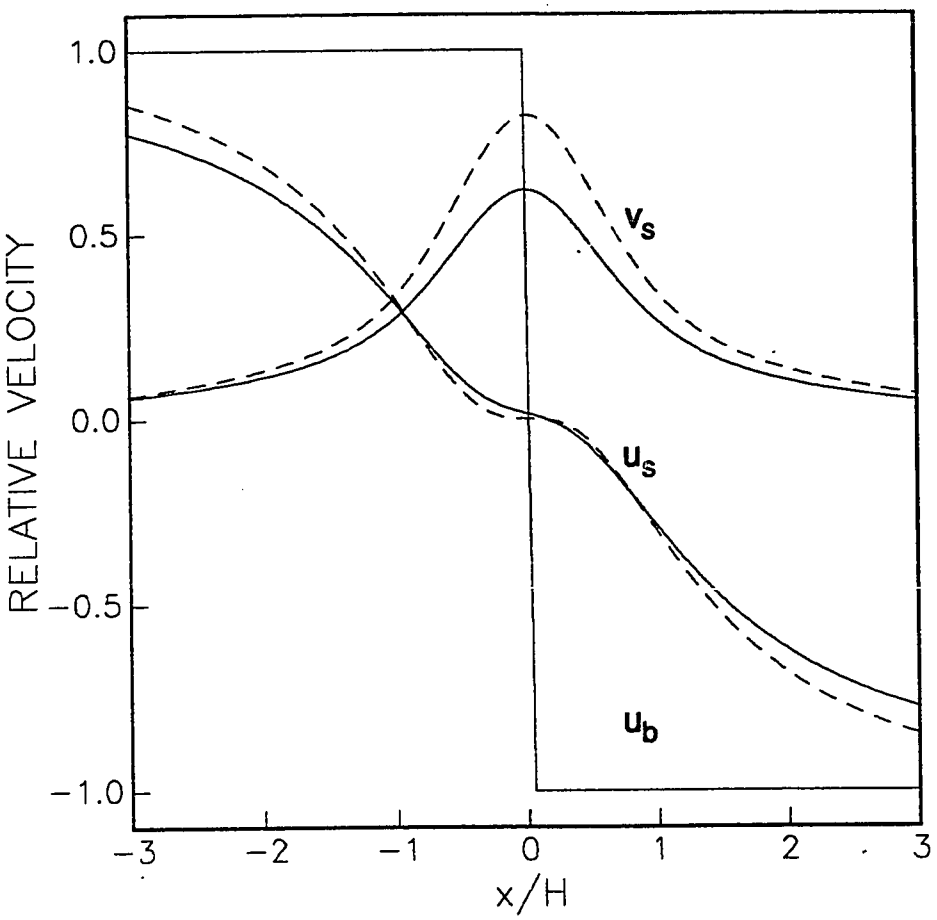

Figure 4-2. Basal and surface velocity anomalies for a step or sharp front in u_b, for visco-elastic rheology. Solid lines: $\log(\eta\omega) = -0.8$, $\nu = 1/3$. Dashed lines: linear viscous solution.

CHAPTER 5

NON-LINEAR (POWER LAW) FORWARD SOLUTIONS

5.1 Rheology and flow law

The previous chapters have all considered linear viscous or visco-elastic rheologies, which allowed analytic solutions for the given geometry and boundary conditions. We now wish to consider a power law rheology, which is more realistic for glacier ice. This power law rheology for glacier ice has been studied by many workers (Nye, 1953; Glen, 1955; Shreve and Sharp, 1970; Raymond, 1973) and is usually referred to as Glen's flow law. The form of this flow law is

$$\dot{e}_{ij} = A\tau^{n-1}\tau_{ij} \tag{5-1a}$$

Here $\dot{e}_{ij}$ is the strain rate tensor, A is the inverse viscosity parameter, τ is the second invariant of the stress deviator tensor, and τ_{ij} is the stress deviator tensor. The parameter n is the exponent in the flow law and is generally considered to have a value of about 3 (Paterson, 1981). The flow law can also be written using a viscosity parameter B, which is defined $B \equiv [1/2]A^{-1/n}$. This form of the flow law is

$$\tau_{ij} = \frac{2B^n}{\tau^{n-1}}\dot{e}_{ij} \tag{5-1b}$$

Thus we can define an effective viscosity of the ice η^{eff}:

$$\eta^{eff} \equiv \frac{2B^n}{\tau^{n-1}} \tag{5-2}$$

It is very important to note that this effective viscosity is dependent on the stress distribution within the ice. Both the steady-state and anomalous velocity distributions can affect this stress distribution and thus affect the effective viscosity. The effective viscosity in turn affects the flow for both the steady-state and anomalous velocity distributions. *Therefore the steady-state and anomalous flows are coupled, and in general can not be separated.* This coupling is examined in more detail in Section 5.4.

With the power law rheology, analytic solutions can be determined only for very

simple problems. The more complicated problems which we wish to consider require the use of numerical models which are solved on a computer. The specific model which we are going to use is a finite element model developed by Raymond (1978). Additional details of this model are in Raymond and others (1986), and Pfeffer (1987). The finite element model, given the proper boundary conditions, calculates the velocity and stress distributions throughout the modelled section.

5.2 Geometry, boundary conditions, and model parameters

5.2.1 Geometry and boundary conditions

The geometry which we wish to use with the finite element model is a planar slab (see Figure 2-1). However, the model can not directly consider a slab of infinite length. For the boundary conditions which we wish to apply, this difficulty can be avoided by specifying "periodic boundary conditions" at the ends of the model.

This is done by modelling only a small longitudinal section of the planar slab. The periodic boundary conditions mean that the section is assumed to repeat itself in an infinite series. This means that the velocity and stress at one end of the modelled section must be identical to the velocity and stress at the other end. Given the basal and surface boundary conditions, the finite element model calculates a solution which satisfies this requirement that the velocity and stress at the ends be equal. Consideration of this method shows that it is entirely analagous to the assumed periodicity of a fast Fourier transform.

The basal and surface boundary conditions are similar to those of Chapters 2 and 4. A velocity anomaly is prescribed at the bed, with longitudinal component u_b and normal component v_b. (Although the steady-state and anomalous solutions are in general coupled, a solution for steady-state basal sliding (not changing in the x direction) can be linearly superposed with other solutions, because steady-state sliding does not affect the strain-rate and thus does not affect the effective viscosity. This means that steady-state basal sliding need not be considered in the boundary conditions. See Section 5.4.2.) The surface is assumed to be stress free, except for atmospheric pressure. Since this surface stress boundary condition is built in to the finite element model, the only boundary condition which must be explicitly input to the model is the anomalous basal velocity.

5.2.2 Model parameters

The first model parameters involve the grid of the finite element model. The organization of the nodal numbering system, and the coordinates of each node, must be specified. For the periodic boundary conditions, an example of the nodal numbering system is shown in Figure 5-1. The coordinates of the nodes will depend on the problem which we are trying to model. It is convenient to non-dimensionalize these coordinates by the ice thickness H; thus the y-coordinate of the surface nodes (and the thickness of the ice) is equal to 1. The basal nodes have a y-coordinate of 0. The intermediate nodes between the surface and the bed have y-coordinates with values between 0 and 1. The domain of the x-coordinates depends on the length of the slab being modelled.

The parameters which control the ice rheology must also be specified. For our model we will specify incompressibility; this means that the non-linear equivalent of Poisson's ratio is equal to 0.5. The viscosity parameter B must be chosen; it is convenient to choose a value of 0.5 (for justification of this see Section 5.3.3). A value of 3 for the exponent n in the flow law will be used, which is intermediate in the range of accepted values. These choices of B and n give a value of one for the inverse viscosity parameter A.

The density of the ice ρ, and the body force components per unit mass (longitudinal component $g\sin\gamma$ and normal component $-g\cos\gamma$, where g is the acceleration of gravity and γ is the bed slope angle) must be specified. We will use $\rho = 900\ kg\ m^{-3}$ and $g = 9.8\ N\ kg^{-1}$; the bed slope angle γ will vary depending on the specific situation which we are modelling. Along with the boundary conditions, these will control the total stress distribution within the ice and the resulting deformation and velocity.

Finally, since the finite element model works by an iterative technique, convergence criteria must be established. This is done by looking at the value of a parameter ε which measures the difference between velocity solutions for successive iterations. If ε is less than a chosen small value, the solution is considered to be converged. A maximum number of iterations is also specified.

5.3 Non-linear transfer functions for harmonic basal velocity anomalies

5.3.1 No bed slope

We will now calculate non-linear "transfer functions" which will be a direct comparison with the linear transfer functions of Chapter 2. Since we expect that the steady-state and anomalous flows for the non-linear rheology will be coupled, the non-linear transfer functions will first be calculated for the case with no steady-state flow. This is done by specifying no bed slope (e.g., no longitudinal component of the body force), and no steady-state basal sliding. The basal boundary condition will be a prescribed harmonic velocity anomaly, either in the longitudinal or normal component. The amplitude of these anomalies will be set equal to one. The output from the finite element model will then give the velocity at all the surface nodes, which gives the longitudinal component of the surface velocity u_s and the normal component of the surface velocity v_s.

To calculate the transfer functions, the finite element model is run for basal anomalies with a series of different dimensionless wavelengths λ/H. For each of these wavelengths, the resulting surface velocity components will have amplitudes which are some fraction of the basal amplitude of one (the wavelength at the surface will be the same as the wavelength at the base). These fractional surface amplitudes are then the magnitude of the non-linear transfer functions. We expect that either a longitudinal or a normal velocity component at the bed will cause both a longitudinal and a normal component at the surface, and that the relative phases between the basal and the surface components will be similar to the relative phases for the linear rheology.

When these non-linear transfer functions are calculated, it turns out that our assumptions about the cross-component effects and the relative phases are correct. Thus when we prescribe a basal velocity anomaly in the longitudinal component u_b, this results in surface velocity anomalies for both the longitudinal component u_s and the normal component v_s. The phase of u_s is either the same as the phase of u_b or shifted 180° (which is equivalent to a sign change). The phase of v_s lags the phase of u_b by 90° in space (which is equivalent to a 90° phase lead in time for propagation in the $+x$ direction).

If we prescribe a basal velocity anomaly in the normal component v_b, this results in surface velocity anomalies for both the u_s and v_s. The phase of v_s is the same as the phase

of v_b. The phase of u_s lags the phase of v_b by 90^o in space.

Thus the non-linear transfer functions follow a similar pattern to the linear transfer functions of Chapter 2. We can therefore plot these non-linear transfer functions in a manner similar to the linear transfer functions. Both the linear and the non-linear transfer functions are plotted in Figure 5-2.

In this figure, comparison of the linear transfer functions with the non-linear transfer functions (with no bed slope) shows systematic differences. The main differences are that the magnitudes of the non-linear transfer functions T_s^{uu} and T_s^{uv} are considerably less than the magnitudes of the corresponding linear transfer functions; while the magnitudes of the non-linear transfer functions T_s^{vu} and T_s^{vv} are similar to the magnitudes of the corresponding linear transfer functions. Thus for the non-linear rheology there is less effect at the surface than with the linear rheology for a given longitudinal harmonic basal anomaly u_b. The effect at the surface for a given normal harmonic basal velocity anomaly v_b is similar for both the linear and the non-linear rheologies. Note that for the non-linear rheology, the transfer function T_s^{uv} is less than the transfer function T_s^{vu}, instead of being equal as with the linear rheology. Therefore these transfer functions are plotted separately in Figure 5-2.

Furthermore, the boundaries between the various scales (as described in Chapter 2) for longitudinal harmonic basal velocity anomalies are shifted towards longer wavelengths. In particular, the boundary between the intermediate and the long scales may be viewed as being shifted considerably towards longer wavelengths, since in no case which is tested is T_s^{uu} near to one in value, for the non-linear rheology.

These non-linear effects are a bit difficult to explain. However, it is intuitively obvious that the deformation and associated stresses resulting from a basal velocity anomaly should be greatest near the bed, and decrease towards the surface. (Balise and Raymond, 1985). This was well-shown for the linear rheology of Chapter 2. Since the effective viscosity (Equation (5-1)) depends on the stress distribution, we can see that the effective viscosity will be lowest near the bed and higher towards the surface. We expect that this will tend to even further decrease the surface effects of a basal anomaly, as is in fact the case for a longitudinal basal velocity anomaly u_b. However, the surface effects for a normal basal velocity anomaly are not decreased, which is somewhat counter-intuitive. The only explanation for this might be due to the gradient of the effective viscosity tending to

be in the normal direction (from the bed towards the surface), with the magnitude of this gradient being greatest near the bed. This could reasonably result in a damping of longitudinal flows near the bed, while normal flows near the bed would not be similarly damped, and might even be decreased less than the decrease which occurs with no effective viscosity gradient.

5.3.2 Sloped bed

The question now arises of what effect a steady-state velocity distribution will have on the non-linear transfer functions. Since we expect that steady-state basal sliding will not affect the anomalous surface motion which results from a basal velocity anomaly, we will instead examine the effects of steady-state deformation within the ice. This can be modelled by specifying a sloped bed for the planar slab. This means that there will be a longitudinal component of the body force (due to gravity) acting on the ice; thus, there will be steady-state deformation in the ice and a steady-state longitudinal velocity component which increases towards the surface.

Specifically, we will prescribe a longitudinal component for the body force, with the geometry and the coordinate system being unchanged. This is equivalent to having a sloped bed. We will then prescribe a basal velocity anomaly only (with no steady-state sliding). This gives a combination of deformation within the ice due to both the steady-state longitudinal body force and the anomalous basal velocity. This allows us to study the effect of a sloped bed (with the associated longitudinal body force) on the non-linear transfer functions, and to compare this with the case for no bed slope which was calculated in the previous section.

The non-linear transfer functions for a sloped bed are plotted in Figure 5-3. (The non-linear transfer functions for the case with no bed slope are also plotted for comparison.) Inspection of this figure shows that the transfer functions T_s^{uu} and T_s^{uv} are further decreased in magnitude for a sloped bed, as compared to the case of the transfer functions with no bed slope. The boundary between the intermediate and the long scales (as mentioned in the previous section) is shifted towards even longer wavelengths. The transfer function T_s^{vu} is also decreased in magnitude, but is still greater than T_s^{uv}. Surprisingly, the transfer function T_s^{vv} increases in magnitude.

The analysis of these effects due to the interaction of a steady-state deformation with an anomalous velocity depends on the effect on the effective viscosity of the steady-state and anomalous stress distributions. A detailed analysis of these interactions is done in Section 5.4.

5.3.3 Important dimensionless numbers

Experimenting with various combinations of the input parameters for the finite element model allows the determination of a few simple dimensionless numbers, for a harmonic basal velocity anomaly. We first specify a given model grid with given coordinates for the nodes. We then choose either a longitudinal or a normal basal velocity anomaly. These anomalies have the form:

$$u_b = U_b \sin kx \tag{5-3a}$$

$$v_b = V_b \sin kx \tag{5-3b}$$

Here U_b and V_b are the respective amplitudes of the longitudinal and normal basal velocity anomalies.

With these choices, we can then determine the important dimensionless numbers. A given set of these dimensionless numbers will then always result in a certain dimensionless surface velocity anomaly, no matter how the constituents of the dimensionless numbers are varied. (The surface velocity anomaly is non-dimensionalized by dividing it by the amplitude of the basal velocity anomaly).

The most obvious of the dimensionless numbers is the exponent n in the flow law. If this exponent is changed, the surface velocity effects from a basal velocity anomaly change, since changing n changes the rheology and the effective viscosity.

The second important dimensionless number is the dimensionless wavelength of the basal velocity anomaly λ/H. Varying this wavelength changes the surface effects since a different transfer function value is used. This is obvious given the plots for the transfer functions (Figures 5-2 and 5-3).

The last important dimensionless number is not so obvious. We know that we have not yet considered in this section the viscosity parameter B and the basal shear stress $\rho g H \sin\gamma$. It turns out that if we combine these, the flow law exponent n, and the amplitude

of the harmonic basal velocity anomaly (U_b or V_b), gives us the third dimensionless number. This dimensionless number is the ratio of the amplitude of the basal velocity anomaly, to the theoretical steady-state surface deformation velocity. The theoretical steady-state surface deformation velocity is simply the (longitudinal) surface velocity which would exist if there were no basal velocity anomaly and no steady-state basal sliding. This surface deformation velocity is due to the component of gravity which is parallel to the bed and surface (the longitudinal component of the body force), and occurs only with a sloped bed. This velocity is calculated in many references. We will denote it as u_s^d:

$$u_s^d = \frac{2A}{n+1} H[\rho g H \sin\gamma]^n \tag{5-4}$$

For a longitudinal basal velocity anomaly, our dimensionless number is then U_b/u_s^d. For a normal basal velocity anomaly, our dimensionless number is V_b/u_s^d. No matter what the constituent parameters of this dimensionless number are, experimenting with the finite element model shows that the dimensionless surface velocity effects do not change if this dimensionless number U_b/u_s^d or V_b/u_s^d does not change (provided that the other dimensionless numbers and the grid system and nodal coordinates do not change). In particular, the value chosen for the viscosity parameter B is not important, as long as it results in a reasonable value of the ratio U_b/u_s^d or the ratio V_b/u_s^d.

5.3.4 Limited validity of non-linear transfer functions

It would be convenient if the non-linear transfer functions, which are a function of wavelength (or wave number), could be applied to any Fourier transformed basal velocity anomaly. This would be similar to the application of the linear transfer functions of Chapter 2, and would allow the determination of the Fourier transformed surface velocity, which could then be inverse Fourier transformed. However, a little thought shows that this process is not valid for the non-linear transfer functions. This is true because in a Fourier analysis, motion at any wave number affects the effective viscosity, thus changing the motion at other wave numbers and in effect changing the transfer functions for these other wave numbers. The non-linear transfer functions were calculated only for motion at any single wave number, and are therefore only valid for motion at any single wave number. To calculate the surface effects of a basal velocity anomaly which has harmonic components at various different wave numbers, it is necessary to run the finite element model

directly for that specified basal anomaly.

Although the non-linear transfer functions are not very useful for directly analyzing the surface effects of complicated basal velocity anomalies, these transfer functions are useful for studying the general effects of the non-linear rheology. This has been briefly examined in the previous sections and will be studied in more detail in the following section.

5.4 Coupling of steady-state and anomaly flows

5.4.1 Effect of anomaly flow on steady-state flow

We know that the steady-state and anomalous flows are coupled, since they both affect the effective viscosity η^{eff}. We have briefly examined the effect of a steady-state deformation (due to gravity and a sloped bed) on the anomalous non-linear transfer functions; now we will examine the effect of the velocity anomalies on the steady-state deformation.

This can be done by specifying various angles γ for the bed slope in combination with various prescribed basal velocity anomalies. We will use harmonic anomalies, since these are easiest to systematically describe. Anomalies in both the longitudinal and the normal components of the basal velocity will be used.

The steady-state deformation due to gravity and the sloped bed results in the theoretical longitudinal surface velocity u_s^d; there is no steady-state normal component to the surface velocity. We will compare this theoretical surface velocity, with the mean of the longitudinal component of the actual surface velocity which occurs when a basal anomaly (with a mean of zero) interacts with steady-state deformation. This mean of the longitudinal component of the actual surface velocity will be denoted as $\overline{u}_s$. This comparison can be described by a dimensionless ratio which is $\overline{u}_s/u_s^d$. This ratio gives the actual mean surface velocity, as a fractional multiple of the surface deformation velocity (due to the sloped bed) which would occur with no basal velocity anomaly.

Experimenting with various combinations of parameters shows that the dimensionless numbers detailed in Section 5.3.3 are also the important numbers for this case. We therefore set n=3, choose a dimensionless wavelength λ/H, and then vary the ratio U_b/u_s^d or the ratio V_b/u_s^d. The results of these calculations are plotted in Figure 5-4.

This figure shows that in all cases the ratio $\overline{u}_s/u_s^d$ is equal to or greater than one. This occurs because the basal velocity anomalies result in an anomalous stress distribution in the ice, which decreases the effective viscosity, as compared to the effective viscosity which would exist with only steady-state deformation. This can be referred to as "strain-rate softening". This strain-rate softening allows greater deformation from the gravitational component which is parallel to the sloped bed. This causes a greater mean surface velocity than that which would occur with no velocity anomaly.

As the ratios U_b/u_s^d or V_b/u_s^d are increased, the resulting ratio $\overline{u}_s/u_s^d$ also increases. This is because as the velocity anomaly becomes a greater portion of the total velocity distribution, the proportion of the stress distribution due to the velocity anomaly increases, resulting in proportionally greater strain-rate softening. This allows proportionally greater deformation due to gravity, and results in a greater mean surface velocity as compared to the surface velocity which would occur with a lower magnitude velocity anomaly.

If we vary the dimensionless wavelength, Figure 5-4 shows that shorter wavelengths result in a greater mean surface velocity. Thus the strain-rate softening (with a constant value for the dimensionless number U_b/u_s^d or V_b/u_s^d) is greater for shorter wavelength anomalies. This is to be expected, since shorter wavelength anomalies result in higher stresses in the ice. Of interest are the details that at short wavelengths, the strain-rate softening is greater for a normal basal velocity anomaly than for a longitudinal basal velocity anomaly; while at long wavelengths, the strain-rate softening is less for a normal basal velocity anomaly than for a longitudinal basal velocity anomaly. No simple explanation is apparent for these details.

The figure also shows that there is very little strain-rate softening when the ratio U_b/u_s^d or V_b/u_s^d is less than or equal to 0.2 (i.e., for this value of U_b/u_s^d or V_b/u_s^d the value of the ratio $\overline{u}_s/u_s^d$ is very close to one). For ratios greater than 0.2, the increase in the strain-rate softening is somewhat linear. No obvious explanation has been identified for this somewhat linear relation.

5.4.2 Effect of steady-state flow on anomaly flow

The effect of a steady-state flow on the anomaly flow has been briefly examined in Section 5.3.2. We will now examine in more detail how the deformation due to gravity and a sloped bed affects the anomalous velocity distribution.

This deformation under the force of gravity will be greatest near the bed and decrease towards the surface (as is also true for the deformation due to a basal velocity anomaly). Thus the stresses associated with the steady-state deformation will be greatest near the bed and decrease towards the surface. This is the same pattern of stress distribution as that described in Section 5.3.1 for the basal velocity anomaly. We thus expect a further decrease in the surface effects of a longitudinal basal velocity anomaly, beyond the decrease which occurs when the rheology is changed from linear to non-linear. This decrease was in fact seen in Section 5.3.2 for a harmonic longitudinal basal velocity anomaly. The non-linear transfer functions T_s^{uu} and T_s^{uv} decreased in value when the effects of a sloped bed were added (see Figure 5-3).

Furthermore, the non-linear transfer function T_s^{vv} increased in value in Section 5.3.2 (for a harmonic normal basal velocity anomaly with a sloped bed). Although this is somewhat counter-intuitive (given the changes in the effective viscosity from the steady-state deformation associated with the sloped bed), a possible explanation for this increase was developed at the end of Section 5.3.1. This explanation was based on the fact that the gradient of the effective viscosity is generally normal to the bed (and decreases towards the surface). Therefore a normal velocity component near the bed would not be damped as much as a longitudinal component, and might also be damped less than a normal velocity component with less effective viscosity gradient. Although this explanation was originally developed to compare a simple non-linear harmonic anomaly (with an effective viscosity gradient), to a linear harmonic anomaly (no viscosity gradient); it is an equally plausible explanation for the comparison of a non-linear harmonic anomaly with steady-state deformation, to a non-linear harmonic anomaly without steady-state deformation. There will be a lower effective viscosity gradient for the anomaly without steady-state deformation.

The transfer function T_s^{vu} decreases in value when the effects of a sloped bed are added (again see Section 5.3.2). This contradicts the above explanation for normal motion near the bed. However, this explanation is somewhat tentative. It is plausible that

somehow the effective viscosity changes due solely to a harmonic normal velocity anomaly increase the non-linear transfer function T_s^{vu} (as compared to the linear case); and yet that the effective viscosity changes due to a combination of steady-state deformation and a harmonic normal basal velocity anomaly decrease the non-linear transfer function T_s^{vu} (as compared to the case without steady-state deformation). It seems difficult to further resolve this discrepancy.

It is fairly apparent that decreasing the ratios U_b/u_s^d or V_b/u_s^d will increase the above effects. (This is confirmed by increasing the longitudinal component of the body force in the finite element model.) Thus as we steepen the bed slope, T_s^{uu}, T_s^{uv}, and T_s^{vu} decrease, and T_s^{vv} increases.

This analysis of the effect of steady-state deformation on an anomalous velocity distribution may be summarized as a "stress guide" effect. This stress guide damps the motion from a longitudinal harmonic basal velocity anomaly, thus decreasing the surface effects. It also damps the cross-component (longitudinal) motion from a normal harmonic basal anomaly. The normal motions from a normal anomaly are damped less than in the case with no steady-state deformation, which probably can be explained by continuity arguments requiring that the normal motions be increased since the cross-component longitudinal motion (from a normal basal velocity anomaly) has been decreased.

The above analysis is based on examination of harmonic basal velocity anomalies. However, it seems reasonable that steady-state deformation would affect any form of basal velocity anomaly (and the resulting surface velocity anomaly) in a manner similar to the manner for harmonic anomalies. The exact details would have to be determined for each specific basal anomaly. This is not systematically examined in this dissertation.

A final question to be examined in this section is whether or not steady basal sliding affects an anomalous velocity distribution. We know that the solution for steady sliding (which is simply a uniform longitudinal velocity throughout the ice thickness) should be able to be linearly added to the anomalous velocity distribution. Tests with the finite element model confirm this. The uniform longitudinal velocity does not affect the effective viscosity, and thus does not affect the anomalous motion.

5.5 Hypothetical mini-surge

The finite element model and solutions of this chapter allow us to make a simple example of a hypothetical mini-surge. One possible explanation for mini-surges involves a pressure wave traveling through the basal hydraulic system. We can therefore model a possible mini-surge by specifying a basal velocity pattern which might be associated with this pressure wave.

This problem has been studied by Iken (1981). A sharp pressure wave in the basal hydraulic system will result in rapid cavitation at the bed. If the pressure is then gradually reduced, the cavities will gradually close.

The rapid cavitation will cause a sharp pulse in both components of the basal velocity. When the cavities reach their maximum size, the normal component at the bed v_b will have dropped back to about zero, since the cavities are no longer opening. However, the longitudinal component at the bed u_b will remain relatively high as long as the cavities are open, due to the increase in the effective smoothness of the bed. As the water pressure is gradually reduced and the cavities close, u_b will gradually decrease. The gradually closing cavities will result in a small negative value for v_b.

The basal velocity boundary condition for the hypothetical mini-surge therefore consists of the following pattern: sharp pulses in both u_b and v_b, followed by u_b then gradually decreasing towards zero, while v_b goes to zero and then is slightly negative.

This pattern for the basal boundary condition and the resulting surface velocity pattern from the finite element model are shown in Figure 5-5. (The basal component v_b was in fact set equal to zero in the "slightly negative" region to simplify the model input.) The single basal peaks in u_b and v_b result in a double peak in the longitudinal component of the surface velocity u_s. This double peak is centered above the single basal peaks. The normal component of the surface velocity v_s has a pattern similar to the pattern at the bed for v_b.

The scale of this hypothetical mini-surge is quite important; especially important is the width (in the x direction) of the basal velocity peaks as compared to the thickness of the ice. If the basal velocity peaks are made sufficiently broad, the double peak in u_s is smoothed out, and the surface velocity pattern becomes very similar to the basal velocity pattern.

This non-linear mini-surge model can be compared with a mini-surge model using the linear rheology (the results for the linear rheology were plotted in Figure 2-9). The different rheologies do not cause major qualitative differences in the resulting surface velocity patterns.

5.6 Discussion

The forward solutions, as developed with the finite element model using the non-linear rheology, are somewhat limited. These solutions heavily emphasize harmonic basal anomalies and the resulting transfer functions. As previously mentioned, these transfer functions can not be reliably applied to a Fourier analysis of any arbitrary basal velocity anomaly.

However, the non-linear transfer functions do give some insight into the effects of the non-linear rheology on velocity anomalies. Specifically, the important dimensionless numbers discussed in Section 5.3.3 should be valid for any form of velocity anomaly. Also, the analysis of Section 5.4 should be valid for non-harmonic anomalies. This analysis described the important coupling between steady-state velocity distributions and anomalous velocity distributions; this coupling only occurs with the non-linear rheology.

Although other differences between the linear and non-linear rheologies are quite interesting, this coupling between the steady-state and anomalous flows is probably the most important result of using a non-linear rheology. This means that the complete velocity or stress distributions must be considered for any problems which are examined using non-linear rheologies.

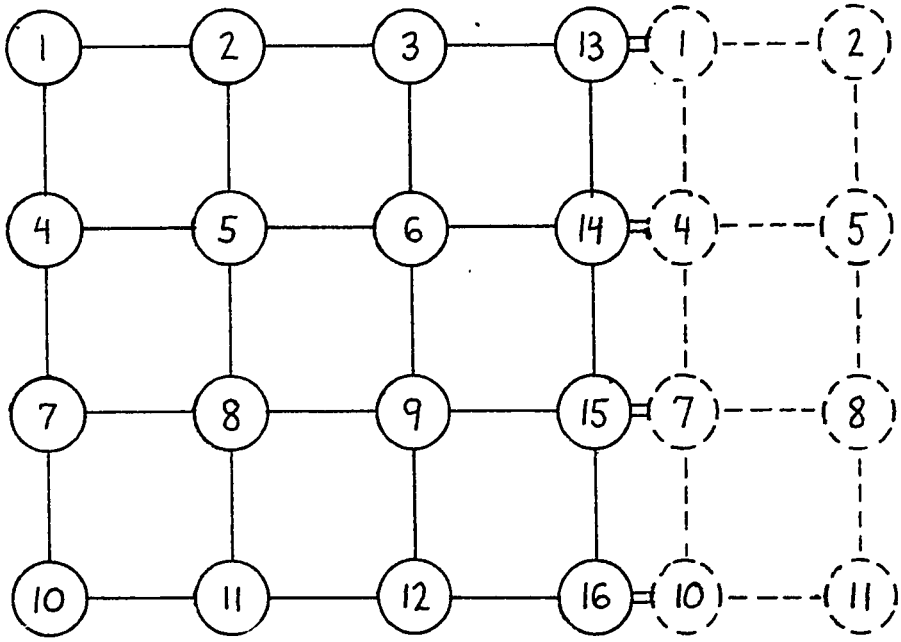

Figure 5-1. Nodal numbering system for periodic boundary condition in finite element model. Actual models had 121 to 231 nodes.

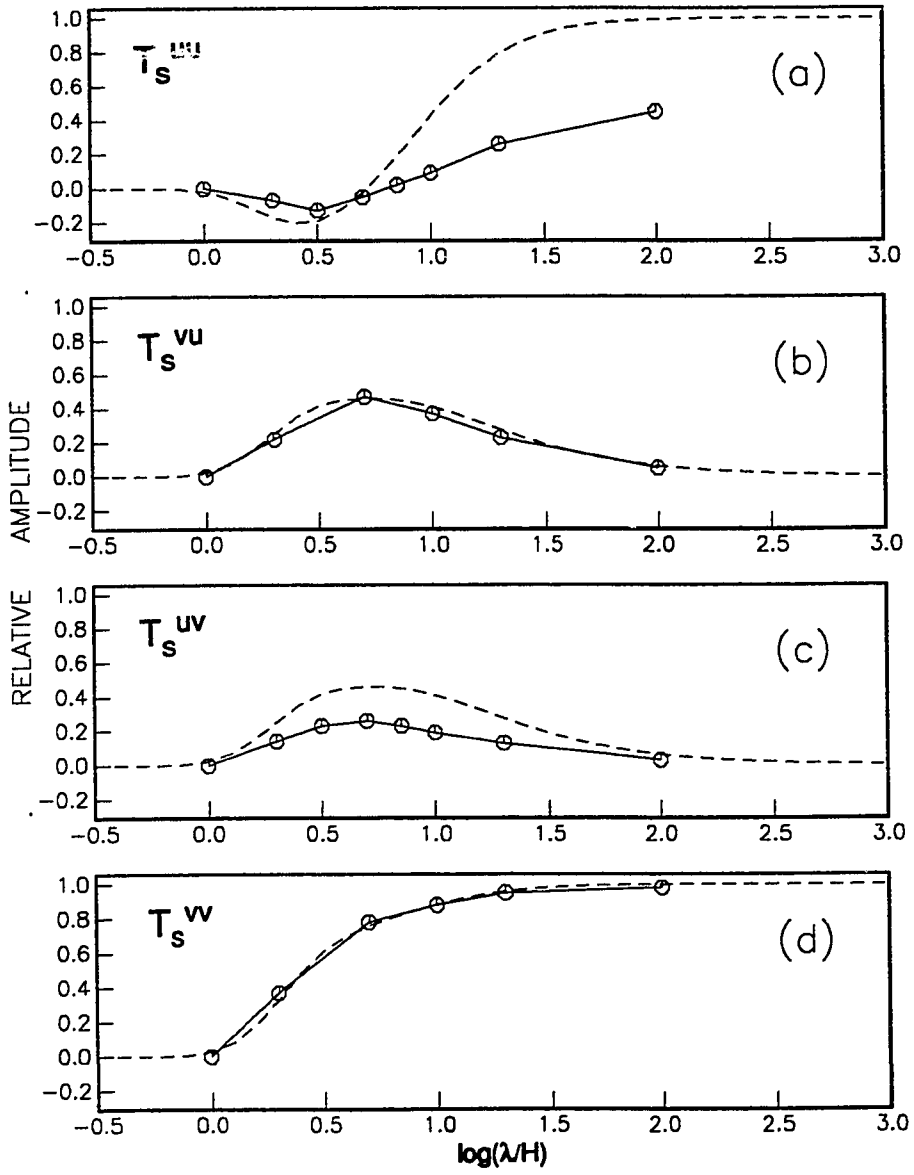

Figure 5-2. Solid lines: non-linear forward transfer functions for harmonic basal velocity anomaly, no bed slope. Dashed lines: corresponding linear transfer functions. (a) T_s^{uu}, (b) T_s^{vu}, (c) T_s^{uv}, and (d) T_s^{vv}.

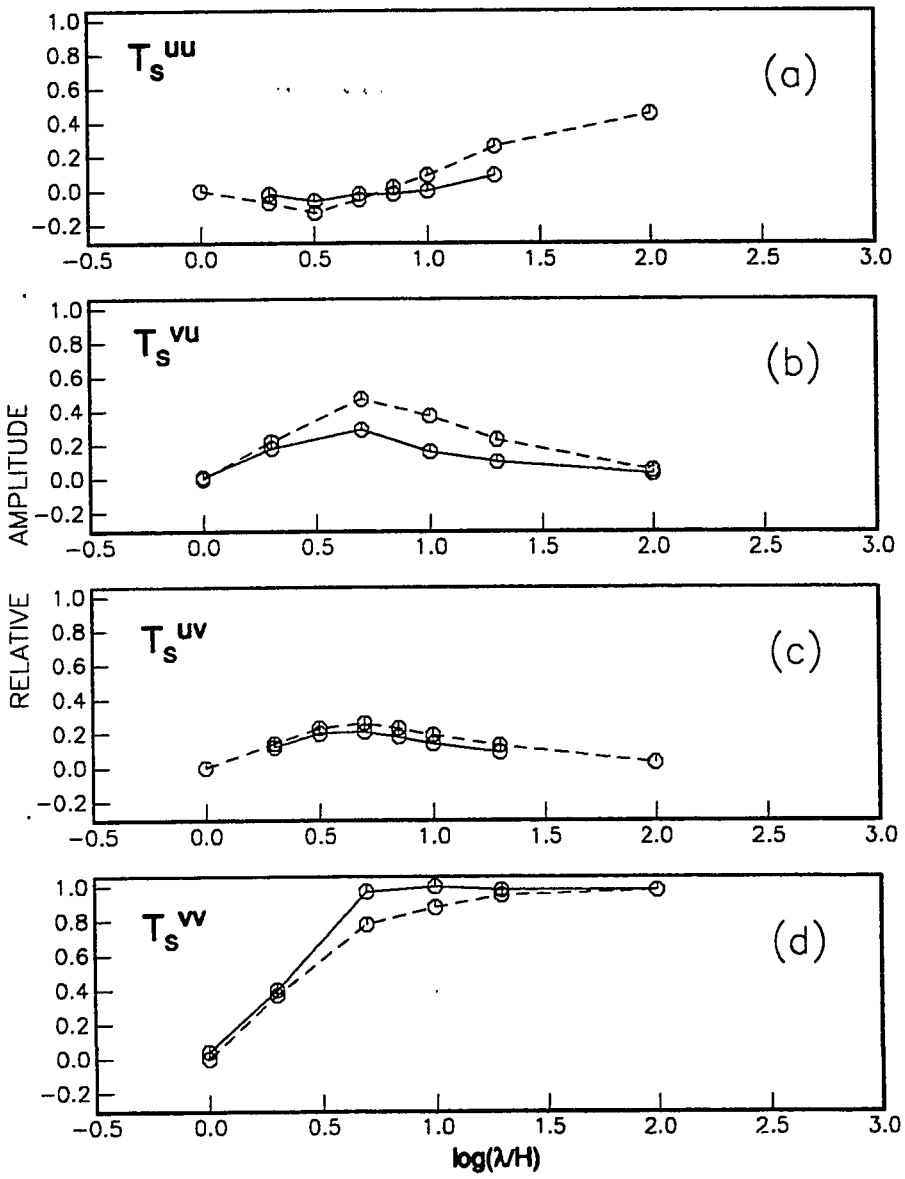

Figure 5-3. Solid lines: non-linear forward transfer functions for harmonic basal velocity anomaly, $U_b/u_s^d = 0.2$ or $V_b/u_s^d = 0.2$ (sloped bed). Dashed lines: corresponding non-linear transfer functions for no bed slope. (a) T_s^{uu}, (b) T_s^{vu}, (c) T_s^{uv}, and (d) T_s^{vv}.

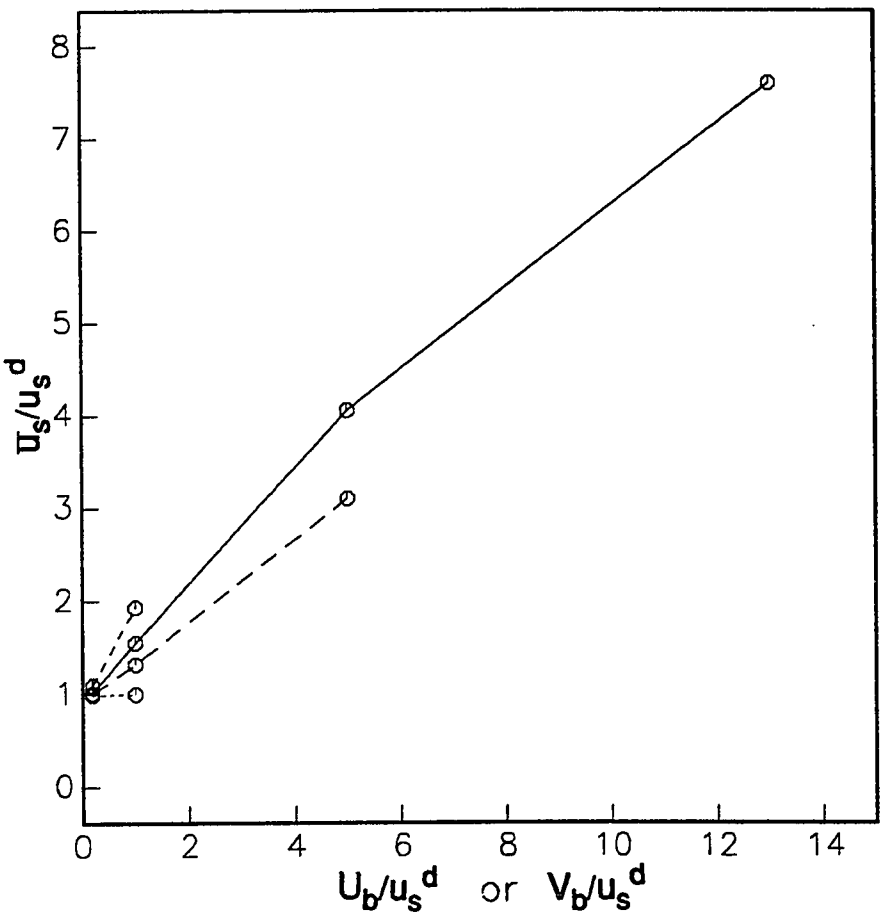

Figure 5-4. Effect of harmonic basal velocity anomalies on mean surface velocity, for non-linear rheology. Solid line: $\bar{u}_s/u_s^d$ plotted as a function of U_b/u_s^d, for $\lambda/H = 2$. Long dashed line: same as solid line except $\lambda/H = 20$. Short dashed line: $\bar{u}_s/u_s^d$ plotted as a function of V_b/u_s^d, for $\lambda/H = 2$. Dotted line: same as short dashed line except $\lambda/H = 20$.

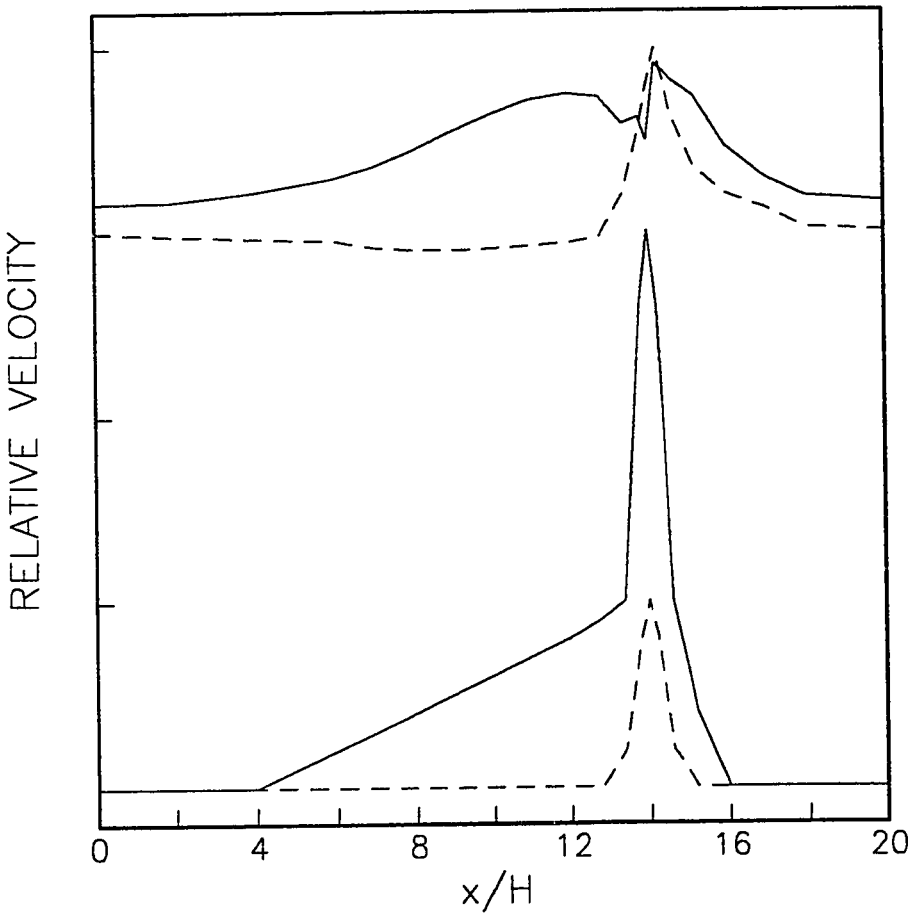

Figure 5-5. Hypothetical mini-surge for non-linear rheology. Surface velocity components (upper curves) for hypothetical basal velocity anomaly (lower curves). Solid lines: u_b and u_s. Dashed lines: v_b and v_s. Here $u_s^d = 0.045$ (sloped bed).

CHAPTER 6

LINEAR VISCOUS INVERSE SOLUTIONS

6.1 Chapter introduction

Understanding sliding velocity distribution in glaciers is an important problem. Typically glacier velocities are measured at the surface, but the velocity of most interest for understanding glacier sliding is the velocity at the glacier bed. For surface velocities which change over a relatively long scale in time or space, the problem of determining basal sliding velocity for a given surface velocity distribution is not too difficult (Haefeli, 1970; Hodge, 1974; Raymond and Harrison, submitted). The calculation of basal sliding velocities for surface velocity patterns which change over a short scale in time or space is more difficult.

Observations of these short-scale changes in surface velocity have been made on various glaciers (e.g., Iken, 1977; Kamb and Engelhardt, 1987). The theory of how relatively short-scale surface velocity patterns relate to basal (and englacial) velocity fields has been developed for flow through a transverse section of a glacier by Reynaud (1973), and Hantz and Lliboutry (1981); only one component of velocity (normal to the section) was considered in these treatments.

In this chapter we will determine possible basal velocity patterns which could be associated with a given surface velocity pattern, when the surface velocity pattern changes over a relatively short scale along a longitudinal section of a glacier. Two components of velocity are allowed. Solving for the basal velocity using a given surface velocity is the "inverse" problem (solving for the surface velocity using a prescribed basal velocity is the "forward" problem; see Chapter 2). The results will be useful for a better understanding of rapid changes in glacier sliding and possible basal processes which may be important in a glacier sliding law.

6.2 Mathematical description of problem

6.2.1 Assumptions, rheology, and geometry

The underlying assumptions are the same as those in Chapter 2. These assumptions can be summarized as solving for an anomalous velocity distribution only, with any steady-state velocity field subtracted out of the problem (which also removes the gravitational force). The anomalous velocity is assumed to be driven by relatively short-scale changes in the glacier dynamics, such as those due to variations in the basal water pressure. The anomalous velocity field is assumed to vary slowly in time so that acceleration terms can be neglected.

A linear viscous rheology is used. (Although a power law rheology is more accurate for glacier ice, calculations using a finite element model show most of the same qualitative features as the linear viscous rheology -- see Chapter 7.)

A planar slab geometry is assumed; coordinates are as shown in Figure 6-1. The velocity is allowed to vary in the x and y directions only. Anomalous motion across the slope in the z direction is zero. Changes in surface topography due to the velocity anomaly are assumed negligible.

6.2.2 Boundary conditions

The boundary conditions are all at the upper surface ($y = H$). (Thus this is not a "well-posed" problem; see Section 6.2.3.) The x and y components of the surface velocity anomaly give two boundary conditions:

$$u|_{y=H} = u_s(x,t) \tag{6-1a}$$

$$v|_{y=H} = v_s(x,t) \tag{6-1b}$$

where u is the x component ("longitudinal component") of the velocity anomaly, and v is the y component ("normal component"). The upper surface is stress free (except for atmospheric pressure), so the stress anomaly on this surface is zero. Treatment is simplified if the derivative in the x direction of the normal stress anomaly on the upper surface is used as the normal stress boundary condition. This derivative must equal zero along the surface:

$$\frac{\partial \sigma_{yy}}{\partial x}\Big|_{y=H} = 0 \tag{6-2a}$$

where σ_{yy} is the normal stress anomaly. The boundary condition for the shear stress at the upper surface is also zero:

$$\sigma_{xy}|_{y=H} = 0 \tag{6-2b}$$

where σ_{xy} is the shear stress anomaly.

6.2.3 Solution method

The field equations for the stress anomaly and the velocity anomaly can most easily be solved by defining a stream function ψ, where $u \equiv \frac{\partial \psi}{\partial y}$, and $v \equiv -\frac{\partial \psi}{\partial x}$. The applicable field equations can then be reduced to

$$\frac{\partial^4 \psi}{\partial x^4} + 2\frac{\partial^4 \psi}{\partial x^2 \partial y^2} + \frac{\partial^4 \psi}{\partial y^4} = 0 \tag{6-3}$$

The problem can be further simplified by using the Fourier transform. The transform of equation (6-3) is:

$$k^4 \hat{\psi} - 2k^2 \frac{\partial^2 \hat{\psi}}{\partial y^2} + \frac{\partial^4 \hat{\psi}}{\partial y^4} = 0 \tag{6-4}$$

where k is the Fourier transform variable (wave number), and $\hat{\psi}$ is the Fourier transform of the stream function. The Fourier transformed boundary conditions, written in terms of $\hat{\psi}$, are (for the surface velocity anomaly)

$$\frac{\partial \hat{\psi}}{\partial y}\Big|_{y=H} = \hat{u}_s(k,t) \tag{6-5a}$$

$$-ik\hat{\psi}|_{y=H} = \hat{v}_s(k,t) \tag{6-5b}$$

For the surface stress anomaly:

$$\left[3k^2 \frac{\partial \hat{\psi}}{\partial y} - \frac{\partial^3 \hat{\psi}}{\partial y^3}\right]_{y=H} = 0 \tag{6-6a}$$

$$\left[\frac{\partial^2\hat{\psi}}{\partial y^2} + k^2\hat{\psi}\right]_{y=H} = 0 \qquad \text{(6-6b)}$$

These four boundary conditions are sufficient to solve for the unknown function $\hat{\psi}$ in Equation (6-4), giving the transformed stream function throughout the ice. In particular, we will use this function at the bed to determine basal velocities. However, the problem is "ill-posed", in that all the boundary conditions are at the surface and none are at the bed (Lanzcos, 1956; Squeak and Diddlesworth, 1987). This means that minor perturbations or errors in the surface velocity boundary condition can cause extreme changes in the velocity pattern calculated at the bed. Some techniques of inverse theory will be used to overcome this difficulty.

The solutions in the following sections will be written in the wave number or space domain, in time-independent form. Thus the solutions are a "snap-shot" of the motion within the ice at a specific time; this viewpoint corresponds with the assumption of negligible change in the surface topography. These fixed spatial solutions could easily be modified to give propagating wave forms. (However, possible changes with time in the surface topography would have to be considered.)

It would also be possible to determine the solutions in the frequency or time domain, solving at a fixed spatial position. For this approach, the spatial pattern of the surface velocity boundary conditions as a function of time would have to be known. This method is mathematically similar to solving in the wave number or space domain, but the solution is not examined in this dissertation.

6.3 Exact velocity solution at bed

6.3.1 Mathematical solution

A solution for Equation (6-4) is

$$\hat{\psi} = \frac{A(k)}{k}e^{-ky} + B(k)ye^{-ky} + \frac{C(k)}{k}e^{ky} + D(k)ye^{ky} \qquad \text{(6-7)}$$

If this solution is substituted into the boundary conditions (Equations (6-5) and (6-6)), the resulting four equations can be solved for the four unknown coefficients A, B, C, and D. This gives

$$A = \frac{1}{2}\left[-kHe^{kH}\hat{u}_s + [1-kH]e^{kH}i\hat{v}_s\right] \tag{6-8a}$$

$$B = \frac{1}{2}\left[e^{kH}\hat{u}_s + e^{kH}i\hat{v}_s\right] \tag{6-8b}$$

$$C = \frac{1}{2}\left[-kHe^{-kH}\hat{u}_s + [1+kH]e^{-kH}i\hat{v}_s\right] \tag{6-8c}$$

$$D = \frac{1}{2}\left[e^{-kH}\hat{u}_s - e^{-kH}i\hat{v}_s\right] \tag{6-8d}$$

These coefficients give the solution for the transformed stream function $\hat{\psi}$. This can be used to determine the transformed components of the velocity anomaly, at any depth. We are specifically interested in the velocity at the bed. The exact solutions for the Fourier transforms of the longitudinal and normal components of the basal velocity anomaly are:

$$\hat{u}_b = \frac{1}{2}\left[[1-kH]e^{-kH} + [1+kH]e^{kH}\right]\hat{u}_s + \frac{1}{2}\left[kHe^{-kH} + kHe^{kH}\right]i\hat{v}_s \tag{6-9a}$$

$$\hat{v}_b = \frac{1}{2}\left[kHe^{-kH} + kHe^{kH}\right]i\hat{u}_s + \left[[1+kH]e^{-kH} + [1-kH]e^{kH}\right]\hat{v}_s \tag{6-9b}$$

The basal velocity can more easily be written in terms of inverse transfer functions (where "inverse" here means from the surface to the bed). T_b^{uu} will be defined as the magnitude of transfer from u at the surface to u at the bed. T_b^{vu}, T_b^{uv}, and T_b^{vv} are similarly defined. These inverse transfer functions are then written:

$$T_b^{uu} \equiv \frac{1}{2}\left[[1-kH]e^{-kH} + [1+kH]e^{kH}\right] \tag{6-10a}$$

$$T_b^{vu} = T_b^{uv} \equiv \frac{1}{2}\left[kHe^{-kH} + kHe^{kH}\right] \tag{6-10b}$$

$$T_b^{vv} \equiv \frac{1}{2}\left[[1+kH]e^{-kH} + [1-kH]e^{kH}\right] \tag{6-10c}$$

The inverse transfer functions are plotted in Figure 6-2. As the non-dimensional wave number kH goes to infinity, the magnitude of all four inverse transfer functions goes to infinity also. This can be contrasted with the corresponding forward transfer functions calculated in Chapter 2 (see Figure 2-3). The magnitude of the forward transfer functions is always less than or equal to one.

6.3.2 Information and error for exact basal velocity solution

If real data are used for the surface velocity anomaly (the surface velocity boundary conditions), this data will contain both information and error. The information (signal) is assumed to be greatest at low wave numbers (because the basal signal when transferred to the surface is increasingly attenuated as the wave number increases; see Chapter 2). The error (noise) at the surface is assumed to be "white" as a function of wave number (Jaech, 1985). Thus the noise-to-signal ratio at the surface increases as the wave number increases.

When the surface data are transferred to the bed, both the signal and the noise are multiplied by the same inverse transfer functions. Therefore the noise-to-signal ratio for the calculated basal velocity anomaly, as a function of wave number, will be the same as that at the surface, and will increase as the wave number increases. Furthermore, the inverse transfer functions (from surface to bed) also increase as the wave number increases. This means that the error at high wave numbers at the bed can be very large, and can in fact dominate the entire signal. When viewed in the space domain, the true information at the bed may be totally masked by a large basal error resulting from relatively small errors in the high wave number components at the surface. This problem can be minimized by modifying the exact solution.

6.4 Modifications to exact solution: filtering data

6.4.1 General theory

One obvious modification is to limit the error in some way. A simple method would be to limit the inverse transfer functions at high wave numbers, and thus limit the error at high wave numbers. For example, the inverse transfer functions could be multiplied (in the wave number domain) by a filter which had a value which was near to one for low wave numbers (for which the inverse transfer function values are small), but tapered towards zero for high wave numbers (for which the inverse transfer function values are large). However, applying a filter to the inverse transfer functions can be viewed as changing the physics of the problem.

Another choice is to apply the filter to the surface data (which have been Fourier transformed), instead of filtering the inverse transfer functions. When the basal velocity anomaly is then calculated using the filtered data and the exact inverse transfer functions, the results will be identical to those using unfiltered data but filtered inverse transfer functions (for a given filter).

An example of the equations for calculating the basal velocity, using filtered inverse transfer functions, is

$$\hat{u}_b = [\hat{F}T_b^{uu_s}]\hat{u}_s \tag{6-11a}$$

where $\hat{F}$ is the filter and $T_b^{uu_s}$ is the inverse transfer function. The same example for the equations for calculating the basal velocity, using filtered data, is

$$\hat{u}_b = T_b^{uu_s}[\hat{F}\hat{u}_s] \tag{6-11b}$$

Mathematically these equations are the same. The only difference between the two methods is that it is easier to justify "filtering the data" than it is to justify "changing the physics".

If a filter is applied which selectively decreases the high wave number components of the surface data, the error at the bed can be limited. However, the true information at high wave numbers is also limited. Thus we have less error but also less information. This effect must be considered when the filter parameters are chosen. Hopefully these parameters can be specified so that the error at the bed is reduced enough to see the true signal; and yet leave enough information present at high wave numbers so that interesting features in the basal velocity pattern are not eliminated. These criteria are somewhat subjective, and are discussed more quantitatively in the next section.

6.4.2 Analysis of resolution and accuracy

The analysis of resolution and accuracy will be applied to the data for the surface velocity anomaly, these surface data after they have been filtered, and the basal velocity anomaly which results when the filtered surface data are transferred to the bed.

The resolution at the bed can be tested by looking at a given wavelength component in the surface data (where wavelength $\lambda \equiv 2\pi/k$). Perfect resolution would result if this component was not filtered, and was just multiplied by the appropriate inverse transfer

function to calculate the amplitude of that wavelength component at the bed. Thus the resolution at the bed will depend directly on the filter. We can define a resolution length to be the wavelength at which the filter reduces the amplitude of that wavelength component by a factor of $1/e$. Shorter wavelengths are reduced in amplitude by a factor greater than $1/e$. This resolution length could then be easily calculated by looking at a particular filter as a function of wavelength.

The accuracy is not quite so easy to define. If we compare the filtered surface data with the actual measured data, it is reasonable to say that the filtered data are accurate provided that they are within the error bounds of the measured data. (These error bounds are determined by uncertainties in surveying, etc.) However, the accuracy of any calculated basal velocity can not be exactly determined, since the true basal velocity is not known. The best approach is to assume that the filter which most reduces the high wave number components is the filter which will give the most accurate basal velocity, since the error increases with increasing wave number.

Therefore, to retain accuracy in the filtered surface velocity anomaly, and to also obtain as much accuracy as possible in the calculated basal velocity anomaly, the filter should be chosen which most reduces the high wave number components of the data, and yet allows the surface velocity to remain within the error bounds.

This procedure will give the most accurate filter, considering both the surface and basal velocities. The basal resolution will be somewhat reduced.

6.4.3 Gaussian filter

The filter that we will look at is a Gaussian (in the wave number domain). The equation for this Gaussian is:

$$\hat{F} = \exp\left[-\frac{1}{2}\left[\frac{k}{\sigma k_{max}}\right]^2\right] \tag{6-12}$$

Here σ is the non-dimensional standard deviation, as a fraction of the maximum wave number k_{max}. The filter has a maximum value of one, centered about k=0. If a fast Fourier transform routine is used to transform the data both positive and negative wave number components exist, so the filter can easily be applied to this transformed data.

The adjustable parameter in this filter is σ. A plot of a Gaussian with σ=0.15 is shown in Figure 6-3a. Also shown is a plot of the filter when transformed to the space domain, in Figure 6-3b. This curve also has the qualitative form of a Gaussian, with no sidebands. Since in the space domain the filter is convolved with the data (which is equivalent to multiplication in the wave number domain), a filter with no sidebands in the space domain means that spikes in the data set will not result in ringing when the data are filtered. This is a desirable feature for the filter, and viewing the filter in the space domain is a simple way to check whether or not ringing can occur.

A broad Gaussian in the wave number domain (σ large) will result in little loss of information at the bed. However, the error at the bed will be high. If the Gaussian is made narrower (σ small), the error at the bed will decrease but more information will be lost. The particular value of σ which is used to filter a given data set should be based on the analysis of resolution and accuracy. This value can best be determined by progressively decreasing the standard deviation σ from some relatively high starting value. For some sufficiently small σ the filtered surface velocity, as viewed in the space domain, will just reach the error bounds at some point. The value of σ which causes the error bounds to be reached will depend on both the range of the error bars, and the particular spatial form of the surface data. The filter parameter σ cannot be chosen only as a function of the range of the error bars.

6.5 Modifications to exact solution: trade-off of roughness vs. misfit

6.5.1 General theory

Instead of filtering the surface data, an alternate approach is to limit the calculated basal velocity anomalies in some way. Since errors in the data are expected to introduce predominantly high wave number noise in the calculated basal velocities, it is reasonable to attempt to limit the "roughness" of these basal velocities. However, if we modify the basal velocity, the surface velocity must also be modified, so that the surface and basal velocities can still be related by the physics of the exact inverse transfer functions. (The modification of the surface velocity is justified by the presumption of errors in the surface data.) There will then be a "misfit" between the modified surface velocity and the actual

surface data. If the basal velocity is made smoother, the amount of surface misfit increases. Thus there is a trade-off between the (basal) roughness and the (surface) misfit.

We will minimize the sum of this roughness and misfit, with the trade-off being controlled by an adjustable parameter. The minimization must be subject to a side condition, which is the requirement that the modified surface velocity (i.e., the surface data as adjusted by the presumed error), be exactly related via the inverse transfer functions to the calculated basal velocity.

The definition for the roughness of the basal velocity which we will use is: the square of the magnitude of the longitudinal (x direction) derivative of the basal velocity. Any order of derivative can be used. We will minimize the roughness of both components of the basal velocity.

Minimizing the zeroth order derivative would limit the amplitude of the basal velocity. Minimizing the first derivative would limit the steepness of the velocity as a function of x; this means that we are minimizing $[\partial u/\partial x]^2$ at the bed, which is equivalent to limiting the basal longitudinal strain rate and the basal longitudinal stress. (We are also minimizing $[\partial v/\partial x]^2$ at the bed, which limits one part of the basal shear stress; but we do not want to minimize $[\partial u/\partial y]^2$, and thus we are not limiting the total basal shear stress.) Minimizing the second longitudinal derivative of the basal velocity limits the smoothness of the velocity as a function of x; this means that we are minimizing $[\partial^2 u/\partial x^2]^2$ at the bed, which will limit the basal longitudinal strain rate gradient and the basal longitudinal stress gradient. This is equivalent to limiting the steepness of the basal longitudinal strain rate and the steepness of the basal longitudinal stress as a function of x. (For the second derivative we are also minimizing $[\partial^2 v/\partial x^2]^2$.)

It is reasonable to assume that one of the above quantities (zeroth, first, or second derivatives) is the correct function to use in the minimization. The general mathematical solution will be written in terms of any nth order derivative. We can then calculate and compare the different minimizations for different orders of derivative, using actual surface data.

6.5.2 Mathematical method

To minimize the equations for a spatial derivative (with respect to x), while operating in the wave number domain, the equations are minimized as a function of the wave number k. Since the Fourier transform is orthogonal, this method will result in a minimization when inverse transformed to the space domain. If a discrete Fourier transform is used, the minimization applies to the equations for each discrete wave number.

We will do this minimization for both components of the basal velocity anomaly. This means that we could do this minimization in two different ways: we could either minimize a sum which includes both components $\hat{u}_b$ and $\hat{v}_b$ of the Fourier transformed basal velocity anomaly, or we could minimize two separate sums (one for $\hat{u}_b$ and the other for $\hat{v}_b$). For the first method, the resulting smoothed solutions for $\hat{u}_b$ and $\hat{v}_b$ are completely coupled (i.e., there is only one set of assumed errors at the surface). For the second method, the resulting smoothed solutions for $\hat{u}_b$ and $\hat{v}_b$ (and related quantities, such as the assumed errors at the surface) are not required to be coupled. (This means that the assumed errors at the surface will be different for the solution for $\hat{u}_b$ as compared to the solution for $\hat{v}_b$.) However, for the first method the form of the solutions for $\hat{u}_b$ and $\hat{v}_b$ is more complicated than the form of these solutions for the second method. This occurs because the equations to be minimized for the first method are more complicated, since they include terms for both $\hat{u}_b$ and $\hat{v}_b$ in one sum.

We therefore choose the second method, which minimizes two separate sums, since the resulting velocity solutions will be simpler and more easily understood. This means that we are actually doing two separate but parallel problems. The solutions will not be coupled except as specifically stated.

We wish to minimize the sum of the basal roughness and the surface misfit; this sum will be called S_{ub} for the equation applying to the Fourier transformed basal velocity component $\hat{u}_b$, and S_{vb} for the equation applying to the Fourier transformed basal velocity component $\hat{v}_b$. The sum for $\hat{u}_b$ is

$$S_{ub} = \hat{u}_b(k)^{(n)}\hat{u}_b(k)^{(n)*} + \beta\left[\hat{e}_u(k)\hat{e}_u(k)^* + \hat{e}_v(k)\hat{e}_v(k)^*\right] \qquad (6\text{-}13a)$$

The sum for $\hat{v}_b$ is

$$S_{vb} = \hat{v}_b(k)^{(n)}\hat{v}_b(k)^{(n)*} + \beta\left[\hat{\varepsilon}_u(k)\hat{\varepsilon}_u(k)^* + \hat{\varepsilon}_v(k)\hat{\varepsilon}_v(k)^*\right] \tag{6-13b}$$

Here $\hat{u}_b(k)^{(n)}\hat{u}_b(k)^{(n)*}$ and $\hat{v}_b(k)^{(n)}\hat{v}_b(k)^{(n)*}$ are the Fourier transforms of the roughness, with the superscript (n) signifying that these roughnesses are for the nth longitudinal spatial derivative. The misfit is $\hat{\varepsilon}_u(k)\hat{\varepsilon}_u(k)^* + \hat{\varepsilon}_v(k)\hat{\varepsilon}_v(k)^*$, where $\hat{\varepsilon}_u$ is the assumed error in the transform of the longitudinal component of the surface data $\hat{u}_s$, and $\hat{\varepsilon}_v$ is the assumed error in the transform of the normal component of the surface data $\hat{v}_s$. (The * means the complex conjugate; thus we are minimizing a real number which is the sum of the squares of the moduli of the complex quantities.) The misfit is not required to be the same in Equations (6-13a) and (6-13b), and in fact will differ between the two solutions. (This difference would not occur if we were minimizing a sum which included both $\hat{u}_b$ and $\hat{v}_b$, since we would only have one set of equations.)

The adjustable trade-off parameter is β; higher β values give more roughness and less misfit. For simplicity the value of β will be the same in both equations. This parameter is not a function of the wave number k. Since the basal velocity is a function of the inverse transfer functions, which increase with increasing wave number, not allowing β to vary with k has the effect of biasing the minimization towards less roughness at higher wave numbers. This is useful because the surface noise-to-signal ratio is assumed to be high at higher wave numbers, and thus any calculated basal roughness is less meaningful at these higher wave numbers.

The side conditions which must be added to Equations (6-13) are that the physics of the problem are satisfied. These side conditions are written:

$$\hat{u}_b^{(n)} = [ik]^n T_b^{uu}[\hat{u}_s + \hat{\varepsilon}_u] + [ik]^n T_b^{vu}[i\hat{v}_s + i\hat{\varepsilon}_v] \tag{6-14a}$$

for Equation (6-13a), and

$$\hat{v}_b^{(n)} = [ik)]^n T_b^{uv}[i\hat{u}_s + i\hat{\varepsilon}_u] + [ik]^n T_b^{vv}[\hat{v}_s + \hat{\varepsilon}_v] \tag{6-14b}$$

for Equation (6-13b). These equations are in fact the nth derivative of Equations (6-9), with the Fourier transformed surface data $\hat{u}_s$ and $\hat{v}_s$ modified by the assumed errors $\hat{\varepsilon}_u$ and $\hat{\varepsilon}_v$. The data are the same for Equations (6-14a) and (6-14b); the assumed errors are not required to be the same in both equations. The quantity $(ik)^n$ is the Fourier transform of the nth longitudinal spatial derivative.

The side conditions are then separated into their real and imaginary parts, and are added to Equations (6-13), using Lagrange multipliers. (Note that the particular terms in the real and imaginary parts of the side conditions will depend on the order of derivative n.) This gives the total quantities to minimize:

$$S_{ub}{}^{total} \equiv \hat{u}_b{}^{(n)}\hat{u}_b{}^{(n)*} + \beta[\hat{\varepsilon}_u\hat{\varepsilon}_u{}^* + \hat{\varepsilon}_v\hat{\varepsilon}_v{}^*] \tag{6-15a}$$

$$+ 2\lambda_{u1}\mathrm{Re}\left[\hat{u}_b{}^{(n)} - [ik]^n T_b{}^{uu}[\hat{u}_s + \hat{\varepsilon}_u] - [ik]^n T_b{}^{vu}[i\hat{v}_s + i\hat{\varepsilon}_v]\right]$$

$$+ 2\lambda_{u2}\mathrm{Im}\left[\hat{u}_b{}^{(n)} - [ik]^n T_b{}^{uu}[\hat{u}_s + \hat{\varepsilon}_u] - [ik]^n T_b{}^{vu}[i\hat{v}_s + i\hat{\varepsilon}_v]\right]$$

and

$$S_{vb}{}^{total} \equiv \hat{v}_b{}^{(n)}\hat{v}_b{}^{(n)*} + \beta[\hat{\varepsilon}_u\hat{\varepsilon}_u{}^* + \hat{\varepsilon}_v\hat{\varepsilon}_v{}^*] \tag{6-15b}$$

$$+ 2\lambda_{v1}\mathrm{Re}\left[\hat{v}_b{}^{(n)} - [ik]^n T_b{}^{uv}[i\hat{u}_s + i\hat{\varepsilon}_u] - [ik]^n T_b{}^{vv}[\hat{v}_s + \hat{\varepsilon}_v]\right]$$

$$+ 2\lambda_{v2}\mathrm{Im}\left[\hat{v}_b{}^{(n)} - [ik]^n T_b{}^{uv}[i\hat{u}_s + i\hat{\varepsilon}_u] - [ik]^n T_b{}^{vv}[\hat{v}_s + \hat{\varepsilon}_v]\right]$$

The Lagrange multipliers are λ_{u1}, λ_{u2}, λ_{v1}, and λ_{v2}; these are real numbers. The real parts are written as $Re(\,)$; the imaginary parts are written as $Im(\,)$. The imaginary parts are defined to be the magnitude of the imaginary quantity and are real numbers. Thus the total quantities being minimized $S_{ub}{}^{total}$ and $S_{vb}{}^{total}$ are real quantities.

To minimize Equations (6-15), we take their multi-dimensional gradient. The components of the gradient for Equation (6-15a) are defined:

$$\nabla \equiv \left[\frac{\partial}{\partial Re(\hat{u}_b{}^{(n)})}, \frac{\partial}{\partial Im(\hat{u}_b{}^{(n)})}, \frac{\partial}{\partial Re(\hat{\varepsilon}_u)}, \frac{\partial}{\partial Im(\hat{\varepsilon}_u)}, \frac{\partial}{\partial Re(\hat{\varepsilon}_v)}, \frac{\partial}{\partial Im(\hat{\varepsilon}_v)}\right] \tag{6-16a}$$

The components of the gradient for Equation (6-15b) are:

$$\nabla \equiv \left[\frac{\partial}{\partial Re(\hat{v}_b{}^{(n)})}, \frac{\partial}{\partial Im(\hat{v}_b{}^{(n)})}, \frac{\partial}{\partial Re(\hat{\varepsilon}_u)}, \frac{\partial}{\partial Im(\hat{\varepsilon}_u)}, \frac{\partial}{\partial Re(\hat{\varepsilon}_v)}, \frac{\partial}{\partial Im(\hat{\varepsilon}_v)}\right] \tag{6-16b}$$

Each term of the gradient of Equations (6-15) is then set equal to zero. This gives six equations from Equation (6-15a), to use for the solution of $\hat{u}_b{}^{(n)}$ and its associated unknowns; and six equations from Equation (6-15b), to use for the solution of $\hat{v}_b{}^{(n)}$ and its associated unknowns. We then add the fact that both the real and imaginary parts of the

side conditions must be satisfied. (Again, the particular terms in the real and imaginary parts will depend on n.) This gives two additional equations for $\hat{u}_b^{(n)}$ and its associated unknowns, for a total of eight; and two additional equations for $\hat{v}_b^{(n)}$ and its associated unknowns, also for a total of eight. There are a total of eight unknowns in the equations for $\hat{u}_b^{(n)}$, and a total of eight unknowns in the equations for $\hat{v}_b^{(n)}$. It is thus possible to solve for the complex quantities $\hat{u}_b^{(n)}$ and $\hat{v}_b^{(n)}$, which can then simply be divided by $(ik)^n$ to get $\hat{u}_b$ and $\hat{v}_b$. Suitable algebraic manipulations yield the general solutions for $\hat{u}_b$ and $\hat{v}_b$. These solutions are:

$$\hat{u}_b = \frac{T_b^{uu}\hat{u}_s + T_b^{vu}i\hat{v}_s}{1 + \frac{1}{\beta}k^{2n}\left[[T_b^{uu}]^2+[T_b^{vu}]^2\right]} \tag{6-17a}$$

$$\hat{v}_b = \frac{T_b^{uv}i\hat{u}_s + T_b^{vv}\hat{v}_s}{1 + \frac{1}{\beta}k^{2n}\left[[T_b^{uv}]^2+[T_b^{vv}]^2\right]} \tag{6-17b}$$

The quantities $\hat{u}_b$, $\hat{v}_b$, $\hat{u}_s$, and $\hat{v}_s$ may be complex. These solutions apply for basal roughness which is dependent on any nth order longitudinal derivative of the basal velocity.

6.5.3 Effects of applying trade-off solutions

The effect of the trade-off solutions can perhaps most easily be looked at by calculating the effect as filters. Inspection of Equations (6-17) shows that the trade-off approach can be viewed as applying one filter to both $\hat{u}_s$ and $\hat{v}_s$, and then calculating $\hat{u}_b$ using the exact inverse transfer functions T_b^{uu} and T_b^{vu}; while a different filter is applied to both $\hat{u}_s$ and $\hat{v}_s$ for use in the calculation of $\hat{v}_b$, where $\hat{v}_b$ is then calculated using the exact inverse transfer functions T_b^{uv} and T_b^{vv}. The reason that we have two different filters is because we separated the equations for $\hat{u}_b$ and $\hat{v}_b$, at the beginning of Section 6.5.2. (Note that in the filtering approach of Section 6.4, a single filter was applied to both $\hat{u}_s$ and $\hat{v}_s$, with the filtered surface velocities then being used for the calculation of both $\hat{u}_b$ and $\hat{v}_b$.)

This means that we can rewrite Equations (6-17) in the form:

$$\hat{u}_b = \hat{F}_{ub}T_b^{uu}\hat{u}_s + \hat{F}_{ub}T_b^{vu}i\hat{v}_s \tag{6-18a}$$

$$\hat{v}_b = \hat{F}_{vb}T_b^{uv}i\hat{u}_s + \hat{F}_{vb}T_b^{vv}\hat{v}_s \tag{6-18b}$$

Here $\hat{F}_{ub}$ (the filter for $\hat{u}_b$) is defined

$$\hat{F}_{ub} \equiv \frac{1}{1 + \frac{1}{\beta} k^{2n} \left[[T_b^{uu}]^2 + [T_b^{vu}]^2 \right]} \tag{6-19a}$$

And $\hat{F}_{vb}$ (the filter for $\hat{v}_b$) is defined

$$\hat{F}_{vb} \equiv \frac{1}{1 + \frac{1}{\beta} k^{2n} \left[[T_b^{uv}]^2 + [T_b^{vv}]^2 \right]} \tag{6-19b}$$

These effective filters for the trade-off solutions are just one divided by the denominators in Equations (6-17).

These equations show that increasing the order of derivative n will in general result in a smoother basal velocity. Decreasing the value of the trade-off parameter β will also result in a smoother basal velocity. Examples of the filters $\hat{F}_{ub}$ and $\hat{F}_{vb}$, and their inverse Fourier transforms (the filters as viewed in the space domain), are plotted in Figures 6-4. The filters in the wave number domain have forms qualitatively similar to Gaussians. Sidebands exist in the space domain, but are relatively small.

The two modified versions of the surface velocity that result from applying the filters $\hat{F}_{ub}$ and $\hat{F}_{vb}$, could also be calculated directly by adding the error terms $\hat{\varepsilon}_u$ and $\hat{\varepsilon}_v$ to the surface data. (These modified versions of the surface velocity are equivalent to the terms in the side conditions (Equations (6-14)) which include the measured surface velocity and the assumed errors.) However, as previously noted, the solutions for $\hat{\varepsilon}_u$ and $\hat{\varepsilon}_v$ are different in the $\hat{u}_b$ equations as compared to the $\hat{v}_b$ equations; and an explicit mathematical solution for the error terms shows that each single error term is a function of both components of the surface data. It is much easier to see the form of the modified surface velocity by using the filters in Equations (6-18).

It is also possible to calculate a different modified surface velocity anomaly, with Fourier transformed components which we will call $\hat{u}_s^m$ and $\hat{v}_s^m$, that corresponds exactly with both components $\hat{u}_b$ and $\hat{v}_b$ of the calculated basal velocity anomaly, via the inverse transfer functions. This modified surface velocity is not exactly the same as the surface velocity which results from applying the filters $\hat{F}_{ub}$ and $\hat{F}_{vb}$ in Equations (6-18) (e.g., the filtered surface velocity on the right sides of the equations), since here we will use only a single version of the surface velocity to calculate the basal velocity, while using Equations

(6-18) is equivalent to using two different forms of the surface velocity to calculate the basal velocity. Actually the different approaches do not result in greatly different forms of the surface velocity, and it is very important to note that the basal velocity is exactly the same in both cases.

The equation for calculating the modified longitudinal component $\hat{u}_s^m$ of the surface velocity anomaly is

$$\hat{u}_s^m = T_s^{uu}\hat{u}_b - iT_s^{vu}\hat{v}_b \tag{6-20a}$$

The equation for calculating the modified normal component $\hat{v}_s^m$ of the surface velocity anomaly is

$$\hat{v}_s^m = -iT_s^{uv}\hat{u}_b + T_s^{vv}\hat{v}_b \tag{6-20b}$$

Here T_s^{uu}, T_s^{vu}, T_s^{uv}, and T_s^{vv} are the exact forward transfer functions (see Balise and Raymond, 1985). At first glance it would appear that we can now calculate a filter which gives $\hat{u}_s^m$ from $\hat{u}_s$, and another filter which gives $\hat{v}_s^m$ from $\hat{v}_s$. These filters would not be the same as the effective filters in Equations (6-18). We could call these new effective filters $\hat{F}_{us}$ and $\hat{F}_{vs}$. However, these new filters are not simple; in fact, both filters will be functions of both components of the surface data set $\hat{u}_s$ and $\hat{v}_s$. Thus the filters will vary, depending on the specific data which are being examined. It is therefore not particularly useful to explicitly write the equations for effective filters $\hat{F}_{us}$ and $\hat{F}_{vs}$ which determine $\hat{u}_s^m$ and $\hat{v}_s^m$. These modified components of the surface velocity are instead most easily determined by first calculating the basal velocity by using Equations (6-17), and next applying Equations (6-20) to yield this form of the modified surface velocity.

This single version of the modified surface velocity is very useful, since we can easily compare it with the original surface data to determine the error between u_s^m and u_s, and the error between v_s^m and v_s. The error terms $\hat{\varepsilon}_u$ and $\hat{\varepsilon}_v$ in the equations of Section 5.2 are not the same as the error here. The error determined by comparing this modified surface velocity with the surface data will be the basis of our choice for the exact parameters to use in the trade-off solution. For any given order of derivative n, we must apply a resolution and accuracy approach (detailed in Section 4.2), to choose the value of the trade-off parameter β. For some particular value of β, the modified surface velocity will reach the error bounds in the space domain at some point for the surface data. This value of β can easily be determined by progressively decreasing it, from some relatively high starting

value. (At the high starting value u_s^m and v_s^m will be will within the error bounds, but the calculated basal velocity will be very noisy.) The value of β which just allows the surface error bounds to be reached, will give the smoothest basal velocity anomaly which still has a corresponding surface velocity anomaly within the error bounds of the surface data.

Unfortunately, there is one difficulty with applying the analysis of resolution and accuracy to the trade-off solution. The problem is that ringing in the modified surface velocity may preclude ever getting this velocity within the error bounds, for any reasonable value of the trade-off parameter β. This ringing can be severe if the surface data have especially sharp maxima or minima in their spatial pattern. This happens because the trade-off approach can be viewed as consisting of first convolving the spatial form of the effective filters F_{ub} and F_{vb} (Figure 6-4b) with the surface data, then calculating the basal velocity using the exact inverse transfer functions, and finally calculating the modified surface velocity using the forward transfer functions. The convolution of the filter sidebands with any spikes in the surface data will result in ringing, and this ringing will be carried through the following calculations. The only solution to this problem is to expand the error bounds as necessary, if the surface data have many rapid changes in spatial pattern.

6.6 Application of theory to Variegated Glacier mini-surges

6.6.1 Fitting data to theory

The mini-surges of Variegated Glacier in Alaska have been well described in several papers (e.g. Kamb and Engelhardt, 1987). Among the data collected during these mini-surges are the displacement and the longitudinal strain rate as functions of time, measured at various fixed spatial positions along the centerline of the glacier surface. (These spatial positions actually move with the slow movement of the glacier surface, but this does not materially affect the calculations in this chapter for the rapidly propagating mini-surges.) The change in displacement over a certain time interval can be divided by the length of the time interval to give the average velocity during this interval. This process gives the surface velocity as a function of time at the fixed spatial position. The strain rate data can also be converted to the longitudinal component of the surface velocity as a function of time at a fixed spatial position; however, the process is more complicated and involves

certain assumptions. This conversion is explained and carried out in Raymond and Malone (1986).

When the surface velocity during a mini-surge is examined, it consists of a "background" steady-state component, and an anomalous component which only occurs during the mini-surge. The cross-glacier velocity component (when known) is small. The surface velocity anomaly typically consists of a velocity wave of several *km* spatial extent, which propagates down-glacier at several hundred $m\ hr^{-1}$.

To apply the particular equations which have been developed in this chapter, it is necessary to convert the calculated surface velocity anomaly from a function of time at a fixed spatial position, to a function of longitudinally varying spatial position at a fixed time. To do this conversion it is necessary to know the wave propagation speed in the x direction, and also to know how the shape of the wave, as a function of varying longitudinal position on the glacier surface, changes with time. The wave propagation speed seems to be fairly constant for a given mini-surge, and is constrained by measurements of when various velocity peaks passed various points along the glacier centerline. (Typically there were three to five of these centerline locations where data were collected on the glacier.) Unfortunately the changes in the wave shape are not so easily constrained, because the velocity wave (as a function of time) typically does not have a consistent pattern, or a consistent change in pattern, when the data from the different spatial measurement positions are compared. Given the very limited spatial resolution of the data, the best assumptions that can be made about the surface velocity anomaly are that the pattern of this propagating anomaly does not change, but that the overall amplitude of the pattern varies with time. Thus a spatial wave shape must be fairly arbitrarily based on the pattern as a function of time at a chosen surface measurement position, even though using data from a different measurement position would give different results. A wave amplitude decay or increase factor α (for overall amplitude changes with time) is then applied, which is based on the total strain and displacement at the various measurement points (see Raymond and Malone (1986) for details of calculating α). This decay or increase factor is assumed to be exponential.

The equation for converting the longitudinal component u_s of the surface velocity anomaly, as a function of time, to velocity as a function of spatial position then is

$$u_s(x,t_o)|_{x=x_o-w[t-t_o]} = e^{-\alpha[t-t_o]}u_s(x_o,t-t_o) \qquad (6\text{-}21)$$

Here x_o is the longitudinal coordinate of the fixed position on the glacier centerline where the surface data were collected; and t_o is the fixed time at which the data are being viewed, when converted to a function of varying longitudinal coordinate x. The wave propagation speed in the down-glacier direction is w.

A similar equation applies to the normal component v_s of the surface velocity anomaly. (The cross-glacier component of the velocity anomaly is assumed to be negligible.) However, for most of the mini-surges data were not collected for the displacement normal to the glacier surface, thus making it impossible to determine v_s (since in no case were strain rate data collected allowing determination of this velocity component). Therefore some assumptions about v_s are usually necessary. One possible assumption is to require that $v_b = 0$ (giving a boundary condition for u_s at the surface and v_b at the bed); the theory would then have to be modified so that v_s would be one of the outputs (along with u_b). Other possible assumptions are to either guess the form of v_s, or to simply require that $v_s = 0$. These last two assumptions require no modification of the theory.

Requiring that $v_b = 0$ is not compatible with some theories of sudden changes in glacier velocities, which is usually thought to involve basal cavitation (Iken, 1981). Requiring that $v_b = 0$ also contradicts the one case which we will examine where both u_s and v_s are known. (In this case the known surface velocity will be seen to be related to significant anomalies in both components of the basal velocity; in fact, for this case the amplitude of v_b is substantially larger than the amplitude of v_s. See Section 6.6.2.2.) We therefore conclude that we are forced to guess v_s in the cases where it is not known, or at least to require that $v_s = 0$, rather than require that $v_b = 0$. The cases where we either know or guess a reasonable form for v_s can be compared with the cases where we set $v_s = 0$.

A final adjustment to the data is made necessary by the fact that the mathematical computations are done using a discrete fast Fourier transform. This requires 2^n evenly spaced data points (where here n is any positive integer). For both the displacement and strain rate data, zeros were added to both ends of the data sets to reach the next higher value of n. (For the displacement data, points were first interpolated between the known data points to result in a smoother, more continuous curve, with even spacing.) The extension of the data sets also minimizes problems which can be caused by the fact that the fast

Fourier transform assumes that the signal is periodic.

6.6.2 Velocity from survey data

6.6.2.1 Surface velocity calculation

The theory can now be applied to mini-surge data from Variegated Glacier. The first data which we will examine are displacement data obtained by standard surveying techniques. We will limit our examination of this survey data to the mini-surge which occurred on 15 July 1980. Very good data exist (Kamb and Engelhardt, 1987) which allow the calculation of both the longitudinal component u_s and the normal component v_s of the surface velocity anomaly. In particular, we will use the data collected at 6.5 *km* on the glacier centerline (measured down-glacier from the head).

The wave shapes at 6.5 *km* for u_s and v_s, as functions of time, are assumed to be reasonably representative of the form of the surface velocity anomaly. Data from other locations on the glacier centerline support this assumption, and also allow the determination of the wave propagation speed w and the wave amplitude decay factor α. Here w is calculated to be 8520 $m\,d^{-1}$, and α is calculated to be $-0.29\ d^{-1}$. These then allow the calculation of u_s and v_s as functions of spatial position. Plots of the longitudinal component $u_s(x,t_o)$ and the normal component $v_s(x,t_o)$ of the surface velocity anomaly are shown in Figures 6-5a and 6-5b, with $x = 0$ being at 6.5 *km*, and $t_o = 15.49\ d$ (just before noon on 15 July 1980). Identical plots of $u_s(x,t_o)$ and $v_s(x,t_o)$ are also shown in parts a and b of Figures 6-6, 6-7, and 6-8, in order to make using these figures easier.

6.6.2.2 Gaussian filter and basal velocity calculation

We next apply a Gaussian filter to the Fourier transformed data as discussed in Section 6.4. The standard deviation σ is chosen as explained in Section 6.4.2. One value of σ is used to filter both u_s and v_s. This is done both to simplify the calculations and because the error in u_s is better known than the error in v_s. The error in u_s is based on possible survey errors of about 1 *cm*, with surveys being done approximately every *hr*. This results in error bars of $\pm 0.25\ m\,d^{-1}$ for u_s. If a Gaussian filter in the wave number domain with $\sigma = 0.137$ is applied to the transformed data $\hat{u}_s$, these error bounds will just be reached in

the space domain at one point ($x = 1299\ m$). This same filter applied to $\hat{v}_s$ results in a maximum error of $0.62\ m\ d^{-1}$ (at $x = 1299\ m$). The filtered components of the surface velocity anomaly will be denoted by the superscript f. The filtered components u_s^f and v_s^f (viewed in the space domain) are shown in Figures 6-5a and 6-5b.

The filtered data are then transferred to the bed using the exact inverse transfer functions. The resulting basal velocity components u_b and v_b are also shown in Figures 6-5a and 6-5b. This is the presumed pattern of the basal velocity anomaly at $t = 15.49\ d$ during the mini-surge. For u_b, the dominant feature is the large positive spike. This spike is centered under the down-glacier peak in u_s at the surface. The up-glacier peak in u_s at the surface corresponds only with a minor basal velocity peak. The double maximum seen in u_s does not appear to be related to a significant double maximum in u_b, since u_b consists of one dominant velocity peak.

The pattern for v_b is dominated by down-drop down-glacier of the major peak in u_b, and uplift up-glacier of this peak. No current theories of glacier mini-surges seem to support such a pattern, although it would not be impossible if a substantial deformable layer existed beneath the glacier sole. However, we must also consider problems with the mathematical theory of this chapter which could result in such a pattern. These problems are:

(1) Inaccurate rheology. However, as previously mentioned, a power law rheology shows most of the same effects.

(2) No allowance for transverse motions. Since the glacier is constrained to move in two dimensions only, it is possible that adding the third dimension would result in a significantly different pattern for v_b.

(3) No allowance for voids in the ice. These are not considered by our theory. It is quite possible that water-filled or air-filled voids exist in the glacier. If these were compressed in the down-glacier region of the mini-surge, this would be equivalent to the calculated down-drop of the ice at the bed in this region. Similarly, if voids opened in the up-glacier region of the mini-surge, this would be equivalent to the calculated uplift at the bed in this region. This situation seems quite plausible.

We will now use the same data and filter, except that we will set $v_s = 0$. This comparison is important, because the mini-surge of 15 July 1980 is the only one which we will

examine where v_s is well known. Setting $v_s = 0$ (but with u_s still based on the data), and then applying the Gaussian filter and the inverse transfer functions, results in the basal velocity anomaly shown in Figures 6-5a and 6-5b. The longitudinal component u_b of the basal velocity is considerably different from the case when the component v_s was not set equal to zero, but the normal component v_b is quite similar to the case when v_s was not set equal to zero. This result is interesting since it shows that changes in v_s may be related to major changes in u_b, and only minor changes in v_b. For this particular case, the figures show that setting $v_s = 0$ changes u_b from a single dominant peak to a double peak. This emphasizes the importance of knowing the correct form of v_s. For this mini-surge with a Gaussian filter, if the correct form of v_s is used, the double peak in u_s is seen to be related to only a single major peak in u_b; if v_s is incorrectly set equal to zero, the double peak in u_s is incorrectly thought to be related to a double peak in u_b.

6.6.2.3 Trade-off solutions and basal velocity calculations

We now apply a trade-off solution to the data for the mini-surge of 15 July 1980. For this trade-off solution, we need to choose a trade-off parameter β, and an order of derivative n to use in the minimization. The value of β which allows the modified surface velocity to reach the error bounds will depend on the order of derivative n.

The first case which we will examine is for $n = 0$. For this situation, a value of $\beta = 1350$ allows the error bars for u_s of $\pm 0.25\ m\ d^{-1}$ to be reached by the modified longitudinal component u_s^m of the surface velocity anomaly, at $x = 1417\ m$. For this same value of β, the maximum error in the modified normal component v_s^m of the surface velocity anomaly is $0.84\ m\ d^{-1}$, at $x = 1299\ m$. This modified surface velocity anomaly which this trade-off solution results in is plotted in Figures 6-6a and 6-6db (Figures 6-6a and 6-6b also show the unmodified surface velocity.) The basal velocity anomaly for this trade-off solution is also plotted in Figures 6-6a and 6-6b. This basal velocity is seen to be quite similar to the basal velocity in Figures 6-5a and 6-5b (which are for the Gaussian filter). Again, u_b has a single dominant peak; and v_b has down-drop down-glacier and uplift up-glacier of the peak in u_b. The same reasoning of Section 6.6.2.2 can be applied to v_b here.

The next case to examine is for $n = 1$. For this case, a value of the trade-off parameter $\beta = 1250$ allows the error bounds for u_s to be reached by the modified longitudinal

component u_s^m, at $x = 1299\ m$. The maximum error in the modified normal component v_s^m is $0.77\ m\ d^{-1}$, also at $x = 1299\ m$. These modified components of the surface velocity anomaly are plotted in Figures 6-7a and 6-7b, and are similar to the results in Figures 6-6a and 6-6b (for which $n = 0$), although somewhat smoother. The basal velocity anomaly for $n = 1$ is also plotted in Figures 6-7a and 6-7b. These basal velocity components are again somewhat similar to the case where $n = 0$ in Figures 6-6a and 6-6b. However, besides both basal velocity components being somewhat smoother and of lower amplitude, there is more evidence of a double peak in u_b for the case where $n = 1$ (Figure 6-7a), as compared to u_b for the case where $n = 0$ (Figure 6-6a). The down-drop in the down-glacier part of v_b has also been substantially reduced.

We next set $n = 2$. Here a value of $\beta = 3650$ allows the error bounds for u_s to be reached by u_s^m, again at $x = 1299\ m$; the maximum error in v_s^m is $0.73\ m\ d^{-1}$, also at $x = 1299\ m$. The modified components of the surface velocity anomaly are plotted in Figures 6-8a and 6-8a. These are slightly smoother than for the case with $n = 1$; of particular interest is the fact that the double peak in u_s has been somewhat reduced. The components of the basal velocity anomaly for $n = 2$ are also plotted in Figures 6-8a and 6-8b. These are also slightly smoother than the basal velocity components for $n = 1$, and of somewhat lower amplitude. The double peak in u_b is pronounced.

If higher values of n were examined (which is not done in this dissertation), the modified surface velocity and associated basal velocity would become even smoother. At some value of n the double peak in both u_s and u_b would probably be smoothed out. Since physical arguments for setting a particular value of n are not compelling, we can not really determine with this trade-off approach whether u_b has a single peak or a double peak. We do know from the data, however, that u_s appears to have a double peak for this particular mini-surge. This would indicate that the value of n chosen should not modify the surface data u_s such that the double peak is eliminated. Since higher values of n tend to reduce the double peak in u_s (e.g. as is the case for $n = 2$), we can reach a tentative conclusion that the lowest value of n ($n = 0$) is the most accurate, or at least better than values of $n = 2$ or higher. We will therefore restrict our examination of trade-off solutions for other mini-surges to solutions with $n = 0$.

The final situation which we will use for the mini-surge of 15 July 1980 is to set $v_s = 0$, for a trade-off solution with $n = 0$. The same trade-off parameter ($\beta = 1350$) is used

as was used for the case where v_s was not set equal to zero. The basal velocity anomaly for the case with $v_s = 0$ is plotted in Figures 6-6a and 6-6b. These results are similar to those for the Gaussian filter, in which setting $v_s = 0$ caused a change from a single dominant peak in u_b to a double peak. For the trade-off solution with $v_s = 0$ the double peak in u_b is quite pronounced. This situation again underscores the necessity of accurately knowing v_s if we hope to successfully determine u_b.

6.6.3 Velocity from strain meter data

6.6.3.1 Surface velocity calculations

The other data from Variegated Glacier which we will use are data from wire strain meters. Details of the data collection, and the calculation of velocities from strain rates, are explained in Raymond and Malone (1986). Good data for the longitudinal strain rate component at the surface were obtained in 1979, 1980, and 1981. (As previously noted, the strain meters were not set up to collect data for the strain rate component normal to the surface.) We will consider data from three mini-surges: 11 July 1979, 15 July 1980, and 14 July 1981.

For the mini-surge of 11 July 1979, the clearest wave form for the longitudinal component u_s of the surface velocity, as a function of time, is calculated from strain rate data which were obtained on the glacier centerline 7.5 *km* down-glacier from the head. Data from other positions along the glacier centerline are used to determine a wave propagation speed of $w = 8160\ m\ d^{-1}$, and a wave amplitude decay factor of $\alpha = -0.82\ d^{-1}$. The longitudinal component of the surface velocity anomaly can then be calculated as a function of spatial position. This component $u_s(x,t_o)$ is plotted in Figure 6-9a (and identically in Figure 6-10a). Note the short spatial scale over which the surface velocity anomaly has relatively rapid changes in magnitude and sign. Here $x = 0$ is at 7.5 *km*, and $t_o = 11.19\ d$ (in the early morning on 11 July 1979). The normal component v_s of the surface velocity is not known.

The strain meter data from the mini-surge of 15 July 1980 give a longitudinal component of the surface velocity which is quite similar to that same velocity component obtained by surveying (see Section 6.6.2). Since the survey data also allow the calculation of v_s for this mini-surge, the survey data are more useful than the strain meter data in this

case. Due to the similarity of the data for u_s, and the lack of strain meter data for v_s, it seems reasonable to limit the analysis of this mini-surge to the survey data (which were analyzed in the previous sections).

Good longitudinal strain rate data at the surface were also obtained for the mini-surge of 14 July 1981. We will use data which were collected on the centerline 4.7 *km* down-glacier from the head. Data from various positions on the glacier centerline determine a wave propagation speed of $w = 6480\ m\ d^{-1}$. The wave amplitude decay factor is determined to be $\alpha = -0.30\ d^{-1}$. The longitudinal component of the surface velocity anomaly is then calculated as a function of spatial position, and is plotted in Figure 6-11a (and identically in Figure 6-12a). Note the relatively long spatial scale of the surface velocity anomaly. For this plot of $u_s(x,t_o)$ $x = 0$ is at 4.7 *km*, and $t_o = 14.87\ d$ (in the evening on 14 July 1981). The normal component v_s of the surface velocity is not known.

6.6.3.2 Gaussian filters and basal velocity calculations

We will now apply Gaussian filters to the Fourier transformed velocities. However, we first need to determine error bounds for these velocity data in the space domain. These error bounds are chosen to be approximately the same fraction of the total range of the surface velocity data, as the error bars were for the mini-surge of 15 July 1980. This fraction is about one fifth.

We start with the velocity data for the mini-surge of 11 July 1979. The error bars are chosen to be $\pm 1.0\ m\ d^{-1}$. Applying a Gaussian filter with a standard deviation of $\sigma = 0.196$, to the Fourier transformed longitudinal component of the surface velocity, results in these error bars being reached in the space domain at $x = -1339m$. The filtered longitudinal component u_s^f of the surface velocity anomaly is plotted in Figure 6-9a.

We next need to decide what to use for the unknown normal component v_s of the surface velocity anomaly. Experimenting with various possible forms for v_s, and comparing the resulting basal velocities to the basal velocity for the case where $v_s = 0$, shows no major consistent differences between the two situations. We therefore conclude that the best choice is to set $v_s = 0$, although we will have no way of knowing whether or not the resulting basal velocity anomaly is correct. Since the component v_s is set equal to zero it does not need to be filtered.

The basal velocity components u_b and v_b are then calculated by using the exact inverse transfer functions, applied to the filtered surface velocity (with $v_s = 0$). These components of the basal velocity anomaly are shown in Figures 6-9a and 6-9b. The pattern of these basal velocity components, although somewhat rough, is similar to the pattern at the surface for u_s; the amplitude is much greater at the bed than at the surface. Since we do not know v_s, we can not necessarily expect the pattern of the calculated basal velocity to be accurate, although we can conclude that the rapid changes are important. The double peak in both basal velocity components may or may not exist. The large amplitude of the basal velocity is certainly significant. This shows that a large amplitude basal anomaly (with a rapidly changing spatial pattern) is probably necessary to cause a rapidly changing surface velocity anomaly, of much smaller amplitude.

We now examine the mini-surge of 14 July 1981. Here the longitudinal component u_s of the surface velocity anomaly is of smaller amplitude, and with a less rapidly changing spatial pattern, than that component for the mini-surge of 11 July 1979. The error bars for u_s on 14 July 1981 are taken to be $\pm 0.20\ m\ d^{-1}$ (about one fifth of the overall amplitude of u_s). A Gaussian filter with $\sigma = 0.047$ is applied, which results in the error bounds being reached by u_s^f at $x = 1080\ m$. This filtered longitudinal component of the surface velocity anomaly is plotted in Figure 6-11a. The normal component v_s of the surface velocity anomaly is again taken to be zero (since no data to determine it exist).

The resulting basal velocity components are calculated, and are plotted in Figures 6-11a and 6-11b. The basal component u_b is very similar to the surface component u_s in both pattern and amplitude. We conclude that in this case (as contrasted to the case for 11 July 1979), the surface anomaly is smooth enough that a much larger amplitude basal anomaly is not required.

The basal component v_b has down-drop down-glacier, followed by uplift up-glacier. This is probably explained by the reasoning in Section 6.6.2.2, with the additional qualification that v_s is not known and was somewhat arbitrarily set equal to zero.

6.6.3.3 Trade-off solutions and basal velocity calculations

Trade-off solutions for the basal velocity anomalies, for the mini-surges of 11 July 1979 and 14 July 1981, can be briefly examined. We restrict our solutions to the case where $n = 0$.

For 11 July 1979, we have previously determined error bars for u_s of $\pm 1.0\ m\ d^{-1}$. A value of the trade-off parameter $\beta = 2550$ allows these error bars to be reached, by the modified component u_s^m, at $x = -1450\ m$. This modified longitudinal component of the surface velocity anomaly is plotted in Figure 6-10a. (The surface component v_s, which is not known, is set equal to zero. However, it is important to note that the modified normal component of the surface velocity v_s^m is not necessarily equal to zero, as is shown by examination of Equations (6-17) and (6-20b); but v_s^m is small relative to u_s^m.) The resulting components u_b and v_b of the basal velocity anomaly are plotted in Figures 6-10a and 6-10b.

The basal velocity for this case is fairly similar to the results obtained with the Gaussian filter, although the spatial pattern is smoother and the amplitude is reduced (which may at least in part be due to the expanded error bars.) We again conclude that a relatively large amplitude basal anomaly, with rapidly changing spatial pattern, is necessary to cause a much smaller amplitude surface anomaly with a similar rapidly changing spatial pattern.

For the mini-surge of 14 July 1981, minor ringing problems occur (see Section 6.5.3). This problem exists especially since the error bars for u_s are relatively small ($\pm 0.20\ m\ d^{-1}$). However, a value of the trade-off parameter $\beta = 200$ results in an error for the modified longitudinal component u_s^m of $0.21\ m\ d^{-1}$, at $x = 1080\ m$. This is very close to the error bars of $\pm 0.20\ m\ d^{-1}$, so we will use this value of β. This modified longitudinal component u_s^m of the surface velocity anomaly is plotted in Figure 6-12a (again, v_s is set equal to zero, and v_s^m is small). The basal velocity components u_b and v_b are plotted in Figures 6-12a and 6-12b. The results are again somewhat similar to the results using a Gaussian filter, although with a somewhat rougher spatial pattern and a greater amplitude. In particular, the double peak in the basal component u_b is much more pronounced in this case, and less down-drop exists in v_b. However, these differences between the Gaussian and trade-off solutions are not too significant, especially when we consider the lack of knowledge about v_s. The conclusion which we can reach for the mini-surge of 14 July

1981, is that a large amplitude basal anomaly with rapid changes in spatial pattern is not required for the relatively smooth surface anomaly.

6.7 Discussion

The examination of possible basal velocity anomalies for the three mini-surges -- one in 1979, one in 1980, and one in 1981 -- allows us to reach some conclusions on the general pattern of the mini-surges. In addition, the three mini-surges were each chosen as being somewhat representative of the other mini-surges for their particular year; this allows us to also reach some tentative conclusions about the evolution of the mini-surges from year to year.

The first general conclusion about the mini-surges is that the amplitude of the basal velocity anomaly is highly variable. In particular, mini-surges for which the surface velocity pattern changes rapidly over a relatively short spatial scale (e.g., the mini-surge of 11 July 1979) seem to be associated with relatively high-magnitude basal velocity anomalies; while mini-surges for which the surface velocity pattern is smoother (e.g., the mini-surge of 14 July 1981) are associated with lower-magnitude basal velocity anomalies.

A comparison of the basal magnitudes for 1979, 1980, and 1981 also can be construed as evidence that the amplitude decreases from year to year. This decrease from year to year appears to apply to both the longitudinal and normal components of the basal velocity. If we assume that the mini-surges are caused by a pressure wave in the basal hydraulic system (Humphrey and others, 1986; Kamb and Engelhardt, 1987), something affecting this system must be changing from year to year in order to cause the decrease in the amplitude of the basal velocity anomaly. The year to year thickness increase of the glacier in the region of the mini-surges is a possible cause, although this increase was only on the order of 2% per year (Raymond and Harrison, submitted). More likely causes for the decrease in amplitude of the basal velocity anomaly are some change in the layout of the basal hydraulic system, and changes in the dynamics of the pressure waves. All of these possible causes for year to year changes in the mini-surges are quite speculative, since the theory of what actually causes mini-surges is not well developed.

Conclusions can also be reached on the spatial pattern of the basal velocity anomaly during the mini-surges. This basal pattern appears to generally be more complex for

shorter-scale surface velocity anomalies. In particular, the longitudinal component u_b appears to have multiple peaks for 11 July 1979 (and perhaps 14 July 1981), but only a single dominant peak for 15 July 1980. Unfortunately these conclusions are of limited value for 1979 and 1981 due to lack of data for the normal component v_s of the surface velocity. Comparing the solution using the known normal component of the surface velocity with the solution setting this component equal to zero in Figures 6-6a has shown that the correct form for v_s (which was known for 15 July 1980) can substantially affect the pattern of u_b. It is of course quite interesting that for this case where v_s is well known, only a single peak results in u_b. This would indicate that u_b could possibly only have a single peak in the other mini-surges also, even though the calculations for these other mini-surges (using data for only u_s and with $v_s = 0$) show multiple peaks.

The theoretical model which we have used does not really allow conclusions about the pattern of v_b. The problems with the model which restrict accurate determination of v_b were mentioned in Section 6.6.2.2. A reasonable conclusion is that there is some sort of compression of the system (ice, air, water and sediment) in the down-glacier region of the mini-surge, with this compression being relaxed in the up-glacier region.

It is very important to emphasize that these conclusions are dependent on the accuracy of the solution process. In particular, errors are probably introduced by the assumptions involved in the calculation of the spatial pattern of the surface velocity (which was calculated from the velocity data as a function of time at a fixed spatial position). This emphasizes the fact that better spatial-resolution surface data are necessary in order to yield more conclusive results for the basal velocity during the mini-surges. Both u_s and v_s need to be measured (note that the data for v_s for 15 July 1980 significantly affected the calculation of both velocity components at the bed).

It is possible that adding a third velocity component (cross-glacier) to the model, and especially somehow allowing for the opening and closing of voids (which would be difficult to model), would help in a better understanding of the normal velocity component at the bed v_b. A non-linear rheology might also significantly affect the results (this possibility is examined in Chapter 7). However, even the relatively simple model which we have used allows a fair understanding of the basal velocity anomalies during the mini-surges of Variegated Glacier.

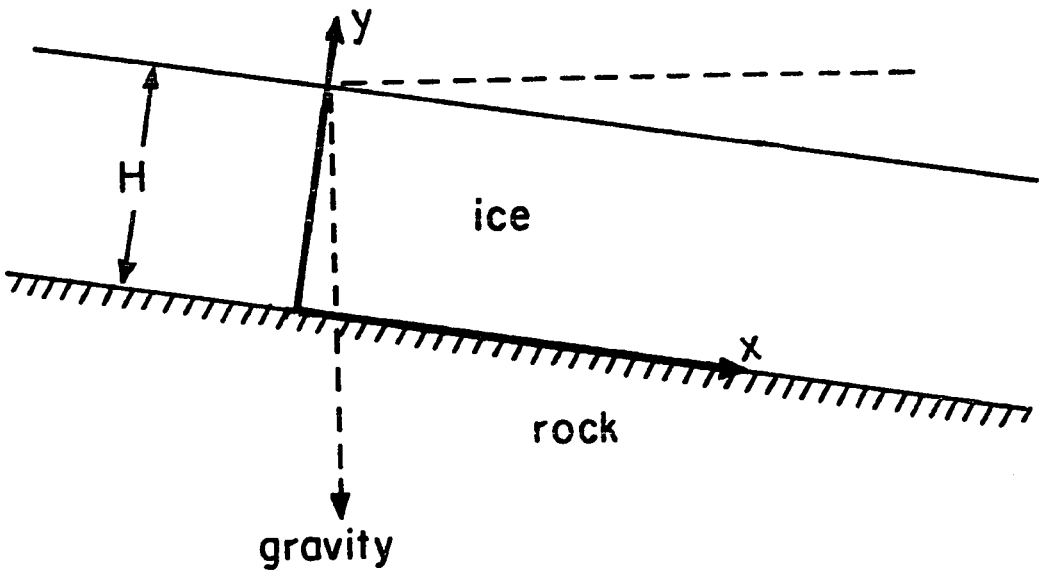

Figure 6-1. Definition of geometrical quantities and coordinate system.

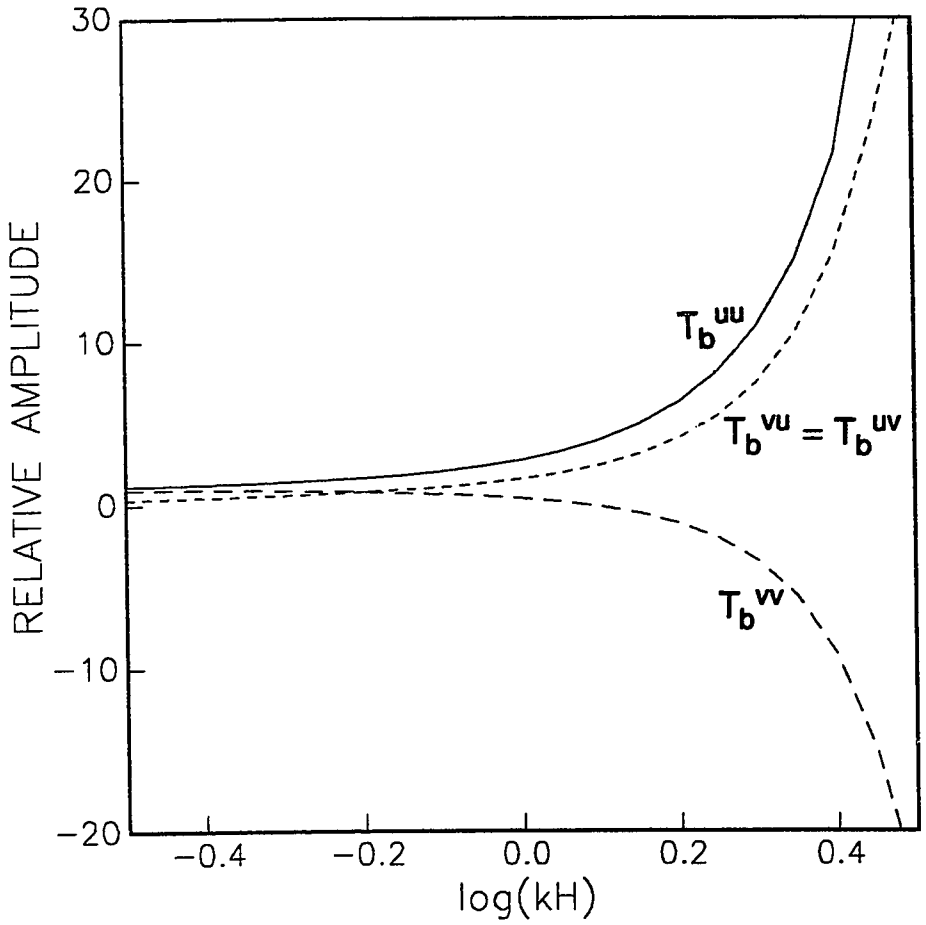

Figure 6-2. Inverse transfer functions for linear viscous rheology. Solid line: T_b^{uu}. Short dashed line: $T_b^{vu} = T_b^{uv}$. Long dashed line: T_b^{vv}.

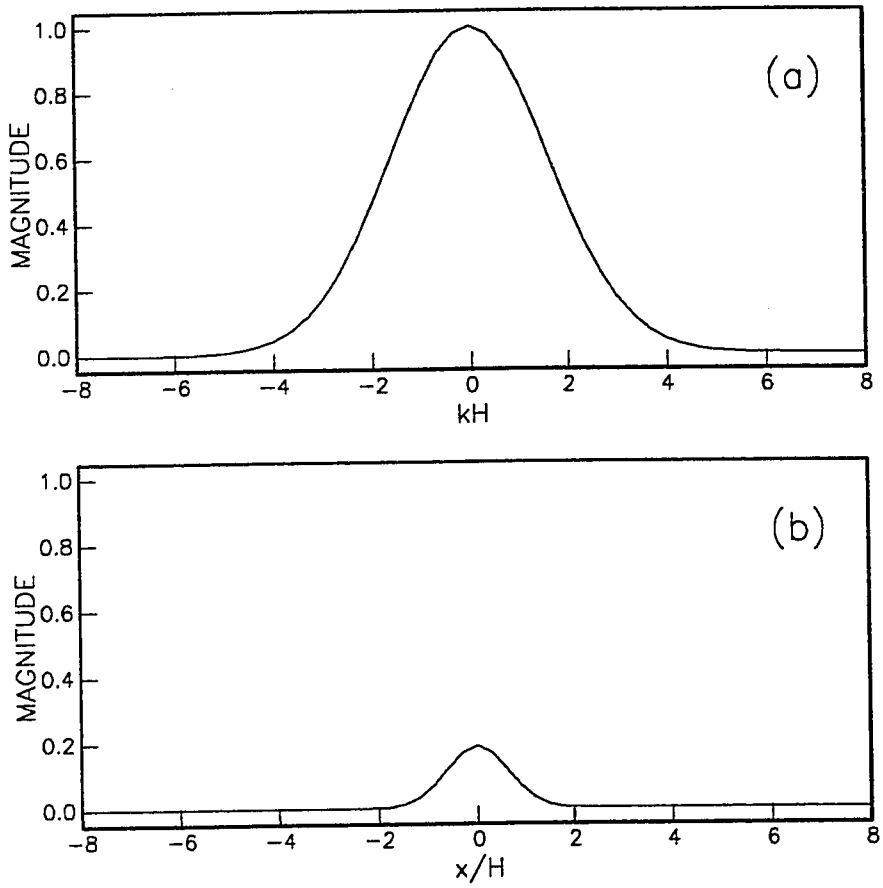

Figure 6-3. Gaussian filter, $\sigma/H = 0.15$. (a) Viewed in the wave number domain, and (b) viewed in the space domain.

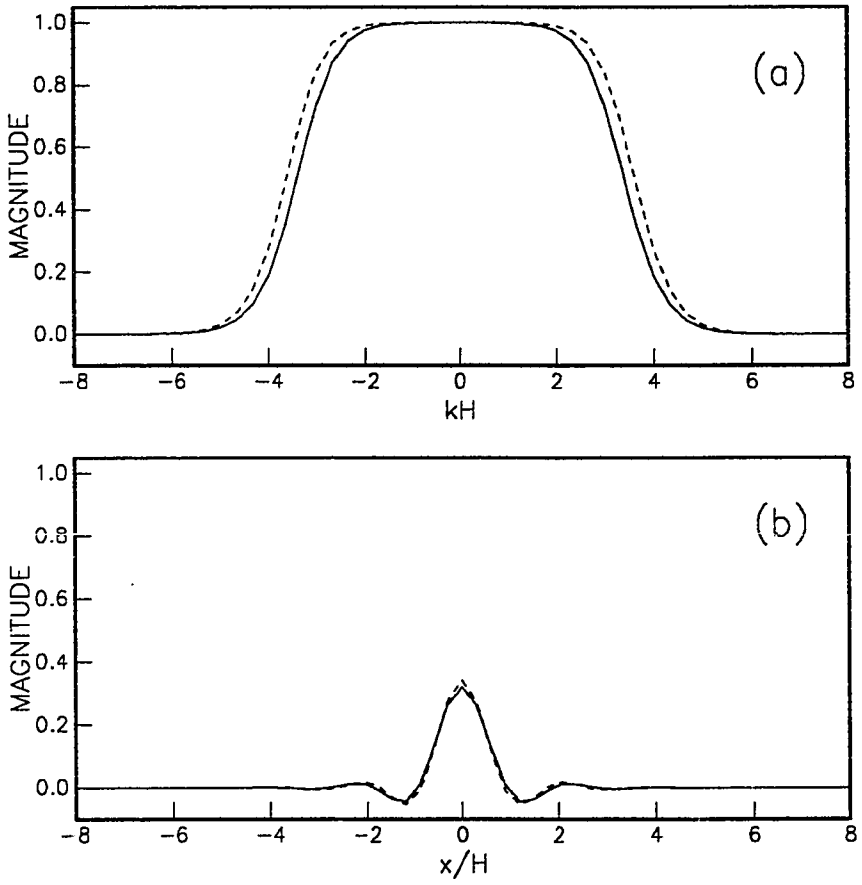

Figure 6-4. Effective filters for trade-off solutions, $n = 0$, $\beta = 7000$. (a) Wave number domain: solid line, $\hat{F}_{ub}$; dashed line, $\hat{F}_{vb}$. (b) Space domain: solid line, F_{ub}; dashed line, F_{vb}.

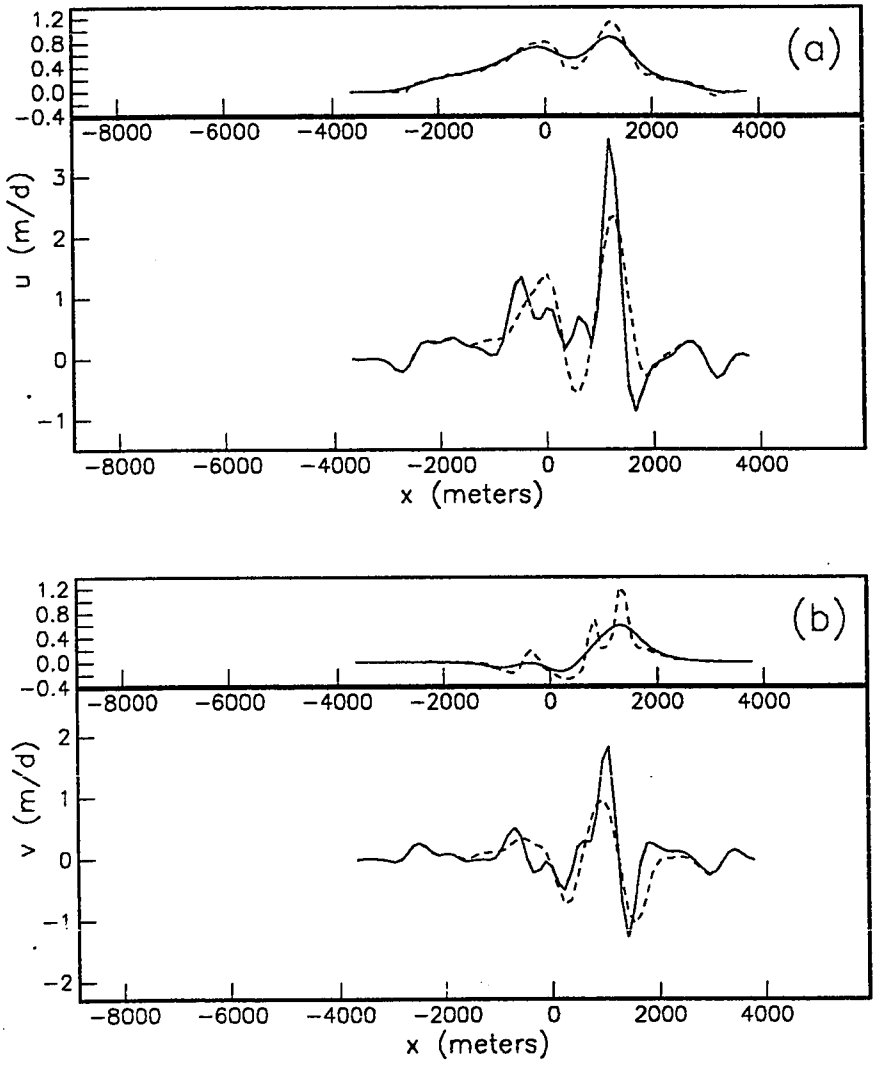

Figure 6-5. Surface and basal velocity components for mini-surge of 15 July 1980, for linear viscous rheology, $x = 0$ at 6.5 *km*. (a) Longitudinal velocity components: upper dashed line, u_s as actually measured; upper solid line, u_s^f calculated using Gaussian filter ($\sigma = 0.137$); lower solid line, u_b calculated using same filter; and lower dashed line, u_b calculated using same filter with v_s set equal to zero. (b) Normal velocity components: upper dashed line, v_s as actually measured; upper solid line, v_s^f calculated using Gaussian filter ($\sigma = 0.137$); lower solid line, v_b calculated using same filter; and lower dashed line, v_b calculated using same filter with v_s set equal to zero.

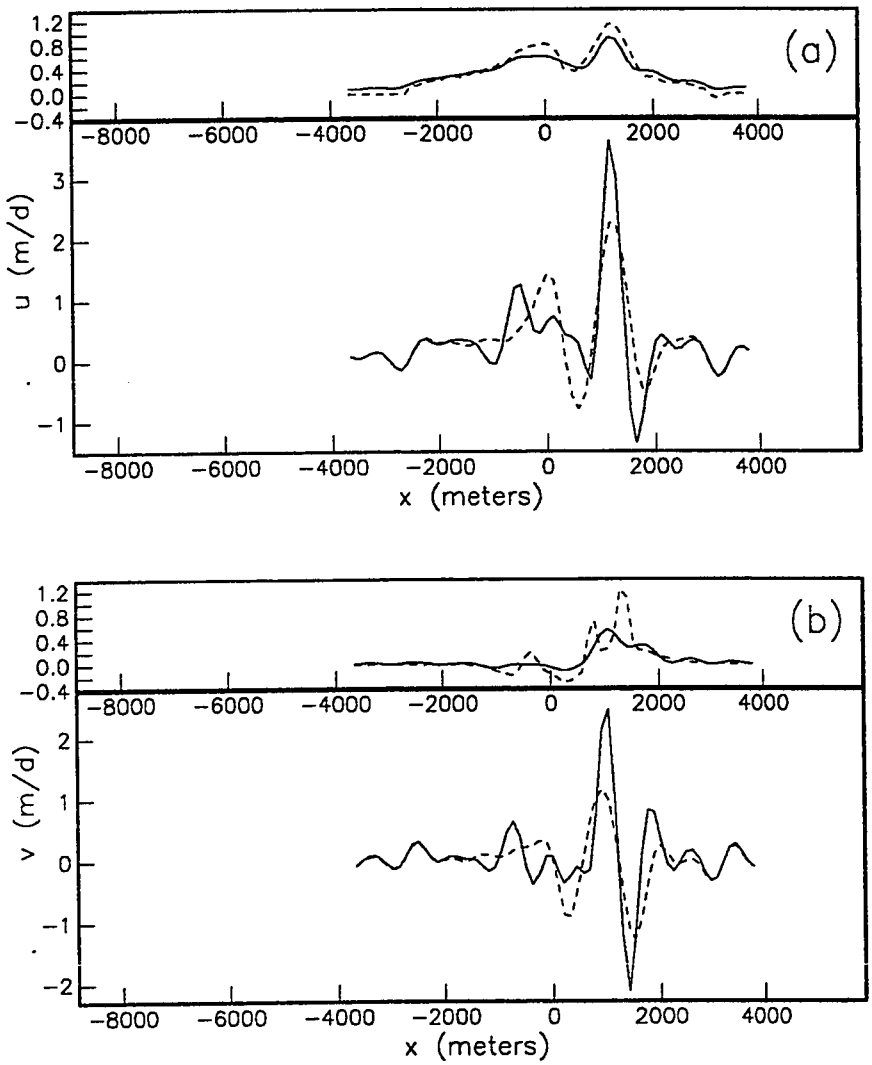

Figure 6-6. Surface and basal velocity components for mini-surge of 15 July 1980, for linear viscous rheology, $x = 0$ at 6.5 *km*. (a) Longitudinal velocity components: upper dashed line, u_s as actually measured; upper solid line, u_s^m calculated using trade-off solution ($n = 0$, $\beta = 1350$); lower solid line, u_b calculated using same trade-off solution; and lower dashed line, u_b calculated using same trade-off solution with v_s set equal to zero. (b) Normal velocity components: upper dashed line, v_s as actually measured; upper solid line, v_s^m calculated using trade-off solution ($n = 0$, $\beta = 1350$); lower solid line, v_b calculated using same trade-off solution; and lower dashed line, v_b calculated using same trade-off solution with v_s set equal to zero.

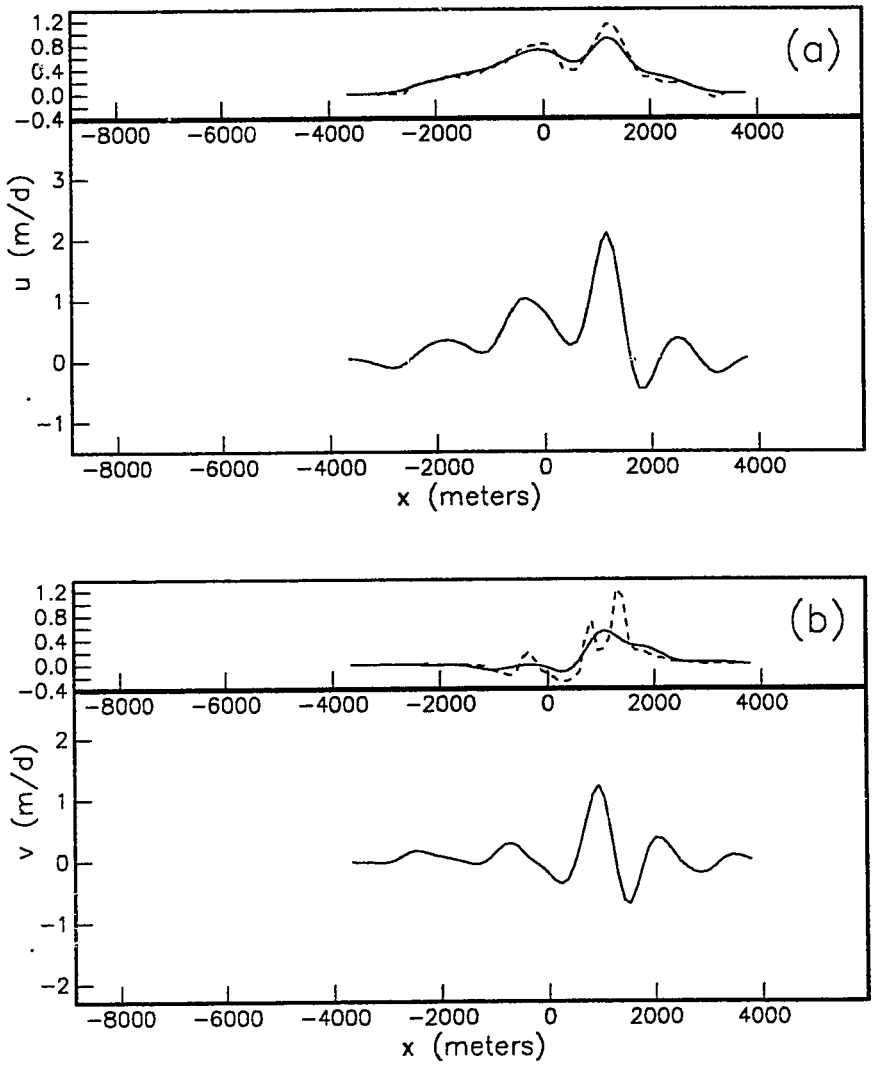

Figure 6-7. Surface and basal velocity components for mini-surge of 15 July 1980, for linear viscous rheology, $x = 0$ at 6.5 *km*. (a) Longitudinal velocity components: upper dashed line, u_s as actually measured; upper solid line, u_s^m calculated using trade-off solution ($n = 1$, $\beta = 1250$); and lower solid line, u_b calculated using same trade-off solution. (b) Normal velocity components: upper dashed line, v_s as actually measured; upper solid line, v_s^m calculated using trade-off solution ($n = 1$, $\beta = 1250$); and lower solid line, v_b calculated using same trade-off solution.

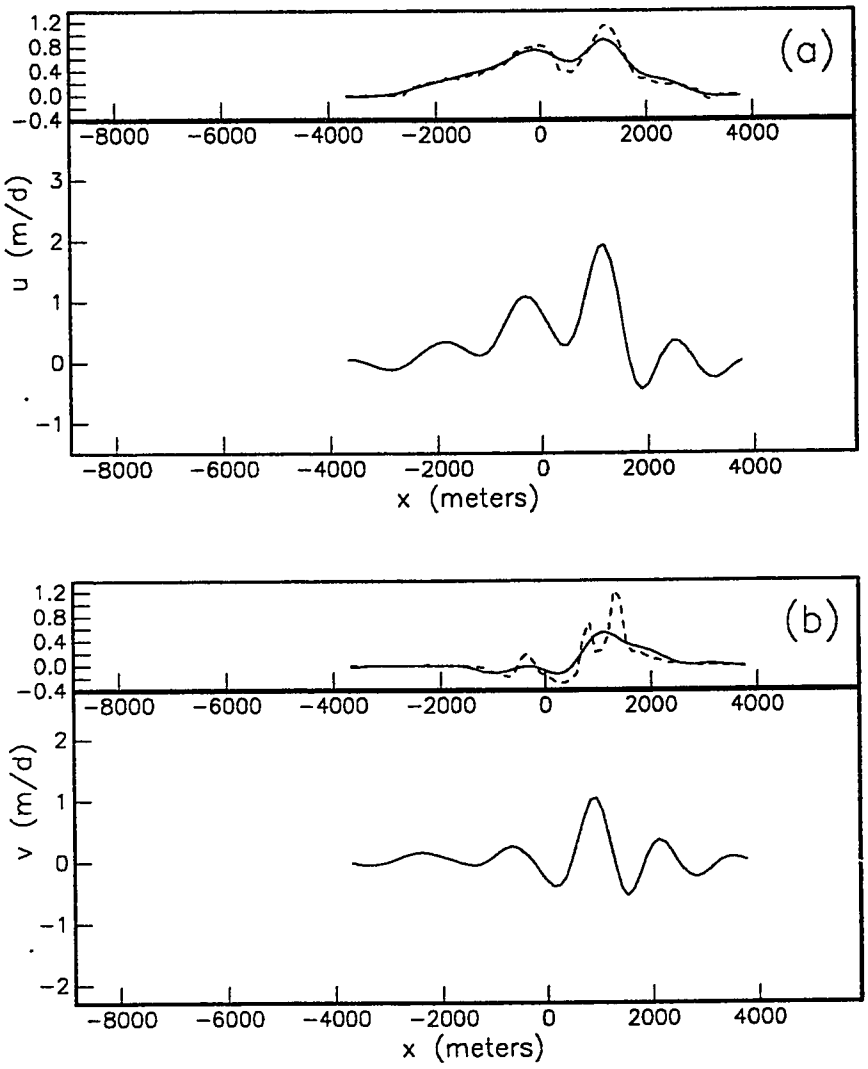

Figure 6-8. Surface and basal velocity components for mini-surge of 15 July 1980, for linear viscous rheology, $x = 0$ at 6.5 *km*. (a) Longitudinal velocity components: upper dashed line, u_s as actually measured; upper solid line, u_s^m calculated using trade-off solution ($n = 2$, $\beta = 3650$); and lower solid line, u_b calculated using same trade-off solution. (b) Normal velocity components: upper dashed line, v_s as actually measured; upper solid line, v_s^m calculated using trade-off solution ($n = 2$, $\beta = 3650$); and lower solid line, v_b calculated using same trade-off solution.

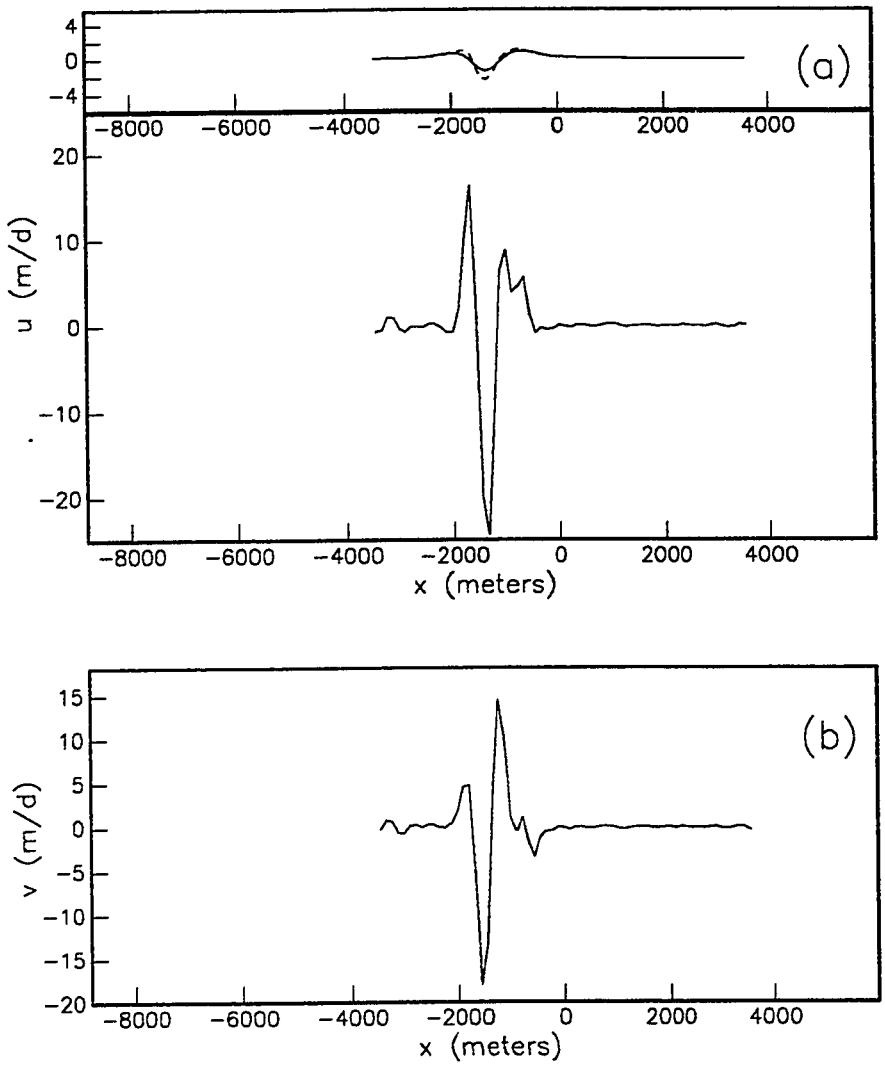

Figure 6-9. Surface and basal velocity components for mini-surge of 11 July 1979, for linear viscous rheology, $x = 0$ at 7.5 *km*. (a) Longitudinal velocity components: upper dashed line, u_s as actually measured; upper solid line, u_s^f calculated using Gaussian filter ($\sigma = 0.196$); and lower solid line, u_b calculated using same filter. (b) Normal component of basal velocity v_b calculated using Gaussian filter ($\sigma = 0.196$).

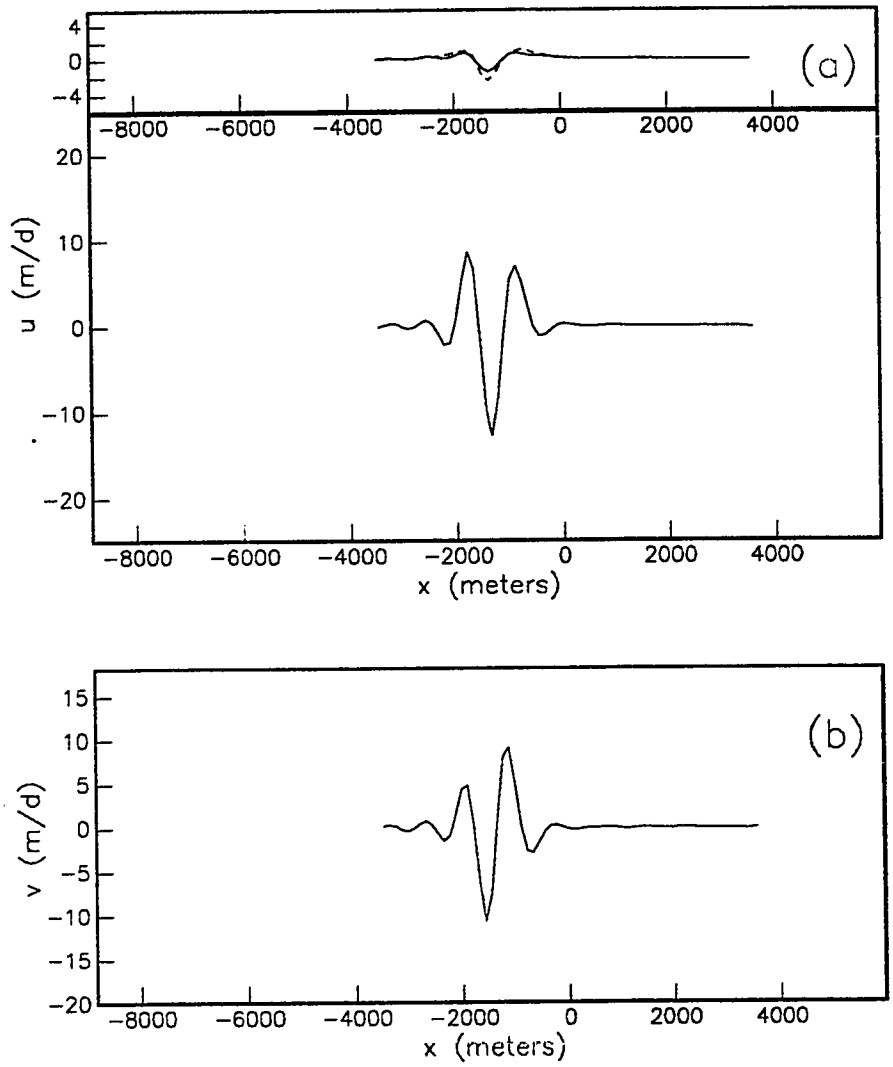

Figure 6-10. Surface and basal velocity components for mini-surge of 11 July 1979, for linear viscous rheology, $x = 0$ at 7.5 *km*. (a) Longitudinal velocity components: upper dashed line, u_s as actually measured; upper solid line, u_s^m calculated using trade-off solution ($n = 0$, $\beta = 2550$); and lower solid line, u_b calculated using same trade-off solution. (b) Normal component of basal velocity v_b calculated using trade-off solution ($n = 0$, $\beta = 2550$).

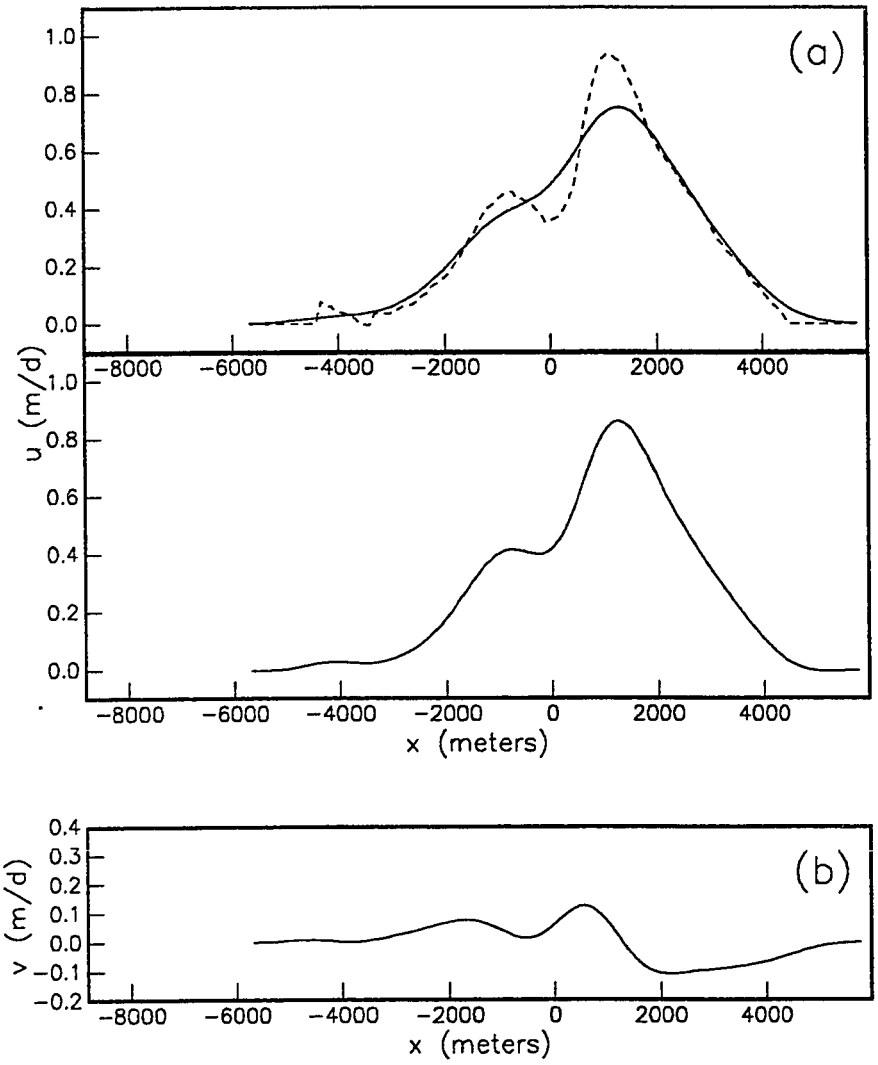

Figure 6-11. Surface and basal velocity components for mini-surge of 14 July 1981, for linear viscous rheology, $x = 0$ at 4.7 *km*. (a) Longitudinal velocity components: upper dashed line, u_s as actually measured; upper solid line, u_s^f calculated using Gaussian filter ($\sigma = 0.047$); and lower solid line, u_b calculated using same filter. (b) Normal component of basal velocity v_b calculated using Gaussian filter ($\sigma = 0.047$).

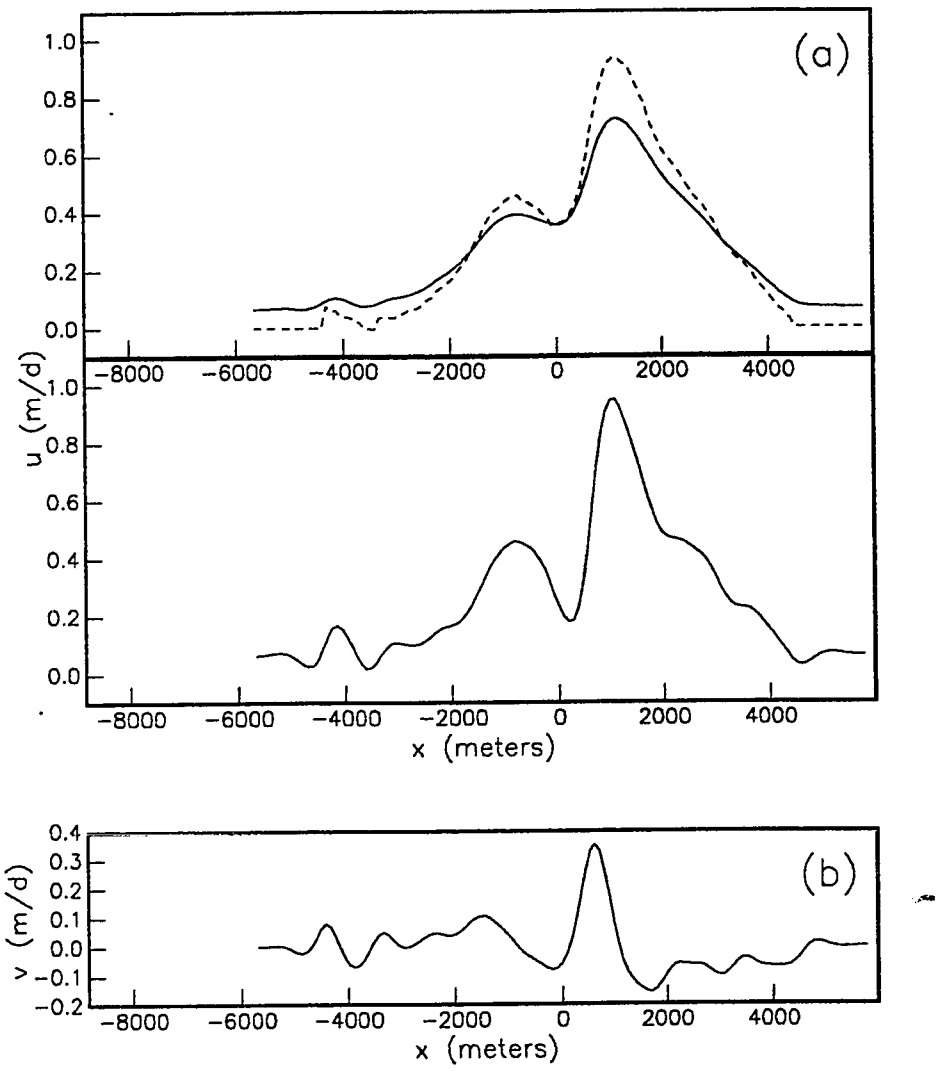

Figure 6-12. Surface and basal velocity components for mini-surge of 14 July 1981, for linear viscous rheology, $x = 0$ at 4.7 *km*. (a) Longitudinal velocity components: upper dashed line, u_s as actually measured; upper solid line, u_s^m calculated using trade-off solution ($n = 0$, $\beta = 200$); and lower solid line, u_b calculated using same trade-off solution. (b) Normal component of basal velocity v_b calculated using trade-off solution ($n = 0$, $\beta = 200$).

CHAPTER 7

NON-LINEAR (POWER LAW) INVERSE SOLUTIONS

7.1 Chapter introduction

The application of inverse theory to problems which involve non-linear rheologies is considerably more complicated than this application for linear rheologies. Because of the non-linearity, an analytic solution to non-linear inverse problems is generally not possible. Numerical methods must be used. Even with these methods, simplifying assumptions such as linear approximations must often be made. In no case can a solution to the non-linear inverse problem be guaranteed (Booker, unpublished).

We are trying to determine the basal velocities which would cause the known measured surface velocities, using the non-linear Glen's flow law rheology. Two possible methods of solving this inverse problem will be investigated. The first of these methods involves using the Frechet derivative (Backus and Gilbert, 1967). For our application, the Frechet derivative is a linear approximation of how the surface velocity changes for small changes in the basal velocity. The second method which we will use is simply trial and error. For both of these methods we will use the finite element model described in Chapter 5.

Since we are using a non-linear rheology, the steady-state and anomalous motions will be coupled (see Chapter 5). Thus we will in general be solving for the total velocity and the total stress (rather than just the anomalous velocity and stress as was the case for linear rheologies).

7.2 Frechet derivative method for velocity inversion

7.2.1 Brief description of method

The Frechet derivative method for non-linear inverse problems is based on a systematic study of small perturbations in the basal velocity. When these small perturbations are made, there will be associated small perturbations in the surface velocity. If a

reasonably accurate initial estimate of the basal velocity can somehow be determined, the resulting surface velocity will be close to the measured surface velocity, and will only need small changes to exactly match this measured surface velocity. These necessary small changes in the surface velocity can be composed of linear sums of the small surface perturbations which resulted from the small perturbations which were systematically made in the basal velocity; thus the necessary changes to the initial estimate of the basal velocity (to make the resulting surface velocity correspond with the measured surface velocity) can be linearly back-calculated.

The Frechet derivative method is described in more detail in the following sections.

7.2.2 Initial estimate of basal velocity

To use the Frechet derivative method, the first step is to make the initial estimate of the total basal velocity. This estimate should be close to the actual solution for the total basal velocity (where the actual solution for the total basal velocity is the basal velocity which results in a total surface velocity which exactly matches the total measured surface velocity). This is necessary for the Frechet derivative method to yield good results, since this method depends on the linear superposition of small perturbations in the basal velocity. This is a linear approximation which is only valid in the vicinity of the actual solution. See Section 7.2.4 for details on the application of the Frechet derivative.

Unfortunately it can be very difficult to accurately guess the basal velocity. A trial and error approach can be used, but this is generally time-consuming and expensive. The best simple guess that we can use is a basal velocity solution using a linear rheology. These solutions can be determined by the analytical inverse theory methods of Chapter 6.

7.2.3 Calculation of Frechet derivative

We next calculate the Frechet derivative. This means that we must systematically perturb the initial estimate of the basal velocity solution and calculate the resulting perturbations in the surface velocity.

Since we are using a finite element model, this systematic perturbation is straightforward. We start with the initial estimate of the total basal velocity. We will define the longitudinal component of this estimate at a basal node i as u_b^i (where $i = 1$ to n for n basal

nodes); similarly we will define the normal component of this estimate as v_b^i. Each basal velocity component at each basal node is in turn perturbed by a small amount δ_u (for u_b^i) or δ_v (for v_b^i). (These perturbation amounts do not change for different basal nodes.) Each perturbation of a single basal velocity component at a single basal node can result in perturbations of both surface velocity components at all the surface nodes. These resulting surface perturbations will be referred to as δu_s^{ij} and δv_s^{ij}, where the first superscript i refers to the basal node and velocity component which was perturbed, and the second superscript j refers to the surface nodes. (These surface perturbations are the difference between the surface solution that results from the initial estimate of the total basal velocity, and the surface solution that results when the initial estimate of the total basal velocity is perturbed.)

Since perturbations in either basal velocity component affect both surface velocity components, it is convenient, for n basal nodes, to let the superscript i range from 1 to $2n$ for the surface perturbations δu_s^{ij} and δv_s^{ij}. This allows us to continue to use this simple notation for the surface perturbations even with the cross-component effects. We simply specify that $i = 1$ to n refers to perturbations in u_b^i at basal nodes 1 to n, and that $i = n+1$ to $2n$ refers to perturbations in v_b^i at basal nodes 1 to n.

We can further simplify the notation by similarly letting the superscript j range from 1 to $2n$. Here $j = 1$ to n will refer to the resulting perturbations in the total longitudinal component of the surface velocity at the surface nodes 1 to n, and $j = n+1$ to $2n$ will refer to the perturbations in the normal component of the surface velocity at the surface nodes 1 to n. (The normal component need not be referred to as "total" since it only has an anomalous part.) We can then combine these surface perturbations into one single function which we will simply refer to as δu_s^{ij}. This function is in fact a $2n$ by $2n$ matrix.

The elements of this matrix are then divided by the amount of the basal velocity perturbation: δ_u for $i = 1$ to n, and δ_v for $i = n+1$ to $2n$. The resulting matrix is the Frechet derivative, which we will refer to as $\delta u_s^{ij}*$. This derivative gives the proportional change in the surface velocity components at all surface nodes for a small change in either basal velocity component at any basal node.

7.2.4 Application of Frechet derivative

To apply the Frechet derivative, we first calculate the "necessary change" in the total surface velocity. This necessary change is the difference between the measured total surface velocity (which we are trying to match) and the modelled total surface velocity which results from the initial estimate of the total basal velocity. We will define this necessary change as δu_s^j. Again, we let the superscript j for $j = 1$ to n refer to the longitudinal component of the surface velocity at the surface nodes 1 to n, and we let $j = n+1$ to $2n$ refer to the normal component of the surface velocity at the surface nodes 1 to n.

We can then solve for the necessary change in the total basal velocity which will cause the necessary change in the surface velocity, by using the Frechet derivative. This necessary change in the total basal velocity will be defined as δu_b^i, where $i = 1$ to $2n$ again refers to both u_b and v_b at the n basal nodes. The equations to solve are:

$$\delta u_b^i \, \delta u_s^{ij*} = \delta u_s^j \tag{7-1}$$

These equations are solved for δu_b^i. The total basal velocity solution will be the solution which results from adding these necessary changes in the total basal velocity δu_b^i to the initial estimate of the total basal velocity. This total basal velocity solution can be considered to be an exact solution to the linearized non-linear inverse problem. If the Frechet derivative δu_s^{ij*} perfectly described all changes in the surface velocity resulting from any changes in the basal velocity, then our calculated total basal velocity solution would result in a surface solution which was exactly equal to the measured total surface velocity.

7.2.5 Smoothing

However, the Frechet derivative is not likely to be perfect, since it is based on a linear perturbation approach for a non-linear rheology. Furthermore, even if the Frechet derivative were perfect, it would not be desirable to exactly match the measured total surface velocity, because this measured velocity contains errors (from surveying inaccuracies, etc.). Both of these problems can be dealt with by first smoothing the measured total surface velocity which we are attempting to match, or alternately smoothing our solution for the total basal velocity (since these two smoothed velocities will be related through the non-linear physics modelled by the finite element model).

This smoothing process can be carried out by the methods of Chapter 6: either a filtering approach or a trade-off approach. For the filtering approach, since we are operating in the space domain, the filters are convolved with the total basal velocity (the filters were multiplied in the wave number domain in Chapter 6). This is a discrete convolution because of the discrete velocity representation of the finite element model.

The trade-off approach for smoothing the total basal velocity solution is considerably more complicated for the non-linear rheology used here than for the linear rheology of Chapter 6. This is because the transfer functions for the linear rheology can be written as a diagonal matrix (in the wave number domain); while the Frechet derivative (which is the equivalent of the non-linear transfer functions for a particular problem in the space domain) is not a diagonal matrix. Working in the wave number domain would not greatly simplify the non-linear problem, since the Frechet derivative still could not be written as a diagonal matrix. (The reason for this is that for the non-linear rheology, motion at any wave number affects the effective viscosity and therefore affects the transfer functions at other wave numbers; see Chapter 5.)

The application of the filtering and trade-off approaches in Chapter 6 did not show a clear advantage of one method over the other. We will therefore use the filtering approach for smoothing the velocities in this chapter, since it is computationally simpler.

7.2.6 Iterating and convergence

To test whether or not the Frechet derivative method works for a specific case, we first calculate the "adjusted" total surface velocity which results from the smoothed adjusted initial estimate of the total basal velocity (adjusted by the "necessary changes" δu_b^i, and smoothed by the methods of the previous section). This adjusted total surface velocity is then compared with the "unadjusted" total surface velocity which results from the unadjusted initial estimate of the total basal velocity. If the match between the adjusted surface velocity and the measured surface velocity is better than the match between the unadjusted surface velocity and the measured surface velocity, then the application of the Frechet derivative may be considered successful.

If the Frechet derivative is working successfully, it is possible to use an iteration process to more closely match the measured surface velocity. This process involves using the

smoothed adjusted basal velocity as the new initial estimate of the basal velocity. This new initial estimate is then perturbed, and a new Frechet derivative is calculated. This new Frechet derivative is then used to further adjust the basal velocity. This process can be repeated, to more and more closely match the measured surface velocity.

The other possible result of the initial application of the Frechet derivative is that the adjusted surface velocity has a poorer match to the measured surface velocity (compared to the match between the unadjusted surface velocity and the measured surface velocity). For this case, we can say that the solution is not converging. The application of the Frechet derivative will not be successful unless we can somehow get a better initial estimate for the basal velocity. This emphasizes the importance of a good initial estimate.

7.3 Trial and error method for velocity inversion

7.3.1 Correcting guesses based on non-linear transfer functions

The other method which we will investigate for non-linear inverse solutions is trial and error. This means that we will guess a total basal velocity solution, use it as the basal boundary condition in the finite element model, and then see how closely the resulting total surface velocity matches the measured total surface velocity. Adjustments can then be made to the basal velocity in an attempt to better match the surface velocity. (The Frechet derivative method is simply a systematic way to do this adjustment, but if there is an intuitive basis for making changes the trial and error method can actually be computationally more efficient.)

Fortunately we have some basis for making the adjustments to the basal velocity. This basis is the information of the non-linear transfer functions determined in Chapter 5. For the non-linear rheology these transfer functions are not exactly correct for non-harmonic velocity patterns (due to each wave number component of the velocity affecting the stress distribution and thus affecting the effective viscosity). However, the information from the non-linear transfer functions can still be used as a first guess of how to adjust the basal velocity, to get a surface velocity pattern which more closely matches the measured surface velocity.

More specifically, these transfer functions are used as follows. If we wish to adjust a long-scale feature of the surface velocity, we make a similar adjustment to the basal velocity, since we know that there is not much attenuation in long-scale features between the base and the surface. At intermediate and short scales, an adjustment to the basal velocity must be greater in amplitude than the desired change at the surface, since there is considerable attenuation between the base and the surface at these scales. At the very short scale, changes in the surface velocity are very difficult to predict from adjustments in the basal velocity, since there is extreme attenuation at this scale.

The cross-component effect of the transfer functions must also be considered (e.g. T_s^{uv} and T_s^{vu}). The possible 180° phase change in T_s^{uu} is also important. These effects must be considered at the intermediate and short scales.

7.3.2 Problems with cross-component effects and phase changes

The problem with the cross-component effect for the trial and error method, is that adjusting either velocity component at the base can change both velocity components at the surface (at the intermediate and short scales). Thus if we wish to change the total longitudinal velocity component at the surface u_s^t by adjusting the total longitudinal velocity component at the base u_b^t, we may also cause changes in the normal velocity component at the surface v_s. (The normal component of the surface velocity v_s does not have a steady-state part; thus this component is anomalous only and there is no need to refer to the "total".) Similarly, adjusting the normal velocity component at the base v_b in order to change v_s, may also cause changes in u_s^t.

Thus the cross-component effect can result in undesired changes in the surface velocity pattern. As an additional complication, it may actually be better to adjust the opposite component at the base, compared to the surface component which we wish to change, at the intermediate and short scales. (E.g., we can adjust u_b^t to change v_s, and adjust v_b to change u_s^t.) This is especially true when the transfer function T_s^{uu} is near to zero in value, if we wish to change u_s^t. At this scale the only way to cause significant changes in u_s^t is to adjust v_b.

The 180° phase change which is part of the transfer function T_s^{uu} at short wavelengths must also be considered. This means that if we desire a positive change in a short-scale

feature of the surface velocity component u_s^t, it is likely that a negative adjustment to the associated short-scale feature of the basal velocity component u_b^t will be necessary.

7.4 Velocity inversion of Variegated Glacier mini-surge data

7.4.1 Inversion attempt using Frechet derivative

We will now apply the simple non-linear inverse theory which we have developed in the previous sections to data from Variegated Glacier. We will only attempt the non-linear inversion for data from one mini-surge. We will use the mini-surge of 15 July 1980 since this has the best data (the measured surface velocity at 6.5 *km*, see Chapter 6).

In this section we will apply the Frechet derivative method. This method requires an initial estimate of the total basal velocity. For this initial estimate we will use a solution for the basal velocity from the linear inversion methods of Chapter 6. Specifically, we will use the basal velocity solution which results when a Gaussian filter is applied to the surface velocity, with the basal velocity then calculated using the exact inverse transfer functions. In addition, for the initial estimate of the non-linear basal velocity solution, we will multiply the linear solution by 1.5. This is to allow for the increased attenuation between the base and the surface with the non-linear rheology (see Chapter 5).

This initial estimate of the total basal velocity is shown in Figures 7-1. The resulting total surface velocity is also shown in these figures. This surface velocity is the total surface velocity which results from using a sloped bed (with bed slope comparable to the bed slope of Variegated Glacier) combined with the initial estimate of the basal velocity anomaly. (The sloped bed is actually modelled by simply including a longitudinal component of gravity in the body force, which would give a surface velocity from ice deformation of $u_s^d = 0.3\ m\ d^{-1}$ if there were no basal velocity anomaly and no steady-state sliding (unchanging in the x direction). This corresponds to the long-term average measured surface velocity of Variegated Glacier in the region of the mini-surges when basal sliding is not included (Raymond and Harrison, in press).)

Our modelled surface velocity shows the effects of coupling between the steady-state flow (from the sloped bed) and the anomalous flow (from the prescribed basal velocity anomaly). This coupling becomes evident if we observe that the strain-rate softening from

the velocity anomaly increases the steady-state longitudinal component of the surface velocity (subtracting off the surface velocity anomaly) to about $u_s^s = 1.3\ m\ d^{-1}$, as compared to the surface velocity with no velocity anomaly of $u_s^d = 0.3\ m\ d^{-1}$ (for this bed slope angle).

The measured total surface velocity during the mini-surge is also shown in Figures 7-1. It is important to note that this measured surface velocity may include contributions from three essentially different mechanisms: steady-state basal sliding, steady-state deformation due to the sloped bed, and the basal velocity anomaly. Of these three mechanisms, steady-state basal sliding is the only one not included in the modelled velocity distribution. However, it is not certain that steady-state sliding occurs during mini-surges (most of the perceived steady-state motion at the surface over the time-span of a given mini-surge may in fact be due to increased strain-rate softening from the velocity anomaly, which results in an increased longitudinal deformation velocity due to the sloped bed). If steady-state sliding appears to be necessary to match the measured velocity pattern, we could easily add this steady-state sliding to our prescribed basal velocity in the model; or the Frechet derivative might directly give us the amount of steady-state sliding in the basal velocity.

If we now compare the measured surface velocity with the modelled surface velocity (resulting from the initial estimate of the basal velocity), major differences are apparent. In particular, the modelled strain-rate softening resulting from our initial estimate of the basal velocity is much greater than the strain-rate softening which is evident in the measured surface velocity (although both surface velocities have longitudinal components, subtracting the surface velocity anomalies, which are greater than $u_s^d = 0.3\ m\ d^{-1}$). Furthermore the surface velocity pattern resulting from the initial estimate does not match the measured surface velocity pattern very well. Hopefully the application of the Frechet derivative will reduce these differences between the modelled and measured surface velocities.

Ideally, the Frechet derivative would be calculated using a sloped bed (to correspond to the bed slope of Variegated Glacier). Then the initial estimate of the total basal velocity could then be adjusted to attempt to match the total surface velocity during the mini-surge of 15 July 1980. This calculation of the Frechet derivative using the sloped bed is desirable because of the coupling between steady-state deformation (due to the longitudinal component of gravity for a sloped bed) and the velocity anomaly (due to the prescribed basal velocity anomaly).

However, here the Frechet derivative was actually calculated with no bed slope. This difference between the ideal and actual methods used to calculate the Frechet derivative is equivalent to the difference between the non-linear transfer functions of Chapter 6 with and without a sloped bed. Although these differences are noticeable, the qualitative patterns are similar.

The Frechet derivative is then used to adjust our initial estimate of the total basal velocity. The adjusted total basal velocity must then be smoothed. For this we use a Gaussian filter.

The smoothed adjusted total basal velocity, the resulting total surface velocity, and the measured total surface velocity are shown in Figures 7-2. Careful numerical comparison of these velocities with the velocities shown in Figures 7-1 (the unadjusted velocities) shows that the application of the Frechet derivative has somewhat improved the match between the modelled u_s^t and the measured u_s^t. However, the match between the modelled v_s and the measured v_s has in fact been made a little worse by the application of the Frechet derivative.

A more major problem is that the application of the Frechet derivative does not significantly reduce the amount of strain-rate softening from the velocity anomaly. Thus u_s^s for the modelled surface velocity (resulting from the adjusted basal velocity) is still much greater than u_s^s for the measured surface velocity. Especially, the total longitudinal component of the surface velocity which results from the application of the Frechet derivative is still too great in the region of the greatest basal velocity anomaly.

This leads us to the basic conclusion that the overall amount of strain-rate softening must somehow be reduced. Neither our initial estimate of the total basal velocity nor the application of the Frechet derivative results in low enough strain-rate softening. This indicates that a reduction in the strain-rate softening must be accomplished by some direct method.

Two possible methods are: (1) changing the rheology, and (2) reducing the average basal strain rate by simplifying the form of the basal anomaly (this means that the initial estimate of the basal velocity must be simplified).

Changing the rheology is not a very good choice, since the Glen's flow law which we are using has been shown to be a good approximation for the rheology of glacier ice.

It is true that during mini-surges primary creep may be important along with visco-elastic effects; however, Chapter 4 showed that visco-elastic effects did not significantly affect the surface velocity pattern for a basal anomaly. On the balance it seems best to stay with the chosen non-linear rheology.

This leaves the choice of simplifying the basal anomaly to reduce the average basal stress. This is in essence a trial and error approach for making the initial estimate of the basal velocity. Once a better initial estimate is arrived at the Frechet derivative can be recalculated and applied to further improve this better estimate. However, time and money constraints did not allow the recalculation of the Frechet derivative. Instead, we proceed directly to the trial and error method for determining the non-linear inverse solution.

7.4.2 Inversion using trial and error

For the trial and error method, we need a first guess for the total basal velocity for the mini-surge of 15 July 1980. This is analagous to the initial estimate of the total basal velocity for the Frechet derivative method. We know that the initial estimate used for the Frechet derivative method resulted in too much strain-rate softening. We will therefore simplify this initial estimate to reduce the strain-rate softening, and then use this simplified velocity as a first guess for the trial and error method.

To simplify the basal velocity, we prescribe only a single peak in u_b^t (instead of the several peaks, with one dominant peak, which resulted from the linear inverse solution). We center this peak under the dip between the peaks at the surface in the measured form of u_s^t. We will initially set $v_b = 0$. We will also initially not prescribe any steady-state basal sliding.

This first guess for the total basal velocity is shown in Figure 7-3a. The resulting total surface velocity is shown in Figures 7-3b and 7-3c. This calculation is done with a sloped bed, which would result in a surface velocity of $u_s^d = 0.3\ m\ d^{-1}$ if there were no basal velocity (corresponding to the situation for Variegated Glacier in the region of the mini-surges).

In Figures 7-3 we note that simplifying the basal velocity has reduced the strain-rate softening, so that the steady-state longitudinal component of the surface velocity u_s^s resulting from our initial guess of the basal velocity is about equal to u_s^s for the measured

surface velocity. However, the pattern of our modelled surface velocity could use considerable improvement in order to better match the measured surface velocity. Specifically, the up-glacier peak in our modelled u_s^t is too large, and the down-glacier peak has multiple oscillations, as compared to the measured surface velocity. Also, the magnitude of our modelled v_s is too large when compared to the measured velocity.

The next step in the trial and error method is experimenting with changes in the basal velocity pattern, to see if the match between the modelled and the measured surface velocities can be improved. For the mini-surge of 15 July 1980, this experimentation was carried out through a process of 20 trial and error solutions, with each solution taking advantage of the information learned from the previous solution. It was also decided that matching the measured total longitudinal component of the surface velocity was more important than matching the measured normal component of the surface velocity, since details about the spatial pattern of the normal component are not as reliable.

Using this trial and error method, it was found that a fairly close match could be obtained between the modelled and the measured total longitudinal components of the surface velocity, by using a basal velocity anomaly with both a total longitudinal component u_b^t and a normal component v_b. The final velocity patterns which result in this close match for the total longitudinal component of the surface velocity are shown in Figures 7-4. Both of the basal velocity components have a single positive peak. The peak in u_b^t corresponds to an anomalous increase in the sliding velocity. The peak in v_b corresponds to basal uplift (cavitation). There is no negative part to v_b, but gradual down-drop after the basal uplift is still quite plausible due to the inaccuracies of the modelling process.

It is interesting to note that steady-state basal sliding (not changing in the x direction) is only evident in the part of the modelled mini-surge which is down-glacier from the peaks in the basal velocity (i.e., the part of the mini-surge which precedes the velocity peaks in time, since the mini-surge propagates in the down-glacier direction). Up-glacier of the peaks in the basal velocity, both basal velocity components go to zero (i.e., in the part of the mini-surge which follows the velocity peaks in time). However, given the possible inaccuracies of the rheology and the modelling process, we can not say for certain that steady-state basal sliding does not still occur following the peaks in the basal velocity.

Unfortunately, the match between the modelled and the measured normal components

of the surface velocity is not very good. Trial and error did not yield an improvement in this match without substantially worsening the match between the modelled and the measured longitudinal components.

Several explanations are possible for this inability to simultaneously match the measured values of both u_s^t and v_s. These explanations are:

(1) The rheology is probably at least somewhat incorrect. However, as previously mentioned, it does not seem possible to greatly improve the rheology.

(2) Transverse (cross-glacier) effects could be affecting the measured surface velocity. Unfortunately, no good data exist which would allow an accurate examination of these effects.

(3) Ice compression, or compression of voids, could enter the problem. Again, no good data exist which would allow this to be examined.

(4) The surface data for v_s are not very detailed. Thus a good match to the measured v_s may be somewhat irrelevant. Also, these poor surface data are part of the reason it is difficult to calculate the importance of explanations (1), (2), and (3).

The conclusions from the trial and error solution shown in Figures 7-4 tor the mini-surge of 15 July 1980 can be summarized as follows. First, it is likely that u_b^t has only a single peak; otherwise, the strain-rate softening is too great for the surface velocity to be matched. The second conclusion is that there is quite likely basal uplift (cavitation) associated with the peak in u_b^t (this is seen from the peak in v_b). This uplift may precede the peak in u_b^t. The uplift is not as well constrained as the evidence for only a single peak in u_b^t. Finally, steady-state basal sliding may only occur in the part of the mini-surge which precedes the peaks in the basal velocity in time. This conclusion is also not certain.

7.4.3 Importance of length of finite element model

An important question that should be answered is whether or not interactions from the periodicity of the finite element model can cause some of the strain-rate softening which is seen with the modelling of velocity anomalies. That is, the model is actually representing a repeating series of sections, only one of which we examine; but each of these sections contains an identical velocity anomaly. Thus the anomalies in the two sections immediately adjacent to the section which we are examining might significantly affect

the stress distribution in the examined section, thereby increasing the strain-rate softening. This problem is similar to the problems caused by the assumed periodicity of the fast Fourier transform (see Chapter 2), although for the linear rheology with which we used the fast Fourier transform the problem is possible direct interactions between the periodic anomalies.

Experimenting with the length of the finite element model leads to the conclusion that longitudinal interactions (associated with the periodicity) occur over much greater lengths for the non-linear rheology than for a linear rheology. For a linear rheology, the interaction length is of the order of $5H$ to $10H$ (where H is the ice thickness); for the non-linear rheology with a prescribed basal velocity anomaly and a sloped bed, the interaction length is of the order of $20H$ to $30H$.

Thus the length of the finite element model which was used in Section 7.4.2 for the final trial and error mini-surge inversion was made equal to about $35H$. This prevented the assumed periodicity of the velocity anomalies from affecting the strain-rate softening in the examined section, and thus giving erroneously high values for the steady-state longitudinal component of the surface velocity u_s^s. (The length of the finite element model for the "first guess" trail and error solution, and for all of the Frechet derivative solutions in Section 7.4.1, was only equal to about $16H$. Although this shorter length results in some excess strain-rate softening from periodic interactions, it does not account for a major portion of the excessive strain-rate softening which occurs in the Frechet derivative solution.)

It is important to note that longitudinal interactions will occur in cases other than the specific case which we have examined (a prescribed velocity anomaly with a sloped bed). The length over which these interactions are important may vary from case to case. However, the case which we have examined shows that this interaction length is considerably longer for the non-linear rheology than for the linear rheology, and we can reasonably expect that the interaction length for the non-linear rheology will always be of the order of $20H$ to $30H$.

7.5 Basal shear stress calculations for Variegated Glacier mini-surge

7.5.1 Determination of basal shear stress

Among the outputs from the finite element model are the total residual forces at all nodes. For a reasonably converged solution, these residuals should be small at the interior nodes. However, at the basal nodes the force residuals must support the basal boundary stress which will be associated with a sloped bed or a prescribed basal velocity anomaly.

These force residuals at the basal nodes can be distributed over the length between nodes to find the total basal shear stress τ_b' (this is the sum of the steady-state basal shear stress $\rho g H \sin\gamma$ due to the sloped bed, and the anomalous basal shear stress). For varying lengths between nodes, half of the length both up and down-glacier from a given node is used.

Unfortunately, there is a problem with pressure oscillations in many finite element models (Sani and others, 1981). These oscillations occur in the model which we are using. Although these oscillations do not affect the convergence of the velocity solutions, they will affect the force residuals at the nodes. This in turn affects the direct calculation of the basal shear stress from these residuals. However, this problem can be dealt with fairly well by applying a running mean to the calculated basal shear stress. In our case we have used a three-point running mean, with the end values weighted proportionally to their distance from the center value.

These procedures allow a reasonably accurate calculation of the total basal shear stress. We can then calculate the total basal shear stress associated with the trial and error basal velocity solution for the mini-surge of 15 July 1980. This total basal shear stress τ_b' is shown in Figure 7-5a. Here τ_b' has a reasonably smooth pattern, and is generally positive for most of the mini-surge. In particular, there is a positive peak in τ_b' both up-glacier and down-glacier from the basal velocity peak of the mini-surge. However, there is a substantial negative region in τ_b' between the positive peaks. This region of negative basal shear stress corresponds with the positive peak in the longitudinal component of the basal velocity u_b'.

This form of correspondence between the anomalous basal shear stress and the anomalous longitudinal component of the basal velocity for the non-linear rheology could

possibly be expected, based on the relation between the anomalous basal shear stress and the anomalous longitudinal component of the basal velocity developed in Chapter 3 for a linear rheology (where the relation is given by a transfer function T^{τ} which is always negative). However, it is quite surprising that the total basal shear stress is negative. This does not seem physically reasonable, but the modelled velocity solution gives derivatives $\partial u/\partial y$ and $\partial v/\partial x$ which result in this negative basal shear stress. The probable solution to this problem is that in the region of very high strain rates associated with the mini-surges, the correct rheology is different than the rheology which we have used (e.g., primary or tertiary creep effects might be important). Thus for the correct rheology, the total basal shear stress could always be positive. Nevertheless, we will continue to use Glen's flow law as our non-linear rheology, because a more accurate rheology for the mini-surges has not been determined.

A check of the basal shear stress solution from the finite element model is to see if the average basal shear stress equals the theoretical basal shear stress for no basal velocity anomaly $\rho g H \sin\gamma$. This check matches within about ten per cent for our non-linear inverse solution, for the mini-surge of 15 July 1980. (It does not match exactly because of the application of the running mean and the non-uniform node spacing.)

7.5.2 Does a sliding law hold?

It is interesting to more closely examine the relation between the total basal velocity and the total basal shear stress to see what form a sliding law has during the mini-surge of 15 July 1980.

For a sliding law with only a fixed parameter W, the basal shear stress will increase as the longitudinal component of the basal velocity increases (see Chapter 3). However, the sliding law parameter can also be variable; this is almost certainly the situation during the mini-surges of Variegated Glacier. (This variation in the sliding law parameter during mini-surges is probably due to a large controlling effect on the parameter from basal water pressure.) Thus during the mini-surges the relation between the basal shear stress and the basal velocity will vary according to the varying sliding law parameter.

Since we have solved for both the basal shear stress and the basal velocity for the mini-surge of 15 July 1980 (using the trial and error method), we can easily derive the

implied distribution of the varying sliding law parameter. Rearranging Equation (3-3) gives us a solution for this varying sliding law parameter $W(x)$:

$$W(x) = \frac{u_b{}'(x)}{\tau_b{}'(x)} \tag{7-2}$$

(Here all of the terms refer to the total quantities; $W(x)$ may include both steady-state and anomalous parts.) The solution for $W(x)$ from the non-linear basal shear stress and basal velocity solutions for the mini-surge of 15 July 1980 is shown in Figure 7-5b.

This resulting pattern which we have derived for the sliding law parameter W can be described fairly simply. For most of the mini-surge W is generally positive. In particular, there is a pronounced positive peak down-glacier from the basal velocity peak. However, in the region of the positive peak in $u_b{}'$ (with a corresponding negative peak in $\tau_b{}'$), W has a pronounced negative peak.

This varying form for W can be related to possible models for mini-surges. These models ascribe the velocity changes to a pressure wave in the basal hydraulic system. In actual measurements at fixed spatial locations during mini-surges, the basal water pressure increases abruptly and then decreases gradually, as the mini-surge propagates down-glacier (Kamb and Engelhardt, 1987). Thus during the mini-surges we expect an abrupt increase in W (resulting in increased sliding for a given level of basal shear stress) followed by a decrease back to normal levels.

The results in Figures 7-5 do show an abrupt increase in W in the down-glacier part of the mini-surge, which probably corresponds to the start of the basal water pressure wave. However, the results then show a negative peak in W; this is due to the negative total basal shear stress which we have derived in this part of the mini-surge, which is probably not correct (as explained in Section 7.5.1). In reality, the basal shear stress in this zone is probably near to zero but still positive; this means that the substantial negative peak in W should actually be part of the positive peak. Thus the negative parts of $\tau_b{}'$ and W in Figures 7-5 probably correspond in physical reality to a low basal shear stress and a continued large positive value for the sliding law parameter, which are associated with the peak in the basal water pressure. The sliding law parameter then gradually decreases back to a small value (in the up-glacier direction).

7.6 Comparison of linear and non-linear solutions

7.6.1 Comparison of basal velocity solutions

It is interesting to compare the basal velocity solutions obtained using the linear and non-linear rheologies for the mini-surge of 15 July 1980. Since the solution for the non-linear rheology is the total basal velocity solution, we must derive a corresponding total basal velocity solution for the linear rheology (only the anomalous basal velocity solutions were calculated for the linear rheology in Chapter 6). This total linear basal velocity solution is calculated in Appendix D, for an inverse solution using a Gaussian filter.

We first compare the longitudinal components of the total basal velocity solutions. The solution for the total longitudinal component of the basal velocity u_b^t for the mini-surge of 15 July 1980 using the linear rheology is shown in Figure D-1a. The corresponding solution for u_b^t using the non-linear rheology is shown in Figure 7-4a (using the trial and error method). These solutions both show a pronounced pulse or peak in u_b^t. The magnitudes of these peaks for the two rheologies are similar (4 to 5 $m\ d^{-1}$). However, the peaks in the basal velocity are located in significantly different spatial positions: the peak for the non-linear rheology is up-glacier a distance equivalent to about $5H$ (where H is the ice thickness) as compared to the peak for the linear rheology.

This difference between the solutions using the two different rheologies has two possible explanations. A very likely possibility is simply that the inverse solutions are not necessarily absolutely correct; thus the difference between the two rheologies may not be as large as it appears. The other possibility is that the two rheologies really are this different. A simple physical explanation for this difference between the two rheologies is that for the non-linear rheology the coupling of the steady-state velocity (from the longitudinal body force) with the anomalous velocity results in a significant shift in the basal velocity pattern, as compared to the case for the linear rheology for which no coupling exists.

The correspondence is better between the two rheologies for the solutions for the normal components of the basal velocity. The solution for the normal component of the basal velocity v_b for the mini-surge of 15 July 1980 using the linear rheology is shown in Figure D-1b; the corresponding solution for v_b using the non-linear rheology is shown in Figure

7-4b. (These solutions can be easily compared because the normal component of the velocity does not have a steady-state part for either rheology.) Both of these solutions have a positive peak in about the same spatial location (with a magnitude of about 1.5 $m\ d^{-1}$). The linear solution also has a negative peak (preceding the positive peak in time) which is not matched in the non-linear solution. However, given the previously discussed inaccuracies in the data for this component at the surface v_s, and the fact that the non-linear solution did not result in a good match for v_s, the difference between the linear and non-linear solutions for v_b does not seem physically significant.

7.6.2 Comparison of basal shear stress solutions and sliding law parameters

The total basal shear stress solution for the mini-surge of 15 July 1980 using a linear rheology (see Figure D-2a in Appendix D) can be compared with the total basal shear stress solution for this mini-surge using a non-linear rheology (Figure 7-5a). Comparison of the linear and the non-linear solutions shows a somewhat similar pattern. For both of these solutions the total basal shear stress $\tau_b{}'$ is generally positive for most of the mini-surge, with a substantial negative region for $\tau_b{}'$ somewhat down-glacier from the middle of the modelled section. The magnitude of $\tau_b{}'$ differs for the two rheologies but is within the same order of magnitude; furthermore, the magnitude of $\tau_b{}'$ for the linear rheology will depend on the value chosen for the dynamic viscosity η (see Appendix D).

For both rheologies, the region of negative total basal shear stress corresponds with the major positive region in the total longitudinal component of the basal velocity $u_b{}'$. However, since the major positive region in $u_b{}'$ is down-glacier for the linear rheology as compared to the non-linear rheology, the corresponding negative region for $\tau_b{}'$ is also down-glacier for the linear rheology as compared to the non-linear rheology.

The total basal shear stress $\tau_b{}'$ for the linear rheology is also rougher in pattern than $\tau_b{}'$ for the non-linear rheology. This is to be expected, since the linear basal velocity pattern is rougher than the non-linear basal velocity pattern. We also used a smoothing process (the three-point running mean) for $\tau_b{}'$ for the non-linear rheology; for the linear rheology $\tau_b{}'$ was not smoothed.

It is also interesting to compare the total sliding law parameter W for the linear and the non-linear rheologies, for the mini-surge of 15 July 1980. (The linear solution is

shown in Figure D-2b; the non-linear solution is shown in Figure 7-5b.) In general, both of the solutions are positive; this is physically reasonable. Both of these solutions also have a negative peak in W corresponding to the negative peak in τ_b'. As previously mentioned, these negative peaks are not physically realistic. The non-linear solution has a positive peak in W immediately down-glacier from the negative peak; while the linear solution has a positive peak immediately up-glacier from the negative peak. These may both be associated with the pressure wave in the basal hydraulic system. However, the non-linear positive peak in W is in a much more reasonable position (preceding the basal velocity peak) than is the linear peak in W (which follows the velocity peak).

It is also possible to gain some insight into the solution for W for the mini-surge by looking at the linear sliding law solutions in Chapter 3. These linear solutions may help to explain the extreme form for the total sliding law parameter W that is seen in the non-linear solution for the mini-surge (Figure 7-5b). This is because the peak in the longitudinal component of the basal velocity during a mini-surge is somewhat similar to the linear case examined in Chapter 3 for a step in the longitudinal component of the basal velocity, since both of these cases involve rapid changes in the basal velocity. In the example of Chapter 3, the step in the longitudinal component of the basal velocity is associated with sharp changes from positive to negative in the anomalous sliding law parameter (see Figures 3-6). Although the solution for the mini-surge in this chapter uses the total quantities and a non-linear rheology, and the solution in Chapter 3 uses the anomalous quantities and a linear rheology, both solutions show the possibility of rapid changes in the sliding law parameter.

7.7 Discussion

This chapter cannot be viewed as a complete examination of the non-linear inverse solutions for Variegated Glacier mini-surges. Ideally, the Frechet derivative method would have been applied to its full potential. This could have been done by using the best solution obtainable from trial and error as a new initial solution for the Frechet derivative method. It is possible that this could have further improved the match of the modelled and measured surface velocities, particularly for the normal component v_s. As previously mentioned, time and money constraints prevented this further application of the Frechet derivative. Also the motivation is not strong, in view of the many uncertainties.

It would also be interesting to examine other mini-surges, besides the mini-surge of 15 July 1980. However, this mini-surge has the best surface velocity data, so it yields the most certain conclusions about the basal velocity and the basal shear stress.

The information from the non-linear inverse solutions can be summarized as three important conclusions, which were not evident from the linear inverse solutions. These conclusions are:

(1) The strain-rate softening during a mini-surge results in a substantial steady-state longitudinal component of the surface velocity u_s^s. Thus the pattern of the basal velocity anomaly must be relatively simple; otherwise, the strain-rate softening is too great and the modelled value of u_s^s is greater than the measured value.

(2) The interaction length during mini-surges is quite long ($20H$ to $30H$). This means that mini-surges will have effects over long lengths in both space and time, for propagating mini-surges.

(3) The combination of high strain-rate softening and long interaction lengths means that any long-term averages over time spans which include mini-surges must be very carefully calculated. As an example of this, the steady-state basal sliding velocity could be given an erroneously high value, when in actuality part of the effect was substantially increased ice deformation from the strain-rate softening associated with mini-surges.

These conclusions from the non-linear inverse solutions are quite valuable. These conclusions show the importance of non-linear effects for short-scale velocity variations in glaciers.

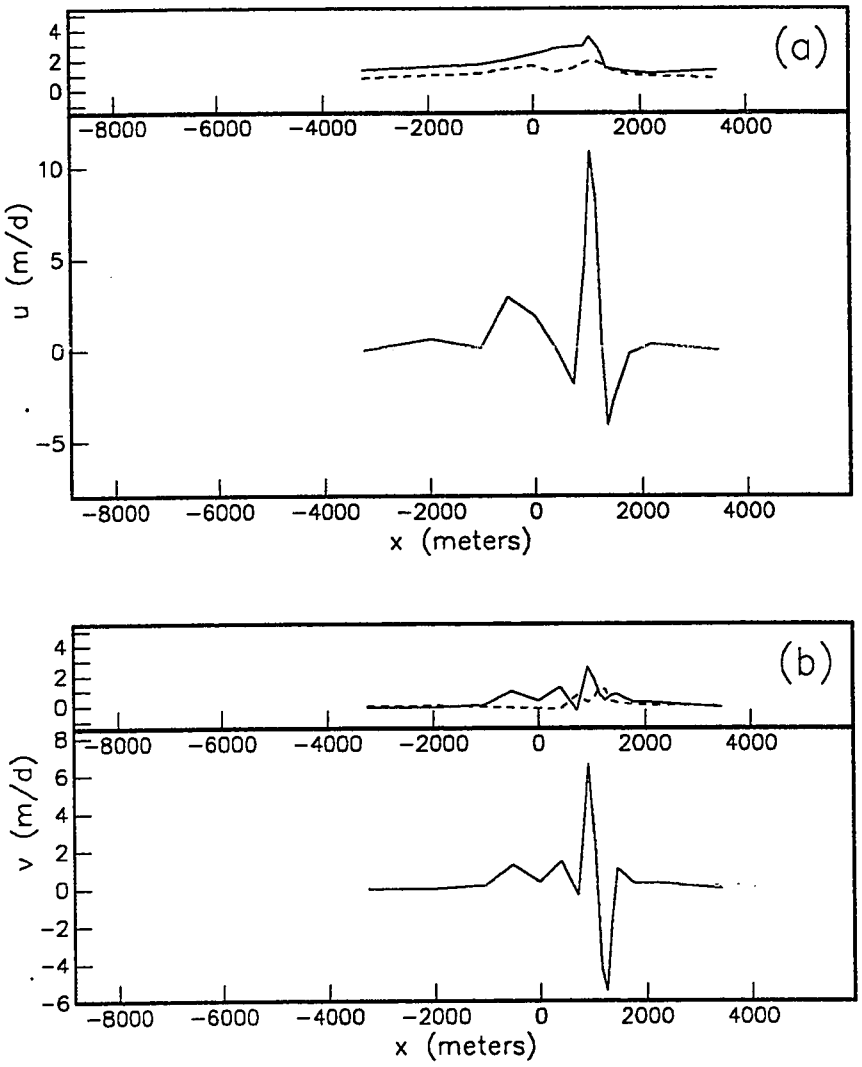

Figure 7-1. Total surface and basal velocity components for mini-surge of 15 July 1980, for non-linear rheology, $u_s^d = 0.3\ m\ d^{-1}$, $x = 0$ at 6.5 *km*. (a) Longitudinal velocity components: upper dashed line, u_s^t as actually measured; upper solid line, u_s^t corresponding to initial estimate of basal velocity (for Frechet derivative method); lower solid line, initial estimate of u_b^t for Frechet derivative method. (b) Normal velocity components: upper dashed line, v_s as actually measured; upper solid line, v_s corresponding to initial estimate of basal velocity (for Frechet derivative method); lower solid line, initial estimate of v_b for Frechet derivative method.

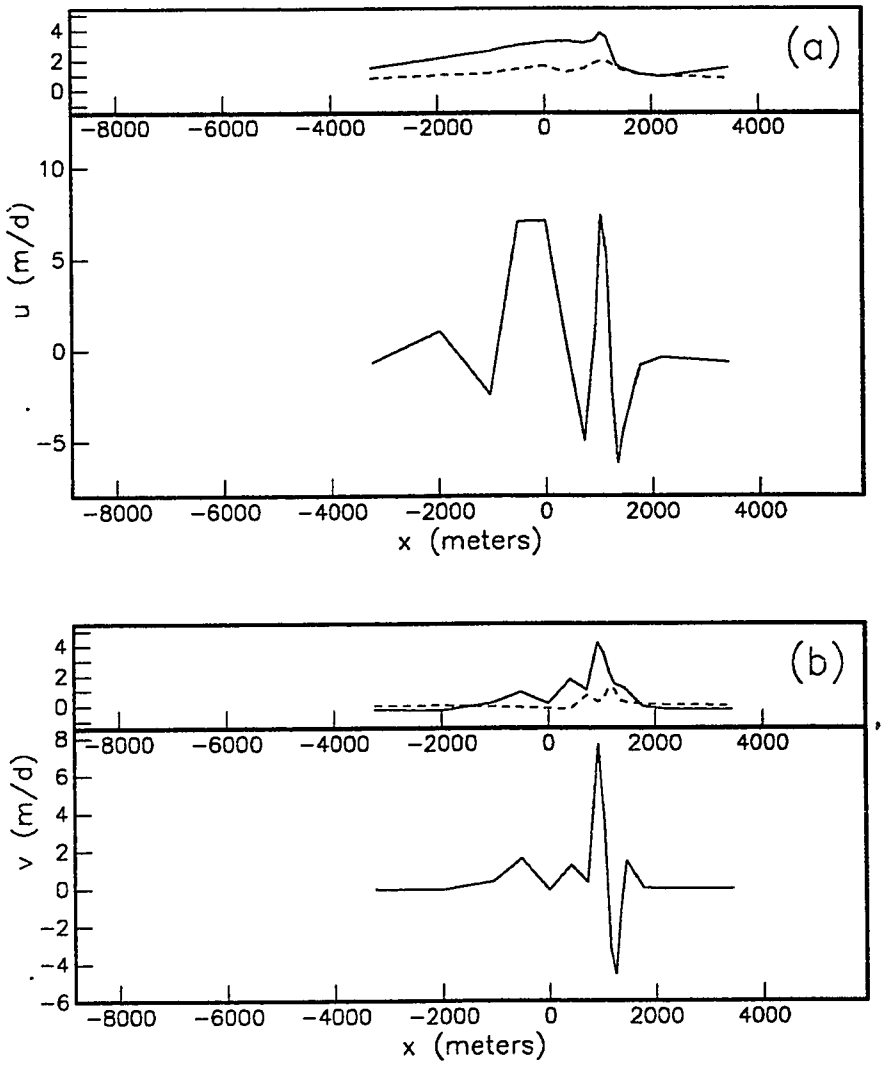

Figure 7-2. Total surface and basal velocity components for mini-surge of 15 July 1980, for non-linear rheology, $u_s^d = 0.3\ m\ d^{-1}$, $x = 0$ at 6.5 *km*. (a) Longitudinal velocity components: upper dashed line, u_s^t as actually measured; upper solid line, u_s^t corresponding to smoothed adjusted initial estimate of basal velocity (for Frechet derivative method); lower solid line, smoothed adjusted initial estimate of u_b^t for Frechet derivative method. (b) Normal velocity components: upper dashed line, v_s as actually measured; upper solid line, v_s corresponding to smoothed adjusted initial estimate of basal velocity (for Frechet derivative method); lower solid line, smoothed adjusted initial estimate of v_b for Frechet derivative method.

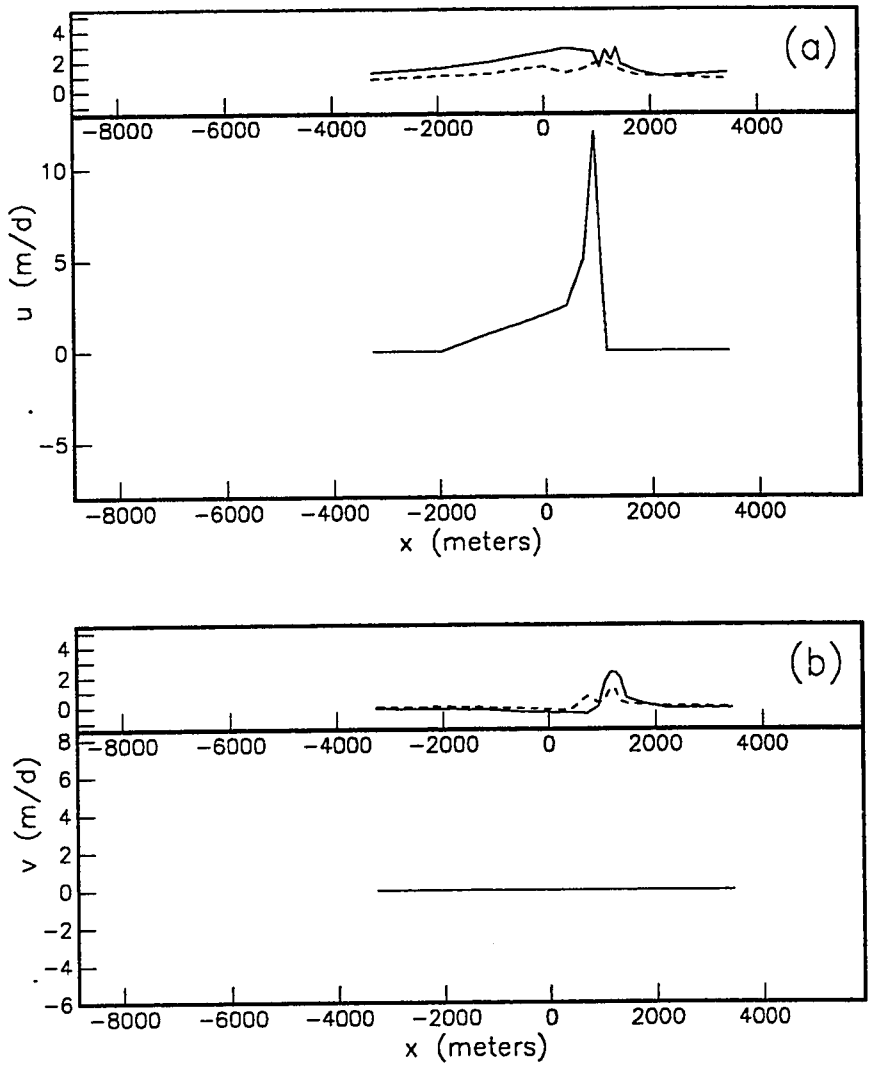

Figure 7-3. Total surface and basal velocity components for mini-surge of 15 July 1980, for non-linear rheology, $u_s^d = 0.3\ m\ d^{-1}$, $x = 0$ at 6.5 *km*. (a) Longitudinal velocity components: upper dashed line, u_s^t as actually measured; upper solid line, u_s^t corresponding to first guess of basal velocity (for trial and error method); lower solid line, first guess of u_b^t for trial and error method. (b) Normal velocity components: upper dashed line, v_s as actually measured; upper solid line, v_s corresponding to first guess of basal velocity (for trial and error method); lower solid line, first guess of v_b for trial and error method.

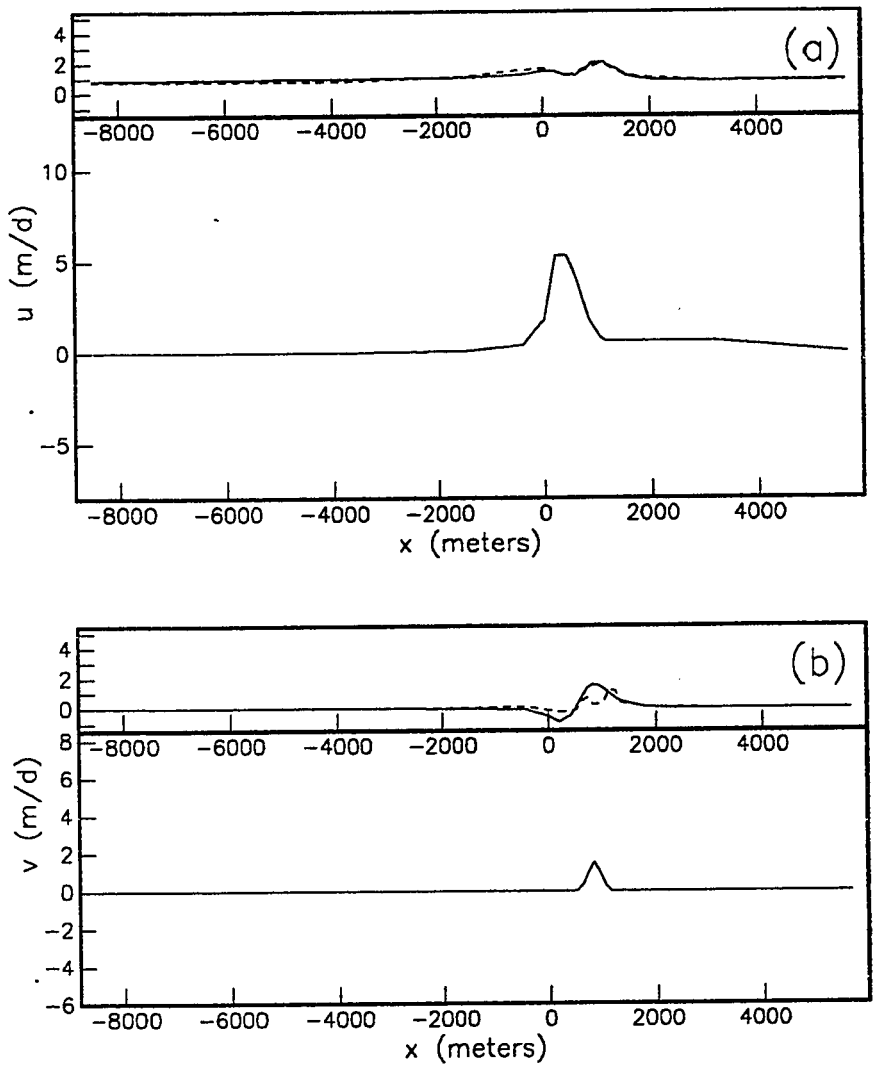

Figure 7-4. Total surface and basal velocity components for mini-surge of 15 July 1980, for non-linear rheology, $u_s^d = 0.3\ m\ d^{-1}$, $x = 0$ at 6.5 *km*. (a) Longitudinal velocity components: upper dashed line, u_s^t as actually measured; upper solid line, u_s^t corresponding to final guess of basal velocity (for trial and error method); lower solid line, final guess of u_b^t for trial and error method. (b) Normal velocity components: upper dashed line, v_s as actually measured; upper solid line, v_s corresponding to final guess of basal velocity (for trial and error method); lower solid line, final guess of v_b for trial and error method.

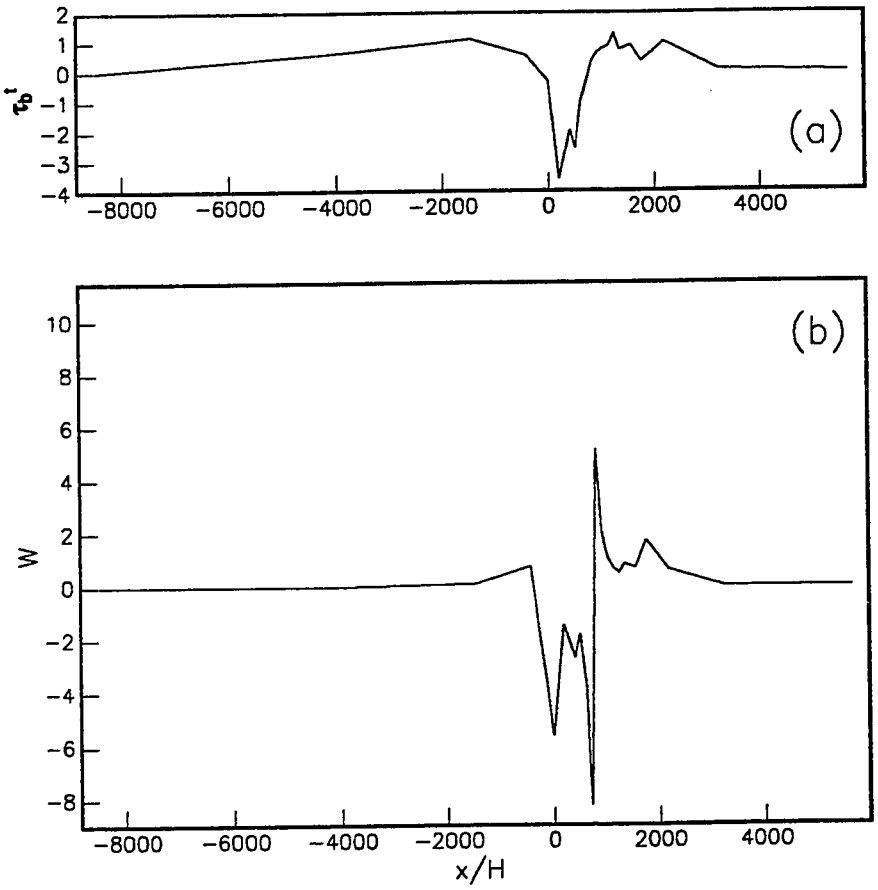

Figure 7-5. (a) Total basal shear stress τ_b^t for mini-surge of 15 July 1980, for non-linear rheology, $u_s^d = 0.3\ m\ d^{-1}$, $x = 0$ at 6.5 *km*, from final guess for trial and error method. Stress units correspond to $u_s^d = 0.3\ m\ d^{-1}$. (b) Sliding law parameter determined as $W = u_b^t/\tau_b^t$, where all quantities include both steady-state and anomalous parts, for u_b^t from Figure 7-4a and τ_b^t from Figure 7-5a.

CHAPTER 8

CONCLUSIONS

The relation between surface and basal velocities in glaciers for relatively short-scale velocity anomalies is dependent on several important factors. The first of these is the exact spatial form of the velocity anomaly. The effects of spatial form are most easily described by looking at the length L of a prescribed basal velocity anomaly (e.g., a harmonic wavelength), with L compared to the thickness H of the glacier. The surface effects are then categorized for different ratios of L to H. Four different length scales can be defined.

For a linear viscous rheology or a visco-elastic rheology, the characteristics of the flow at the four scales is as follows. At very short scales ($L \leq 1H$) there is essentially no response at the surface. At short scales ($1H \leq L \leq 5H$) the surface response is of the order of half of the magnitude of the basal anomaly. Anomalies in either the longitudinal or normal components of the basal velocity will cause anomalies in both components at the surface; in particular, these cross-component effects show that substantial anomalous normal motions at the surface may be induced by deformation even though the basal velocity anomaly has only a longitudinal component. The spatial form of the longitudinal component at the surface may be very different from that component at the bed. At intermediate scales ($5H \leq L \leq 10H$) the magnitude of the surface response is generally greater than the magnitude at the short scale. Cross-component effects are similar to the short scale. The spatial form of the longitudinal component at the surface will more closely follow that component at the bed. At the long scale ($10H \leq L$) the velocity anomaly at the surface is essentially the same as the velocity anomaly at the bed. These relationships can be exactly described by analytically determined transfer functions which relate the surface and basal velocity anomalies.

The assumed rheology of the ice is also important. A realistic non-linear rheology results in smaller amplitude effects at the surface when compared to the results for linear rheologies, for a given length scale. The boundaries between the different scales are also shifted towards longer wavelengths. Furthermore, for the non-linear rheology the steady-state and anomalous flow patterns are coupled, because both affect the effective viscosity of the ice. Thus it is not possible to separately consider the anomalous flow. In general,

steady-state deformation due to gravity reduces the surface effects of any basal velocity anomalies, due to a stress guide effect. Also, the velocity anomalies cause strain-rate softening of the ice, resulting in an increase in the mean surface deformation velocity, as compared to the steady-state flow for no velocity anomaly. These effects complicate solutions for the non-linear rheology.

The assumed rheology of the ice also affects the interaction length, over which a localized basal velocity anomaly can affect the surface velocity pattern. For the linear viscous rheology, this interaction length is on the order of $5H$ (where H is the ice thickness); for the non-linear rheology the interaction length can be as great as $20H$ to $30H$.

The inversion of actual data from Variegated Glacier mini-surges (attempting to calculate basal velocity from the measured surface velocity) shows several important points. The first of these is that the magnitude of the basal velocity anomalies during the mini-surges is considerably greater than the magnitude of the resulting surface velocity anomalies, by a factor of up to about 10. This means that the basal velocity during the mini-surges is comparable to the velocity during the main surge of Variegated Glacier (although the mini-surges only affect a narrow zone which relatively rapidly propagates down-glacier, while the main surge involves most of the glacier). Second, it is very difficult to determine how much of the normal motion at the surface is caused by normal motions at the bed, and how much is caused by cross-component effects (from longitudinal motions at the bed). This means that it is not possible to to determine the amount of cavitation which may occur at the bed during the rapid velocity changes of the mini-surges. Finally, an inversion using the non-linear rheology shows that the basal velocity anomaly must be relatively simple in pattern, at least for the particular mini-surge examined (15 July 1980). If the pattern is not simple, the associated strain-rate softening results in an excessive longitudinal velocity component at the glacier surface. This is consistent with the results for a basal sliding law, which show that excessively rapid basal velocity changes result in physically unreasonable basal shear stresses.

The velocity inversion of Variegated Glacier data emphasizes the importance of adequate data. In particular, the spatial resolution of the data from Variegated Glacier is not good. Good time series data exist, but major errors are quite likely introduced by the assumptions necessary to convert this data to a function of varying spatial position. Thus it would be very desirable if future measurements were made with significantly improved

spatial resolution. All directional components of the surface velocity need to be measured, at a reasonable number of spatial positions, and more or less simultaneously. Any basal velocity data which might be obtained from borehole measurements would also greatly help in constraining the basal velocity calculations.

BIBLIOGRAPHY

Backus, G. E., and Gilbert, J. F. 1967. Numerical applications of a formalism for geophysical inverse problems. *Geophysical Journal of the Royal Astronomical Society*, vol. 13, pp. 247-276.

Balise, M. J., and Raymond, C. F. 1985. Transfer of basal sliding variations to the surface of a linearly viscous glacier. *Journal of Glaciology*, vol. 31, pp. 308-318.

Bindschadler, R. 1983. The importance of pressurized subglacial water in separation and sliding at the glacier bed. *Journal of Glaciology*, vol. 29, pp. 3-19.

Boulton, G. S., and Hindmarsh, R. C. A. 1987. Sediment deformation beneath glaciers: rheology and geological consequences. *Journal of Geophysical Research*, vol. 92, pp. 9059-9082.

Churchill, R. V. 1972. *Operational Mathematics*. New York, McGraw-Hill Book Co.

Clarke, G. K. C. 1987. Subglacial till: a physical framework for its properties and processes. *Journal of Geophysical Research*, vol. 92, pp. 9023-9036.

Echelmeyer, K. A., and Kamb, B. 1986. Stress-gradient coupling in glacier flow: II. Longitudinal averaging in the flow response to small perturbations in ice thickness and surface slope. *Journal of Glaciology*, vol. 32, pp. 285-298.

Engelhardt, H. F., Harrison, W. D., and Kamb, B. 1978. Basal sliding and conditions at the glacier bed as revealed by bore-hole photography. *Journal of Glaciology*, vol. 20, pp. 469-508.

Flugge, W. 1967. *Viscoelasticity*. Waltham, Mass., Blaisdell Publishing Co.

Glen, J. W. 1955. The creep of polycrystalline ice. *Proceedings of the Royal Society of London,* A228, pp. 519-538.

Haefeli, R. 1970. Changes in the behavior of the Unteraargletscher in the last 125 years. *Journal of Glaciology,* vol. 9, pp. 195-212.

Hantz, D., and Lliboutry, L. 1981. The inverse problem for valley glacier flow. *Journal of Glaciology,* vol. 27, pp. 179-184.

Harrison, W. D., Raymond, C. F., and MacKeith, P. 1986. Short period motion events on Variegated Glacier as observed by automatic photography and seismic methods. *Annals of Glaciology,* vol. 8, pp. 82-89.

Hodge, S. M. 1974. Variations in the sliding of a temperate glacier. *Journal of Glaciology,* vol. 13, pp. 349-369.

Humphrey, N., Raymond, C., and Harrison, W. 1986. Discharges of turbid water during the mini-surges of Variegated Glacier, Alaska. *Journal of Glaciology,* vol. 32, pp. 195-207.

Hutter, K., 1983. *Theoretical glaciology.* Dordrecht, D. Reidel Publishing Co./Tokyo, Terra Scientific Publishing Co.

Hutter, K., Leger, F., and Spring, U. 1981. First-order stresses and deformations in glaciers and ice sheets. *Journal of Glaciology,* vol.27, pp. 227-270.

Hutter, K., and Olunloyo, V. O. S. 1980. On the distribution of stress and velocity in an ice strip, which is partly sliding over and partly adhering to its bed, by using a Newtonian viscous approximation. *Proceedings of the Royal Society of London,* A373, pp. 385-403.

Iken, A. 1977. Variations of surface velocities of some alpine glaciers measured at intervals of a few hours. Comparison with Arctic glaciers. *Zeitschrift fur Gletscherkunde und Glazialgeologie,* Bd. 13, H. 1/2 (1977), pp. 23-25.

Iken, A. 1981. The effect of the subglacial water pressure on the sliding velocity of a glacier in an idealized numerical model. *Journal of Glaciology,* vol. 27, pp. 407-421.

Iken, A., and Bindschadler, R. A. 1986. Combined measurements of subglacial water pressure and surface velocity of Findelengletscher, Switzerland: conclusions about drainage system and sliding mechanism. *Journal of Glaciology,* vol. 32, pp. 101-119.

Iken, A., Rothlisberger, H., Flotron, A., and Haeberli, W. 1983. The uplift of Unteraargletscher at the beginning of the melt season - a consequence of water storage at the bed? *Journal of Glaciology,* vol. 29, pp. 28-47.

Jaech, J. L. 1985. *Statistical Analysis of Measurement.* London/New York, Van Nostrand.

Kamb, B. 1970. Sliding motion of glaciers: theory and observation. *Reviews of Geophysics and Space Physics,* vol. 8, pp. 673-728.

Kamb, B., and Echelmeyer, K. A. 1986. Stress-gradient coupling in glacier flow: I. Longitudinal averaging of the influence of ice thickness and surface slope. *Journal of Glaciology,* vol. 32, pp. 267-284.

Kamb, B., and Engelhardt, H. 1987. Waves of accelerated motion in a glacier approaching surge: the mini-surges of Variegated Glacier, Alaska. *Journal of Glaciology,* vol. 33, pp. 27-46.

Krimmel, R. B., and Vaughan, B. H. 1987. Columbia Glacier, Alaska: changes in velocity 1977-1986. *Journal of Geophysical Research,* vol. 92, pp. 8961-8968.

Lanczos, C. 1956. *Applied Mathematics.* Englewood Cliffs, N.J., Prentice Hall.

Langdon, J., and Raymond, C. 1978. "Numerical calculation of adjustment of a glacier surface to perturbations in ice thickness." Academy of Sciences of the U.S.S.R. Section of Glaciology of the Soviet Geophysical Committee and Institute of Geography, Publ. no. 32, pp. 233-239.

Lliboutry, L. 1975. Loi de glissement d'un glacier sans cavitation. *Ann. Geophys.*, vol. 31, pp. 207-226.

Nye, J. F. 1952. The mechanics of glacier flow. *Journal of Glaciology*, vol. 2, pp. 82-93.

Nye, J. F. 1953. The flow law of ice from measurements in glacier tunnels, laboratory experiments and the Jungfraufirn borehole experiment. *Proceedings of the Royal Society of London,* A219, pp. 477-489.

Nye, J. F. 1969. A calculation on the sliding of ice over a wavy surface using a Newtonian viscous approximation. *Proceedings of the Royal Society of London,* A311, pp. 445-467.

Papoulis, A. 1962. *The Fourier Integral and its Applications.* New York, McGraw-Hill Book Co.

Paterson, W. S. B. 1981. *The Physics of Glaciers.* Oxford, England, Pergammon Press Ltd.

Peltier, W. R. 1974. The impulse response of a Maxwell Earth. *Reviews of Geophysics and Space Physics,* vol. 12, pp. 649-669.

Pfeffer, W. T. 1987. *(unpublished doctoral dissertation)* Structure and deformation in a propagating surge front.

Raymond, C. F. 1973. Inversion of flow measurements for stress and rheological parameters in a valley glacier. *Journal of Glaciology*, vol. 12, pp. 19-44.

Raymond, C. F. 1978. Numerical calculation of glacier flow by finite element methods. Final technical report for National Science Foundation Grant No. DPP74-19075.

Raymond, C. F., and Harrison, W. D. *(submitted)* Evolution of the geometry and motion of Variegated Glacier preceding its surge.

Raymond, C., Johannesson, T., Pfeffer, T., and Sharp, M. 1986. Propagation of a glacier surge into stagnant ice. *Journal of Geophysical Research*, vol. 92, pp. 9037-9049.

Raymond, C. F., and Malone, S. 1986. Propagating strain anomalies during mini-surges of Variegated Glacier, Alaska, U.S.A. *Journal of Glaciology*, vol. 32, pp. 178-191.

Reynaud, L. 1973. Flow of a valley glacier with a solid friction law. *Journal of Glaciology*, vol. 12, pp. 251-258.

Sani, R. L., Gresho, P. M., Lee, R. L., and Griffiths, D. F. 1981. The cause and cure (!) of the spurious pressures generated by certain FEM solutions of the incompressible Navier-Stokes equations: Part 1. *International Journal for Numerical Methods in Fluids*, vol. 1, pp. 17-43.

Shreve, R. L., and Sharp, R. P. 1970. Internal deformation and thermal anomalies in lower Blue Glacier, Mount Olympus, Washington, U.S.A. *Journal of Glaciology*, vol. 9, pp. 65-86.

Squeak, P. P., and Diddlesworth, I. R. 1987. The influence of ptarmigan population dynamics on the thermal regime of the Laurentide Ice Sheet: the surface boundary condition. *The Physical Basis of Ice Sheet Modelling* (Proceedings of the Vancouver Symposium). IAHS Publ. no. 170. pp. 381-384.

Vivian, R. 1980. The nature of the ice-rock interface: the results of investigation on 20,000 m^2 of the rock bed of temperate glaciers. *Journal of Glaciology*, vol. 25, pp. 267-277.

Weertman, J. 1957. On the sliding of glaciers. *Journal of Glaciology*, vol. 3, pp. 33-38.

Whillans, I. M., and Johnsen, S. J. 1983. Longitudinal variations in glacial flow: theory and test using data from the Byrd Station strain network, Antarctica. *Journal of Glaciology*, vol. 29, pp. 78-97.

APPENDIX A

LINEAR VISCOUS FORWARD SOLUTIONS: SURFACE TOPOGRAPHIC EFFECTS

A.1 Effect of surface geometry changes on surface velocity solutions

The velocity solutions in this dissertation have been calculated for a planar slab geometry. However, even if this simple geometry is assumed to be a valid approximation for the geometry of real glaciers, we have seen that basal velocity anomalies can cause surface velocity anomalies which have a normal component, and thus can affect this planar geometry. The effects of variations in surface slope have been addressed by many authors (e.g., Nye, 1969; Langdon and Raymond, 1978; Hutter, 1983; Kamb and Echelmeyer, 1986; Echelmeyer and Kamb, 1986). The question to be addressed here is how possible evolving changes in surface geometry will affect the calculated surface velocity solutions which result from basal velocity anomalies.

We can first look at the case when the anomalous velocity distribution occurs over a long enough time period (at a given spatial position) such that a reasonably steady-state situation evolves. Assuming that surface geometry changes are not simply propagated away (see Section A.2), these changes will cause a surface velocity which will eventually begin to oppose further surface geometry changes. The evolution of these surface geometry changes and the eventual steady-state surface geometry is an interesting problem, which is not addressed here. For this long-term situation, which allows significant surface geometry changes, surface velocity solutions calculated using the assumption of a planar geometry are no longer very useful.

A more realistic case is when the anomalous velocity distribution does not occur over long time periods. For this case, we can see that we want the surface velocity anomaly which results from a basal velocity anomaly (using the planar geometry) to dominate over any surface velocity which arises from changes in the surface geometry. Unfortunately, a simple method of checking that the effects of surface geometry changes are minimal is not possible. This problem occurs because the spatial pattern of the surface velocity anomaly associated with any particular basal velocity anomaly depends on the form of the basal

anomaly. This means that for some forms of basal velocity anomaly the surface velocity arising from the evolving surface geometry will dominate the surface velocity anomaly which results from a basal velocity anomaly for the planar geometry, even though the surface geometry changes are very small. (E.g., for a harmonic longitudinal basal velocity anomaly with a wavelength near to $5.2H$, the calculated longitudinal component of the surface velocity anomaly u_s for the planar geometry will be near to zero; while the calculated normal component of the surface velocity anomaly v_s for the planar geometry will be substantial, causing a significant geometry change and thus soon resulting in a significant value for u_s).

However, we can say that in general, if the surface slope variation has not become very large, then the calculated surface velocity solution for the planar geometry will still be approximately valid. This is a reasonable requirement for the accuracy of the planar slab approximation, and will be valid for most forms of an anomalous velocity distribution.

It would also be possible to calculate the initial surface geometry changes which would result from an initial calculated surface velocity (associated with a given basal velocity anomaly), and to then see what surface velocity would be caused by these geometry changes. Then the combination of the initial surface velocity and the velocity from the geometry changes could be used to calculate further geometry changes, through an iterative process (such as a finite difference model). Using this method, the amount of geometry change which could occur without significantly affecting the surface velocity (as compared to the initial surface velocity) could be determined. However, this would be a complicated process which is not done in this dissertation. Instead, we will look at the simpler requirement that surface slope variations be minimized.

A.2 Minimizing surface slope variations

As stated in the previous section, minimizing surface slope variations should minimize the possible effects of surface geometry changes on the solutions which we have calculated for a planar slab geometry. Two possible mechanisms exist which would result in minimal surface slope variations when a surface velocity anomaly occurs.

The first of these mechanisms is that the surface velocity anomaly may occur over only a short time at any given spatial position. Either a spatially-fixed anomaly might

occur over only a short time period, or else a propagating anomaly might have a short enough spatial extent and a large enough propagation speed such that the anomaly does not occur at any spatial position for an extended time. This simply means that surface geometry changes would not have time to evolve to any great extent.

The other mechanism requires that any evolving surface geometry changes simply be propagated away down-glacier. Provided that the surface slope variations are initially small, a simple stream-line calculation shows that these surface slope variations will only change very slowly provided that:

$$u_s^t >> v_s \tag{A-1}$$

Here u_s^t is the total longitudinal component of the surface velocity, and v_s is the total normal component of the surface velocity; u_s^t can have both steady-state (not changing in the x direction) and anomalous parts, while v_s will only have an anomalous part.

This equation can be satisfied in three different ways. First, the anomalous longitudinal component of the surface velocity can be much greater than v_s; however, this can only occur for relatively long-scale anomalies (which do not have a significant normal component at the bed). Second, the steady-state longitudinal deformation velocity at the surface (due to a sloped bed) can be much greater than v_s. Third, steady-state basal sliding will result in a corresponding steady-state longitudinal component of the surface velocity; this can also be much greater than v_s. For all three of these situations $u_s^t >> v_s$, and the surface slope variations will remain small.

When the surface slope variations are minimized, the planar slab geometry will be essentially correct. Although in certain specific cases even small slope variations can significantly affect the accuracy of the calculated surface velocity anomalies, for most situations the calculated solutions will be correct even if small surface slope variations occur.

APPENDIX B

LINEAR ELASTIC COMPRESSIBLE FORWARD SOLUTIONS

B.1 Geometry, constitutive equations, and boundary conditions

In this appendix we will use an elastic compressible rheology for the modelling of short-scale velocity variations in glaciers. The solutions using this rheology can be used to derive solutions for a visco-elastic rheology (see Chapter 4).

The geometry is a planar slab. This geometry is well-described elsewhere in this dissertation.

The constitutive equations for the elastic compressible rheology are

$$\sigma_{ij} = \left[K - \frac{2}{3}\mu\right] e_{kk}\delta_{ij} + 2\mu e_{ij} \tag{B-1}$$

Here σ_{ij} are the nine stress components and e_{ij} are the nine strain components. The elastic bulk modulus is K, and the elastic shear modulus is μ. Repeated indices indicate summation and δ_{ij} is the Kronecker delta.

These constitutive equations can be separated into two parts: one part relating the sum of the normal stresses to the sum of the normal strains, and the other part relating the stress deviator components to the strain deviator components. Summing Equations (B-1) for the normal components, we get

$$\sigma_{kk} = 3Ke_{kk} \tag{B-2}$$

To relate the stress deviator components to the strain deviator components, these deviators must first be defined. The stress deviators are defined:

$$\tau_{ij} \equiv \sigma_{ij} - \frac{1}{3}\sigma_{kk}\delta_{ij} \tag{B-3a}$$

The strain deviators are defined:

$$\zeta_{ij} \equiv e_{ij} - \frac{1}{3}e_{kk}\delta_{ij} \tag{B-3b}$$

These deviators are then substituted into Equations (B-1). The sums of the normal

components which are in the resulting equation can be related by Equation (B-2) and cancel out. The remaining terms give a set of equations relating the stress deviators to the strain deviators:

$$\tau_{ij} = 2\mu\zeta_{ij} \tag{B-3c}$$

To use Equations (B-2) and (B-3c) in the correspondence principle in Chapter 4, we must take the Laplace transform, after first taking the time derivative of Equation (B-2). The Laplace transform is defined:

$$\tilde{f}(s) \equiv \int_0^\infty e^{-st} f(t) dt \equiv L\{f(t)\} \tag{B-4a}$$

Here s is the transform variable. The inverse Laplace transform is then defined:

$$f(t) \equiv \int_{c-i\infty}^{c+i\infty} e^{st} \tilde{f}(s) ds \tag{B-4b}$$

(This means that a time derivative transforms to a simple algebraic function of the transform variable s; see Chapter 4.)

Taking the Laplace transform of the time derivative of Equation (B-2) we get

$$s\tilde{\sigma}_{kk} = 3Ks\tilde{e}_{kk} \tag{B-5a}$$

Taking the Laplace transform of Equation (B-3c) we get

$$\tilde{\tau}_{ij} = 2\mu\tilde{\zeta}_{ij} \tag{B-5b}$$

(In these equations we have set $\sigma(0)$ and $e(0)$ equal to zero to simplify the mathematics of our solution process.)

The four boundary conditions are the same as Chapters 2 and 4, with a stress-free upper surface (except for atmospheric pressure), and a prescribed basal velocity anomaly (with longitudinal component u_b and normal component v_b).

B.2 Solution method

The solution method for an elastic compressible rheology is more complicated than the solution method for a viscous incompressible rheology. This is because the constitutive equations are more complicated for the elastic compressible rheology (although the

equations for the force balance and the kinematic relations are the same for both rheologies). The main difficulty with the constitutive equations for the elastic compressible rheology is that the compressibility does not allow the use of a stream function, since $\partial u/\partial x + \partial v/\partial y \neq 0$.

However, suitable manipulation of the field equations (the constitutive equations, force balance, and kinematic relations) allows them to be reduced to the following reasonable tractable form in the wave number domain:

$$k^4\hat{u} - 2k^2\frac{\partial^2\hat{u}}{\partial y^2} + \frac{\partial^4\hat{u}}{\partial y^4} = 0 \tag{B-6a}$$

$$k^4\hat{v} - 2k^2\frac{\partial^2\hat{v}}{\partial y^2} + \frac{\partial^4\hat{v}}{\partial y^4} = 0 \tag{B-6b}$$

Here $\hat{u}$ is the Fourier transform of the longitudinal velocity component, $\hat{v}$ is the Fourier transform of the normal velocity component, and k is the wave number.

The solution form for these equations is

$$\hat{u} = A_u e^{-ky} + B_u kye^{-ky} + C_u e^{ky} + D_u kye^{ky} \tag{B-7a}$$

$$\hat{v} = A_v e^{-ky} + B_v kye^{-ky} + C_v e^{ky} + D_v kye^{ky} \tag{B-7b}$$

These equations have eight unknown coefficients; however, there are only four boundary conditions. This problem arises because the field equations were differentiated and combined in such a manner as to artificially double the number of coefficients in Equations (B-7). Thus going back to the process used to derive Equations (B-6), we find that we can solve four of the unknown coefficients in Equations (B-7) in terms of the other four unknown coefficients, by substituting Equations (B-7) into the original field equations, and equating exponentials.

Solving for the coefficients A_v, B_v, C_v, and D_v, in terms of the coefficients A_u, B_u, C_u, and D_u, we get

$$A_v = iA_u + i[3 - 4\nu]B_u \tag{B-8a}$$

$$B_v = iB_u \tag{B-8b}$$

$$C_v = -iC_u + i[3 - 4\nu]D_u \tag{B-8c}$$

$$D_v = -iD_u \tag{B-8d}$$

We note that Poisson's ratio $\nu \equiv [K-2/3\mu]/[2K+2/3\mu]$ enters these equations; thus the elastic moduli will enter the velocity solution (unlike the situation for a viscous incompressible rheology where the dynamic viscosity η does not enter the velocity solution).

Using the four boundary conditions and Equations (B-8), it is then possible to solve for the eight unknown coefficients. These solutions are

$$A_u = \left[\frac{5-12\nu+8\nu^2+6kH-8\nu kH+2k^2H^2+[3-4\nu]e^{2kH}}{[3-4\nu]e^{-2kH}+10-24\nu+16\nu^2+4k^2H^2+[3-4\nu]e^{2kH}}\right]\hat{u}_b \tag{B-9a}$$

$$+\left[\frac{4-12\nu+8\nu^2-2k^2H^2}{[3-4\nu]e^{-2kH}+10-24\nu+16\nu^2+4k^2H^2+[3-4\nu]e^{2kH}}\right]i\hat{v}_b$$

$$B_u = \frac{[-3+4\nu-2KH-e^{2kH}]\hat{u}_b + [-3+4\nu+2kH-e^{2kH}]i\hat{v}_b}{[3-4\nu]e^{-2kH}+10-24\nu+16\nu^2+4k^2H^2+[3-4\nu]e^{2kH}} \tag{B-9b}$$

$$C_u = \left[\frac{[3-4\nu]e^{-2kH}+5-12\nu+8\nu^2-6kH+8\nu kH+2k^2H^2}{[3-4\nu]e^{-2kH}+10-24\nu+16\nu^2+4k^2H^2+[3-4\nu]e^{2kH}}\right]\hat{u}_b \tag{B-9c}$$

$$+\left[\frac{-4+12\nu-8\nu^2+2k^2H^2}{[3-4\nu]e^{-2kH}+10-24\nu+16\nu^2+4k^2H^2+[3-4\nu]e^{2kH}}\right]i\hat{v}_b$$

$$D_u = \frac{[e^{-2kH}+3-4\nu-2kH]\hat{u}_b + [-e^{-2kH}-3+4\nu-2kH]i\hat{v}_b}{[3-4\nu]e^{-2kH}+10-24\nu+16\nu^2+4k^2H^2+[3-4\nu]e^{2kH}} \tag{B-9d}$$

$$A_v = \left[\frac{-4+12\nu-8\nu^2+2k^2H^2}{[3-4\nu]e^{-2kH}+10-24\nu+16\nu^2+4k^2H^2+[3-4\nu]e^{2kH}}\right]i\hat{u}_b \tag{B-10a}$$

$$+\left[\frac{5-12\nu+8\nu^2-6KH+8\nu kH+2k^2H^2+[3-4\nu]e^{2kH}}{[3-4\nu]e^{-2kH}+10-24\nu+16\nu^2+4k^2H^2+[3-4\nu]e^{2kH}}\right]\hat{v}_b$$

$$B_v = \frac{[-3+4\nu-2kH-e^{2kH}]i\hat{u}_b + [3-4\nu-2kH+e^{2kH}]\hat{v}_b}{[3-4\nu]e^{-2kH}+10-24\nu+16\nu^2+4k^2H^2+[3-4\nu]e^{2kH}} \quad \text{(B-10b)}$$

$$C_v = \left[\frac{4-12\nu+8\nu^2-2k^2H^2}{[3-4\nu]e^{-2kH}+10-24\nu+16\nu^2+4k^2H^2+[3-4\nu]e^{2kH}}\right]i\hat{u}_b \quad \text{(B-10c)}$$

$$+ \left[\frac{[3-4\nu]e^{-2kH}+5-12\nu+8\nu^2+6kH-8\nu kH+2k^2H^2}{[3-4\nu]e^{-2kH}+10-24\nu+16\nu^2+4k^2H^2+[3-4\nu]e^{2kH}}\right]\hat{v}_b$$

$$D_v = \frac{[-e^{-2kH}-3+4\nu+2kH]i\hat{u}_b + [-e^{-2kH}-3+4\nu-2kH]\hat{v}_b}{[3-4\nu]e^{-2kH}+10-24\nu+16\nu^2+4k^2H^2+[3-4\nu]e^{2kH}} \quad \text{(B-10d)}$$

Substituting these coefficients into Equations (B-7) gives the Fourier transformed velocity solution at any depth in the glacier.

B.3 Surface velocity solution

The velocity solution of most interest is the velocity at the surface. For a prescribed basal velocity anomaly with Fourier transformed longitudinal component $\hat{u}_b$ and Fourier transformed normal component $\hat{v}_b$, the resulting transformed surface velocity solution is

$$\hat{u}_s = \left[\frac{[8-16\nu+8\nu^2+4kH-4\nu kH]e^{-kH} + [8-16\nu+8\nu^2-4kH+4\nu kH]e^{kH)}}{[3-4\nu]e^{-2kH}+10-24\nu+16\nu^2+4k^2H^2+[3-4\nu]e^{2kH}}\right]\hat{u}_b \quad \text{(B-11a)}$$

$$- \left[\frac{[-4+12\nu-8\nu^2+4kH-4\nu kH]e^{-kH} + [4-12\nu+8\nu^2+4kH-4\nu kH]e^{kH}}{[3-4\nu]e^{-2kH}+10-24\nu+16\nu^2+4k^2H^2+[3-4\nu]e^{2kH}}\right]i\hat{v}_b$$

$$\hat{v}_s = - \left[\frac{[4-12\nu+8\nu^2+4kH-4\nu kH]e^{-kH} + [-4+12\nu-8\nu^2+4kH-4\nu kH]e^{kH}}{[3-4\nu]e^{-2kH}+10-24\nu+16\nu^2+4k^2H^2+[3-4\nu]e^{2kH}}\right]i\hat{u}_b \quad \text{(B-11b)}$$

$$+ \left[\frac{[8-16\nu+8\nu^2-4kH+4\nu kH]e^{-kH} + [8-16nu+8\nu^2+4kH-4\nu kH]e^{kH}}{[3-4\nu]e^{-2kH}+10-24\nu+16\nu^2+4k^2H^2+[3-4\nu]e^{2kH}}\right]\hat{v}_b$$

Here $\hat{u}_s$ is the Fourier transform of the longitudinal component of the surface velocity anomaly, and $\hat{v}_s$ is the Fourier transform of the normal component of the surface velocity anomaly.

These equations can also be written in terms of transfer functions:

$$\hat{u}_s = T_s^{uu}\hat{u}_b - T_s^{vu}i\hat{v}_b \tag{B-12a}$$

$$\hat{v}_s = -T_s^{uv}i\hat{u}_b + T_s^{vv}\hat{v}_b \tag{B-12b}$$

Here the transfer functions are defined

$$T_s^{uu} \equiv \frac{[8-16\nu+8\nu^2+4kH-4\nu kH]e^{-kH} + [8-16\nu+8\nu^2-4kH+4\nu kH]e^{kH)}}{[3-4\nu]e^{-2kH}+10-24\nu+16\nu^2+4k^2H^2+[3-4\nu]e^{2kH}} \tag{B-13a}$$

$$T_s^{vu} \equiv \frac{[-4+12\nu-8\nu^2+4kH-4\nu kH]e^{-kH} + [4-12\nu+8\nu^2+4kH-4\nu kH]e^{kH}}{[3-4\nu]e^{-2kH}+10-24\nu+16\nu^2+4k^2H^2+[3-4\nu]e^{2kH}} \tag{B-13b}$$

$$T_s^{uv} \equiv \frac{[4-12\nu+8\nu^2+4kH-4\nu kH]e^{-kH} + [-4+12\nu-8\nu^2+4kH-4\nu kH]e^{kH}}{[3-4\nu]e^{-2kH}+10-24\nu+16\nu^2+4k^2H^2+[3-4\nu]e^{2kH}} \tag{B-13c}$$

$$T_s^{vv} \equiv \frac{[8-16\nu+8\nu^2-4kH+4\nu kH]e^{-kH} + [8-16nu+8\nu^2+4kH-4\nu kH]e^{kH}}{[3-4\nu]e^{-2kH}+10-24\nu+16\nu^2+4k^2H^2+[3-4\nu]e^{2kH}} \tag{B-13d}$$

Note that $T_s^{vu} \neq T_s^{uv}$, except in the incompressible limit as Poisson's ratio ν goes to 1/2.

These transfer functions are plotted in Figure B-1, for a value of $\nu = 1/3$, which is approximately correct for glacier ice. These transfer functions are not qualitatively different from the transfer function for a viscous incompressible rheology (see Figure 2-3 in Chapter 2). In the incompressible limit (as ν goes to 1/2) the two sets of transfer functions are identical.

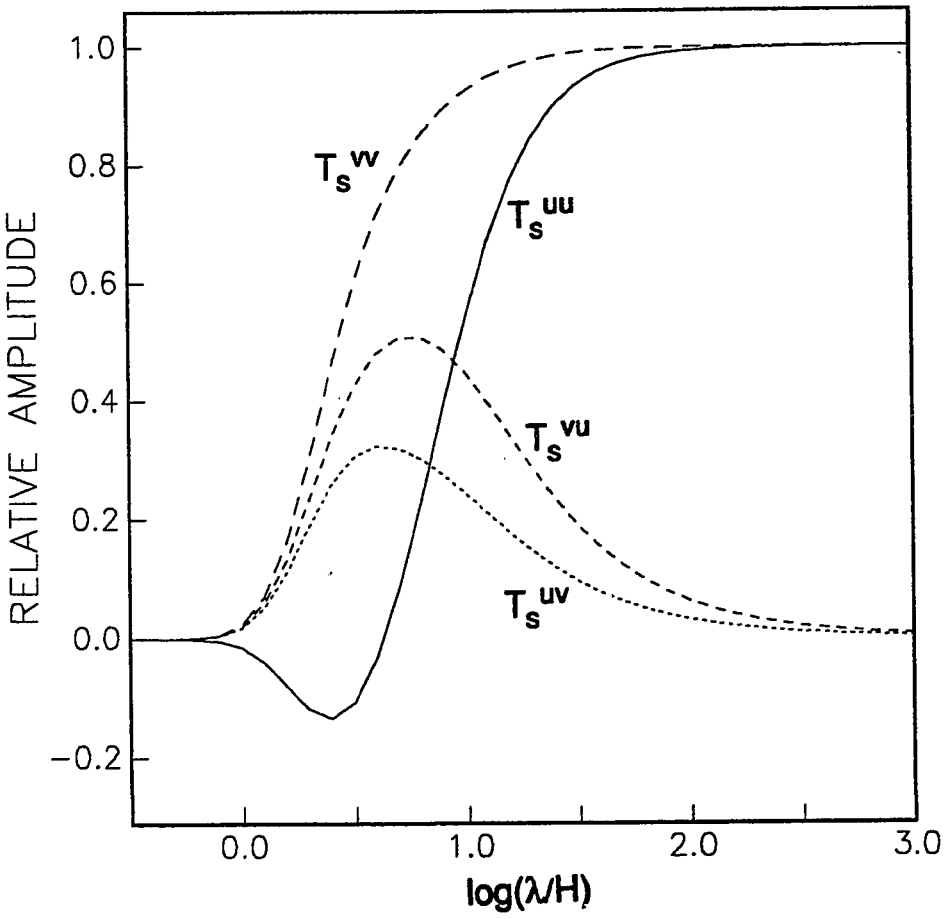

Figure B-1. Forward transfer functions for elastic compressible rheology. Solid line, T_s^{uu}; short dashed line, T_s^{vu}; dotted line, T_s^{uv}; and long dashed line, T_s^{vv}.

APPENDIX C

DETAILED COEFFICIENTS FOR VISCO-ELASTIC FORWARD SOLUTIONS

C.1 Coefficients for longitudinal component of surface velocity

The solution for the Laplace transform of the Fourier transform of the longitudinal component of the surface velocity $\tilde{u}_s$ is written as Equation (4-7a) in Chapter 4, for the visco-elastic rheology. This solution contains coefficients which are not explicitly written out. These coefficients are α_1, β_1, γ_1, α_2, β_2, γ_2, a, b, and c.

To explicitly write these coefficients, we will first define the following more basic coefficients (where k is the wave number and H is the ice thickness):

$$p_{11} \equiv [6+6kH]e^{-kH} + [6-6kH]e^{kH} \tag{C-1a}$$

$$p_{12} \equiv [8+5kH]e^{-kH} + [8-5kH]e^{kH} \tag{C-1b}$$

$$p_{13} \equiv \left[\frac{32}{3} + \frac{8}{3}kH\right]e^{-kH} + \left[\frac{32}{3} - \frac{8}{3}kH\right]e^{kH} \tag{C-1c}$$

$$p_{21} \equiv -6kHe^{-kH} - 6kHe^{kH} \tag{C-2a}$$

$$p_{22} \equiv [3-5kH]e^{-kH} + [-3-5kH]e^{kH} \tag{C-2b}$$

$$p_{23} \equiv \left[8 - \frac{8}{3}kH\right]e^{-kH} + \left[-8 - \frac{8}{3}kH\right]e^{kH} \tag{C-2c}$$

$$q_1 \equiv 3e^{-2kH} + 6 + 12k^2H^2 + 3e^{2kH} \tag{C-3a}$$

$$q_2 \equiv 4e^{-2kH} + 8 + 4k^2H^2 + 4e^{2kH} \tag{C-3b}$$

$$q_3 \equiv \frac{7}{3}e^{-2kH} + \frac{50}{3} + \frac{4}{3}k^2H^2 + \frac{7}{3}e^{2kH} \tag{C-3c}$$

We then can write the solutions for the unknown coefficients in terms of these more basic coefficients, and in terms of the bulk modulus K, the shear modulus μ, and the dynamic viscosity η:

$$\alpha_1 \equiv K^2\mu^2 p_{11} \tag{C-4a}$$

$$\beta_1 \equiv 2K^2\mu\eta p_{11} + 2K\mu^2\eta p_{12} \tag{C-4b}$$

$$\gamma_1 \equiv K^2\eta^2 p_{11} + 2K\mu\eta^2 p_{12} + \mu^2\eta^2 p_{13} \tag{C-4c}$$

$$\alpha_2 \equiv K^2\mu^2 p_{21} \tag{C-5a}$$

$$\beta_2 \equiv 2K^2\mu\eta p_{21} + 2K\mu^2\eta p_{22} \tag{C-5b}$$

$$\gamma_2 \equiv K^2\eta^2 p_{21} + 2K\mu\eta^2 p_{22} + \mu^2\eta^2 p_{23} \tag{C-5c}$$

$$a \equiv K^2\mu^2 q_1 \tag{C-6a}$$

$$b \equiv 2K^2\mu\eta q_1 + 2K\mu^2\eta q_2 \tag{C-6b}$$

$$c \equiv K^2\eta^2 q_1 + 2K\mu\eta^2 q_2 + \mu^2\eta^2 q_3 \tag{C-6c}$$

C.2 Coefficients for normal component of surface velocity

The solution for the Laplace transform of the Fourier transform of the normal component of the surface velocity $\tilde{\bar{v}}_s$ is written as Equation (4-7b) in Chapter 4, for the viscoelastic rheology. This solution also contains coefficients which are not explicitly written out. These coefficients are α_3, β_3, γ_3, α_4, β_4, γ_4, a, b, and c.

The solutions for a, b, and c are given by Equations (C-6). To explicitly write the remaining coefficients, we will again define the following more basic coefficients (where k is the wave number and H is the ice thickness):

$$p_{31} \equiv [6-6kH]e^{-kH} + [6+6kH]e^{kH} \tag{C-7a}$$

$$p_{32} \equiv [8-5kH]e^{-kH} + [8+5kH]e^{kH} \tag{C-7b}$$

$$p_{33} \equiv \left[\frac{32}{3} - \frac{8}{3}kH\right]e^{-kH} + \left[\frac{32}{3} + \frac{8}{3}kH\right]e^{kH} \tag{C-7c}$$

$$p_{41} \equiv -6kHe^{-kH} - 6kHe^{kH} \tag{C-8a}$$

$$p_{42} \equiv [-3-5kH]e^{-kH} + [3-5kH]e^{kH} \tag{C-8b}$$

$$p_{43} \equiv \left[-8 - \frac{8}{3}kH\right]e^{-kH} + \left[8 - \frac{8}{3}kH\right]e^{kH} \tag{C-8c}$$

We then can write the solutions for the unknown coefficients in terms of these more basic coefficients, and in terms of the bulk modulus K, the shear modulus μ, and the dynamic viscosity η:

$$\alpha_3 \equiv K^2\mu^2 p_{31} \tag{C-9a}$$

$$\beta_3 \equiv 2K^2\mu\eta p_{31} + 2K\mu^2\eta p_{32} \tag{C-9b}$$

$$\gamma_3 \equiv K^2\eta^2 p_{31} + 2K\mu\eta^2 p_{32} + \mu^2\eta^2 p_{33} \tag{C-9c}$$

$$\alpha_4 \equiv K^2\mu^2 p_{41} \tag{C-10a}$$

$$\beta_4 \equiv 2K^2\mu\eta p_{41} + 2K\mu^2\eta p_{42} \tag{C-10b}$$

$$\gamma_4 \equiv K^2\eta^2 p_{41} + 2K\mu\eta^2 p_{42} + \mu^2\eta^2 p_{43} \tag{C-10c}$$

APPENDIX D

LINEAR BASAL SHEAR STRESS CALCULATIONS FOR THE MINI-SURGE OF 15 JULY 1980

D.1 Basal shear stress solution for Gaussian filter

It is interesting to examine the basal shear stress for the mini-surge of Variegated Glacier on 15 July 1980, using a linear viscous rheology. We can calculate the anomalous basal shear stress for this mini-surge if we know the longitudinal component of the basal velocity anomaly, by using the transfer function T^{τ} which was derived in Chapter 3 (see Equation (3-21c). Rewriting Equation (3-21b), we get

$$\hat{\tau}_b = T^{\tau}\hat{u}_b \tag{D-1}$$

Here $\hat{u}_b$ will be the Fourier transform of the inverse solution for the longitudinal component of the basal velocity anomaly (instead of a prescribed longitudinal component of the basal velocity). The term $\hat{\tau}_b$ is the transform of the basal shear stress anomaly.

The inverse solution for $\hat{u}_b$ for the mini-surge of 15 July 1980 is derived in Chapter 6. We will use the solution which results from using a Gaussian filter (see Figure 6-5a). It is then simple to calculate $\hat{\tau}_b$, which can be inverse transformed to get the basal shear stress anomaly in the space domain.

D.2 Relation of basal shear stress solution to basal velocity solution

Our motivation for calculating the basal shear stress anomaly for the mini-surge of 15 July 1980 is two-fold. First, we wish to compare this basal shear stress solution using the linear rheology with the basal shear stress solution using a non-linear rheology; this comparison is done in Chapter 7. (This means that the viscosity units for η in Equation (D-1) must be chosen to match the units of the finite element model.) Second, we wish to examine the relation of the basal shear stress solution to the basal velocity solution (a comparison of this relation for the linear and non-linear rheologies is also done in Chapter 7). Therefore we will now examine the relation of the basal shear stress solution to the basal velocity solution.

We know that the basal shear stress anomaly is related to the basal velocity anomaly by Equation (D-1), for the linear viscous rheology. However, what we are really interested in is whether or not some form of sliding law holds during the mini-surge. This means that we want to put the basal shear stress and the basal velocity into a sliding law, and then solve for the sliding law parameter which would relate the given basal shear stress to the given basal velocity.

The linear sliding law which we will use is given by Equation (3-3) in Chapter 3. Rearranging this sliding law, we solve for the sliding law parameter:

$$W = \frac{u_b^{\,t}}{\tau_b^{\,t}} \tag{D-2}$$

Here W is the total sliding law parameter (the sum of the steady-state and anomalous parts), $u_b^{\,t}$ is the total longitudinal component of the basal velocity, and $\tau_b^{\,t}$ is the total basal shear stress. (The exponent m in the sliding law has been set equal to one for the linear rheology and thus is not explicitly written in Equation (D-2).)

This equation relates the total longitudinal component of the basal velocity to the total basal shear stress; but our solutions for the basal velocity (in Chapter 6) and the basal shear stress (in Section D.1) are for the anomalies only. This means that we must first calculate the total basal shear stress and the total longitudinal component of the basal velocity for the mini-surge of 15 July 1980, before we can solve Equation (D-2). This is easy to do.

To calculate the total longitudinal component of the basal velocity, we must add any steady-state basal sliding velocity (not changing in the x direction) to the velocity anomaly. For the mini-surge of 15 July 1980, we will use a steady-state sliding velocity of 0.3 $m\,d^{-1}$. This is based on calculations for the average sliding velocity at this time for this region of Variegated Glacier from Raymond and Harrison (in press). This value also somewhat matches the form of the basal velocity resulting from the non-linear inversion in Chapter 7 (although in the solution in Chapter 7 the sliding velocity was actually about 0.6 $m\,d^{-1}$ before the peak in the mini-surge, and about zero after the peak).

This steady-state sliding velocity is then added to the longitudinal component of the basal velocity anomaly for this mini-surge of 15 July 1980. The longitudinal component of the basal velocity anomaly is solved with a linear inversion using a Gaussian filter (with

$\sigma = 0.137H$, see Figure 6-5a in Chapter 6). The resulting total longitudinal component of the basal velocity u_b^t for this mini-surge is plotted in Figure D-1a. The normal component of the basal velocity (which has no steady-state part) for this mini-surge is plotted in Figure D-1b for reference.

To calculate the total basal shear stress τ_b^t for the mini-surge of 15 July 1980, we simply add the steady-state basal shear stress $\rho g H \sin\gamma$ to the anomalous basal shear stress. (The stress units here are chosen to match the stress units used in the finite element model in Chapter 7.) The resulting total basal shear stress for this mini-surge is plotted in Figure D-2a.

We then solve Equation (D-2) for the total sliding law parameter W. The resulting solution is plotted in Figure D-2b. In general the sliding law parameter is positive. However, there is a negative peak corresponding with the negative peak in τ_b^t. There is also a positive peak immediately up-glacier from the negative peak. This pattern does not well match the expected pattern of W for a mini-surge. (For an analysis of the expected pattern of the W for a mini-surge see Section 7.5.2; for a comparison of the linear and non-linear solutions for W see Section 7.6.2.)

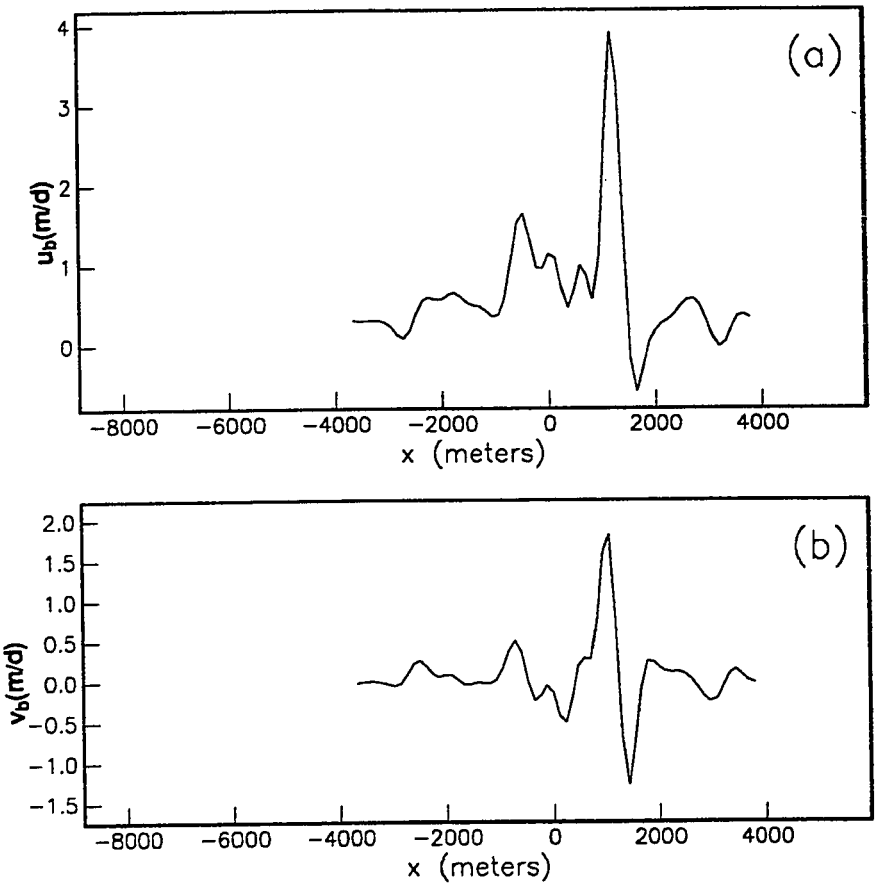

Figure D-1. Solid line: total longitudinal component of basal velocity for mini-surge of 15 July 1980, for linear viscous rheology, calculated using Gaussian filter ($\sigma = 0.137$), including steady-state basal sliding of 0.3 $m\ d^{-1}$, $x = 0$ at 6.5 *km*. Dashed line: normal component of basal velocity v_b for same mini-surge calculated using same filter.

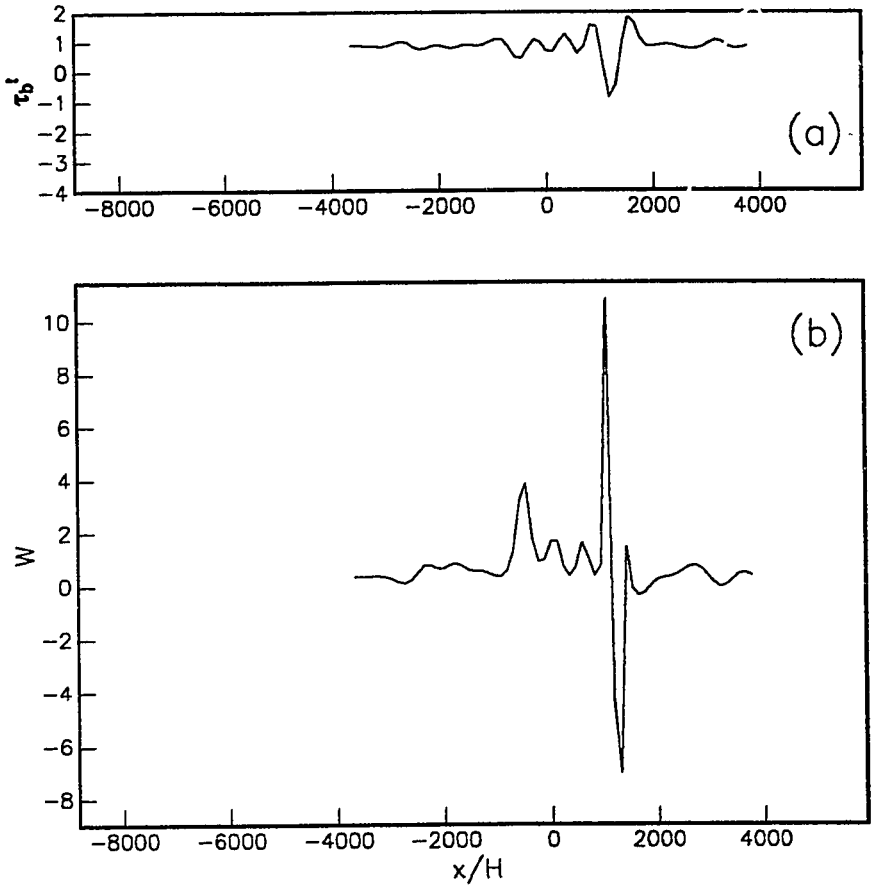

Figure D-2. (a) Total basal shear stress for mini-surge of 15 July 1980, for linear viscous rheology, calculated using Gaussian filter ($\sigma = 0.137$), units corresponding to non-linear solution in Figure 7-5a, $x = 0$ at 6.5 *km* (calculated using $\rho g H \sin\gamma = 0.85$, $\eta = 0.25$). (b) Sliding law parameter determined as $W' = u_b'/\tau_b'$, where all quantities include both steady-state and anomalous parts, for u_b' from Figure D-1 and τ_b' from Figure D-2a.

VITA

Michael John Balise

Born: March 31, 1955, Seattle, Washington

B.Fr. University of Washington, U.S.A., 1977

B.Sc. University of Washington, U.S.A., 1979

Ph.D. University of Washington, U.S.A., 1988